Factorization and Non-Local $1/m_b$ Corrections in the Decay $\bar{B} \to X_s\gamma$

Dissertation

zur Erlangung des Grades

"Doktor der Naturwissenschaften"

am Fachbereich Physik, Mathematik und Informatik

der Johannes Gutenberg-Universität

in Mainz

Michael Benzke

geboren in Essen

Mainz, 2011

Tag der Promotion: 10. Juni 2011

Abstract

In this thesis, a systematic analysis of the $\bar{B} \to X_s\gamma$ photon spectrum in the endpoint region is presented. The endpoint region refers to a kinematic configuration of the final state, in which the photon has a large energy $m_b - 2E_\gamma = \mathcal{O}(\Lambda_{\rm QCD})$, while the jet has a large energy but small invariant mass. Using methods of soft-collinear effective theory and heavy-quark effective theory, it is shown that the spectrum can be factorized into hard, jet, and soft functions, each encoding the dynamics at a certain scale. The relevant scales in the endpoint region are the heavy-quark mass m_b, the hadronic energy scale $\Lambda_{\rm QCD}$ and an intermediate scale $\sqrt{\Lambda_{\rm QCD} m_b}$ associated with the invariant mass of the jet. It is found that the factorization formula contains two different types of contributions, distinguishable by the space-time structure of the underlying diagrams. On the one hand, there are the direct photon contributions which correspond to diagrams with the photon emitted directly from the weak vertex. The resolved photon contributions on the other hand arise at $\mathcal{O}(1/m_b)$ whenever the photon couples to light partons. In this work, these contributions will be explicitly defined in terms of convolutions of jet functions with subleading shape functions. While the direct photon contributions can be expressed in terms of a local operator product expansion, when the photon spectrum is integrated over a range larger than the endpoint region, the resolved photon contributions always remain non-local. Thus, they are responsible for a non-perturbative uncertainty on the partonic predictions. In this thesis, the effect of these uncertainties is estimated in two different phenomenological contexts. First, the hadronic uncertainties in the $\bar{B} \to X_s\gamma$ branching fraction, defined with a cut $E_\gamma > 1.6\,\text{GeV}$ are discussed. It is found, that the resolved photon contributions give rise to an irreducible theory uncertainty of approximately 5 %. As a second application of the formalism, the influence of the long-distance effects on the direct CP asymmetry will be considered. It will be shown that these effects are dominant in the Standard Model and that a range of $-0.6 < A_{CP}^{\rm SM} < 2.8\,\%$ is possible for the asymmetry, if resolved photon contributions are taken into account.

Contents

Chapter 1

Introduction

1.1 Motivation: Why we fight

Today, the Standard Model of particle physics (SM) is able to explain most of the physics at microscopic scales. Mathematically it corresponds to a gauge theory based on the local symmetry group $SU(3)_c \times SU(2)_L \times U(1)_Y$, which naturally decomposes into a strong ($SU(3)_c$) and an electroweak sector ($SU(2)_L \times U(1)_Y$).

Based on the symmetry group of the strong sector, the Lagrangian of quantum chromodynamics (QCD) is derived, which describes the fundamental interactions between colored particles, i.e., quarks and gluons. Due to the non-abelian nature of the strong interaction a perturbative calculation of physical processes involving quarks and gluons is only possible at energy scales above $\sim 1\,\mathrm{GeV}$, where the strong coupling constant is small.

The electroweak sector of the SM exhibits several interesting features that are not present in QCD. First, *all* fermions are charged under the electroweak gauge group and therefore participate in the weak interaction. Second, its symmetry group $SU(2)_L \times U(1)_Y$ is spontaneously broken down to $U(1)_{EM}$ which generates the masses of the heavy vector bosons $W^{\pm}$ and Z. In the SM, this symmetry breaking is realized by the introduction of a new scalar doublet field with a non-vanishing vacuum expectation value (VEV). In this realization the *Higgs* boson appears as a new physical particle, which has yet to be discovered in experiments. Finally, there are Yukawa couplings between quarks of different flavor. After diagonalizing the quark mass matrix, these give rise to flavor changing interactions, whose strength is encoded in the Cabibbo-Kobayashi-Maskawa (CKM) mixing matrix. Possible physical complex phases in this mixing matrix lead to violations of the charge-parity (CP) symmetry.

Modern particle physics strives to improve our understanding of natural processes at the quantum level. Through the analysis of decays of quark-antiquark bound states (mesons) it is possible to determine free parameters of the SM like the CKM matrix elements as well to discover physics beyond the SM (BSM). One particularly interesting process of this type is the decay of a B meson into a photon and a charmless hadronic final state with

non-zero strangeness:

$$\bar{B} \to X_s\gamma\,.$$

The particle $\bar{B}$ includes charged (B^-) as well as neutral ($\bar{B}^0$) B mesons with a bottom quantum number of -1. The corresponding process with a bottom quantum number of +1 can be deduced by CP conjugation. This decay is interesting for several reasons. First it plays an important role in the determination of the CKM matrix element V_{ub} via the semi-leptonic decay $\bar{B} \to X_u l\bar{\nu}$. To a good approximation the hadronic uncertainties of this decay and $\bar{B} \to X_s\gamma$ are equal and therefore it is possible to eliminate this uncertainty in the measurement of V_{ub} through a measurement of the $\bar{B} \to X_s\gamma$ decay rate [1,2]. Second, direct CP violation may be observed by comparing $\bar{B} \to X_s\gamma$ to its CP conjugate process. Finally, the process is mediated by the flavor changing neutral current (FCNC) $b \to s\gamma$. In the SM such a process is only possible at loop level (see first diagram in Figure 1.1). This opens a possible window into BSM physics, since new particles can contribute to

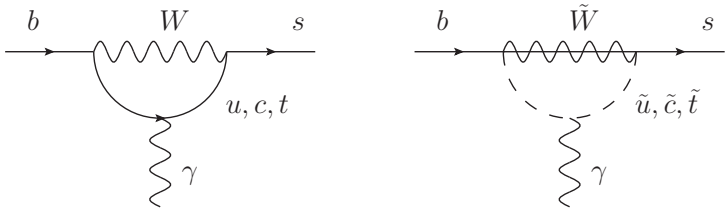

Figure 1.1: The $b \to s\gamma$ FCNC in the SM (left) and in the MSSM (right).

loop diagrams even if there is not enough energy to produce them directly. One example would be the FCNC in the minimal supersymmetric standard model (MSSM) containing a squark and a chargino (see second diagram in Figure 1.1). Furthermore, certain extra-dimensional models can introduce FCNCs at the tree level, which would also cause a measurable deviation from the SM prediction. For a recent review dealing with $\bar{B} \to X_s\gamma$ in BSM models see [3].

The decay $b \to s\gamma$ itself is mediated by the weak interaction. However, theoretical predictions are complicated by the fact that the quarks are not free but bound into hadrons by the strong force. Since the QCD coupling constant is large at the typical hadronic energy scales, a purely perturbative approach is inappropriate. *Effective field theories* allow to separate the calculation into a high-energy (perturbative) and a low-energy (non-perturbative) part. While the high-energy part can in principle be determined to any order in perturbation theory, the effect of the low-energy part can be estimated by the use of phenomenological models. Together with the uncertainties of the perturbative calculation these *hadronic uncertainties* principally restrict the precision of any prediction concerning the $\bar{B} \to X_s\gamma$ decay in the SM as well as BSM.

In the past considerable progress has been made in the ambitious endeavor of calculating the decay rate of $\bar{B} \to X_s\gamma$ as precisely as possible. The starting point for all calculations is an effective theory in which all fields with a mass above the typical energy scale of B decays (the bottom-quark mass m_b) are integrated out. At leading order the transition is then

mediated by a single local operator Q_7, containing just a photon, a bottom- and a strange-quark. Since the mass of the decaying b-quark is large compared to the energy scale of the hadronic binding effects, it is possible to use a further effective theory that implements an expansion in powers of the inverse heavy-quark mass $1/m_b$. The appropriate theory is the *heavy-quark effective theory* (HQET, for a throughout review see e.g. [4]). As will be shown, the first term in this expansion corresponds to the decay of a free quark, which can be calculated perturbatively. Corrections to this result are suppressed by at least $1/m_b$. Today, the perturbative calculation of the decay rate has been performed up to next-to-next-to-leading order (NNLO) in renormalization-group improved perturbation theory [5]. However, experimental measurements only include $\bar{B} \to X_s\gamma$ decays with photon energies above $\sim 1.7\,\text{GeV}$. In this so called *endpoint region* the hadronic jet X_s has an energy of the order of the large scale m_b while its invariant mass is much smaller at the order of $\sqrt{m_b\Lambda_{\text{QCD}}}$ which itself is much larger than the hadronic energy scale Λ_{QCD}. Due to this particular setup, it is no longer possible to employ an expansion in terms of local operators (OPE). Also, potentially large logarithms appear in the perturbative calculation, which need to be resummed to make the perturbative expansion meaningful. This resummation is possible within the framework of the *soft collinear effective theory* (SCET) [6,7]. Alternatively it is possible to extrapolate the experimental data to a photon cut outside the endpoint region. For a cut $E_\gamma > 1.6\,\text{GeV}$ the perturbative calculation yields a branching fraction of [5]

$$\mathcal{B}(\bar{B} \to X_s\gamma) = (3.15 \pm 0.23) \cdot 10^{-4}.$$

A dedicated analysis of cut-related effects and uncertainties gives the slightly lower value $\mathcal{B}(\bar{B} \to X_s\gamma) = (2.98 \pm 0.26) \cdot 10^{-4}$ [8]. The errors given above consist of higher order perturbative uncertainties (3%), parametric dependencies (3%), a charm-quark mass interpolation ambiguity (3%) and—most significantly—non-perturbative uncertainties (5%). The size of these non-perturbative uncertainties was estimated by naive dimensional analysis. In order to systematically study these effects one has to go beyond the leading power in the heavy-quark expansion. Some of these effects have already been considered [2,9,10], but a dedicated analysis was missing.

The primary goal of this work is to use SCET for a systematic study of subleading power[1] corrections to the $\bar{B} \to X_s\gamma$ decay in the endpoint region, which has not been performed before. It was shown in [11, 12] that the differential decay rate of $\bar{B} \to X_s\gamma$ obeys a factorization formula at leading power in the SCET expansion

$$d\Gamma(\bar{B} \to X_s\gamma) = H \cdot J \otimes S\,,$$

where $\otimes$ denotes a convolution. Each of the components describe the physics at a certain scale (hard, intermediate and soft). While the *hard function* H and the *jet function* J are perturbatively calculable, the soft function S is related to a hadronic matrix element. When integrating the differential rate over a range much larger than the endpoint region

[1]The term "subleading" always refers to higher order terms in the expansion parameter of the effective theory, while "next-to-leading" refers to higher order terms of the perturbative expansion in the coupling.

(i.e. including photons with an energy such that $m_b - 2E_\gamma \gg \Lambda_{\rm QCD}$) the expression above reduces to an expansion in terms of local operators [13]. In this thesis a new factorization formula for the differential rate in the endpoint region, valid at any order in the $1/m_b$ expansion will be established. It will introduce matrix elements of non-local operators that do not reduce to local ones in the integrated rate [14]. In the end, the effect of these non-perturbative uncertainties on the integrated decay rate, as well as on the direct CP violation will be estimated. The main results of this work have been published in [15, 16]. It will turn out, that the factorization resolves several issues of the partonic calculation, such as large logarithms and dependencies on low-energy parameters like the strange quark mass. The numerical analysis of the non-perturbative effects will show that the irreducible uncertainty of the partonic prediction of the branching fraction amounts to approximately 5 %. Furthermore, it will be found that these effects dominate the prediction of the SM CP asymmetry.

1.2 Structure of the Thesis

This work can be roughly divided into two parts, with the borderline running between Section 5.2.6 and 5.3. Before that line the theoretical background will be extensively reviewed, in order to motivate the approach and put it into a conceptual context. Afterwards the new findings of this work will be presented.

The first part starts with a brief review of the experimental situation in Section 1.3. Chapter 2 will then introduce the fundamental concepts of the partonic calculation of the $\bar{B} \to X_s\gamma$ branching fraction. This includes the derivation of an appropriate set of operators and a discussion of the influence of renormalization. During the presentation several issues concerning the calculation will be noted. One of these issues are the corrections due to the binding of the partons into hadronic states. In Chapter 3 the heavy-quark effective theory will be introduced, which offers a way to deal with hadrons that contain one heavy quark. The soft-collinear effective theory, which offers a systematic way to resum large logarithms and deal with the breakdown of the local OPE will be discussed in Chapter 4. Following up, the subleading contributions in the SCET expansion are considered in Chapter 5. The first part of this chapter will discuss the subleading contributions due to an interference of the electromagnetic dipole operator with itself. The second part will then set the stage for the systematic analysis of *all* subleading contributions, by discussing the matching of QCD onto SCET. This analysis is explicitly performed in Chapter 6. Chapters 7 and 8 will then apply the results of the analysis in two different phenomenological contexts, i.e., the irreducible non-perturbative uncertainty on the prediction of the $\bar{B} \to X_s\gamma$ branching fraction and the direct CP asymmetry. Chapter 9 will sum up the results and draw conclusions. Finally, three appendices contain information on the penguin function, the set of parameters used in this work, and a complete list of the SCET operators up to a suppression of $1/m_b$ compared to the leading power.

1.3 Experimental Status of $\bar{B} \to X_s\gamma$

In order to illustrate the motivation behind the complex theoretical apparatus developed for describing rare inclusive B decays the experimental situation is briefly reviewed (for a more detailed review see [17, 18]). The primary quantity of interest is the branching fraction of B meson decays mediated by a flavor changing neutral current. One of the most important processes of this type is the decay into a photon and a charmless hadronic final state with non-zero strangeness. In contrast to the experimental point of view, which prefers exclusive measurements for easier background elimination, it is more desirable from a theoretical perspective to measure an inclusive process, since this makes the difficult modeling of the hadronic final states unnecessary.

In the dedicated *B factories* BaBar [19] and Belle [20] the B mesons are produced by operating an electron positron collider at the $\Upsilon(4S)$ resonance, which predominantly decays into pairs of neutral (B^0, $\bar{B}^0$) or charged (B^+, B^-) B mesons (in approximately equal parts). These in turn primarily decay into charmed final states via the CKM favored charged current process $b \to cW^-$. There are two ways to measure the much smaller branching fraction into the charmless final state $X_s\gamma$, which is mediated by an FCNC. In the so called "semi-inclusive" method several exclusive decays into a strange final state and a photon are measured separately and added up. The "fully inclusive" method only reconstructs the photon[2]. Since $\bar{B} \to X_s\gamma$ is dominated by the two-body decay $b \to s\gamma$ the photon energy spectrum peaks at $E_\gamma \approx m_b/2$, while the deviations from a δ-function are due to gluon bremsstrahlung and hadronic effects within the meson. This distinctive form of the spectrum can be used to identify the photons from a $\bar{B} \to X_s\gamma$ decay.

However, there are several background processes that render the identification of the $\bar{B} \to X_s\gamma$ photons difficult (see Figure 1.3). On the one hand there is the continuum background. One component of this continuum is due to photons radiated from the initial state electrons before their annihilation $e^+e^- \to \gamma\bar{q}q$ (called "Continuum ISR" in Figure 1.3). Another arises from the decay of inclusively produced π^0/η, which subsequently decay via $\pi^0/\eta \to \gamma\gamma$, with one undetected photon (called "Continuum π^0" in Figure 1.3). When using the semi-inclusive method, this continuum background is reduced due to kinematical constraints and the beam energy constraint, while for the inclusive methods event shapes have to be used to identify signal events.

On the other hand there is the $B\bar{B}$ background, which refers to processes in which the B mesons are produced, but then decay via a process other than $\bar{B} \to X_s\gamma$. The main component of this background is due to $B \to X\pi^0$ or $B \to X\eta$ followed by $\pi^0/\eta \to \gamma\gamma$. In order to get rid of this background some lower cutoff on the photon energy is imposed. It is this cutoff, that leads to the breakdown of the local OPE and potentially gives rise to the large logarithms in the perturbative calculation. Generally, the experimental uncertainties become larger as the cutoff on the photon energy is lowered, as can be illustrated with the

[2]With high enough statistics a lepton tag (the lepton originates from the semi-leptonic decay of the other B meson) can be used to reduce the background [22].

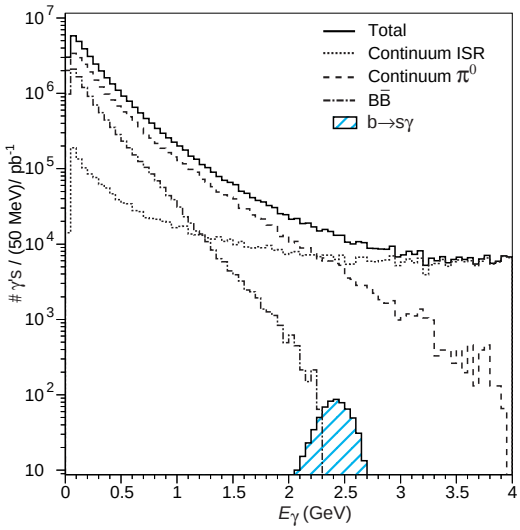

Figure 1.2: Numbers of photons from various background processes and the signal for $b \to s\gamma$, taken from [21]. See text for the explanation of the different graphs.

latest fully inclusive data of the BELLE collaboration [22].

$$\begin{aligned}
\mathcal{B}(\bar{B} \to X_s\gamma)_{E_\gamma > 2\,\mathrm{GeV}} &= (3.02 \pm 0.10_{\mathrm{stat}} \pm 0.11_{\mathrm{syst}}) \cdot 10^{-4} \\
\mathcal{B}(\bar{B} \to X_s\gamma)_{E_\gamma > 1.9\,\mathrm{GeV}} &= (3.21 \pm 0.11_{\mathrm{stat}} \pm 0.16_{\mathrm{syst}}) \cdot 10^{-4} \\
\mathcal{B}(\bar{B} \to X_s\gamma)_{E_\gamma > 1.8\,\mathrm{GeV}} &= (3.36 \pm 0.13_{\mathrm{stat}} \pm 0.25_{\mathrm{syst}}) \cdot 10^{-4} \\
\mathcal{B}(\bar{B} \to X_s\gamma)_{E_\gamma > 1.7\,\mathrm{GeV}} &= (3.45 \pm 0.15_{\mathrm{stat}} \pm 0.40_{\mathrm{syst}}) \cdot 10^{-4}
\end{aligned}$$

The first error is statistical, while the second one is systematic and includes uncertainties due to background subtraction.

The shape of the photon spectrum and therefore the differential decay rate $d\Gamma/dE_\gamma$ is of interest as well, as it contains information about the heavy-quark parameters, which are related to the b-quark mass and its movement inside the hadron. Also, for a comparison of experimental data with the perturbative calculation an even lower cutoff is necessary than the ones achieved in measurements so far. For this purpose one assumes a certain model for the shape of the photon spectrum and calculates extrapolation factors [23], which are defined as the ratio between branching fractions with minimum photon energies above and at 1.6 GeV.

The current experimental world average for a photon energy of $E_\gamma > 1.6\,\mathrm{GeV}$ is given as [24]

$$\mathcal{B}(\bar{B} \to X_s\gamma) = (3.55 \pm 0.24 \pm 0.09) \cdot 10^{-4}\,,$$

where the first error is the combined statistical and systematic, while the second error is due to the extrapolation. As a final remark it is noted that inclusive experiments only measure the sum of $\bar{B} \to X_s\gamma$ and $\bar{B} \to X_d\gamma$. The $\bar{B} \to X_d\gamma$ part is subtracted by calculating the ratio of the two decays in the SM.

In order to proceed with precision physics at the intensity frontier in the future, two super-B factories – Belle II and SuperB in Italy – have been proposed. Their design and physics case can be read off from the latest progress reports of the two collaborations [25,26].

In conclusion, the experimental situation motivates a theoretical treatment that is able to describe the photon spectrum of the $\bar{B} \to X_s\gamma$ decay in the endpoint region. The following chapters will introduce the appropriate framework and will work out its impact on the theoretical prediction.

Chapter 2

The Decay $\bar{B} \to X_s\gamma$ in Full QCD

In this chapter all the ingredients necessary to perform a partonic calculation of the $\bar{B} \to X_s\gamma$ decay rate will be discussed. The phrase "partonic" refers to the interpretation of hadrons as the sum of their constituent partons whose interactions can be perturbatively calculated. Of course, this interpretation ignores effects of confinement, which are very relevant and will be considered in the next chapter. The first ingredient is the weak effective Lagrangian that is necessary to describe flavor-changing processes. It can be derived by systematically integrating out the heavy degrees of freedom, which will be done in Section 2.1. Along the way it will be demonstrated how the new effective terms in the Lagrangian can be obtained from a local operator product expansion. In Section 2.1.3 it will then be shown how the effective couplings of the new operators are determined at the appropriate scale. Using these results the differential decay rate in the parton model is calculated in Section 2.2.

2.1 The Weak Effective Lagrangian

The starting point for all calculations concerning radiative B decays is the weak effective Lagrangian. The general procedure of deriving effective theories will be discussed in this section. As an example the heavy gauge bosons $W^{\pm}$ will be explicitly integrated out. Since there are no leptons in radiative B decays only the quark sector will be considered. The presentation in this section will follow to some extent the comprehensive discussions in in [27, 28].

2.1.1 Integrating out the Heavy Degrees of Freedom

On the elementary level the decay $\bar{B} \to X_s\gamma$ is mediated by the decay of a b-quark via the weak interaction. In addition, the b-quark is bound into a hadron by the strong interaction. The Standard Model Lagrangian necessary to describe such a process was introduced by Glashow, Weinberg, and Salam. After spontaneous symmetry breaking (SSB) it is given

by [29]

$$
\begin{aligned}
\mathcal{L}_{\text{SM}} &= \mathcal{L}_{\text{quark}} + \mathcal{L}_{\text{CC}} + \mathcal{L}_{\text{W,kin}} + \mathcal{L}_{\text{Z}} + \mathcal{L}_{\text{Field}} + \mathcal{L}_{\text{Higgs}} \\
\mathcal{L}_{\text{quark}} &= \sum_i \left[\bar{u}^i(i\not{D} - m_u^i)u^i + \bar{d}^i(i\not{D} - m_d^i)d^i\right] \\
\mathcal{L}_{\text{CC}} &= \sum_{i,j} \Big[\frac{g}{2\sqrt{2}}\,\bar{u}^i\gamma^\mu(1-\gamma_5)V_{ij}d^j\,W_\mu^+ + \frac{g}{2\sqrt{2}}\,\bar{d}^i\gamma^\mu(1-\gamma_5)V_{ij}^*u^j\,W_\mu^-\Big] \\
\mathcal{L}_{\text{W,kin}} &= -\frac{1}{2}(\partial_\mu W_\nu^+ - \partial_\nu W_\mu^+)(\partial^\mu W^{-\nu} - \partial^\nu W^{-\mu}) + M_W^2 W_\mu^+ W^{-\mu}
\end{aligned}
\tag{2.1}
$$

where the sum runs over all quark families and u^i and d^i represent the up- and down-type quarks of the ith family and $m_{u,d}^i$ are the corresponding masses. The fields $W_\mu^\pm$ are massive $SU(2)_L$ gauge bosons and g is the associated coupling constant. Since the Lagrangian is given in the mass basis the charged currents (indicated by the subscript CC) contain the CKM mixing matrix V_{ij}, that gives rise to family changing interactions [30]. The expressions for $\mathcal{L}_{\text{Z}}$, which encodes the flavor-diagonal couplings of the Z-bosons and its kinetic term, as well as those for $\mathcal{L}_{\text{Field}}$ and $\mathcal{L}_{\text{Higgs}}$, which contain the self-interaction terms of the gauge fields and the Higgs sector introduced in order to achieve SSB, are not explicitly given. Finally the covariant derivative is given by

$$
iD_\mu = i\partial + e_q e A_\mu + g_s A_\mu^a T^a\,, \tag{2.2}
$$

where e and g_s are the electromagnetic and strong coupling constants, e_q is the quark charge in units of e ($e_u = 2/3$, $e_d = -1/3$), T^a are the $SU(3)_c$ color generators and A_μ and A_μ^a are the photon and gluon gauge fields.

The typical energy scale of B decays is set by the mass m_b of the heavy b-quark. Since heavier fields can not be produced directly it is convenient to use an effective field theory (EFT) obtained by removing the heavy modes as dynamical degrees of freedom. The effective theory must nevertheless include the corrections due to virtual contributions of these heavy particles. A consistent way to construct the EFT is to start with the generating functional of the full SM and integrate out the heavy fields in the path integral formalism. In the case of B decays these are the heavy gauge bosons fields $W_\mu^\pm$ and Z_μ and the top quark field t. The generating functional can be written as

$$
Z[J] = \int \mathcal{D}\phi\, \exp\Big[i\int d^4x\,[\mathcal{L}_{\text{SM}} + J(x)\phi(x)]\Big]. \tag{2.3}
$$

Here $\phi(x)$ represents all fields that can be external in the theory at hand and $J(x)$ are the associated external sources. The symbol $\int \mathcal{D}\phi$ stands for the path integral over all fields of the theory. The Feynman propagator of a field is then given by

$$
\begin{aligned}
D_F(x-y) &= \langle 0|\mathbf{T}\phi(x)\phi(y)|0\rangle \\
&= \frac{1}{Z[0]}\left(-i\frac{\delta}{\delta J(x)}\right)\left(-i\frac{\delta}{\delta J(y)}\right) Z_0[J]\Big|_{J=0} \\
&= \frac{\int \mathcal{D}\phi\,\phi(x)\phi(y)\exp\left[i\int d^4x\,\mathcal{L}_{\phi,\text{kin}}\right]}{\int \mathcal{D}\phi\,\exp\left[i\int d^4x\,\mathcal{L}_{\phi,\text{kin}}\right]}\,,
\end{aligned}
\tag{2.4}
$$

where Z_0 is the generating functional containing only the free field Lagrangian of ϕ, $\delta/(\delta J)$ is a functional derivative and **T** indicates a time-ordered product. The quantity in the denominator of the last line of (2.4) is called a functional determinant and will always cancel in the perturbative calculation of correlation functions. In order to integrate out the W bosons from the SM generating functional the sources of $W^{\pm}$ are set to zero and the exponential is split as follows

$$Z[J] = \int \mathcal{D}\phi \, \exp\left[i \int d^4x \, \mathcal{L}_{\mathrm{W,kin}}\right] \exp\left[i \int d^4x \, \mathcal{L}_{\mathrm{CC}}\right] \exp\left[i \int d^4x \, \mathcal{L}_{\mathrm{Field}}\right] \times \exp\left[i \int d^4x \, [\mathcal{L}_{\mathrm{rem}} + J(x)\phi(x)]\right].$$

The last term containing $\mathcal{L}_{\mathrm{rem}}$ can be deduced from Equation (2.1) and is independent of the W fields. If one is only interested in the effective Lagrangian for the quark fields, the self-interaction term $\mathcal{L}_{\mathrm{Field}}$ can be ignored as well. After expanding the exponential containing the interaction terms in $\mathcal{L}_{\mathrm{CC}}$, the path integral over the W bosons can be explicitly performed by using (2.4). One finds

$$\begin{aligned}
&\int \mathcal{D}W^+\mathcal{D}W^- \exp\left[i \int d^4x \, \mathcal{L}_{\mathrm{W,kin}}\right] \left(1 - \frac{1}{2} \int d^4x d^4y \, \mathcal{L}_{\mathrm{CC}}(x)\mathcal{L}_{\mathrm{CC}}(y) + \dots\right) \\
&= \int \mathcal{D}W^+\mathcal{D}W^- \exp\left[i \int d^4x \, \mathcal{L}_{\mathrm{W,kin}}\right] \\
&\qquad \times \left(1 - \frac{g^2}{16} \int d^4x d^4y \, (J^{+\mu}W^+_\mu + J^{-\mu}W^-_\mu)_x (J^{+\nu}W^+_\nu + J^{-\nu}W^-_\nu)_y + \dots\right) \\
&= \int \mathcal{D}W^+\mathcal{D}W^- \exp\left[i \int d^4x \, \mathcal{L}_{\mathrm{W,kin}}\right] \\
&\qquad \times \left(1 - \frac{g^2}{16} \int d^4x d^4y \, (J^+_\mu(x)J^-_\nu(y) + J^-_\mu(x)J^+_\nu(y)) D_F^{\mu\nu}(x-y) + \dots\right).
\end{aligned}$$

Here the charged currents are defined as $J^+_\mu = \bar{u}^i \gamma^\mu (1-\gamma_5) V_{ij} d^j$ and $J^-_\mu = (J^+_\mu)^\dagger$. The terms in the last line can be resummed into an exponential which introduces non-local interaction terms in the new effective Lagrangian. These terms do not depend on the W fields which have been integrated out. The remaining path integral over the kinetic part of the W Lagrangian is identical to the functional determinant mentioned above and drops out in the definition of correlation functions. After integrating out the W bosons the effective Lagrangian for the quarks can therefore be written as

$$\mathcal{L}_{\mathrm{eff}} = \mathcal{L}_{\mathrm{quark}} + \mathcal{L}_{\mathrm{int,\ eff}} + \mathcal{L}_{\mathrm{Z}} + \mathcal{L}_{\mathrm{Higgs}}, \tag{2.5}$$

with

$$\mathcal{L}_{\mathrm{int,\ eff}} = i \frac{g^2}{16} \int d^4y \, (J^+_\mu(x)J^-_\nu(y) + J^-_\mu(x)J^+_\nu(y)) D_F^{\mu\nu}(x-y).$$

In the unitary gauge one has

$$D_F^{\mu\nu}(x-y) = \int \frac{d^4k}{(2\pi)^4} \frac{-i}{k^2 - M_W^2} \left(g^{\mu\nu} - \frac{k^\mu k^\nu}{M_W^2} \right) e^{-ik(x-y)}.$$

Up to this point the Lagrangians of the full and effective theory are equivalent for any process without external W bosons. At tree level, the momentum k of the propagator is of the same order as the external momenta which are by definition much smaller than the W mass M_W, i.e., $k^2 \ll M_W^2$. It is therefore possible to expand the propagator $D_F^{\mu\nu}$ in powers of $1/M_W^2$. This expansion effectively rewrites the non-local interaction functional as a series of local ones. One arrives at

$$\begin{aligned}
&\int d^4y \, J_\mu^+(x) J_\nu^-(y) \, D_F^{\mu\nu}(x-y) \\
&= \int d^4y \, J_\mu^+(x) \int \frac{d^4k}{(2\pi)^4} \frac{i}{M_W^2} \left(g^{\mu\nu} + \frac{1}{M_W^2}(k^2 g^{\mu\nu} - k^\mu k^\nu) + \dots \right) e^{-ik(x-y)} \int d^4p \, J_\nu^-(p) \, e^{-ipy} \\
&= J_\mu^+(x) \, \frac{i}{M_W^2} \left(g^{\mu\nu} + \frac{1}{M_W^2}(\partial^2 g^{\mu\nu} - \partial^\mu \partial^\nu) + \dots \right) J_\nu^-(x).
\end{aligned}$$

Summing up, one might say that integrating out the W bosons at tree level introduced a sum of effective local-interaction functionals of arbitrary dimension. The higher dimensional terms are suppressed by appropriate powers of $1/M_W^2$. In canonical quantum field theory this corresponds to a sum of local operators. Beyond the tree level, these operators will have coefficients that encode the difference between the full and effective theory due to virtual effects of the particles which have been integrated out. Writing an EFT in terms of local operators is called the operator product expansion [31]. It is important to note that this local expansion was only possible due to the large mass scale M_W. Later on, EFTs will be introduced in which such a large scale is missing. These will also give rise to non-local operators. The leading order term in the local expansion is given by

$$\mathcal{L}^{(1)}_{\text{int, eff}} = -\frac{g^2}{8M_W^2} \, J_\mu^-(x) J^{+\mu}(x). \tag{2.6}$$

This is the well-known Fermi interaction of weak decays with the Fermi constant defined as $G_F/\sqrt{2} = g^2/(8M_W^2)$. The apparent weakness of the weak interaction is due to the $1/M_W^2$ suppression of the leading contribution.

2.1.2 The Wilson Coefficients

In the above derivation of the effective Lagrangian, corrections due to the strong interaction have been ignored. Since QCD is still part of the effective theory, the effective description resembles the one of QCD in the infrared (IR). However, high-virtuality gluons enter loop diagrams together with other fields that are integrated out. In this case the momentum of the heavy particle can become large and a naive expansion of the heavy propagator in

powers of k^2/M_W^2 is no longer possible. This practical problem can be systematically dealt with in the framework of the heavy-mass expansion (see [32] and references therein). In the so-called *matching procedure* the high-virtuality gluon corrections are absorbed into the coefficients of the local operators in the OPE. These can then be determined by comparing the effects of the gluonic corrections in the effective and the full theory. Since the coefficients encode the physics of gluons with a large virtuality, this calculation can be performed in perturbation theory. As an example one might consider the four-fermion operator in (2.6). In the case of $\bar{B} \to X_s\gamma$ one has to deal with

$$Q_1^c := \bar{s}_i\gamma^\mu(1-\gamma_5)c_i\,\bar{c}_j\gamma_\mu(1-\gamma_5)b_j, \tag{2.7}$$

where indices i, j now represent color quantum numbers. The QCD corrections to a process with four external quarks in the full and effective theory are shown in Figure 2.1.2. The first

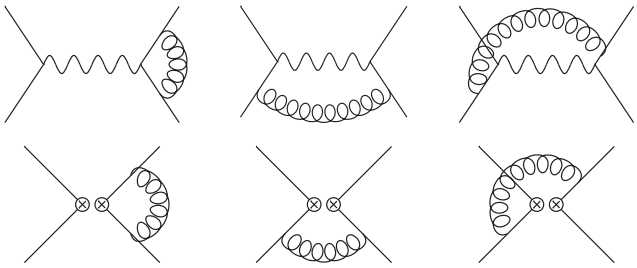

Figure 2.1: NLO QCD corrections to the four-quark process in the full (first line) and the effective theory (second line). Two crossed circles denote the insertion of a four-quark operator.

diagram in each line gives rise to the renormalization of the quark currents. Since the quark currents are conserved the divergence of these diagrams is canceled by the field-strength renormalization of the quark fields. Furthermore, the finite terms of these diagrams are the same in the full and effective theory. Therefore they do not contribute to the coefficient of the effective theory operator. Calculating the last two diagrams in the effective theory and in $4-2\varepsilon$ dimensions to regulate the divergences yields (suppressing the factor $\frac{G_F}{\sqrt{2}}V_{cs}^*V_{cb}$)

$$i\mathcal{M} = -6i\,\frac{\alpha_s}{4\pi}\left(\frac{1}{\varepsilon} + \ln\frac{\mu^2}{-p^2} + \text{constant}\right)\bar{s}_i\gamma^\mu(1-\gamma_5)T^a_{ij}c_j\,\bar{c}_k\gamma_\mu(1-\gamma_5)T^a_{kl}b_l, \tag{2.8}$$

where T^a_{ij} are the $SU(3)_c$ generators and μ is the renormalization scale. Since the coefficients are by definition independent from the IR degrees of freedom, the external particles can be treated as massless and it can be assumed that they all the same momentum. The four-quark operator in (2.8) can be related to Q_1^c by the following relation for the generators:

$$T^a_{ij}T^a_{kl} = \frac{1}{2}\left(\delta_{il}\delta_{kj} - \frac{1}{N_c}\delta_{ij}\delta_{kl}\right). \tag{2.9}$$

where N_c is the number of colors. This obviously introduces a second operator with a different color structure[1]

$$Q_2^c := \bar{s}_i \gamma^\mu (1-\gamma_5) c_j \, \bar{c}_j \gamma_\mu (1-\gamma_5) b_i. \tag{2.10}$$

This effect is called the mixing of two operators under QCD renormalization. In order to renormalize all operators of the effective theory the diagrams in the second line of Figure 2.1.2 have to be calculated with operator insertions of Q_1^c and Q_2^c. Then a matrix-valued operator renormalization constant has to be introduced to absorb all divergences:

$$Q_i = Z_{ij} Q_j^{\text{ren}}. \tag{2.11}$$

After renormalization the result of the effective theory calculation can be compared to the full theory calculation of the diagrams in the first line of Figure 2.1.2 and the difference must be accounted for by coefficients of the effective operators. Note that there is no divergence in the full theory since the full W propagator renders the loop integral finite. The full theory diagrams therefore contain logarithms of the type $\ln \frac{M_W^2}{-p^2}$. Comparing this to the logarithmic terms in (2.8) reveals that the scale μ takes the role of a factorization scale, that divides the result into a high-energy part contained in the coefficients and a low-energy part encoded in the matrix elements of the effective operators. At NLO the coefficients of the operators Q_1^c and Q_2^c are given by

$$\begin{aligned} C_1(\mu) &= 1 + \frac{3}{N_c} \frac{\alpha_s}{4\pi} \left(\ln \frac{M_W^2}{\mu^2} - \frac{11}{6} \right), \\ C_2(\mu) &= -3 \frac{\alpha_s}{4\pi} \left(\ln \frac{M_W^2}{\mu^2} - \frac{11}{6} \right). \end{aligned} \tag{2.12}$$

The coefficients of the effective theory operators are called *Wilson coefficients* [33].

The general procedure outlined above can be summarized as follows. In order to construct an effective theory appropriate for energies below the electroweak scale M_W the fields above that scale have to be integrated out. This corresponds to writing down a sum of all local operators allowed by the symmetries and quantum numbers of the problem and suppressed by powers of $1/M_W$:

$$\mathcal{L}_{\text{eff}} = \mathcal{L}_{\text{quark}} - \frac{G_F}{\sqrt{2}} V_{\text{CKM}}^* V_{\text{CKM}} \sum_i C_i Q_i + \mathcal{O}\left(\frac{1}{M_W^2} \right). \tag{2.13}$$

The Wilson coefficients C_i can be interpreted as coupling constants of the new interactions in the effective theory. But since the full theory is known they can also be calculated from the SM. Since the coefficients encode the effects of the high-virtuality modes of the full theory they can be calculated perturbatively, by comparing the results of the effective and of the full theory at a large scale. Thereby a dependence on this factorization scale

[1] Note that the operators Q_1^c and Q_2^c often have reversed names in the literature.

is introduced into the coefficients. This scale dependence cancels if the matrix elements of the operators are calculated at the same scale and in the same scheme. However, for a certain low-energy process like a meson decay the matrix element of the effective operators must be renormalized at the low scale. This can potentially introduce large logarithms in the Wilson coefficients. For $\mu = 1\,\text{GeV}$ the $\mathcal{O}(\alpha_s)$ corrections to the Wilson coefficients are only suppressed by a factor of $\frac{\alpha_s}{\pi} \ln \frac{M_W^2}{\mu^2} \sim 0.9$ compared to the leading-order term resulting in a bad convergence of the perturbative series. This problem can be solved by resumming large logarithms by means of the *renormalization group* (RG) [34].

2.1.3 The Renormalization Group

In order to derive the renormalization group equations (RGE) one considers the dependence of the Wilson coefficients on the scale μ. Since this scale was introduced by splitting the calculation in a low- and a high-energy part, the product of the Wilson coefficients with the operator matrix elements renormalized at μ is formally independent of the scale. Using (2.11) one has

$$\begin{aligned}
&\frac{d}{d\ln\mu}\sum_i C_i(\mu)\langle Q_i^{\text{ren}}(\mu)\rangle = 0 \\
=&\sum_{i,j}\left(\left[\frac{d}{d\ln\mu}C_i(\mu)\right](Z^{-1})_{ij}(\mu)\,\langle Q_j\rangle + C_i(\mu)\left[\frac{d}{d\ln\mu}(Z^{-1})_{ij}(\mu)\right]\langle Q_j\rangle\right) \\
=&\sum_{i,j,k}\left(\left[\frac{d}{d\ln\mu}C_i(\mu)\right]\langle Q_i^{\text{ren}}(\mu)\rangle - C_i(\mu)\,(Z^{-1})_{ik}(\mu)\left[\frac{d}{d\ln\mu}Z_{kj}(\mu)\right]\langle Q_j^{\text{ren}}(\mu)\rangle\right) \\
=&\sum_i\left(\frac{d}{d\ln\mu}C_i(\mu) - \sum_j C_j(\mu)\gamma_{ji}\right)\langle Q_i^{\text{ren}}(\mu)\rangle,
\end{aligned}$$

where the *anomalous dimension matrix* γ is defined as

$$\gamma_{ji} = \left[Z^{-1}\frac{d}{d\ln\mu}\,Z\right]_{ji}. \tag{2.14}$$

It only depends implicitly on the scale μ through the strong coupling constant α_s. Under the assumption that the operators of the expansion are linearly independent this yields the RGE of the Wilson coefficients:

$$\frac{d}{d\ln\mu}\vec{C}(\mu) = \gamma^T(\alpha_s(\mu))\,\vec{C}(\mu). \tag{2.15}$$

By solving this equation it is possible to relate the Wilson coefficients at a certain scale to the coefficients at any other scale. This solves the problem of the large logarithms. The coefficients are calculated at the electroweak scale where the logarithms are small and the

perturbative expansion is valid. Then they are "run down" to the low-energy scale by using the solution of the RGE. The solution to (2.15) is given by

$$\vec{C}(\mu) = T_{\alpha_s} \exp \int_{\alpha_s(\mu_0)}^{\alpha_s(\mu)} d\alpha_s \, \frac{\gamma^T(\alpha_s)}{\beta(\alpha_s)} \, \vec{C}(\mu_0), \tag{2.16}$$

where the exponential of a matrix is defined by its Taylor expansion and the ordering symbol T_{α_s} sorts the matrices in order of increasing values of the parameter α_s with larger values standing to the left. The QCD β-function is defined as $\beta(\alpha_s) = \frac{d\alpha_s}{d\ln\mu}$. For the case of $\bar{B} \to X_s\gamma$ the matching scale μ_0 corresponds to the weak scale μ_W which is of the order of the W or t-quark mass. The Wilson coefficients are subsequently "run" down to the bottom-quark mass scale $\mu_b \sim m_b$.

2.1.4 The Operator Basis

So far the effective theory only contains the current-current operators Q_1^c and Q_2^c that arose by integrating out the W bosons from diagrams like the first one in Figure 2.2. They form a complete set under QCD renormalization, i.e., no new operators are introduced by QCD corrections. However, by integrating out all other modes above the electroweak scale additional effective operators arise that are relevant for the $\bar{B} \to X_s\gamma$ decay. In fact, it will be established in Section 2.2 that $Q_{1,2}$ do not even give rise to a LO matrix element. Still, due to RG running their contribution is very relevant (see Section 2.1.5). In the full effective Lagrangian there appear six more operators. First there are the dimension-6 *QCD penguin operators* that originate from the second diagram in Figure 2.2. The external

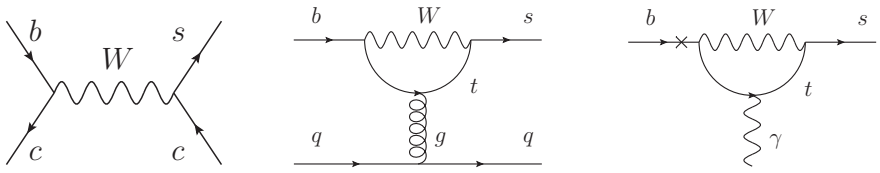

Figure 2.2: SM diagrams relevant for the $\bar{B} \to X_s\gamma$ decay. The diagrams give rise to current-current, penguin and electromagnetic dipole operators, respectively.

current coupling to the gluon can be decomposed into a $V-A$ and a $V+A$ structure. The short-hand notation $V-A$ represents a current with vector minus axial vector structure $\bar{q}\gamma^\mu(1-\gamma_5)q$ while $V+A$ correspondingly represents $\bar{q}\gamma^\mu(1+\gamma_5)q$. Furthermore the current can contain quarks of any flavor lighter than the electroweak scale ($q = u, d, c, s, b$). When QCD corrections are included also different color structures are possible. In total, there are four QCD penguin operators. More operators are introduced by the last diagram in Figure 2.2. It contains the insertion of a mass operator into the b-quark line, which gives rise to a chirality changing dimension 5 operator. This diagram goes by the name of *electromagnetic dipole* or electromagnetic penguin operator. Finally, there is also a

chromomagnetic dipole operator where the photon in the last diagram is replaced by a gluon. A complete set of linearly independent operators that again closes under QCD renormalization is given by [35]

$$\begin{aligned}
Q_1^q &= (\bar{q}b)_{V-A}\,(\bar{s}q)_{V-A}\,, & Q_2^q &= (\bar{q}_i b_j)_{V-A}\,(\bar{s}_j q_i)_{V-A}\,,\\
Q_3 &= (\bar{s}b)_{V-A}\sum\nolimits_q (\bar{q}q)_{V-A}\,, & Q_4 &= (\bar{s}_i b_j)_{V-A}\sum\nolimits_q (\bar{q}_j q_i)_{V-A}\,,\\
Q_5 &= (\bar{s}b)_{V-A}\sum\nolimits_q (\bar{q}q)_{V+A}\,, & Q_6 &= (\bar{s}_i b_j)_{V-A}\sum\nolimits_q (\bar{q}_j q_i)_{V+A}\,,\\
Q_{7\gamma} &= \frac{-em_b}{8\pi^2}\,\bar{s}\sigma_{\mu\nu}(1+\gamma_5)F^{\mu\nu}b\,, & Q_{8g} &= \frac{-gm_b}{8\pi^2}\,\bar{s}\sigma_{\mu\nu}(1+\gamma_5)G^{\mu\nu}b\,,
\end{aligned} \tag{2.17}$$

where the sums run over all quark flavors lighter than the electroweak scale. The complete effective Lagrangian, necessary to describe the decay $b \to s\gamma$ at leading order in $1/M_W^2$ is given by

$$\mathcal{L}_{\text{eff}} = \mathcal{L}_{\text{quark}} - \frac{G_F}{\sqrt{2}}\sum_{q=u,c}\lambda_q\left(C_1\,Q_1^q + C_2\,Q_2^q + \sum_{i=3,\ldots,6} C_i\,Q_i + C_{7\gamma}\,Q_{7\gamma} + C_{8g}\,Q_{8g}\right) + \text{h.c.}\,, \tag{2.18}$$

where $\lambda_q = V_{qb}V_{qs}^*$ and the Wilson coefficients C_i depend on the scale μ at which the operators are renormalized. The unitarity of the CKM matrix $\lambda_u + \lambda_c + \lambda_t = 0$ has been used to rewrite the coefficients of the penguin operators. Under QED renormalization additional operators can mix with the operator basis given above, but due to the smallness of the electromagnetic coupling α these effects turn out to be subleading and will be ignored here. It is an advantage of the effective theory approach, that radiative FCNC decays can be expressed in terms of matrix elements of the operators in (2.17) with Wilson coefficients that are independent of the process. New physics can enter the calculation either through the introduction of new operators and/or through additional contributions to the Wilson coefficients of the operators in (2.17).

2.1.5 The Wilson Coefficients at the Correct Scale

The effective Lagrangian derived in the previous section can now be used to calculate the $b \to s\gamma$ decay rate. In order to do so one writes down all contributing diagrams up to $\mathcal{O}(G_F)$, i.e., with one insertion of an effective operator and including QCD to the desired order. Since the effective couplings in form of the Wilson coefficients are themselves calculated by a perturbative expansion in α_s it is necessary to introduce a systematic way to define the order of the calculation. In the so called *leading logarithmic* (LL) approximation the Wilson coefficients are determined by a matching at $\mathcal{O}(\alpha_s^0)$ followed by running using the $\mathcal{O}(\alpha_s^1)$ correction to the anomalous dimension matrix. This running is necessary to resum large logarithms of the ratio of the large matching scale and the much lower scale of the b decay. The LL approximation resums logarithms of the form $(\alpha_s \ln \frac{\mu_W}{\mu_b})^n$. The large scale μ_W can be equal to the mass of any of the integrated out particles while the low-energy scale μ_b is the scale of the process at hand. To complete the leading-order calculation the matrix elements must be calculated at the low-energy scale $\mu_b \sim m_b$. In general these

matrix elements are non-perturbative quantities, but to a first approximation (that will be justified later on in Chapter 3) it is possible to perform their calculation in a perturbative expansion in powers of α_s. For a leading-order calculation only tree-level matrix elements need to be considered. All the necessary steps (matching, running, and calculation of the matrix elements) have been performed first in [36]. However, there is one subtlety related to the determination of the anomalous dimension matrix at $\mathcal{O}(\alpha_s)$. Determining the 6×6 sub-matrix that induces the mixing between the four-quark operators $Q_{1\ldots6}$ requires the calculation of the UV divergent part of the one-loop diagrams in the effective theory (e.g., the first diagram in Figure 2.3). The same is true for the mixing in the dipole sector. For

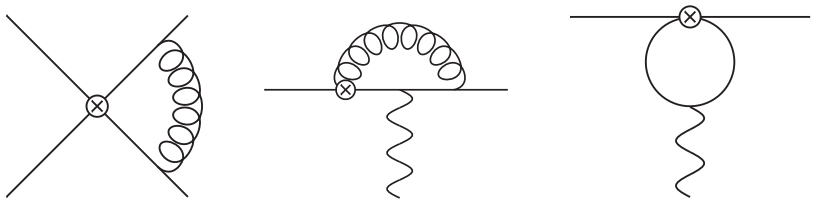

Figure 2.3: Diagrams relevant for the calculation of the LO anomalous dimension. Effective operators are now denoted by one crossed circle. The last diagram actually vanishes in certain renormalization schemes (see text).

example the second diagram in Figure 2.3 is responsible for the mixing of Q_{8g} into $Q_{7\gamma}$. Finally the mixing of the four-quark operators $Q_{1\ldots6}$ into the dipole operators $Q_{7\gamma,8g}$ is mediated by the third diagram of Figure 2.3. It is an interesting feature of the operator set (2.17) that these diagrams yield a renormalization scheme dependent result [37]. Indeed, this dependence cancels between the first order anomalous dimension and the one-loop matrix elements. It is convenient to introduce renormalization scheme invariant Wilson coefficients C_i^{eff} through [38]

$$C_{7\gamma}^{\text{eff}} = C_{7\gamma} + \sum_{i=1}^{6} y_i C_i \,, \qquad C_{8g}^{\text{eff}} = C_{8g} + \sum_{i=1}^{6} z_i C_i \,, \tag{2.19}$$

where y_i, z_i depend on the scheme. In the 't Hooft-Veltman scheme all y_i and z_i are zero, while in the naive dimensional regularization scheme $y_5 = -1/3$, $y_6 = -1$, and $z_5 = 1$, and all other y_i and z_i vanish. Since the diagram vanishes in any four-dimensional renormalization scheme it is necessary to perform a two-loop calculation to obtain the complete leading-order contribution to the anomalous dimension. The complete calculation has first been performed in [37] and afterwards confirmed in [39]. In the LL approximation

the Wilson coefficients at the scale μ can be written as [40]

$$\begin{aligned}
C_i(\mu) &= \sum_{j=1}^{8} k_{ij}\eta^{a_j} \qquad (\text{i}=1\ldots 6),\\
C_{7\gamma}^{\text{eff}}(\mu) &= \eta^{\frac{16}{23}} C_{7\gamma}(M_W) + \frac{8}{3}\left(\eta^{\frac{14}{23}} - \eta^{\frac{16}{23}}\right) C_{8g}(M_W) + C_1(M_W)\sum_{i=1}^{8} h_i \eta^{a_i}, \qquad (2.20)\\
C_{8g}^{\text{eff}}(\mu) &= \eta^{\frac{14}{23}} C_{8g}(M_W) + C_1(M_W)\sum_{i=1}^{8} \bar{h}_i \eta^{a_i},
\end{aligned}$$

where

$$\begin{aligned}
C_1(M_W) &= 1,\\
C_{7\gamma}(M_W) &= \frac{3x_t^3 - 2x_t^2}{4(x_t-1)^4}\ln x_t + \frac{-8x_t^3 - 5x_t^2 + 7x_t}{24(x_t-1)^3}, \qquad (2.21)\\
C_{8g}(M_W) &= \frac{-3x_t^2}{4(x_t-1)^4}\ln x_t + \frac{-x_t^3 + 5x_t^2 + 2x_t}{8(x_t-1)^3},
\end{aligned}$$

with $x_t = m_t^2/M_W^2$ and $\eta = \alpha_s(M_W)/\alpha_s(\mu)$. The calculable parameters a_i, h_i, $\bar{h}_i$, and k_{ij} are given in Table XXVII of reference [40] (with reversed names of C_1 and C_2). A numerical study of these Wilson coefficients at a scale $\mu \sim m_b$ demonstrates that $C_{7\gamma}^{\text{eff}}$ is strongly enhanced by the QCD corrections associated with the operator Q_1^q [41]. This enhancement is also responsible for a strong μ_b dependence of the Wilson coefficients, that is not compensated in the leading-order calculation [42]. Since the exact value of the scale is arbitrary, the μ_b dependence gives rise to an uncertainty of the calculated quantities. Varying the scale in the range $m_b/2 < \mu_b < 2m_b$ yields a change of the branching fraction by $\pm 22\,\%$ [44]. As has been shown in [38], this dependence can be significantly reduced by performing an NLO calculation using the next-to-leading logarithmic (NLL) approximation.

The NLL program requires the calculation of the Wilson coefficients through a matching at $\mathcal{O}(\alpha_s^1)$, while the anomalous dimension matrix is needed up to $\mathcal{O}(\alpha_s^2)$. This corresponds to the calculation of two-loop diagrams for the mixing between the four-quark operators and for the mixing between the dipole operators. The mixing between the two sectors even requires calculations at three-loop order. By using the NLL approximation logarithms of the form $\alpha_s(\alpha_s \ln \frac{\mu_W}{\mu_b})^n$ are resummed in addition to the leading order resummation. The NLO matching of the four-quark operators was already performed in [45–47] while the dipole operators were matched in [48, 49]. References [46, 47] also contained the complete two-loop anomalous dimension matrix of the four-quark sector. The mixing between the dipole operators was calculated in [50] and the mixing between four-quark and dipole operators in [43]. Finally, the operator matrix elements must be considered at NLO [51] which will be the topic of the next section. As expected, the complete NLL program reduces the dependence of the branching fraction on scale variations notably [43]. Apart

from the dependence on the low-energy scale μ_b there are also uncertainties due to the matching scale μ_W [44] as well as the renormalization scale of the quark masses. While the former scale dependence is already reduced by the NLO calculation, the uncertainty due to charm-quark mass scale μ_c is only introduced at that order. This is explained by the already mentioned fact, that matrix elements containing long-distance charm-quark loops (see the last diagram in Figure 2.3) vanish at the leading order. As has been shown in [52], replacing the pole charm-quark mass by the $\overline{\text{MS}}$ mass at the scale μ_b can enhance the prediction for the branching fraction by $\mathcal{O}(10\,\%)$. It is therefore necessary to consider the NNLO corrections, in order to reduce the dependence on the charm-quark mass scale.

The NNLO calculation (using the NNLL approximation) was performed over the course of many years by a joint effort of several groups. The matching procedure required the calculation of two-loop diagrams for the case of $C_{1\ldots6}$ [53] and three-loop diagrams for $C_{7\gamma,8g}$ [54]. For the mixing between the four-quark [55] and between the dipole [56] operators three-loop calculations are necessary, while the mixing between four-quark and dipole operators even demanded for a four-loop calculation [57]. Running the NNLO Wilson coefficients down by using the solution to the RGE in NNLL approximation additionally resums logarithms of the form $\alpha_s^2(\alpha_s \ln \frac{\mu_W}{\mu_b})^n$. In order to reduce the scale dependence through the charm-quark mass the calculation of three-loop matrix elements containing a charm-quark loop must be performed. So far this has only been done in the so-called large-β_0 approximation [58]. Although this approximation does not reduce the scale dependence on μ_c by itself, it serves as a starting point for an interpolation of the charm-quark mass to physical values [59]. All the above results, together with the $\mathcal{O}(\alpha_s^2)$ matrix elements for $O_{7\gamma}$ [58, 60–62] were merged in [5] to produce the current final word on the perturbative NNLO calculation of the $\bar{B} \to X_s\gamma$ branching fraction for a sufficiently low cut on the photon energy. It was demonstrated that going beyond the NLO did indeed significantly reduce the scale dependencies (see Figure 2.4). The left plot in Figure 2.4 illustrates how

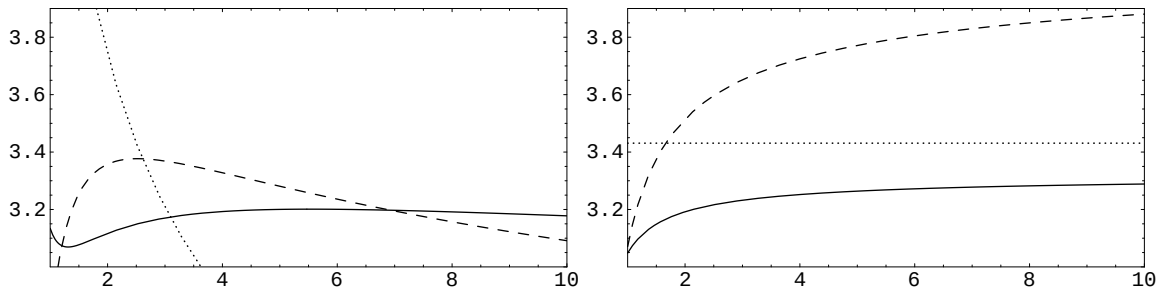

Figure 2.4: Branching fraction ($\cdot 10^{-4}$) plotted versus the variation of the low-energy scale μ_b (left plot) and versus the charm-quark mass scale μ_c (right plot). Dotted, dashed, and solid lines represent LO, NLO, and NNLO respectively. Plots taken from [5].

the variations of the branching fraction due to variations of the low-energy scale μ_b decrease when going to higher orders in α_s. The uncertainty due to the μ_c variations on the other hand is only introduced at NLO and decreases at the NNLO (right plot). In [5] the total uncertainty of the branching fraction due to scale variations was estimated to be 3 % by

varying the scales in a range between one half and two times their central value.

This concludes the discussion of the effective Lagrangian required for the description of low-energy weak decays: In addition to the usual QCD and QED Lagrangian for the quark sector it contains the effective local operators $Q_{1\ldots8g}$. Their coefficients are calculated from the full theory to a certain order in α_s. In oder to resum large logarithms they are subsequently run down to the low-energy scale of the process by solving the RGE. Today, these Wilson coefficients are known at NNLO through a matching at $\mathcal{O}(\alpha_s^2)$ and a running in the NNLL approximation. However, up-to-date calculations of the $\bar{B} \to X_s\gamma$ branching fraction [5] only make use of the NNLO result for $C_{7\gamma}^{\text{eff}}$, while using the NLO result for $C_{1\ldots6,8g}$. For a matching scale of $\mu_W = 160\,\text{GeV}$ and a low-energy scale of $\mu_b = 2.5\,\text{GeV}$ the coefficients are explicitly given in Table 2.1. It can be seen that the current-current

C_1	C_2	C_3	C_4	C_5	C_6	$C_{7\gamma}^{\text{eff}}$	C_{8g}^{eff}
1.123	-0.272	0.020	-0.048	0.010	-0.060	-0.326	-0.184

Table 2.1: Wilson coefficients at the scale $\mu = \mu_b = 2.5\,\text{GeV}$ at NLO (for $C_{1\ldots6,8g}$) and NNLO (for $C_{7\gamma}^{\text{eff}}$).

operators, together with the dipole operators are dominant. The next important step will be the calculation of the $\bar{B} \to X_s\gamma$ decay rate in the framework of the weak effective theory. This will be the topic of the next section.

2.2 The Differential Decay Rate

With the derivation of the weak effective Lagrangian complete, the differential decay rate can now be calculated by the usual methods of quantum field theory. This section discusses these methods and gives the LO and NLO order results in the parton model.

In the rest frame, the decay rate of an initial particle i into a final state f can in general be written as [29]

$$\Gamma(i \to f) = \frac{1}{2M_i}\frac{1}{Vt}\int \frac{d^3p_f}{(2\pi)^2}\frac{1}{2E_f}\,|\langle f|iT|i\rangle|^2, \tag{2.22}$$

where $\langle f|$ represents all final state particles and the phase space integral is taken over all final state momenta. Since the initial state is assumed to have a definite momentum a discrete normalization including the factor $1/V$ must be used. This factor cancels after using "Fermi's Trick" for the square of the momentum conservation δ-function. The transition matrix T contains the dynamics of the scattering process.

When considering radiative B decays, the initial state is a pseudoscalar B meson. The calculations are performed for the case of a neutral $\bar{B}^0$ with a bottom quantum number of -1 that is composed of a b and $\bar{d}$ quark. To a first approximation the light quark $\bar{d}$ does not influence the decay of the heavy b-quark, which corresponds to the assumption of the spectator model. In this case, the decay rate for the charged $B^- \sim b\bar{u}$ meson is

identical to the neutral one. Deviations from this equality will be explicitly mentioned when applicable.

The final state consists of a hadronic part with a net strangeness of -1 and a photon. Due to confinement, the final-state quarks are bound into hadrons. In general, it is not possible to calculate the hadronic matrix element $\langle X_s^{\text{hadr}}\gamma|iT|\bar{B}^0\rangle$ from first principles. The problem is associated with the QCD coupling constant α_s, that becomes large for energy scales at the typical hadronic binding energy, thereby invalidating the perturbative expansion. However, the situation is simplified by considering the inclusive decay rate. This corresponds to the sum over all final states f with strangeness -1 and containing a photon. It will be shown in Section 3.1 that the sum over hadronic matrix elements is then equal to the sum over free quark matrix elements up to corrections proportional to the inverse heavy-quark mass. This equality requires the assumption of *quark-hadron duality*. In the free quark approximation the inclusive decay rate can be written as

$$\Gamma(\bar{B}\to X_s\gamma)=\frac{1}{2m_b}\frac{1}{Vt}\sum_{X_s^{\text{part}}}\int\frac{d^3p_f}{(2\pi)^2}\frac{1}{2E_f}|\langle X_s^{\text{part}}\gamma|i\mathbf{T}\exp\left(i\int d^4x\,\mathcal{L}_{\text{eff}}\right)|b\rangle|^2+\mathcal{O}\left(\frac{1}{m_b}\right), \tag{2.23}$$

where $\mathbf{T}$ is the time ordering symbol from the definition of the transition matrix $T=\mathbf{T}\exp i\int d^4x\,\mathcal{L}$ and the phase space integration is taken over all final state particle momenta. At leading order in α_s there is only one strange-quark (and the photon) in the final state and the transition is only mediated by the operator $Q_{7\gamma}$. The effect of the four-quark operators $Q_{1\ldots6}$ is already included by using the effective Wilson coefficient $C_{7\gamma}^{\text{eff}}$ introduced in (2.19). Thus, it is only necessary to calculate the first diagram in Figure 2.5 that represents the tree-level matrix element $\langle s\gamma|Q_{7\gamma}|b\rangle$. This calculation can be performed by

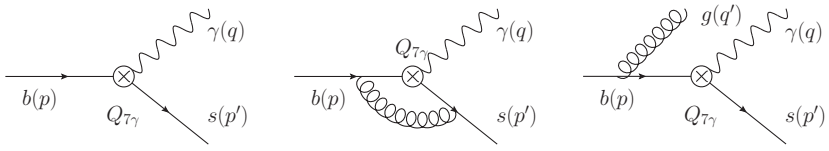

Figure 2.5: Diagrams containing the operator $Q_{7\gamma}$ contributing at LO (first diagram) and NLO (second and third diagram).

using Feynman rules to calculate the invariant matrix element $\mathcal{M}$ related to the transition matrix through $\langle p_f|iT|p_i\rangle=(2\pi)^{(4)}\delta^4(p_i-\sum p_f)i\mathcal{M}_{fi}$. For a vanishing strange-quark mass this diagram is evaluated to

$$i\mathcal{M}_7^{\text{LO}}=\frac{iG_F}{\sqrt{2}}\,C_{7\gamma}^{\text{eff}}(\mu)\lambda_t\,\frac{em_b}{4\pi^2}\,\bar{u}_s(p')\not{q}\not{\varepsilon}^*(1+\gamma_5)u_b(p), \tag{2.24}$$

where u_b and u_s are the quark spinors and the momenta are defined in Figure 2.5. Inserting this result into (2.23) yields the differential decay rate in the free quark approximation at leading order in α_s

$$d\Gamma_{\text{free}}^{\text{LO}}(\bar{B}\to X_s\gamma)=\frac{G_F^2m_b^2\alpha}{2\pi^4}\,|C_7^{\text{eff}}(\mu)\lambda_t|^2E_\gamma^3\,dE_\gamma\,\delta(m_b-2E_\gamma), \tag{2.25}$$

with the photon energy E_γ and the electromagnetic coupling constant $\alpha = e^2/(4\pi)$. As one can see, the LO calculation yields only a δ-function contribution to the photon spectrum located at the photon energy $m_b/2$. Of course, this is to be expected from a simple two-body decay. There are two types of corrections to the form of the spectrum. First, there is a smearing of the peak originating from the fact, that the b-quark is not free but bound into a hadron. This will be the topic of Chapter 3. Second, QCD corrections from gluon bremsstrahlung diagrams introduce a non-trivial photon spectrum, as $b \to s\gamma g$ constitutes a three-body decay. This case will be considered now. To conclude the LO calculation, the total LO decay rate is obtained by integrating over the photon energy which results in

$$\Gamma^{\mathrm{LO}}_{\mathrm{free}}(\bar{B} \to X_s\gamma) = \frac{G_F^2 m_b^5 \alpha}{32\pi^4} \left|C^{\mathrm{eff}}_{7\gamma}(\mu)\lambda_t\right|^2. \tag{2.26}$$

Since the Wilson coefficients are real in the SM, it is not necessary to take their absolute value squared in the above equation. However, the Wilson coefficients will always be assumed to be complex in this work. This simplifies the generalization of the analysis to new-physics models.

2.2.1 Next-to-Leading Order Matrix Elements

The NLO corrections to the decay rate fall into two categories. On the one hand there are the virtual corrections (e.g., the second diagram in Figure 2.5) that contain one additional gluon loop. On the other hand the bremsstrahlung corrections (e.g., the last diagram in Figure 2.5) introduce an additional, non-observable gluon into the final state. At NLO also operators other than $Q_{7\gamma}$ contribute to the decay rate (for examples the diagrams in Figure 2.6). As can be seen from Table 2.1 the Wilson coefficients of the QCD penguin

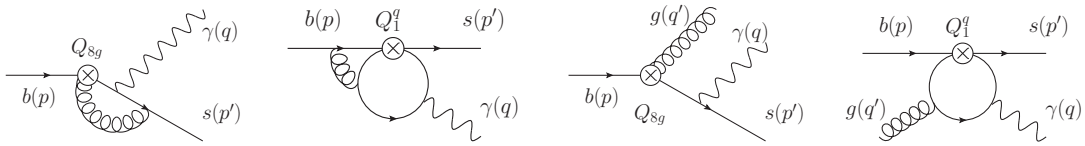

Figure 2.6: Matrix elements containing the operators Q_1^q and Q_{8g}. The first two diagrams depict virtual, the last two bremsstrahlung contributions.

operators $Q_{3\ldots6}$ are numerically small, the corresponding diagrams will therefore be ignored. The diagrams associated with the current-current operator Q_2 vanish as they contain a factor involving the trace of the color matrices T^a, which is zero. This leaves the matrix elements of the operators Q_1^q, $Q_{7\gamma}$ and Q_{8g} to be calculated. In order to determine the NLO differential decay rate the contributions of the processes $b \to s\gamma$ and $b \to s\gamma g$ must be added:

$$\frac{d\Gamma^{\mathrm{NLO}}}{dE_\gamma} = \frac{d\Gamma^{\mathrm{virt}}}{dE_\gamma} + \frac{d\Gamma^{\mathrm{brems}}}{dE_\gamma}. \tag{2.27}$$

The virtual part is determined by squaring the sum of all relevant $b \to s\gamma$ matrix elements up to $\mathcal{O}(\alpha_s)$. This gives rise to interference terms containing different operators. The

interference will always contain one LO ($\mathcal{O}(\alpha_s^0)$) matrix element of $Q_{7\gamma}$ together with an NLO ($\mathcal{O}(\alpha_s^1)$) matrix element of Q_1^q, $Q_{7\gamma}$ or Q_{8g}. Just like the LO, the virtual NLO diagrams describe a three-body process and therefore their contribution to the spectrum is given by a δ-function. As will be shown below the virtual photon corrections to $b \to sg$ are relevant as well.

The NLO bremsstrahlung contributions in $d\Gamma^{\text{brems}}/dE_\gamma$ are due to interferences of all $b \to s\gamma g$ diagrams, which leads to an α_s suppression of the squared matrix elements. These diagrams are responsible for the form of the photon spectrum and were first calculated in [63]. When the contribution of the interference between the matrix elements of the operators Q_i and Q_j to the decay rate of $b \to s\gamma g$ is denoted as $\Gamma_{ij}^{\text{brems}}$ the result can be written as [64, 65]

$$\frac{d\Gamma^{\text{brems}}}{dE_\gamma} = \frac{d\Gamma_{77}^{\text{brems}}}{dE_\gamma} + \frac{d\Gamma_{88}^{\text{brems}}}{dE_\gamma} + \frac{d\Gamma_{11}^{\text{brems}}}{dE_\gamma} + \frac{d\Gamma_{17}^{\text{brems}}}{dE_\gamma} + \frac{d\Gamma_{18}^{\text{brems}}}{dE_\gamma} + \frac{d\Gamma_{78}^{\text{brems}}}{dE_\gamma}, \tag{2.28}$$

where all terms except the first two are completely finite and given by (for $m_s = 0$)

$$\begin{aligned}
\frac{d\Gamma_{11}^{\text{brems}}}{dE_\gamma} &= \frac{G_F^2|\lambda_t|^2\alpha m_b^5}{32\pi^4}\,\frac{C_F\alpha_s}{4\pi}\,\frac{1}{m_b}\,|C_1|^2\,2e_u^2\int_0^{\frac{2E_\gamma}{m_b}} dx\,(1-x)\left|1-F\left(\frac{z}{x}\right)\right|^2,\\
\frac{d\Gamma_{17}^{\text{brems}}}{dE_\gamma} &= \frac{G_F^2|\lambda_t|^2\alpha m_b^5}{32\pi^4}\,\frac{C_F\alpha_s}{4\pi}\,\frac{1}{m_b}\,\text{Re}\,(C_1C_{7\gamma}^{\text{eff}*})(-4)e_u\int_0^{\frac{2E_\gamma}{m_b}} dx\,x\,\text{Re}\,\left(1-F\left(\frac{z}{x}\right)\right),\\
\frac{d\Gamma_{18}^{\text{brems}}}{dE_\gamma} &= e_d\,\frac{\text{Re}\,(C_1C_{8g}^{\text{eff}*})}{\text{Re}\,(C_1C_{7\gamma}^{\text{eff}*})}\,\frac{d\Gamma_{17}^{\text{brems}}}{dE_\gamma},\\
\frac{d\Gamma_{78}^{\text{brems}}}{dE_\gamma} &= \frac{G_F^2|\lambda_t|^2\alpha m_b^5}{32\pi^4}\,\frac{C_F\alpha_s}{4\pi}\,\frac{1}{m_b}\,\text{Re}\,(C_{7\gamma}^{\text{eff}*}C_{8g}^{\text{eff}})(-4)e_d\\
&\quad\times\left[4+\left(\frac{2E_\gamma}{m_b}\right)^2+8\frac{m_b}{2E_\gamma}\left(1-\frac{2E_\gamma}{m_b}\right)\ln\left(1-\frac{2E_\gamma}{m_b}\right)\right].
\end{aligned} \tag{2.29}$$

Here $C_F = 4/3$ is the Casimir operator of the fundamental representation of the $SU(3)_c$, e_u and e_d are the charges of up- and down-type quarks in units of e, $z = m_c^2/m_b^2$ and everything about the *penguin function* $F(x)$ is collected in Appendix A.1. Furthermore, the scale dependence of the Wilson coefficients and the QCD coupling α_s has been dropped for brevity and the results were CP-averaged[2]

$$\Gamma = \frac{1}{2}\left(\Gamma + \Gamma^{\text{CP}}\right). \tag{2.30}$$

The contribution to the spectrum due to the interference of two matrix elements of $Q_{7\gamma}$ diverges for $E_\gamma \to m_b/2$. This limit corresponds the emission of a soft bremsstrahlung gluon which gives rise to an IR singularity in the fully integrated decay rate. Fortunately, gauge invariance requires that this singularity cancels when the virtual $\mathcal{O}(\alpha_s)$ corrections

[2]Unless explicitly noted $\bar{B} \to X_s\gamma$ will therefore include $B \to X_{\bar{s}}\gamma$ as well.

are added. Since the divergence is introduced by a phase-space integral this cancellation takes place at the level of decay rates. In order to determine the differential decay rate one has to first integrate the virtual and bremsstrahlung contributions, add them up and subsequently differentiate the result with respect to the limits of integration [51]

$$\begin{aligned}\Gamma(E_0) &= \int_{E_0}^{\frac{m_b}{2}} dE_\gamma \left(\frac{d\Gamma^{\text{brems}}}{dE_\gamma} + \frac{d\Gamma^{\text{virt}}}{dE_\gamma}\right), \\ \frac{d\Gamma(E_\gamma)}{dE_\gamma} &= -\frac{d\Gamma(E_0)}{dE_0}\Big|_{E_0=E_\gamma}.\end{aligned} \tag{2.31}$$

An alternative way is to subtract the divergence in the distribution sense by the introduction of the *plus distribution*. It is defined as

$$\int_0^1 dx \left[\frac{1}{1-x}\right]_+ f(x) = \int_0^1 dx \, \frac{f(x)-f(1)}{1-x}, \tag{2.32}$$

where $f(x)$ is a smooth test function. The spectrum is then given just by the bremsstrahlung contribution with the divergent terms replaced by plus distributions that already include the cancellation of the divergence due to the virtual contribution. Finally, since the virtual contributions are proportional to a δ-distribution they add a constant term to the integrated rate. For $m_s = 0$ the NLO contribution to the differential rate due to the the self interference of the operator $Q_{7\gamma}$ (virtual + bremsstrahlung) is given by

$$\begin{aligned}\frac{d\Gamma_{77}^{\text{NLO}}}{dx} &= \frac{G_F^2 |\lambda_t|^2 \alpha m_b^5}{32\pi^4} \frac{C_F \alpha_s}{4\pi} |C_{7\gamma}^{\text{eff}}|^2 \\ &\times \Bigg[-\left(5 + \frac{4\pi^2}{3} + 2\ln\frac{\mu^2}{m_b^2}\right)\delta(1-x) - 4\left[\frac{\ln(1-x)}{1-x}\right]_+ - 7\left[\frac{1}{1-x}\right]_+ \\ &\quad - \frac{x+1}{2}\ln(1-x) + 7 + x - 2x^2\Bigg],\end{aligned} \tag{2.33}$$

with the shorthand notation $x = 2E_\gamma/m_b$. The μ dependence in the term proportional to the δ-function is of ultraviolet (UV) origin and was introduced by the inclusion of the field-strength renormalization in the LO contribution of $Q_{7\gamma}$. The logarithm $\ln(1-x)$ on the other hand is of IR origin and becomes large (but still integrable) for $x \to 1$. There is one more comment in order, concerning the m_b^5 factor in the above expression. Two of the m_b's originate from the normalization of $Q_{7\gamma}$ and should therefore be taken in the same renormalization scheme as the Wilson coefficients [38], while the other three come from on-shell external lines and therefore correspond to pole masses. For that reason the replacement

$$m_b^5 \to m_{b,\,\text{pole}}^3 \overline{m_b}(\mu)^2, \tag{2.34}$$

is implicitly assumed in (2.33). The final contribution to the NLO spectrum is due to the interference of the operator matrix element of Q_{8g} with itself. As in the case of $\Gamma_{77}^{\text{brems}}$ the

differential decay rate $d\Gamma_{88}^{\text{brems}}/dx$ diverges, now for $E_\gamma \to 0$. This IR divergence cancels when adding the virtual photon corrections to the process $b \to sg$. This can once again be considered by introducing plus distributions, but since the photon spectrum in the region of low photon energies is of no interest here, this prescription can be immediately dropped. This leads to [64]

$$\begin{aligned}\frac{d\Gamma_{88}^{\text{brems}}}{dx} &= \frac{G_F^2|\lambda_t|^2\alpha m_b^5}{32\pi^4}\,\frac{C_F\alpha_s}{4\pi}\,|C_{8g}^{\text{eff}}|^2\,e_d^2 \\ &\quad\times\left[(4\ln(1-x)-8-4\ln r)\,\frac{1}{x}+2(x-2)\ln(1-x)+8-x-2x^2+4(x-2)\ln r\right],\end{aligned} \tag{2.35}$$

where only the leading terms in the strange-quark mass in $r = m_s^2/m_b^2$ has been kept. This time it can not be set to zero since this would introduce another divergence. Note, that the appearance of the low-energy scale m_s in the above result is a genuine parton-model effect, since QCD is non-perturbative at such scales. Finally, the b-quark masses in the prefactor are assumed to have the same form as in (2.34).

This completes the discussion of the bremsstrahlung contribution to the differential rate at NLO. In order to calculate the integrated decay rate the remaining virtual contributions must be added and the integral over the photon energy has to be performed. The virtual contributions relevant for divergence cancellation were already calculated in [63], the remaining ones in [51].

2.3 The Integrated Decay Rate

Apart from the photon spectrum given by the differential decay rate, also the integrated decay rate is of phenomenological interest. Its calculation with a lower cutoff on the photon energy will be discussed in this section.

As was demonstrated in Chapter 1 the inclusive decay rate of $\bar{B} \to X_s\gamma$ is experimentally only accessible for large photon energies. The branching fraction is therefore calculated by integrating the differential decay rate only over the endpoint region

$$E_\gamma \in \left[(1-\delta)\frac{m_b}{2}, \frac{m_b}{2}\right] \quad \text{with} \quad \delta \sim \frac{\Lambda_{\text{QCD}}}{m_b}. \tag{2.36}$$

Here E_γ is defined in the b-quark rest frame. Performing this integration over the $Q_{7\gamma}$ self interference in (2.25) and (2.33) up to NLO yields ($m_s = 0$)

$$\begin{aligned}\Gamma_{77}(\delta) = \frac{G_F^2|\lambda_t|^2\alpha m_b^5}{32\pi^4}|C_{7\gamma}^{\text{eff}}|^2\Bigg[1+\frac{C_F\alpha_s}{4\pi}\Big(&-2\ln^2\delta-7\ln\delta+\delta(\delta-4)\ln\delta+10\delta+\delta^2-\frac{2\delta^3}{3} \\ &-5-\frac{4\pi^2}{3}-2\ln\frac{\mu^2}{m_b^2}\Big)\Bigg],\end{aligned} \tag{2.37}$$

with the first term in the round brackets being a Sudakov double logarithm. This result makes a possible problem of partonic calculations in the endpoint region transparent. For small values of δ the logarithms become large and potentially need to be resummed to make the perturbative expansion meaningful. For $\delta \sim \Lambda_{\rm QCD}/m_b$ the logarithm will enhance the NLO correction by a factor of ~ 2.3. As will be motivated in Section 5.2.5 the appropriate scale for α_s is $\mu \sim \sqrt{\Lambda_{\rm QCD} m_b} \sim 1.5\,\text{GeV}$ which leads to $\alpha_s \sim 0.375$. Overall the NLO corrections will therefore not be significantly suppressed, motivating a resummation of the logarithms. Just like in the weak effective theory introduced in Section 2.1, the resummation can be performed by matching onto an appropriate effective theory and solving the RG equations. This effective theory is the *soft collinear effective theory* (SCET) which will be introduced in Chapter 4.

Without resorting to SCET the photon cutoff must be chosen sufficiently low to ensure the applicability of the perturbative expansion. As was discussed in Section 1.3, this requires the extrapolation of the experimental prediction, introducing new systematic uncertainties. As a compromise a photon cutoff of $E_0 = 1.6\,\text{GeV}$ is used in the literature. This corresponds to $\delta = (m_b - 2E_0)/m_b \approx 0.3$ and a logarithmic enhancement of the NLO by ~ 1.2. In [5] all results discussed in this chapter were combined to calculate the branching fraction of $\bar{B} \to X_s\gamma$ with an $E_0 = 1.6\,\text{GeV}$. Due to the scale dependences discussed in Section 2.1.5 a certain value for μ_b and μ_c had to be chosen. For central values of $\mu_b = 2.5\,\text{GeV}$ and $\mu_c = 1.5\,\text{GeV}$ the partial (i.e. including a cut) branching fraction is given by

$$\mathcal{B}(\bar{B} \to X_s\gamma)_{E_\gamma > 1.6\,\text{GeV}} = (3.15 \pm 0.23) \cdot 10^{-4}. \tag{2.38}$$

Apart from the error due to higher order perturbative contributions that are estimated from the scale variations, the error estimate in (2.38) also includes the uncertainty due to the m_c-interpolation as well as parametric and non-perturbative uncertainties. In order to reduce the dependence on the b-quark mass the branching fraction is defined by normalizing the result for the integrated $\bar{B} \to X_s\gamma$ decay rate to that of the semi-leptonic decay rate [66]. Finally, in [8] the effects of the photon energy cut on the partially integrated decay rate have been studied. This analysis yielded a lower theoretical prediction of

$$\mathcal{B}(\bar{B} \to X_s\gamma)_{E_\gamma > 1.6\,\text{GeV}} = (2.98 \pm 0.26) \cdot 10^{-4}. \tag{2.39}$$

2.4 Conclusions of this Chapter

The parton model calculation of the $\bar{B} \to X_s\gamma$ branching fraction discussed in this chapter required sophisticated perturbative calculations and yields an estimate that agrees with the experimental result within their error bars. During the course of the presentation two major topics were noted, whose discussion was postponed to later chapters. First, it is desirable to resum the large logarithms appearing in (2.37). This can be achieved by using SCET, which will be introduced in Chapter 4. Second, there are non-perturbative corrections to the photon spectrum as well as to the integrated decay rate. The next chapter will discuss

how these non-perturbative effects influence the calculation by employing the heavy-quark effective theory.

Chapter 3

Heavy-Quark Effective Theory

The major topic of this Chapter will be the analysis of the hadronic matrix elements that appear in the calculation of decay rates involving hadrons. Due to confinement it is not possible to calculate them in an analytic way. However, by considering an inclusive decay rate only forward scattering matrix elements between heavy-quark states are of relevance. All details and intricacies of this matter are investigated in Section 3.1. Afterwards a systematic way to deal with matrix elements between meson states that consist of one heavy quark plus light degrees of freedom is presented in Section 3.2. The heavy-quark effective theory makes use of the fact that the heavy quark only interacts softly with the light degrees of freedom and is therefore nearly on-shell. In Section 3.3 the operators relevant for the leading order of the $\bar{B} \to X_s\gamma$ decay rate are matched onto HQET and the resulting non-local matrix element expanded in terms of local operators. It turns out that this expansion contains an infinite number of leading order terms that need to be resummed into a shape function. During the course of these calculations a suitable light-cone basis as well as the HQET trace formalism are introduced.

3.1 Hadronic Matrix Elements

One of the major "approximations" adopted in the partonic calculation of the inclusive decay rate in Section 2.2 was to replace the sum over hadronic matrix elements $\langle X_s^{\text{hadr}}\gamma|iT|\bar{B}\rangle$ by a sum over free quark matrix elements $\langle X_s^{\text{part}}\gamma|iT|b\rangle$. It is not immediately clear that this is a valid approximation at all, since the hadrons in the initial and final states are in fact complex entities made out of their valence quarks, sea quarks as well as gluons, constituting a QCD bound state. The typical binding energy for B mesons is of order Λ_{QCD}, also called the confinement scale. Therefore the dynamics of this bound state can not be calculated in perturbative QCD.

However, the situation is simplified for mesons that consist of a heavy and a light quark. In this case the motion of the heavy quark is only slightly influenced by the light degrees of freedom. It is then appropriate to calculate the decay of a *free* heavy quark and account for its *Fermi motion* inside the hadron by convoluting the result with the momentum distri-

bution of the heavy quark [67]. Since the heavy quark is nearly at rest (in the rest system of the meson) the momentum distribution peaks at zero momentum, corresponding to an on-shell heavy quark. This argument motivates the free quark approximation of the preceding Chapter. A more rigorous formulation of this statement is possible in the language of HQET and will be considered now. As it will turn out, the free quark approximation is the first term in an expansion in powers of the inverse heavy-quark mass. Furthermore, the momentum distribution function will be identified with a sum over an infinite set of leading twist operators [68, 69].

So far only a method to deal with the hadronic initial state has been considered. The final state of the matrix elements does not contain mesons with a heavy quark. Instead it can be related to a partonic final state by considering the sum over all exclusive modes. Starting from Equation (2.22) the decay rate can then be written as

$$\begin{aligned}\Gamma(\bar{B}\to X_s\gamma) &= \frac{1}{2M_B}\frac{1}{Vt}\sum_{X_s^{\text{hadr}}}\int\frac{d^3p_f}{(2\pi)^2}\frac{1}{2E_f}|\langle X_s^{\text{hadr}}\gamma|iT|\bar{B}\rangle|^2\\ &= \frac{1}{2M_B}\frac{1}{Vt}\langle\bar{B}|-iT^\dagger\left[\sum_{X_s^{\text{hadr}}}\int\frac{d^3p_f}{(2\pi)^2}\frac{1}{2E_f}|X_s^{\text{hadr}}\gamma\rangle\langle X_s^{\text{hadr}}\gamma|\right]iT|\bar{B}\rangle \qquad (3.1)\\ &= \frac{1}{2M_B}\frac{1}{Vt}\langle\bar{B}|T^\dagger T|\bar{B}\rangle.\end{aligned}$$

In the last step the completeness of the set of states in the large square brackets was used. It is important to note that this set is only complete for transition matrices T that contain operators with a photon field as well as the right quantum numbers to form a strange hadron. The form of the last line of (3.1) suggests the use of the unitarity of the S-Matrix $S^\dagger S = 1$ and therefore

$$T^\dagger T = 2\text{Im}\, T \qquad (3.2)$$

to further simplify the expression for the decay rate. This leads to the optical theorem

$$\begin{aligned}\Gamma(\bar{B}\to X_s\gamma) &= \frac{1}{2M_B}\frac{1}{Vt}\,\text{Im}\,\langle\bar{B}|T|\bar{B}\rangle\\ &= \frac{1}{M_B}\,\text{Im}\,\mathcal{M}(\bar{B}\to\bar{B}) = \frac{1}{2iM_B}\,\text{Disc}\,\mathcal{M}(\bar{B}\to\bar{B})\,,\end{aligned} \qquad (3.3)$$

where $\mathcal{M}$ is the invariant matrix element defined above Equation (2.24). It has to contain at least a photon and a strange-quark propagator in order to contribute to $\bar{B}\to X_s\gamma$. Just like in Section 2.2 the leading order contribution to the transition matrix can be depicted by a diagram containing two operators $Q_{7\gamma}$ (see first diagram in Figure 3.1). When considering these diagrams it should be kept in mind that the in- and outgoing b-quark lines are in fact not contracted with the initial and final states which are still hadronic. But there are more subtleties related to the use of the optical theorem.

First of all it is important to note that the discontinuity prescription in (3.3) implies the sum of *all* possible cuts through each diagram. However, not all cuts contribute to

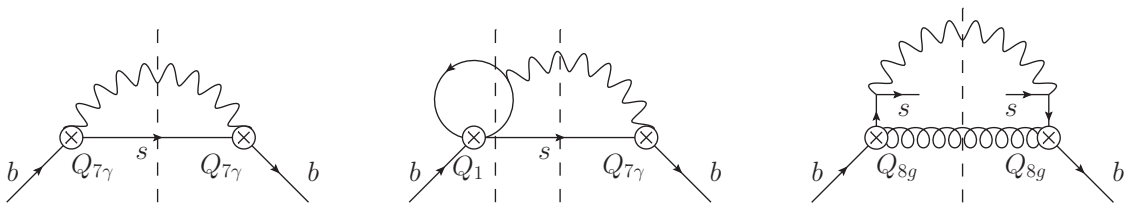

Figure 3.1: Diagrams of forwards matrix elements with cuts (depicted by dashed lines) that contribute to $\bar{B} \to X_s\gamma$.

$\bar{B} \to X_s\gamma$ as can be seen in the second diagram in Figure 3.1. Specifically, the cut related to the dashed line on the left of the diagram corresponds to a decay $b \to s\bar{c}c$. Therefore the the discontinuity must be replaced by a restricted discontinuity that only sums over cuts that contain at least a photon and a strange-quark line. In such a case the matrix element can not be represented by operator products with a single time-ordering prescription (originating from the definition of the transition matrix T). Instead the fields on the in-side (i.e., the side with the ingoing b-quark) of the cut must be time-ordered while the ones on the other side of the cut anti-time-ordered. This can be seen by going back to Equation (3.1) and noting that it contains an adjoint transition matrix $T^\dagger$ which gives rise to an anti-time-ordered operator product. Naively eliminating $T^\dagger$ by using the unitarity relation (3.2) is therefore not allowed in the case of a restricted number of final states. It is possible to systematically include the effects of not time-ordered operator products in the path integral formalism by using the Schwinger-Keldysh approach [70]. A concise recent discussion has been presented in [71]. The final result of this discussion can be summarized by the simple rule that, for diagrams with a restricted set of allowed cuts, the Feynman rules on the out-side of the cut must be complex conjugated. All this is of course not relevant for the leading order contribution due to the operator $Q_{7\gamma}$, as in that case all cuts contribute to $\bar{B} \to X_s\gamma$.

Another important subtlety linked to the use of the optical theorem is related to the appearance of soft particles in the final state. This is illustrated in the third diagram of Figure 3.1. In this example the soft s-quarks are part of the final state, yet they do not correspond to a cut propagator, since cutting an internal line puts the particles on-shell. However, soft particles interact strongly via the strong interaction which implies that they are far off-shell. In the actual calculation soft fields therefore remain uncontracted in the matrix elements.

Following the arguments presented in this section so far, it was possible to eliminate the hadronic final states from the calculation by considering the inclusive rate. The term quark-hadron duality refers to the assumption that this rate is the same for hadronic and partonic final states. Summing up, the $\bar{B} \to X_s\gamma$ decay rate can be written in the following way. For contributions with all cuts relevant to the rate the optical theorem can be used

to write

$$\begin{aligned}\Gamma(\bar{B}\to X_s\gamma) &= \frac{1}{2iM_B}\frac{1}{Vt}\,\mathrm{Disc}\langle\bar{B}|T|\bar{B}\rangle \\ &= \frac{1}{2iM_B}\frac{1}{Vt}\,\mathrm{Disc}\langle\bar{B}|\frac{i}{2}\int d^4x\,d^4y\,\mathbf{T}\{\mathcal{L}(x)\mathcal{L}(y)\}|\bar{B}\rangle \\ &= \frac{1}{2iM_B}\,\mathrm{Disc}\langle\bar{B}|\frac{i}{2}\int d^4x\,\mathbf{T}\{\mathcal{L}(x)\mathcal{L}(0)\}|\bar{B}\rangle\,,\end{aligned} \tag{3.4}$$

where translation invariance was used in the last step. Each of the Lagrangian insertions must contain one of the weak effective operators (for the leading power in $1/M_W$) presented in (2.17) or the corresponding hermitian conjugate. Of course, additional Lagrangian insertions containing QCD or QED vertices are also possible. If certain cuts do not contribute to the rate only the restricted discontinuity may be considered which shall be written as

$$\Gamma(\bar{B}\to X_s\gamma) = \frac{1}{2iM_B}\,\mathrm{Disc}_{\mathrm{restr.}}\langle\bar{B}|\frac{i}{2}\int d^4x\,\mathcal{L}^\dagger(x)\mathcal{L}(0)|\bar{B}\rangle. \tag{3.5}$$

One Lagrangian insertion appears in hermitian conjugated form, since it originated from an anti-time-ordered product of operators or, equivalently, from the adjoint transition matrix in (3.1). The two Lagrangians can only be connected by a cut propagator. Again, additional Lagrangian insertions are possible. They have to appear in time- or anti-time-ordering depending on which side of the cut they are inserted.

The above discussion relates the inclusive decay rate $\bar{B}\to X_s\gamma$ to a forward scattering matrix element between hadronic states. That means that even though one has achieved the elimination of the hadronic final states from the calculation, there is still no way to determine the decay rate from first principles. However, as was already mentioned at the beginning of this section the particular nature of the B-hadron allows for simplifications. The determination of matrix elements between B-meson states does not require the use of full QCD. Instead an effective theory implementing the fact that the heavy quark of the meson is nearly on-shell can be used, which allows for a systematic expansion in the inverse heavy-quark mass and which features additional symmetries. Using this EFT it will still not be possible to actually calculate the hadronic matrix elements, but the symmetries allow one to express the matrix elements in terms of a limited set of parameters, that are process independent and can in principle be determined from experiment. By considering certain ratios of observables it is therefore possible to reduce the effect of non-perturbative physics on a calculation. The appropriate EFT is HQET and will be introduced in the next section. As a closing remark for this chapter on hadronic matrix elements, it should be mentioned that even though a formal expansion in $1/m_b$ is always possible, it does not necessarily lead to a sum of local matrix elements. In fact, it is a major objective of this work to analyze the space-time structure of the operators in the expansion.

3.2 Heavy-Quark Effective Theory

In the previous section the inclusive decay rate was related to a QCD forward matrix element between B-meson states. Although it is not possible to find an exact solution for the meson bound state in QCD, enough is known about the physical situation inside the meson to use a simpler effective theory in place of full QCD. This theory is HQET (for a throughout review see [4]). It is constructed to be equivalent to QCD for the case of the special kinematical configuration present within the hadron: The B-meson consists of a heavy b-quark (in case of the $\bar{B}$) with a mass m_b and a cloud of light quarks, anti-quarks and gluons. These light degrees of freedom and the heavy quark form a bound state with a typical confinement scale of $\mathcal{O}(\Lambda_{\text{QCD}})$ which corresponds to the typical hadronic length scale of $\mathcal{O}(1\,\text{fm})$. The starting point for the construction of HQET is the statement that the heavy-quark mass is much larger than the confinement scale.

$$m_b \gg \Lambda_{\text{QCD}} \tag{3.6}$$

There are two immediate consequences to this statement. First, the Compton wavelength of the heavy quark is $\mathcal{O}(1/m_b \sim 0.01\,\text{fm})$ and therefore much smaller than the resolution that a probe with the energy of the light degrees of freedom can achieve. It follows that in the limit of an infinite heavy-quark mass the light partons have no information about the flavor or the spin orientation of the heavy quark. They see the heavy quark only as a static source for a color field. This gives rise to the spin-flavor symmetry of HQET which is a new symmetry and not present in full QCD but only in the considered kinematic region. As a consequence of this symmetry the decays of different mesons that contain a heavy and a light quark can be related to each other. Equation (3.6) further implies that the heavy quark within the meson interacts only with soft gluons and is therefore nearly on-shell. Its momentum can thus be written as

$$p_b^\mu = m_b v^\mu + k^\mu\,, \tag{3.7}$$

where v is the velocity of the meson and k is the *residual momentum*. Since the meson is a real particle v satisfies $v^2 = 1$ which implies that the residual momentum puts the heavy quark off-shell due to interactions with the light degrees of freedom. The b-quark being close to the mass-shell requires all components of k to be of $\mathcal{O}(\Lambda_{\text{QCD}})$.

The basic idea of HQET is to integrate out a part of the heavy-quark field that represents fluctuations around the mass shell. In order to do this one proceeds in the same way as described in Section 2.1 where the heavy gauge bosons were integrated out of the SM Lagrangian. However, since the heavy quark is still a degree of freedom of HQET it first has to be decomposed into an on- and off-shell part. After performing the path integral over the off-shell part the new non-local operators can be expanded in powers of $1/m_b$. Finally one has to determine the Wilson coefficients by matching full QCD onto the EFT.

The first step is to introduce energy projection operators $P_\pm$ that are defined by

$$P_\pm = \frac{1 \pm \not{v}}{2}\,, \tag{3.8}$$

and that satisfy the usual projection relations $P_\pm^2 = P_\pm$ and $P_+P_- = 0$. Using the operator P_+ (P_-) on an on-shell, i.e., $k = 0$ (anti-)particle spinor returns the spinor itself, while the reverse projection yields zero.

$$\begin{aligned} P_+ u_b(m_b v) &= u_b(m_b v)\,, \qquad & P_- u_b(m_b v) &= 0\,, \\ P_- v_b(m_b v) &= v_b(m_b v)\,, \qquad & P_+ v_b(m_b v) &= 0\,. \end{aligned} \tag{3.9}$$

Consequently, if the particle is slightly off-shell the projection operators decompose the particle spinor into large and small two-component spinors. In the rest frame of the meson the large projection corresponds to the upper two components of the spinor u_b. Therefore the P_+ projection of the heavy-quark spinor only annihilates a quark while the P_- projection annihilates an anti-quark.

In order to construct the HQET Lagrangian describing $\bar{B}$ decays the b-quark field is decomposed by using the relation $P_+ + P_- = 1$. Additionally the strongest x-dependence is factored out. Thus, in momentum space the heavy-quark fields only depend on the residual momentum and there is a separate field for every velocity. This is commonly indicated by a label v on the heavy-quark field, but since only heavy quarks with a single velocity play a role in this work, this label is dropped. This leads to

$$b(x) := e^{-im_b v\cdot x}\tilde{b}(x) = e^{-im_b v\cdot x}(P_+ + P_-)\tilde{b}(x) := e^{-im_b v\cdot x}[h(x) + H(x)]. \tag{3.10}$$

The small component field H which is non-zero only for off-shell quarks is going to be integrated out. After this decomposition the QCD Lagrangian for the heavy quark can be written as

$$\begin{aligned} \mathcal{L}_{\text{QCD}} &= \bar{b}(i\not{D} - m_b)b \\ &\to \bar{h}\, iv\cdot D h - \bar{H}(iv\cdot D + 2m_b)H + \bar{h}\, i\vec{\not{D}} H + \bar{H}\, i\vec{\not{D}} h\,, \end{aligned} \tag{3.11}$$

where the relations $\not{v}h = h$ and $\not{v}H = -H$ have been used and $\vec{D}^\mu$ is defined through $D^\mu = v^\mu v\cdot D + \vec{D}^\mu$. Integrating out the small component field H in the path integral formalism (entirely analogous[1] to the procedure in Section 2.1) introduces a new term in the action functional which is given by

$$S_{\text{eff}} = \int d^4x\, \bar{h}(x)\, i\vec{\not{D}}\, \frac{1}{iv\cdot D + 2m_b}\, i\vec{\not{D}} h(x). \tag{3.12}$$

Since the strong x-dependence was factored out of the heavy-quark fields in (3.10), the derivative acting on h is much smaller than $2m_b$ and the above expression can be expanded in terms of local action functionals. Up to first order in $1/m_b$ this yields

$$S_{\text{eff}} = \int d^4x\, \frac{1}{2m_b}\, \bar{h}(x)\, i\vec{\not{D}}\, i\vec{\not{D}} h(x) + \mathcal{O}\left(\frac{1}{m_b^2}\right). \tag{3.13}$$

[1] In fact, there is one subtlety related to the appearance of the covariant derivative in the functional determinant instead of a normal derivative. However, by choosing the axial gauge $v\cdot A = 0$ the case reduces to the one considered before [72].

Ignoring radiative corrections, which would introduce scale dependent Wilson coefficients for each effective operator, the HQET Lagrangian for the heavy quarks may be written as [73, 74]

$$\begin{aligned}\mathcal{L}_{\text{HQET}} &= \bar{h}\, iv\cdot Dh + \frac{1}{2m_b}\,\bar{h}(x)\, i\vec{\not{D}}\, i\vec{\not{D}}h(x) + \mathcal{O}\left(\frac{1}{m_b^2}\right) \\ &= \bar{h}\, iv\cdot Dh + \frac{1}{2m_b}\,\bar{h}(i\vec{D})^2 h + \frac{1}{4m_b}\,\bar{h}\,\sigma_{\mu\nu} g_s G^{\mu\nu} h + \mathcal{O}\left(\frac{1}{m_b^2}\right),\end{aligned} \tag{3.14}$$

where the field strength tensor G is defined by $ig_sG^{\mu\nu} = [iD^\mu, iD^\nu]$. This Lagrangian is equivalent to the one of QCD in the kinematic region of a slightly off-shell heavy quark. It exhibits several interesting features. First, it is important to note that the covariant derivatives only contain soft gluon fields, since hard fields would put the heavy quark far off-shell, which is outside of the kinematic regime appropriate for HQET. Another important observation is that the leading power term contains no Dirac matrices thereby making the interaction of the heavy quark with (soft) gluons independent of its spin state. Also there is no mass-dependence in the leading term, which implies that the Lagrangian is the same for all heavy quarks. The spin-flavor symmetry mentioned at the beginning of this section is therefore manifest in the HQET Lagrangian of (3.14).

At subleading power in $1/m_b$ two new operators are introduced, given in the second line of (3.14). The first corresponds to the kinetic energy due to the residual momentum, while the second represents the "chromomagnetic" interaction of the heavy-quark spin with the gluon field. The spin-flavor symmetry is therefore broken at subleading power. For problems containing several heavy quarks at different velocity the full Lagrangian is given by a sum of the Lagrangians like (3.14), each with the appropriate velocity. The heavy quarks only interact by the exchange of soft gluons.

This concludes the derivation of the HQET Lagrangian for heavy quarks matched at tree level. But in order to calculate the forward scattering matrix elements of (3.4) it is necessary to also include the the weak effective operators of (2.18). This can in principle be done by using the Lagrangian (2.18) instead of the pure QCD Lagrangian as starting point, then decomposing the b-quark fields as was done in (3.10) and finally integrating out the small component field H. However, an equivalent approach is available that lends itself to the use as a recipe. On the classical level, integrating out a particle corresponds to solving its equation of motion and replacing the field in the Lagrangian by the solution. In the case of the small component field H the solution is formally given by

$$\begin{aligned}H(x) &= (iv\cdot D + 2m_b)^{-1} i\vec{\not{D}}h(x) \\ &= \frac{i\vec{\not{D}}}{2m_b}h(x) + \mathcal{O}\left(\frac{1}{m_b^2}\right).\end{aligned} \tag{3.15}$$

The field H is introduced into the heavy Lagrangian only by the decomposition (3.10) which can therefore immediately be rewritten as

$$b(x) \to e^{-im_b v\cdot x}[h(x) + H(x)] \to e^{-im_b v\cdot x}\left[h(x) + \frac{i\vec{\not{D}}}{2m_b}h(x) + \mathcal{O}\left(\frac{1}{m_b^2}\right)\right]. \tag{3.16}$$

Using this replacement rule in the QCD Lagrangian (3.11) instantly yields the HQET Lagrangian (3.14). The same replacement can be performed in the effective operators $Q_{1\ldots8g}$. This yields an expansion of the operators in powers of $1/m_b$ that can be written as

$$Q_i = \sum_{j=0}^{\infty} C_i^{(j)} Q_i^{(j)} \,, \tag{3.17}$$

with j indicating the suppression of the operator by powers of $1/m_b$ and C representing the Wilson coefficients from the matching onto HQET. They can be calculated perturbatively to the desired order in α_s. However, at this point it is sufficient to perform the matching onto HQET only at tree level.

As an example the leading power contribution to the decay rate in (3.4) will be considered in the next Section. Along the way two important discoveries will be made. On the one hand it will become apparent that an infinite amount of local operators needs to be resummed for the leading contribution in the endpoint region. This will be a further motivation for the introduction of another EFT, namely SCET. On the other hand the calculation will eventually lead to the proof of the statement, that the partonic calculation yields just the leading power of the $1/m_b$ expansion.

3.3 Leading Power Matching and OPE

With an appropriate EFT realizing a systematic expansion in terms of a small parameter $(1/m_b)$ at hand it is now possible to consider the hadronic forward scattering matrix element of (3.4) in more detail. The leading contribution is given by the insertion the operator $Q_{7\gamma}$ and its adjoint which leads to

$$\Gamma(\bar{B} \to X_s\gamma) = \frac{1}{2iM_B} \,\mathrm{Disc}\langle \bar{B}|i \int d^4x \, \frac{G_F^2}{2} |C_{7\gamma}\lambda_t|^2 \mathbf{T}\{Q_{7\gamma}^\dagger(x) Q_{7\gamma}(0)\}|\bar{B}\rangle \,, \tag{3.18}$$

with the scale dependencies of the Wilson coefficient dropped for brevity and $Q_{7\gamma}$ defined in (2.17). Matching $Q_{7\gamma}$ at tree level onto HQET yields

$$\begin{aligned} Q_{7\gamma} &= \frac{-em_b}{8\pi^2} \,\bar{s}\sigma_{\mu\nu}(1+\gamma_5)F^{\mu\nu}b = \frac{-em_b}{4\pi^2} \,\bar{s}\sigma_{\mu\nu}(1+\gamma_5)\partial^\mu A^\nu b \\ &\to \frac{-em_b}{4\pi^2} \, e^{-im_b v\cdot x} \bar{s}\sigma_{\mu\nu}(1+\gamma_5)\partial^\mu A^\nu \left[h + \frac{i\vec{\not{D}}}{2m_b} h + \mathcal{O}\left(\frac{1}{m_b^2}\right)\right]. \end{aligned} \tag{3.19}$$

Inserting the leading power matched expression for $Q_{7\gamma}$ into (3.18) and using Wick's theorem to contract the photon and strange-quark fields yields after some algebra

$$\begin{aligned} \Gamma(\bar{B} \to X_s\gamma) = &\frac{1}{2iM_B} \frac{G_F^2 m_b^2 \alpha}{4\pi^3} \, |C_{7\gamma}\lambda_t|^2 \\ &\times \mathrm{Disc}\langle \bar{B}|i \int \frac{d^4q}{(2\pi)^4} \, \bar{h}(0)\sigma_{\mu\nu}q^\mu \frac{m_b\not{v} + i\not{\partial} - \not{q}}{(m_b v + i\partial - q)^2 + i\varepsilon} \, \sigma_{\alpha\beta}q^\alpha(1+\gamma_5)h(0) \frac{g^{\nu\beta}}{q^2+i\varepsilon}|\bar{B}\rangle, \end{aligned} \tag{3.20}$$

where the strange-quark mass is set to zero. The partial derivatives act on the heavy-quark field and correspond to the residual momentum k in momentum space. Due to the derivatives in the denominator the resulting operator is non-local making it desirable to employ an OPE. This OPE will contain operators that are suppressed by powers of $1/m_b$ and therefore add to the subleading contributions from the expansion of (3.19). Before the expansion is performed the partial derivative will be replaced by a covariant derivative. This yields the propagator in the background field of the soft gluons in the B-meson. It will also be convenient to introduce a light-cone 4-vector-basis and decompose all momenta of the problem in this basis. All the necessary definitions will be collected in the following section.

3.3.1 The Light-Cone Basis

First one introduces a light-like vector $\bar{n}$ that points in the direction of the momentum of the external photon $q = E_\gamma \bar{n}$. Another vector n is defined by the relation $n + \bar{n} = 2v$. The decay products other than the photon will have a large momentum component in this direction. It is then easy to prove that

$$\bar{n}^2 = 0 = n^2, \qquad \bar{n} \cdot v = 1 = n \cdot v, \qquad n \cdot \bar{n} = 2. \tag{3.21}$$

In the B-meson rest frame an appropriate choice for the light-cone vectors would be $n^\mu = (1, 0, 0, 1)$ and $\bar{n}^\mu = (1, 0, 0, -1)$. All 4-vectors can be decomposed in this light-cone basis

$$x^\mu = \frac{n^\mu}{2} \bar{n} \cdot x + \frac{\bar{n}^\mu}{2} n \cdot x + x_\perp^\mu. \tag{3.22}$$

Note that by definition the external momenta of the B-meson $M_B v$, the photon q and the jet $P_X = M_B v - q$ all have vanishing perpendicular components. With this basis at one's disposal the OPE of the s-quark propagator may proceed.

3.3.2 Calculation Continued

In order to expand the HQET operator in Equation (3.20) the propagator is rewritten in a geometric series

$$\begin{aligned} \frac{m_b \not{v} + i \not{D} - \not{q}}{(m_b v + iD - q)^2 + i\varepsilon} &= \frac{m_b \not{v} + i \not{D} - \not{q}}{m_b(m_b - 2E_\gamma) + m_b\, in \cdot D + (m_b - 2E_\gamma) i\bar{n} \cdot D + (iD)^2 + i\varepsilon} \\ &= \frac{m_b \not{v} + i \not{D} - \not{q}}{m_b(m_b - 2E_\gamma + i\varepsilon)} \sum_{i=0}^{\infty} \left[-\frac{in \cdot D}{m_b - 2E_\gamma + i\varepsilon} - \frac{i\bar{n} \cdot D}{m_b} - \frac{(iD)^2}{m_b(m_b - 2E_\gamma + i\varepsilon)} \right]^i . \end{aligned} \tag{3.23}$$

Taking the cut forced by the discontinuity prescription in (3.20) corresponds to the replacement $1/(x+i\varepsilon)^n \to -2\pi i(-1)^n \delta^{(n)}(x)$. For E_γ outside the endpoint region ($m_b - 2E_\gamma \to m_b$) the propagator can thus be expanded in a series of singular terms with higher orders suppressed by powers of $1/m_b$. The first term in this expansion ($i = 0$) yields the expected

momentum conservation δ-function of a two-body decay. At leading power in $1/m_b$ the decay rate in (3.20) is therefore equal to

$$\Gamma(\bar{B} \to X_s\gamma) = \frac{1}{M_B}\frac{G_F^2 m_b^2 \alpha}{4\pi^4}\,|C_{7\gamma}\lambda_t|^2 \int_0^{\frac{m_b}{2}} dE_\gamma\, E_\gamma^3 \langle \bar{B}|\bar{h}(0)\vec{\not{n}}(1+\gamma_5)h(0)|\bar{B}\rangle \delta(m_b - 2E_\gamma)\,, \tag{3.24}$$

where the limits of integration are set by the cuts through the leading power contribution. Note that the axial vector part of the matrix element vanishes due to parity invariance. Also the Dirac matrix $\vec{\not{n}} = \bar{n}\cdot v\not{v} + \vec{\not{n}}$ can be replaced by 1 between two heavy-quark spinors.

So far the heavy-quark expansion was realized at two different points in the calculation. First the dipole operator $Q_{7\gamma}$ was matched onto the leading power HQET operator, then the strange-quark propagator was expanded in powers of $1/m_b$. In order to continue with the systematic expansion the initial and final states must be written in an m_b-independent way. The states are mass-dependent because they are defined as eigenstates of the HQET Lagrangian (3.14) that contains corrections of $\mathcal{O}(1/m_b)$. It is more appropriate to define the external states as eigenstates of only the leading term in (3.14) and include the power corrections as perturbations [75]. From now on all states are considered to be eigenstates of the leading power HQET Lagrangian and the necessary Lagrangian insertions of higher power to compensate for this are implicitly assumed.

By utilizing the heavy-quark symmetries, the remaining matrix element can now be related to a universal form factor that is especially simple in the case of forward scattering. Along with other meson form factors it was introduced by Isgur and Wise in [76]. Even though the case at hand is simple, it is useful for future purposes to derive a systematic way of defining form factors from HQET matrix elements. This can be done by employing the *HQET trace formalism* [77, 78] that is introduced in the next section. Afterwards the calculation of the leading power contribution to $\bar{B} \to X_s\gamma$ is resumed.

3.3.3 The HQET Trace Formalism

Due to the complex interactions of the light degrees of freedom within the meson it is not possible to analytically calculate hadronic matrix elements. Instead they are decomposed into a minimal set of form factors which can then be measured or determined by numerical calculations on a lattice [79, 80]. Through the introduction of HQET it is possible to relate many hadronic matrix elements at a certain order in the $1/m_b$ expansion to a limited number of form factors. The HQET trace formalism offers a systematic way to find these relations.

An important simplification was achieved by using the eigenstates of the leading power HQET Lagrangian as initial and final states. Ignoring the $1/m_b$ corrections, these states correspond to hadrons that contain a heavy quark with infinite mass and the light degrees of freedom. These hadrons have a well defined behavior under the spin and Lorentz transformations. Their ground state can be represented by a direct spinor product $u_h\bar{v}_l$, where u_h is the heavy-quark spinor, satisfying $\not{v}u_h(v) = u_h(v)$ and $\bar{v}_l$ represents the light degrees

of freedom which transform like an anti-quark with velocity v under Lorentz transformations. The light spinor satisfies $\not{v}\bar{v}_l(v) = -\bar{v}_l(v)$. Depending on the spin quantum numbers, the object $u_h\bar{v}_l$ has the correct transformation properties to represent the ground state of a pseudoscalar or a vector meson state. In this work only the pseudoscalar mesons are of interest. In terms of Dirac matrices the states can be written in a covariant way by [77, 78]

$$\mathcal{M}(v) = -\sqrt{M_B}\,\frac{1+\not{v}}{2}\,\gamma_5. \tag{3.25}$$

Note that the factor $\sqrt{M_B}$ enters through the relativistic normalization of the states. In the decay rate (3.24) this factor always cancels.

Even though nothing is known about the interactions of the light degrees of freedom, the hadronic matrix element will have a certain structure. Consider the matrix element

$$\langle \bar{B}(v)|\bar{h}\,\Gamma h|\bar{B}(v')\rangle\,, \tag{3.26}$$

where the heavy-quark fields have a different velocity and Γ represents a general Dirac structure. Due to Lorentz invariance this matrix element corresponds to a spinor product with no open indices. At leading power in HQET the heavy quarks interact with gluons without introducing a Dirac structure at the vertex. Therefore the spinor index corresponding to the heavy quark from the initial and final state is directly connected to the spinor indices of the Dirac structure Γ. The matrix element will thus contain

$$\overline{\mathcal{M}}_{ij}(v)\Gamma_{jk}\mathcal{M}_{kl}(v'). \tag{3.27}$$

The open light quark spinor indices i and l can be contracted to any type of Dirac structure that enters through the complex interactions of the light degrees of freedom. The matrix element can therefore be written as

$$\langle \bar{B}(v)|\bar{h}\,\Gamma h|\bar{B}(v')\rangle = \mathrm{tr}\,[\overline{\mathcal{M}}(v)\Gamma\mathcal{M}(v')\Xi(v,v')]. \tag{3.28}$$

The Dirac matrix Ξ can in principle depend on the scale at which the operators are renormalized. Since the matching to HQET is only performed at tree level here, this dependence has been dropped.

As an example the important case $\Gamma = \gamma^\mu$ will be considered. Since there are two independent external vectors available, the most general form for Ξ is given by

$$\Xi(v,v') = \Xi_0(v,v') + \not{v}\,\Xi_1(v,v') + \not{v}'\,\Xi_2(v,v') + \not{v}\not{v}'\,\Xi_3(v,v'). \tag{3.29}$$

Contributions containing γ_5 are not allowed due to parity invariance. Lorentz invariance on the other hand implies that the scalar functions Ξ_i can only depend on the product $v\cdot v'$. Inserting (3.29) into (3.28) and performing the trace yields

$$\langle \bar{B}(v)|\bar{h}\gamma^\mu h|\bar{B}(v')\rangle = M_B[\Xi_0(v\cdot v') - \Xi_1(v\cdot v') - \Xi_2(v\cdot v') + \Xi_3(v\cdot v')](v^\mu + v'^\mu). \tag{3.30}$$

The expression in square brackets is the Isgur-Wise function $\xi(v \cdot v')$ [76]. It is important to note that this function is the same for all heavy-light mesons due to the HQET flavor symmetry. By using current conservation

$$\int d^3x\, \bar{h}(x)\gamma^0 h(x)|\bar{B}(v)\rangle = 1\,|\bar{B}(v)\rangle\,, \tag{3.31}$$

the normalization of the Isgur-Wise function may be determined. In the forward scattering case $v = v'$ one finds $\xi(1) = 1$. It follows that

$$\langle\bar{B}(v)|\bar{h}\gamma^\mu h|\bar{B}(v)\rangle = 2M_B v^\mu. \tag{3.32}$$

Of course, it is immediately clear from Lorentz invariance that the forward scattering matrix element in (3.32) is proportional to v^μ, but the general procedure will be useful several times later on. With the result (3.32) one is finally able to show that the decay rate at leading power in the heavy-quark expansion corresponds to the decay rate for free quarks. This will be done now.

3.3.4 The Leading Power and the Shape Function

The section started with the definition of the inclusive decay rate in terms of a forward scattering matrix element. The operator of this matrix element was then matched onto HQET at the leading power in $1/m_b$. This gave rise to a non-local HQET operator. Furthermore the external hadron states were replaced by eigenstates of the leading power HQET Lagrangian. After expanding the operator in an OPE, the leading power local HQET matrix element was considered and its form determined by the HQET trace formalism. Inserting the result (3.32) into (3.24) yields

$$\Gamma(\bar{B} \to X_s\gamma) = \frac{G_F^2 m_b^2 \alpha}{2\pi^4}\,|C_{7\gamma}\lambda_t|^2 \int_0^{\frac{m_b}{2}} dE_\gamma\, E_\gamma^3 \delta(m_b - 2E_\gamma)\,, \tag{3.33}$$

which is equivalent to the free quark result in (2.25), just as claimed at the end of Chapter 2.

This naturally leads to the question of at what order in $1/m_b$ corrections do appear. To answer this question higher orders in the matching (3.19) and in the expansion (3.23) must be considered. In addition to the matching the higher power Lagrangian insertions compensating for the use of the leading power eigenstates are relevant. This section will deal with the higher orders of the expansion of the propagator in (3.23).

The expansion in (3.23) was based on the $1/m_b$ suppression of the higher order terms

in the series. After calculating the discontinuity this expansion can be written as[2]

$$\begin{aligned}\frac{m_b\not{v}+i\not{D}-\not{q}}{(m_bv+iD-q)^2+i\varepsilon} \to \frac{-2\pi i}{m_b}\left(\not{v}-\frac{\not{q}}{m_b}+\frac{i\not{D}}{m_b}\right)\\ \times\left[\delta\left(1-\frac{2E_\gamma}{m_b}\right)+\frac{in\cdot D}{m_b}\,\delta'\left(1-\frac{2E_\gamma}{m_b}\right)+\frac{1}{2}\left(\frac{in\cdot D}{m_b}\right)^2\delta''\left(1-\frac{2E_\gamma}{m_b}\right)+\dots\right.\\ \left.-\frac{i\bar{n}\cdot D}{m_b}\,\delta\left(1-\frac{2E_\gamma}{m_b}\right)+\dots+\frac{(iD)^2}{m_b^2}\,\delta'\left(1-\frac{2E_\gamma}{m_b}\right)+\dots\right],\end{aligned} \tag{3.34}$$

where the second line only contains powers of the first term in the square bracket of (3.23), while the third line contains the first power of the second and third term in (3.23). Even though all higher powers are formally suppressed by $1/m_b$ it is possible to assign a certain *scaling* to the δ-functions themselves. It follows, that in the endpoint region ($2E_\gamma/m_b \to 1$) all terms in the second line of (3.34) are of the same order. The concept of scaling will be carefully introduced in Section 4.1, but here it is sufficient to note that the leading singular terms in the second line of (3.34) are all equally important. This phenomenon is called the breakdown of the OPE. It indicates that an HQET based local OPE is not applicable in the kinematic region of $E_\gamma \to m_b/2$. The ad-hoc solution to this problem is to resum the leading singular terms (corresponding to the first term in the square brackets of (3.23)) into a so-called *shape function* [81, 82]. This function only has support in the endpoint region and is defined by its moment expansion under the energy integral. The resummation can explicitly be performed by expanding the propagator (3.23) in a different way

$$\begin{aligned}\frac{m_b\not{v}+i\not{D}-\not{q}}{(m_bv+iD-q)^2+i\varepsilon} = \frac{m_b\not{v}+i\not{D}-\not{q}}{m_b(m_b-2E_\gamma+in\cdot D+i\varepsilon)}\\ \times\sum_{i=0}^{\infty}\left[-\frac{(m_b-2E_\gamma)i\bar{n}\cdot D}{m_b(m_b-2E_\gamma+in\cdot D+i\varepsilon)}-\frac{(iD)^2}{m_b(m_b-2E_\gamma+in\cdot D+i\varepsilon)}\right]^i.\end{aligned} \tag{3.35}$$

Here the higher order terms in the expansion are truly suppressed and the leading power contains the resummed terms of the second line of (3.34)

$$\frac{m_b\not{v}+i\not{D}-\not{q}}{(m_bv+iD-q)^2+i\varepsilon} \to -2\pi i\left(\not{v}-\frac{\not{q}}{m_b}+\frac{i\not{D}}{m_b}\right)\Big[\delta(m_b-2E_\gamma+in\cdot D)+\dots\Big]. \tag{3.36}$$

By inserting this result into the decay rate (3.20) suggests a definition for the leading order shape function through

$$S(m_b-2E_\gamma)=\frac{\langle\bar{B}|\bar{h}\,\delta(m_b-2E_\gamma+in\cdot D)h|\bar{B}\rangle}{2M_B}. \tag{3.37}$$

[2]In order to eliminate derivatives of δ-functions the relation $x\delta'(x)=-\delta(x)$ was used which holds for non-singular test functions.

However, due to the derivative in the argument of the δ-function the shape function does not correspond to a single, local HQET operator. Instead, it is a new non-perturbative object, whose moments can be expressed in terms of HQET matrix elements. Performing a moment expansion returns just the sum of terms in the second line of (3.34) with local matrix elements as coefficients.

$$\begin{aligned} S(m_b - 2E_\gamma) = \frac{\langle \bar{B}|\bar{h}\, h|\bar{B}\rangle}{2M_B}\, \delta(m_b - 2E_\gamma) + \frac{\langle \bar{B}|\bar{h}\, in\cdot Dh|\bar{B}\rangle}{2M_B}\, \delta'(m_b - 2E_\gamma) \\ + \frac{1}{2}\frac{\langle \bar{B}|\bar{h}(in\cdot D)^2 h|\bar{B}\rangle}{2M_B}\, \delta''(m_b - 2E_\gamma) + \dots \end{aligned} \tag{3.38}$$

The first moment was already determined in the leading power calculation above and is equal to 1. The second moment is proportional to the HQET matrix element $\langle \bar{B}|\bar{h} iD^\mu h|\bar{B}\rangle$ which vanishes by applying the equation of motion $iv\cdot Dh = 0$ derived from the leading power Lagrangian [83]. The third moment requires the decomposition of the matrix element $\langle \bar{B}|\bar{h} iD^\mu iD^\nu h|\bar{B}\rangle$ in terms of form factors. This can be achieved by employing the trace formalism of Section 3.3.3

$$\begin{aligned} \langle \bar{B}|\bar{h}\Gamma iD^\mu iD^\nu h|\bar{B}\rangle &= \mathrm{tr}\left[\overline{\mathcal{M}}\Gamma\mathcal{M}\left((g^{\mu\nu} - v^\mu v^\nu)\Xi_0 + \sigma^{\mu\nu}\Xi_1\right)\right] \\ &=: M_B \mathrm{tr}\left[\Gamma\frac{1+\not{v}}{2}\left((g^{\mu\nu} - v^\mu v^\nu)\frac{\lambda_1}{3} + \sigma^{\mu\nu}\frac{i\lambda_2}{2}\right)\frac{1+\not{v}}{2}\right], \end{aligned} \tag{3.39}$$

where the HQET parameters λ_1 and λ_2 are related to the matrix elements of the subleading operators in the HQET Lagrangian (3.14). When inserting these operators into the formula above one finds

$$\langle \bar{B}|\bar{h}(i\vec{D})^2 h|\bar{B}\rangle = 2M_B\lambda_1\,, \tag{3.40}$$

$$\langle \bar{B}|\bar{h}\frac{1}{2}\sigma_{\mu\nu}G^{\mu\nu}h|\bar{B}\rangle = 6M_B\lambda_2\,, \tag{3.41}$$

which suggests the relation of λ_1 to the kinetic energy of the heavy quark within the meson and λ_2 to the hyperfine chromomagnetic interactions. With these definitions the third moment of the leading shape functions calculates to $-\lambda_1/3$ (set $\Gamma = n_\mu n_\nu$). Of course, the resummation can be extended to higher orders in $1/m_b$ for the product of the second or third term in the square brackets of (3.23) with any power of the first term.

The shape function can be systematically derived within the framework of SCET which introduces an appropriate power counting. This will be the topic of Section 4.3.3. There, also corrections of higher order in α_s will be considered. At the leading order in α_s and $1/m_b$ the shape function just replaces the momentum-conservation δ-function in (3.33)

$$\Gamma(\bar{B}\to X_s\gamma) = \frac{G_F^2 m_b^2 \alpha}{2\pi^4}\,|C_{7\gamma}\lambda_t|^2 \int_0^{\frac{M_B}{2}} dE_\gamma\, E_\gamma^3 S(m_b - 2E_\gamma)\,, \tag{3.42}$$

where the upper limit of integration is now $M_B/2$, since the effects of the residual momentum k are taken into account. The shape function thus encodes the form of the photon

spectrum in the endpoint region. Since the deviation of the spectrum from the form of a δ-function is at leading order in α_s related to the residual momentum of the heavy quark, the shape function can also be interpreted as the momentum distribution function of the heavy quark within the meson. This is analogous to the parton distribution functions in the description of proton collisions.

Since the shape function only has support over the endpoint region, it affects the integrated rate only if the limits of integration are in that region (e.g. by the introduction of a lower cut $E_0 \sim m_b/2$ on the photon energy). For a much larger range ($E_0 \to 0$) the shape function might be replaced by its moment expansion, with higher orders being suppressed by powers of $1/m_b$. In that case there is no need to resum the terms in (3.34). For the contributions considered here, the terms of order $1/m_b$ then vanish due to the equation of motion. However, later on subleading shape functions that are also relevant outside the endpoint region will be introduced. These subtleties are not easily analyzed in the framework of HQET, illustrating the demand for a more appropriate EFT (SCET). In the remainder of this chapter the higher power contributions of the local OPE are considered.

3.4 Higher Power Corrections to the Total Rate

In the last Section it was shown that outside the endpoint region the decay rate of $\bar{B} \to X_s\gamma$ can be written as a local OPE in terms of HQET operators with the leading power term corresponding to the free quark result. Corrections due to the expansion of the light quark propagator did only appear at the order $1/m_b^2$. Outside the endpoint region this correction is given by the third moment of the leading order shape function that was found to be proportional to the HQET parameter λ_1. Additional contributions to the order $1/m_b^2$ are introduced by matching $Q_{7\gamma}$ onto subleading HQET operators as prescribed in (3.19) and by Lagrangian insertions. Instead of the matrix element $\langle \bar{B}|\mathbf{T}\{Q_{7\gamma}^\dagger(x)Q_{7\gamma}(0)\}|\bar{B}\rangle$ the decay rate in (3.18) will then contain matrix elements like

$$\langle \bar{B}|\mathbf{T}\{Q_{7\gamma}^{\dagger(1)}(x)Q_{7\gamma}^{(1)}(0)\}|\bar{B}\rangle, \quad \langle \bar{B}|\mathbf{T}\{Q_{7\gamma}^{\dagger(2)}(x)Q_{7\gamma}(0)\}|\bar{B}\rangle \quad \text{or}$$
$$\langle \bar{B}|\mathbf{T}\{Q_{7\gamma}^{\dagger(1)}(x)Q_{7\gamma}(0)\mathcal{L}^{(1)}(y)\}|\bar{B}\rangle \quad \text{etc.}$$

where the superscript (i) denotes the power of $1/m_b$ suppression and $Q_{7\gamma}^{(i)}$ and $\mathcal{L}^{(i)}$ can be read of from (3.19) and (3.14), respectively. Furthermore, the $1/m_b$ term from the OPE can be combined with any other $1/m_b$ suppressed terms. The complete calculation was performed in [84] and resulted in

$$\Gamma(\bar{B} \to X_s\gamma) = \frac{G_F^2 m_b^5 \alpha}{32\pi^4} |C_{7\gamma}\lambda_t|^2 \left[1 + \frac{\lambda_1 - 9\lambda_2}{2m_b^2}\right]. \tag{3.43}$$

This is the final justification for the use of the free quark approximation. If the total inclusive rate is considered, non-perturbative corrections to the free quark result only

appear at order $1/m_b^2$. Of course, the total rate is not accessible by experiment, as was explained in Section 1.3. Thus, a dedicated analysis of the effects in the endpoint region is of interest.

3.5 Conclusions of this Chapter

At the end of Chapter 2 the question of how non-perturbative effects influence the calculation of the $\bar{B} \to X_s\gamma$ decay rate was posed. These effects are encoded in hadronic matrix elements. In this Chapter the heavy-quark effective theory was introduced, which made it possible to expand the matrix elements of the inclusive decay rate in powers of $1/m_b$. Each term in this expansion can be related to a limited set of HQET parameters. These are still not analytically computable, but universal due to the heavy-quark symmetries. In particular it was shown that the leading power contribution corresponds to the free quark result used in Chapter 2 and that, in this framework, the corrections to the total rate appear only at order $1/m_b^2$. During the course of the calculation it was found that the local OPE breaks down in the endpoint region. This was solved by the introduction of the shape function. However, it was left open how radiative corrections affect this approach. In order to deal with this kind of questions the shape functions must be introduced in a more systematic way. This can be done in the framework of SCET, which will be the topic of the next chapter.

Chapter 4

Soft-Collinear Effective Theory

It will be the aim of this chapter to introduce SCET in the context of $\bar{B} \to X_s\gamma$ in the endpoint region and to demonstrate its advantages over the previous approaches. The fundamental concepts of SCET are the systematic separation of the scales involved in the problem and the implementation of an appropriate power counting. In Section 4.1 the kinematics of $\bar{B} \to X_s\gamma$ in the endpoint region are analyzed, which leads to the identification of the relevant scales and to the scaling of the fields. Afterwards, in Section 4.2, SCET will be put forward as the proper EFT to deal with the challenges identified in the previous chapters. This involves the derivation of the Lagrangian up to the required order in the power counting. In order to calculate the differential $\bar{B} \to X_s\gamma$ decay rate, the leading power SCET version of the effective heavy-to-light operator is introduced in Section 4.3 and its Wilson coefficient determined by matching QCD onto the SCET operator. This first matching step separates physics at the hard scale from the lower scales. In a second step, SCET is matched onto HQET thereby proving a complete separation of the different scales for the decay rate. This factorization forms the basis of a resummation of the large logarithms in Section 4.4.

4.1 Kinematics and Power Counting

The two preceding chapters introduced two basic concepts which are important for the analysis of the $\bar{B} \to X_s\gamma$ decay rate. On the one hand a perturbative calculation was used to determine the high-energy behavior of the particles involved. On the other hand an expansion in powers of the inverse heavy-quark mass made it possible to systematically deal with non-perturbative effects. However, both approaches encountered difficulties in the endpoint region of large photon energy that were related to the smallness of the quantity $m_b - 2E_\gamma$. While the perturbative calculation suffered from large logarithms for $E_\gamma \to m_b/2$, the $1/m_b$ expansion produced an infinite amount of leading order matrix elements. More precisely, these difficulties are related to the appearance of several distinct energy scales. First, there is the large energy scale set by the mass of the decaying meson M_B. Second, the size of the hadronic interactions introduce the scale Λ_{QCD}. In the rest frame of the

meson the photon momentum $q = E_\gamma \bar{n}$ can be written as $q = (E_\gamma, 0, 0, -E_\gamma)$, where E_γ is of the same order of magnitude as M_B in the endpoint region. The momentum of the hadronic jet $P_X = M_B v - q$ then corresponds to

$$P_X = (M_B - 2E_\gamma)\frac{\bar{n}}{2} + M_B \frac{n}{2}\,, \tag{4.1}$$

with a large component of order M_B in the n-direction and a small component of order $\Lambda_{\rm QCD}$ in the $\bar{n}$-direction. It will be convenient to introduce the notation

$$x^\mu = (n \cdot x, \bar{n} \cdot x, x_\perp) = (x_+, x_-, x_\perp) \tag{4.2}$$

for any 4-vector decomposed in the light-cone basis of Section 3.3.1, where $x_\perp$ denotes both perpendicular components. Thus, the jet has a large energy $E_X = P_X^0 = M_B - E_\gamma \sim \mathcal{O}(M_B)$ but a small invariant mass $M_X = \sqrt{P_X^2} = \sqrt{M_B(M_B - 2E_\gamma)} \sim \mathcal{O}(\sqrt{\Lambda_{\rm QCD} M_B})$. This invariant mass sets an intermediate scale, which is larger than the hadronic scale $\Lambda_{\rm QCD}$ but smaller than the hard scale M_B. Ratios of these scales are responsible for the large logarithms in the perturbative calculation. Also, a power counting taking into account all the different scales is necessary for a systematic expansion in a small parameter.

In order to implement the appropriate power counting, a small parameter λ is introduced, that parameterizes the difference between the scales by

$$\begin{aligned} \text{hard:} &\quad M_B\,, \\ \text{intermediate:} &\quad \sqrt{\Lambda_{\rm QCD} M_B} = \lambda^{1/2} M_B\,, \\ \text{soft:} &\quad \Lambda_{\rm QCD} = \lambda M_B\,. \end{aligned} \tag{4.3}$$

The parameter λ is therefore of the order[1] $\Lambda_{\rm QCD}/M_B \sim 0.1$. Instead of the meson mass M_B one might also choose the heavy-quark mass m_b, both of which are the same at the leading power in λ. By using the parameter λ, different momenta may be classified by their *scaling* properties. A momentum component is said to scale like λ when its magnitude is of order λm_b. In the context of $\bar{B} \to X_s\gamma$ in the endpoint the following momentum regions are of relevance.

$$\begin{aligned} \text{hard (h):} &\quad (p_+, p_-, p_\perp) \sim (1, 1, 1) \\ \text{hard-collinear (hc):} &\quad (p_+, p_-, p_\perp) \sim (\lambda, 1, \lambda^{1/2}) \\ \text{anti-hard-collinear } (\overline{\text{hc}}): &\quad (p_+, p_-, p_\perp) \sim (1, \lambda, \lambda^{1/2}) \\ \text{soft (s):} &\quad (p_+, p_-, p_\perp) \sim (\lambda, \lambda, \lambda) \end{aligned} \tag{4.4}$$

Unfortunately the naming is not consistent in the literature. Especially in the earlier works [7, 85] soft momenta were often referred to as ultrasoft, while hard-collinear were called collinear. The different momentum modes will now be discussed.

In the case of $\bar{B} \to X_s\gamma$ hard momenta will appear in virtual corrections to the heavy-to-light operators. As was discussed in Section 3.2 the large part of the heavy-quark

[1] Note, that in the literature λ is sometimes defined as $\sqrt{\Lambda_{\rm QCD}/M_B}$.

momentum $m_b v$ is extracted and only the soft residual momentum k remains dynamical. In the endpoint region, the partons making up the final state jet can only have a large momentum component in the primary direction n of the jet momentum (hence the name "collinear"), but are allowed to have small components in the other directions. In the case of a two-body decay of an on-shell heavy quark, the small components vanish. Their origin is therefore dynamical. In order to guarantee the scaling of the invariant mass of the jet, the small components scale as given in (4.4). Soft particles do not change the scaling of either the invariant mass or the jet energy and can therefore also be part of the final state. Furthermore, soft interactions are responsible for the binding of the initial state partons into a hadron. The only particle in the final state with a large momentum component in the $\bar{n}$-direction may be the photon, but intermediate fields can be anti-hard-collinear as well.

The basic idea of the soft collinear effective theory is to introduce separate fields for each necessary momentum mode and then integrate out the modes at the perturbative scales, namely hard fluctuations as well as fluctuations around the light-cone of the hard-collinear particles. SCET therefore separates physics at the hard scale from the physics at the intermediate or lower scale. As will be shown, this additional matching step (in addition to the matching onto HQET) allows for the resummation of the large logarithms that appear in the free parton calculation. Furthermore, since all scales are identified and parameterized by λ, the power counting is definite and there will be no need to explicitly resum an infinite amount of leading order operators as was the case in HQET.

A priori it is not clear that the momentum modes defined in (4.4) are sufficient to describe $\bar{B} \to X_s\gamma$. The requirement is, that the fields of SCET reproduce the correct infrared behavior of the considered QCD processes. The decomposition of an QCD amplitude into the relevant momentum regions corresponds to an analysis using the method of regions [86]. Depending on the problem, certain momentum modes do not contribute due to the appearance of scaleless integrals. It turns out that the momentum modes of (4.4) are indeed sufficient for inclusive decays. The effective theory containing only hard-collinear and soft modes is called SCET-I. The inclusion of anti-hard-collinear modes leads to SCET(hc,$\overline{\text{hc}}$,s) which corresponds to the sum of two SCET-I with interchanged light-cone directions n and $\bar{n}$. The two sectors are connected when matching QCD diagrams onto SCET operators. In the case of exclusive decays, a new momentum mode becomes important. The collinear mode (c) describes the partons inside the hadron with an invariant mass of $\mathcal{O}(\Lambda_{\text{QCD}})$ and scales like $(\lambda^2, 1, \lambda)$ [87, 88]. After matching SCET(hc,c,s) onto a theory containing only collinear and soft modes one arrives at SCET-II. In addition, this theory contains soft-collinear messenger modes (i.e. modes not appearing as external states) with a scaling of $(\lambda^2, \lambda, \lambda^{3/2})$ [89]. Since this work only deals with inclusive decays, SCET-I is the relevant EFT and will henceforth just be referred to as SCET. The following Section will review the derivation of the SCET Lagrangian for inclusive decays.

4.2 Soft-Collinear Effective Theory

The soft-collinear effective theory was first introduced in [6] to solve the problem of large logarithms in the perturbative calculation of $\bar{B} \to X_s\gamma$. This presentation will make use of the position-space formalism presented in [85]. Since the theory is constructed to contain only hard-collinear and soft momentum modes, the QCD fields are decomposed as

$$\psi(x) = \psi_{\rm hc}(x) + q(x)\,, \tag{4.5}$$

where the fields are defined by the scaling of their momenta

$$\partial^\mu \psi_{\rm hc}(x) \sim (\lambda, 1, \lambda^{1/2})\psi_{\rm hc}(x) \quad \text{and} \quad \partial^\mu q(x) \sim (\lambda,\lambda,\lambda)q(x). \tag{4.6}$$

In analogy to the decomposition of the heavy-quark field in HQET, the hard-collinear fields can be decomposed into a large and a small two-component spinor. This time, the small component vanishes if the spinor describes a particle that is exactly on the light-cone. The hard-collinear particles of the final state jet have a large momentum component in one light-cone direction and small components in the other directions and are therefore nearly on the light-cone. The appropriate projection operators are

$$P_n = \frac{\not{n}\bar{\not{n}}}{4} \quad \text{and} \quad P_{\bar{n}} = \frac{\bar{\not{n}}\not{n}}{4}\,, \tag{4.7}$$

which satisfy $P_n u(p_+\bar{n}) = 0$ and $P_n u(p_- n) = u(p_- n)$ for spinors of light-like particles and correspondingly for $P_{\bar{n}}$. As projection operators they furthermore satisfy $P_n + P_{\bar{n}} = 1$ which leads to the following decomposition for hard-collinear fields

$$\psi_{\rm hc}(x) = P_n\psi_{\rm hc}(x) + P_{\bar{n}}\psi_{\rm hc}(x) =: \xi(x) + \eta(x)\,, \tag{4.8}$$

with the decomposed fields satisfying $\not{n}\xi = 0$ and $\bar{\not{n}}\eta = 0$. By calculating the propagator it is possible to assign a certain scaling to the fields themselves.

$$\langle 0|\mathbf{T}\{\xi(x)\bar{\xi}(y)\}|0\rangle = P_n\langle 0|\mathbf{T}\{\psi_{\rm hc}(x)\bar{\psi}_{\rm hc}(y)\}|0\rangle P_{\bar{n}} = \int \frac{d^4p}{(2\pi)^4}\,\frac{\not{n}}{2}\frac{i\bar{n}\cdot p}{p^2+i\varepsilon}e^{-ip(x-y)}\,, \tag{4.9}$$

Since by definition p is a hard-collinear momentum the integrals over the various components scales like $dnp\,d\bar{n}p\,dp_\perp^1\,dp_\perp^2 \sim \lambda^2$. The right hand side of (4.9) therefore scales like λ which implies that $\xi \sim \lambda^{1/2}$. A similar consideration leads to the scaling properties of the remaining fermion fields, where one has to keep in mind that the integration measure for soft integrals scales like λ^4. Summing up, one finds

$$\xi \sim \lambda^{1/2}, \quad \eta \sim \lambda \quad \text{and} \quad q \sim \lambda^{3/2}. \tag{4.10}$$

The gluon fields are decomposed in an analogous way $A^\mu(x) = A^\mu_{\rm hc}(x) + A^\mu_{\rm s}(x)$. Their scaling can be determined by contracting the gluon propagator in a general gauge with the light-cone vectors n and $\bar{n}$. One finds

$$A^\mu_{\rm hc} \sim (\lambda, 1, \lambda^{1/2}) \quad \text{and} \quad A^\mu_{\rm s} \sim (\lambda,\lambda,\lambda)\,, \tag{4.11}$$

which implies that the gluon fields scale just like their momenta. With these fields scalings it is possible to assign a definite scaling to every operator made out of the effective theory fields.

In order to describe the $\bar{B} \to X_s\gamma$ process in the language of SCET it is necessary to determine the Lagrangian for the EFT fields. This is done by using the QCD Lagrangian as a starting point and then decomposing the QCD fields into the SCET fields by using (4.5) and (4.8). This leads to

$$\begin{aligned}\mathcal{L}_{\text{SCET}} &= \bar{\xi}\,\frac{\bar{n}\!\!\!/}{2}\,in\cdot D\xi + \bar{\xi}\,i\not{D}_\perp\eta + \bar{\xi}g\not{A}_{\text{hc}}q + \bar{\eta}\,i\not{D}_\perp\xi \\ &\quad + \bar{\eta}\,\frac{n\!\!\!/}{2}\,i\bar{n}\cdot D\eta + \bar{\eta}g\not{A}_{\text{hc}}q + \bar{q}g\not{A}_{\text{hc}}\xi + \bar{q}g\not{A}_{\text{hc}}\eta + \bar{q}\,i\not{D}_s q\,,\end{aligned} \tag{4.12}$$

where where g is the strong coupling and $D_s = \partial - igA_s$ is the covariant derivative containing only a soft gluon field. Vertices with only one hard-collinear field are forbidden by momentum conservation. In a next step, the fluctuations around the light-cone η are integrated out by solving the classical equation of motion in analogy to the procedure employed in the derivation of the HQET Lagrangian in Section 3.2. The solution is formally given by

$$\eta = -\frac{1}{i\bar{n}\cdot D + i\varepsilon}\frac{\bar{n}\!\!\!/}{2}(i\not{D}_\perp\xi + g\not{A}_{\text{hc}}q). \tag{4.13}$$

In contrast to the derivation of the HQET Lagrangian it is not possible to expand the inverse covariant derivative in the case of SCET. This gives rise to non-local operators in the Lagrangian and necessitates the inclusion of the $+i\varepsilon$ prescription to regularize the inverse derivative. This regularization by $+i\varepsilon$ is arbitrary and drops out in physical quantities [85]. After integrating out the η-field the Lagrangian becomes

$$\begin{aligned}\mathcal{L}_{\text{SCET}} &= \mathcal{L}_\xi + \mathcal{L}_q + \mathcal{L}_{\xi q} \\ \mathcal{L}_\xi &= \bar{\xi}\,\frac{\bar{n}\!\!\!/}{2}\,in\cdot D\xi - \bar{\xi}\,i\not{D}_\perp\frac{1}{i\bar{n}\cdot D}\frac{\bar{n}\!\!\!/}{2}\,i\not{D}_\perp\xi \\ \mathcal{L}_q &= \bar{q}\,i\not{D}_s q - \bar{q}g\not{A}_{\text{hc}}\frac{1}{i\bar{n}\cdot D}\frac{\bar{n}\!\!\!/}{2}g\not{A}_{\text{hc}}q \\ \mathcal{L}_{\xi q} &= \bar{\xi}\left(g\not{A}_{\text{hc}} - i\not{D}_\perp\frac{1}{i\bar{n}\cdot D}\frac{\bar{n}\!\!\!/}{2}g\not{A}_{\text{hc}}\right)q + \bar{q}\left(g\not{A}_{\text{hc}} - g\not{A}_{\text{hc}}\frac{1}{i\bar{n}\cdot D}\frac{\bar{n}\!\!\!/}{2}\,i\not{D}_\perp\right)\xi\,,\end{aligned} \tag{4.14}$$

where the $+i\varepsilon$ prescription has been dropped for brevity. From the field scalings in (4.10) and (4.11) it follows that the kinetic part of the hard-collinear Lagrangian $\mathcal{L}_\xi$ scales like λ^2. Since a position space integral $\int d^4x$ over an operator that contains at least one hard-collinear field scales like λ^{-2} the action is of order λ^0 and thereby contributes to the leading power term. Similarly, the kinetic part of the soft Lagrangian scales like λ^4 which is again canceled in the action by the integral over soft fields. The interaction terms do not scale homogeneously in general and need to be expanded. Specifically, the hard-collinear-soft interaction terms only give rise to subleading contributions starting at $\mathcal{O}(\lambda^{1/2})$.

It should be noted that a Lagrangian derived by the steps above is formally equivalent to QCD as long as the fields are not restricted to a certain momentum region. As a consequence, hard fluctuations do not introduce new operators or change any of the operator coefficients. This no-renormalization property has been discussed in [85]. The situation changes with the introduction of the heavy-to-light operators of the weak effective Lagrangian, which constitute a source for the hard-collinear particles. In that case it is necessary to match the QCD operators onto the SCET operators, order by order in the power counting. These SCET operators of each order are determined by the replacements (4.5) and (4.8) in the QCD operators. However, before explicitly performing the matching, some comments concerning the behavior of the SCET Lagrangian under gauge transformations are in order.

4.2.1 Gauge Transformations and Wilson Lines

With the introduction of separate hard-collinear and soft gluon fields, the Lagrangian is no longer invariant under general $SU(3)_c$ gauge transformations. Instead separate hard-collinear and soft gauge transformations are introduced that do not change the scaling of the transformed fields. The transformations are defined by the scaling of their derivatives $\partial^\mu U_{\rm hc} \sim (\lambda, 1, \lambda^{-1/2}) U_{\rm hc}$ and $\partial^\mu U_{\rm s} \sim (\lambda, \lambda, \lambda) U_{\rm s}$ [12]. From this it is clear that the soft fields do not transform under hard-collinear gauge transformations but transform in the usual way under soft gauge transformations. The hard-collinear fields on the other hand transform under soft as well as hard-collinear gauge transformations. The transformations are given by

$$\begin{aligned} &q \xrightarrow{\rm s} U_{\rm s} q, \quad \xi \xrightarrow{\rm s} U_{\rm s}\xi, \quad A_{\rm s} \xrightarrow{\rm s} U_{\rm s} A_{\rm s} U_{\rm s}^\dagger + \frac{i}{g} U_{\rm s} \big[\partial, U_{\rm s}^\dagger\big], \quad A_{\rm hc} \xrightarrow{\rm s} U_{\rm s} A_{\rm hc} U_{\rm s}^\dagger, \\ &q \xrightarrow{\rm hc} q, \quad \xi \xrightarrow{\rm hc} U_{\rm hc}\xi, \quad A_{\rm s} \xrightarrow{\rm hc} A_{\rm s}, \quad A_{\rm hc} \xrightarrow{\rm hc} U_{\rm hc} A_{\rm hc} U_{\rm hc}^\dagger + \frac{i}{g} U_{\rm hc} \big[D_s, U_{\rm hc}^\dagger\big]. \end{aligned} \tag{4.15}$$

By definition, the kinetic terms of the Lagrangian (4.14) are manifestly invariant under these transformation. However, the invariance is not obvious for the interaction terms. This can be remedied by the introduction of Wilson lines. Of relevance are the Wilson line W and the soft Wilson line S defined by

$$W(x) = \mathbf{P} \exp\left(ig \int_{-\infty}^{0} dt\, \bar{n} \cdot A(x + t\bar{n}) \right), \tag{4.16}$$

$$S(x) = \mathbf{P} \exp\left(ig \int_{-\infty}^{0} dt\, \bar{n} \cdot A_s(x + t\bar{n}) \right), \tag{4.17}$$

where the gluon field A contains hard-collinear as well as soft modes and $\mathbf{P}$ is the path ordering symbol that sorts the gluon fields closer to the lower limit of the integration to the right. By definition the covariant derivative acting only on the Wilson line vanishes $(\bar{n} D W) = 0$ and $(\bar{n} D_s S) = 0$ which implies the important relations

$$\bar{n} \cdot D\, W = W \bar{n} \cdot \partial \quad \text{and} \quad \bar{n} \cdot D_s S = S\, \bar{n} \cdot \partial \tag{4.18}$$

where the covariant derivative is also acting on everything on the right of the Wilson line. Their behavior under gauge transformations is given by

$$W(x) \xrightarrow{\text{s}} U_{\text{s}}(x)W(x), \quad S(x) \xrightarrow{\text{s}} U_{\text{s}}(x)S(x), \quad W(x) \xrightarrow{\text{hc}} U_{\text{hc}}(x)W(x), \quad S(x) \xrightarrow{\text{hc}} S(x), \tag{4.19}$$

where it is assumed that the gauge transformations do not change the fields at infinity, $U(x - \bar{n}\infty) = 1$. With the help of these Wilson lines it is now possible to write down the SCET Lagrangian (4.14) in a manifestly gauge invariant form [85]. However, the Wilson line W contains the soft gluon field and therefore generates an infinite sum of terms with increasing power in λ. In order to determine the SCET Lagrangian as a systematic expansion in terms of λ the Wilson line must be expanded[2]. The leading power in that expansion is just the hard-collinear Wilson line W_{hc}

$$\begin{aligned} W(x) &= W_{\text{hc}}(x) + \mathcal{O}(\lambda)\,, \\ W_{\text{hc}}(x) &= \mathbf{P} \exp\left(ig \int_{-\infty}^{0} dt\, \bar{n} \cdot A_{\text{hc}}(x + t\bar{n}) \right). \end{aligned} \tag{4.20}$$

But there are more terms in the Lagrangian (4.14) that do not scale homogeneously in λ and that therefore need to be expanded.

4.2.2 Expansion and Lagrangian

First it is necessary to expand each vector field in terms of their components. In addition, the soft fields in interaction terms with hard-collinear fields need to be *multipole expanded* [90]. This is because the hard-collinear fields vary much faster in the light-cone direction $\bar{n}$ and in the perpendicular direction than the soft field. It follows that the position argument x scales like $(1, \lambda^{-1}, \lambda^{-1/2})$ and the soft field must be expanded in

$$\begin{aligned} q(x) &= e^{x\cdot\partial} q(0) = e^{n\cdot x\, \bar{n}\cdot\partial/2 + x_\perp\cdot\partial_\perp} e^{\bar{n}\cdot x\, n\cdot\partial/2} q(0) \\ &= \left(1 + x_\perp \cdot \partial_\perp + \frac{1}{2} n\cdot x\, \bar{n}\cdot\partial + \frac{1}{2} x_\perp^\mu x_\perp^\nu \partial_\mu \partial_\nu + \mathcal{O}(\lambda^{3/2}) \right) q(x_-), \end{aligned} \tag{4.21}$$

where $x_- = \frac{n}{2}\bar{n}\cdot x$ and the derivative is taken before one sets $x = x_-$. The complete expansion has been performed up to $\mathcal{O}(\lambda^2)$ in [85] and the full Lagrangian is given there. In this work only the leading power Lagrangian is of relevance as well as the first power of the hard-collinear-soft interactions. They are given by

$$\begin{aligned} \mathcal{L}^{(0)}_{\text{SCET}} &= \bar{\xi} \frac{\bar{\not{n}}}{2} in\cdot D \xi + \bar{\xi}\, i\not{D}_{\text{hc}\perp} \frac{1}{i\bar{n}\cdot D_{\text{hc}}}\, i\not{D}_{\text{hc}\perp} \frac{\bar{\not{n}}}{2} \xi, \\ \mathcal{L}^{(1)}_{\xi q} &= \bar{\xi}\, i\not{D}_{\text{hc}\perp} W_{\text{hc}} q + \bar{q} W^\dagger_{\text{hc}} i\not{D}_{\text{hc}\perp} \xi, \end{aligned} \tag{4.22}$$

where it is implied that all soft fields are evaluated at the position x_-. These terms are invariant under hard-collinear and soft gauge transformations at this order in the power

[2]Note that the soft Wilson line is of order λ^0 due to the scaling of the integration measure dt.

counting, i.e., gauge transformations leave the Lagrangian invariant up to higher power terms. It is convenient to introduce gauge invariant building blocks through [87]

$$\xi_{\rm hc} = W_{\rm hc}^\dagger \xi, \quad \mathcal{A}_{\rm hc}^\mu = W_{\rm hc}^\dagger (i D_{\rm hc}^\mu W_{\rm hc}), \quad i\mathcal{D}_{\rm hc}^\mu = W_{\rm hc}^\dagger i D_{\rm hc}^\mu W_{\rm hc} = i\partial^\mu + \mathcal{A}_{\rm hc}^\mu \,, \tag{4.23}$$

where the brackets indicate that the derivative is only acting on the arguments within the brackets. From the definition of the hard-collinear Wilson line follows that $\bar{n}\cdot\mathcal{A}_{\rm hc} = 0$. This object therefore scales like $(\lambda, 0, \lambda^{-1/2})$. The scaling of the hard-collinear quark field $\xi_{\rm hc}$ is not changed. With these definitions the vertex of a hard-collinear gluon with a hard-collinear and soft quark can be written as

$$\mathcal{L}_{\xi q}^{(1)} = \bar{\xi}_{\rm hc} \mathcal{A}\!\!\!/_{\rm hc} q + \bar{q} \mathcal{A}\!\!\!/_{\rm hc} \xi_{\rm hc} \,, \tag{4.24}$$

which is manifestly gauge invariant at this order.

The Lagrangian (4.14) describes the QCD dynamics of hard-collinear and soft particles. This would be sufficient for the analysis of $\bar{B} \to X_s\gamma$ if the photon was only created at the weak interaction vertices. Since by definition the jet only contains hard-collinear and soft particles (otherwise the invariant mass would not be small) no interactions containing anti-hard-collinear particles would be required. However, at subleading power anti-hard-collinear particles can be created at the weak interaction vertex, which are subsequently converted into a photon. For this conversion it is necessary to introduce the SCET Lagrangian for anti-hard-collinear particles. Its derivation proceeds in exactly the same way as the derivation of the SCET(hc,s) Lagrangian presented above, except that every n and $\bar{n}$ are interchanged. The field ξ will always refer to the large spinor components with an added label n or $\bar{n}$ to indicate the large momentum component. From the definition of the projection operators (4.7) then follows that $\bar{n}\!\!\!/\, \xi_{\bar{n}} = 0$. Also the gauge invariant building blocks $\xi_{\overline{\rm hc}}$ and $\mathcal{A}_{\overline{\rm hc}}^\mu$ are defined analogously to (4.23) by using Wilson lines along the n direction

$$\xi_{\overline{\rm hc}} = W_{\overline{\rm hc}}^\dagger \xi_{\bar{n}}, \quad \mathcal{A}_{\overline{\rm hc}}^\mu = W_{\overline{\rm hc}}^\dagger (i D_{\overline{\rm hc}}^\mu W_{\overline{\rm hc}}). \tag{4.25}$$

In order to implement the photon conversions, the covariant derivatives will also contain the photon field $D = \partial - igA - e_q e A^{\rm em}$. Since the photon is a real particle that moves in the $\bar{n}$-direction only the perpendicular component of the photon field is non-zero and scales like $\lambda^{1/2}$. The complete SCET(hc,$\overline{\rm hc}$,s) Lagrangian is given by the sum of the SCET(hc,s) and SCET($\overline{\rm hc}$,s) Lagrangians. The mixing between the sectors will be considered when matching the weak effective operators from QCD onto SCET.

Although not required in this work, it is mentioned for completeness that the pure gluonic part of QCD can be matched onto SCET in an analogous way [90]. The gluon fields are split into their hard-collinear and soft components with each of the sectors looking the same as in QCD. Interaction terms between the two sectors are restricted by momentum conservation. In the next section the matching of the weak effective operators onto SCET will be performed at leading power in λ. This will lead to an expression, in which the physics of the different scales (4.3) are factorized.

4.3 Factorization at Leading Power

In order to demonstrate the factorization of the differential decay rate, the following steps will be performed. First the effective heavy-to-light operator is matched onto the corresponding SCET operator. Then the differential decay rate is calculated and the emerging non-local operator decomposed into two parts, one of which can be calculated perturbatively the other corresponding to an HQET matrix element. Both matching steps can in principle be performed at any order in α_s at the appropriate scale.

4.3.1 Tree Level Matching

The leading power operator contributing to $\bar{B} \to X_s\gamma$ is derived from $Q_{7\gamma}$ given in (2.17). In order to determine onto which SCET operator $Q_{7\gamma}$ matches exactly, the hard-collinear strange-quark field is decomposed by using Equation (4.8) which at leading power corresponds to the replacement $s \to \xi_n + \mathcal{O}(\lambda)$. Furthermore the field-strength tensor needs to be expanded, leading to

$$Q_{7\gamma} = \frac{-e\overline{m}_b}{8\pi^2}\,\bar{s}\sigma_{\mu\nu}F^{\mu\nu}(1-\gamma_5)b \to \frac{-e\overline{m}_b}{8\pi^2}\,\bar{\xi}_n\, i\frac{\bar{\not{n}}}{2}\, n\cdot\partial \not{A}^{\rm em}_{\perp}(1-\gamma_5)b + \mathcal{O}(\lambda^3)\,, \tag{4.26}$$

where $\overline{m}_b$ is once again the running b-quark mass in the $\overline{\rm MS}$ scheme (see Section 2.2.1). In a second matching step the decay rate will be expressed in terms of a pure HQET matrix element. Thus the b-quark field needs to be replaced by the heavy-quark field h defined in (3.10).

Since the large component of a hard-collinear gluon field scales like λ^0, an arbitrary number of them can be added to any QCD diagram without changing the scaling of that contribution. The effective theory can describe situations where the hard-collinear gluon is emitted from another hard-collinear line. However, when the gluon is emitted from the heavy-quark field, it puts the heavy quark far off-shell (see left diagram in Figure 4.1). These modes are integrated out of the effective theory, which gives rise to an effective

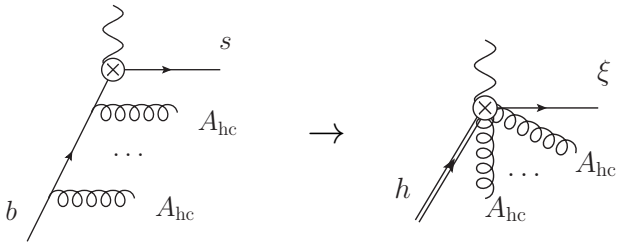

Figure 4.1: Tree-level matching of an heavy-to-light operator. The resummation into a Wilson line includes all gluon permutations in the QCD diagram. The double line corresponds to a heavy-quark field.

operator that emits any number of hard-collinear gluons (right diagram in Figure 4.1). The gluon emissions can be resummed into an eikonal form which just corresponds to the

hard-collinear Wilson line of (4.20). This Wilson line appears to the left of the heavy-quark field, but since it commutes with the photon field, it can be absorbed into the hard-collinear field ξ_n to yield the gauge invariant quantity $\xi_{\rm hc}$. Therefore the sum of all hard-collinear gluon emissions was necessary to generate a gauge invariant operator. At tree level in the strong interaction the operator $Q_{7\gamma}$ therefore matches onto the SCET operator

$$Q_{7\gamma}^{(0)}(x) = \frac{-e\overline{m}_b}{8\pi^2}\, e^{-im_b vx}\bar{\xi}_{\rm hc}(x)\, i\frac{\vec{\not{n}}}{2}\, n\cdot\partial \not{A}_\perp^{\rm em}(x)(1-\gamma_5)h(x_-)\,, \tag{4.27}$$

where the soft field h was multipole expanded as in (4.21) and the superscript (i) on an operator indicates the suppression in powers of $\lambda^{1/2}$ compared to the leading power. When calculating amplitudes containing a heavy-quark field, it is necessary to add the HQET Lagrangian (3.14) to the effective theory Lagrangian of SCET(hc,$\overline{\rm hc}$,s). Due to momentum conservation the HQET Lagrangian only contains soft covariant derivatives D_s. Also, effective operators connecting two or more collinear gluons to the heavy-quark field are not allowed in an effective theory describing the decay of a B-meson into collinear particles [85]. This concludes the tree level matching. Next the effect of virtual corrections will be considered.

4.3.2 Loop Level Matching

Another way to describe the matching performed above is to say that at the tree level the Wilson coefficient of the leading power SCET operator $Q_{7\gamma}^{(0)}$ is just $C_{7\gamma}^{\rm eff}$. At the loop level all QCD diagrams that match onto $Q_{7\gamma}^{(0)}$ (e.g. the first diagram in Figure 4.2) need to be calculated and expanded in powers of λ. The difference to the corresponding effective

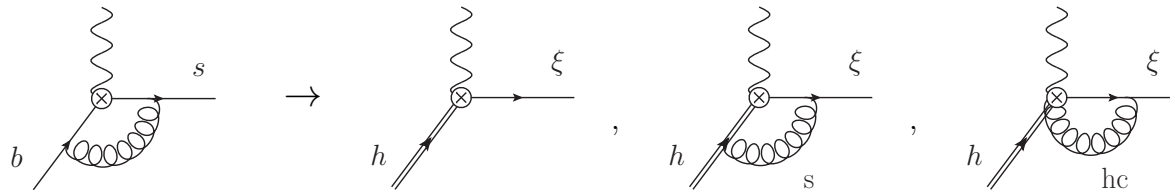

Figure 4.2: At loop level the QCD operator $Q_{7\gamma}$ (on the left) matches onto the SCET diagrams on the right. The gluons in the second and third diagram on the left are soft and hard-collinear, respectively.

theory diagrams (e.g. the other diagrams in Figure 4.2) is accounted for by the Wilson coefficient. In the literature the matching of $Q_{7\gamma}$ onto $Q_{7\gamma}^{(0)}$ is associated with a Wilson coefficient $\mathcal{C}_9$ [7] (not to be confused with the Wilson coefficients of the weak effective

Lagrangian). By evaluating the diagrams in Figure 4.2 this coefficient is calculated to

$$\mathcal{C}_9(\bar{n}\cdot P,\mu) = 1 - \frac{\alpha_s(\mu)C_F}{4\pi}\left[2\ln^2\frac{m_b}{\mu} - 7\ln\frac{m_b}{\mu} + 4\ln\frac{\bar{n}\cdot P}{m_b}\ln\frac{m_b}{\mu}\right.$$
$$\left. +2\ln^2\frac{\bar{n}\cdot P}{m_b} - 2\ln\frac{\bar{n}\cdot P}{m_b} + 2\mathrm{Li}_2\left(1-\frac{\bar{n}\cdot P}{m_b}\right) + \frac{\pi^2}{12} + 6\right], \tag{4.28}$$

where P is the sum of all hard-collinear momenta and μ is the matching scale which must be of the order of the hard scale m_b to keep the logarithms small. The Wilson coefficient depends on the hard-collinear momentum since its large component is of the same order as the hard momenta. It was proven in [7] that gauge invariance requires the Wilson coefficients to depend only on the sum of all hard-collinear momenta instead of each one separately. If the light quark is the only hard-collinear particle in the process, $\bar{n}\cdot P$ is equal to m_b at leading power. Since the Wilson coefficient depends on a momentum that still appears in the matrix element, the terms of the effective Lagrangian need to be represented by a convolution in position space

$$\mathcal{L}^{(0)}_{\text{SCET, eff}} = \frac{G_F}{\sqrt{2}}\,\lambda_t\, C^{\text{eff}}_{7\gamma}(\mu)\int dt\,\tilde{\mathcal{C}}_9(t,\mu)Q^{(0)}_{7\gamma}(x+t\bar{n}) + \dots\,, \tag{4.29}$$

where $\tilde{\mathcal{C}}_9(t,\mu)$ is the Fourier transform of $\mathcal{C}_9(\bar{n}\cdot P,\mu)$, $C^{\text{eff}}_{7\gamma}$ was defined in Section 2.1.5 and the ellipses denote terms originating from other QCD operators that match onto $Q^{(0)}_{7\gamma}$. Due to these terms the complete matching coefficient is given by a sum of products of the weak effective Wilson coefficients C_i and the Wilson coefficients of the matching of QCD onto the SCET operators from [7]. This gives rise to the *hard function* H_γ which is given by [13]

$$\begin{aligned} H_\gamma(\mu_h) =& C^{\text{eff}}_{7\gamma}(\mu_h)\left[1 + \frac{C_F\alpha_s(\mu_h)}{4\pi}\left(-2\ln^2\frac{m_b}{\mu_h} + 7\ln\frac{m_b}{\mu_h} - 6 - \frac{\pi^2}{12}\right)\right] \\ &+ C^{\text{eff}}_{8g}(\mu_h)\frac{C_F\alpha_s(\mu_h)}{4\pi}\left(-\frac{8}{3}\ln\frac{m_b}{\mu_h} + \frac{11}{3} - \frac{2\pi^2}{9} + \frac{2\pi i}{3}\right) \\ &+ C_1(\mu_h)\frac{C_F\alpha_s(\mu_h)}{4\pi}\left(\frac{104}{27}\ln\frac{m_b}{\mu_h} + g(z) + \varepsilon_{\text{CKM}}[g(0)-g(z)]\right), \end{aligned} \tag{4.30}$$

where $\bar{n}\cdot P = m_b$ was used, the matching scale was set to the hard scale $\mu_h \sim m_b$ and $g(z)$ is related to the penguin function (see Appendix A.1) with $z = m_c^2/m_b^2$. Furthermore some small corrections were dropped for brevity and can be taken from Reference [13]. The parameter ε_{CKM} contains a weak phase from the CKM matrix elements that will become important in Chapter 8. Today, the hard function has been explicitly calculated at one loop order and its two loop result has been deduced in [8]. It encodes the effects from hard fluctuations which have been integrated out, while the effective theory reproduces the IR behavior of QCD.

Matching QCD onto SCET was only the first step. In order to achieve a complete separation of scales a second matching step (onto HQET) at a different scale is necessary. The result of this first matching step can be given in terms of the leading power effective Lagrangian mediating the decay $\bar{B} \to X_s\gamma$

$$\mathcal{L}^{(0)}_{\text{SCET, eff}} = \frac{G_F}{\sqrt{2}}\,\lambda_t\, H_\gamma(\mu_h) Q^{(0)}_{7\gamma}(x)\,, \tag{4.31}$$

where the operator $Q^{(0)}_{7\gamma}$ is renormalized at the scale μ_h. This Lagrangian, together with the SCET (4.14) and HQET (3.14) Lagrangians is sufficient to describe $\bar{B} \to X_s\gamma$ at leading power. It will now be used for the calculation of the decay rate.

4.3.3 The Factorization Formula

With the leading power SCET operator at hand, the decay rate for $\bar{B} \to X_s\gamma$ will be calculated for the third time. Due to the systematic power counting of SCET the calculation will naturally lead to the non-local matrix element of Section 3.3.4. Furthermore, the calculation will explicitly demonstrate how the decay rate factorizes into parts, that each contain the physics at a certain scale. This will eventually lead to the resummation of the large logarithms encountered in the partonic calculation. The calculation will once again start from Equation (3.4). The leading power (and leading order in α_s) contribution is made up of two operators $Q^{(0)}_{7\gamma}$ and is illustrated on the left of Figure 4.3. Since cutting the

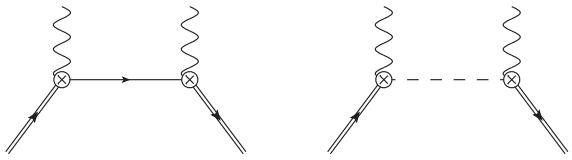

Figure 4.3: Leading power contribution to $\bar{B} \to X_s\gamma$. The left diagram represents the product of SCET operators, while the right diagram depicts the space-time structure of the HQET operator (see text).

photon line does not affect the calculation of the hadronic matrix element, the diagrams will always be drawn with the photon propagator already cut. Here and in the following heavy-quark lines will always be indicated by a double line, while light quarks correspond to single lines. After evaluating the vacuum matrix element of the time-ordered product of photon fields and taking the residue of the photon propagator pole one arrives at

$$\begin{aligned}\frac{d\Gamma}{dE_\gamma} &= \frac{1}{2M_B}\frac{G_F^2\overline{m}_b^2(\mu)\alpha}{4\pi^4}\,|H_\gamma(\mu)\lambda_t|^2 E_\gamma^3\left(-\frac{1}{\pi}\right)\\ &\quad\times \text{Im}\,\langle\bar{B}|i\int d^4x\, e^{i(mv-q)x}\mathbf{T}\{\bar{h}(x_-)\gamma_\perp^\mu(1-\gamma_5)\xi_{\text{hc}}(x)\bar{\xi}_{\text{hc}}(0)\gamma_{\perp\mu}(1-\gamma_5)h(0)\}|\bar{B}\rangle.\end{aligned} \tag{4.32}$$

As there are no hard-collinear particles in the initial or final state, the time-ordered product of the two hard-collinear fields can be perturbatively evaluated between vacuum states.

However, at higher orders in α_s there can be soft gluon interactions between the heavy and hard-collinear lines, making this separate calculation impossible. The solution to this problem is to introduce "sterile" fields with the help of the soft Wilson line in (4.17). One defines

$$\xi_{\rm hc}(x) = S_n(x_-)\xi^{(0)}_{\rm hc}(x), \quad \mathcal{A}^\mu_{\rm hc}(x) = S_n(x_-)\mathcal{A}^{(0)\mu}_{\rm hc}(x)S_n^\dagger(x_-)\,, \tag{4.33}$$

where the label n was added to the soft Wilson line in order to distinguish it from $S_{\bar n}$ which is used in the definition of anti-hard-collinear sterile fields. By using Equation (4.18) it is easy to see that after the introduction of sterile fields the Lagrangian (4.14) no longer mediates soft gluon emissions from hard-collinear particles. This *decoupling transformation* is the basis for an all order factorization proof of the leading power $\bar B \to X_s\gamma$ decay rate. The hard-collinear part of the calculation can be separated from the soft part and since the typical hard-collinear scale is larger than $\Lambda_{\rm QCD}$ it can be perturbatively calculated. This factorization was already proven in [11], but the effective theory approach [12] makes the procedure more transparent. Formally the hard-collinear physics are encoded in the so-called *jet function* $\mathcal{J}$ that can be defined as

$$\langle\Omega|\mathbf{T}\{\xi^{(0)}_{\rm hc}(x)\bar\xi^{(0)}_{\rm hc}(0)\}|\Omega\rangle =: i\int\frac{d^4p}{(2\pi)^4}\,\frac{\bar n\!\!\!/}{2}\,\bar n\cdot p\,\mathcal{J}(p^2)e^{-ipx}\,, \tag{4.34}$$

where Ω is the interacting vacuum and the Dirac structure is determined by the hard-collinear propagator. Inserting this into (4.32) and evaluating the Dirac structures leads to

$$\begin{aligned}\frac{d\Gamma}{dE_\gamma} &= \frac{1}{2M_B}\frac{G_F^2\overline{m}_b^2(\mu)\alpha}{2\pi^4}\,|H_\gamma(\mu)\lambda_t|^2E_\gamma^3\left(-\frac{1}{\pi}\right)\\ &\quad\times{\rm Im}\left[\int d^4x\int\frac{d^4p}{(2\pi)^4}\,e^{i(mv-q-p)x}\bar n\cdot p\,\mathcal{J}(p^2)\langle\bar B|\mathbf{T}\{[\bar hS_n](x_-)[S_n^\dagger h](0)\}|\bar B\rangle\right],\end{aligned} \tag{4.35}$$

where once again parity invariance was used to eliminate the axial vector part. By using the transformations

$$[hS_n]\left(\frac{n}{2}\bar n\cdot x\right) = \int dt\,\delta\left(\frac{\bar n\cdot x}{2}-t\right)[hS_n](tn) = \int d\omega\,e^{i\omega\frac{\bar n x}{2}}\int\frac{dt}{2\pi}\,e^{-i\omega t}[hS_n](tn)\,, \tag{4.36}$$

it is possible to perform the x and p integrations in (4.35) which leads to

$$\begin{aligned}\frac{d\Gamma}{dE_\gamma} &= \frac{1}{2M_B}\frac{G_F^2\overline{m}_b^2(\mu)\alpha}{2\pi^4}\,|H_\gamma(\mu)\lambda_t|^2E_\gamma^3\left(-\frac{1}{\pi}\right)\\ &\quad\times{\rm Im}\left[\int d\omega\,m_b\,\mathcal{J}(m_b(m_b-2E_\gamma+\omega))\int\frac{dt}{2\pi}\,e^{-i\omega t}\langle\bar B|[\bar hS_n](tn)[S_n^\dagger h](0)|\bar B\rangle\right],\end{aligned} \tag{4.37}$$

where the time-ordering symbol was dropped since the HQET fields only create and destroy quarks and their ordering is already dictated by the propagator. It is now useful to define the leading power shape function by

$$S(\omega) := \frac{1}{2M_B}\int\frac{dt}{2\pi}\,e^{-i\omega t}\langle\bar B|[\bar hS_n](tn)[S_n^\dagger h](0)|\bar B\rangle. \tag{4.38}$$

The product of the soft Wilson lines $S_n(tn)S_n^\dagger(0) = [tn, 0]$ is a straight line segment connecting the points tn and 0, with gauge fields closer to the point tn standing to the left of those closer to 0. This finite Wilson line guarantees gauge invariance of the non-local operator. The HQET operator is depicted on the right of Figure 4.3 with a dashed line indicating the finite Wilson line. By taking the complex conjugate of the shape function and using translational invariance, one can show that the shape function is real. Thus the imaginary part prescription in (4.37) only acts on the jet function $\mathcal{J}$ which suggests the definition of a new quantity J that will from now on be called jet function

$$J(p^2) = -\frac{1}{\pi}\mathrm{Im}\,\mathcal{J}(p^2). \tag{4.39}$$

This leads to the fully factorized expression for the leading power differential $\bar{B} \to X_s\gamma$ decay rate

$$\frac{d\Gamma}{dE_\gamma} = \frac{G_F^2\overline{m}_b^2(\mu)\alpha}{2\pi^4}\,|H_\gamma(\mu)\lambda_t|^2 E_\gamma^3 \int_{-p_+}^{\bar{\Lambda}} d\omega\, m_b\, J(m_b(p_+ + \omega))S(\omega)\,, \tag{4.40}$$

where $\bar{\Lambda} = M_B - m_b$ and $p_+ = m_b - 2E_\gamma$. The lower limit of integration is derived from the start of the branch cut (or pole in case of a single particle jet) of the jet function in the complex p^2-plane. The upper limit on the other hand follows from the definition of $\omega = n \cdot k$ and

$$n \cdot P_B > n \cdot p_b \Leftrightarrow M_B > m_b + \omega\,, \tag{4.41}$$

where P_B and p_b are the B-meson and b-quark momenta, respectively. At leading power, $\bar{\Lambda}$ can be set to zero. The shape function defined in (4.38) corresponds to the shape function of Section 3.3.4 which can be shown explicitly by using Equation (4.18) and $S_n(0)S_n^\dagger(0) = 1$ and by writing

$$\begin{aligned}\int \frac{dt}{2\pi}\, e^{-i\omega t}\langle\bar{B}|[\bar{h}S_n](tn)[S_n^\dagger h](0)|\bar{B}\rangle &= \int \frac{dt}{2\pi}\, e^{-i\omega t}\langle\bar{B}|[\bar{h}S_n](0)e^{tn\cdot\overleftarrow{\partial}}[S_n^\dagger h](0)|\bar{B}\rangle \\ &= \langle\bar{B}|\bar{h}(0)\,\delta(\omega - n\cdot\overleftarrow{D})h(0)|\bar{B}\rangle\,,\end{aligned} \tag{4.42}$$

which is equal to the earlier definition by translation invariance. However, this time the shape function arose naturally at leading power in the expansion in λ and no resummation of terms was required. Furthermore, the extension to higher orders in α_s is well defined. The problem posed in the conclusions of Chapter 3 is therefore solved.

The factorization formula (4.40) can also be used to solve the issue of the large logarithms encountered in the partonic calculation. They appeared because not all relevant scales were separated and their ratios could generate large numbers. With the factorization formula at hand, it is now possible to calculate the matching coefficients each at their natural scale and subsequently evolve them to a common scale by using the renormalization group equations. The matching of the hard functions at the hard scale was already discussed above in Section 4.3.2. The matching of the jet function will be the next topic.

4.3.4 Matching the Jet Function

At tree level, the jet function J is related to the propagator of the hard-collinear particle. Taking the imaginary part, the jet function J is calculated to

$$J(m_b(p_+ + \omega)) = \delta(m_b(p_+ + \omega)). \tag{4.43}$$

Inserting this into the decay rate (4.40) leads to the leading power and leading order expression already derived in Section 3.3.4. At NLO the usual procedure is applied of calculating full theory diagrams (in this case SCET) as well as effective theory diagrams (HQET) and absorbing the differences into the Wilson coefficients, i.e., the jet function. The relevant diagrams are given in Figure 4.4. Once again, HQET reproduces the IR

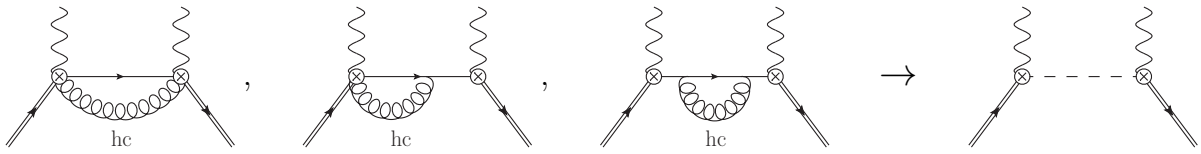

Figure 4.4: NLO matching of the SCET decay rate onto HQET. The mirror of the second diagram is not shown.

behavior of the full theory. This particularly includes the soft gluon corrections to the SCET diagrams [1]. The NLO calculation has been performed in [1, 91] and leads to the renormalized jet function

$$\begin{aligned} m_b\, J(m_b(p_+ + \omega), \mu_i) = \delta(p_+ + \omega) \left[1 + \frac{C_F \alpha_s(\mu_i)}{4\pi} \left(7 - \pi^2\right)\right] \\ + \frac{C_F \alpha_s(\mu_i)}{4\pi} \left[\frac{1}{p_+ + \omega} \left(4 \ln \frac{m_b(p_+ + \omega)}{\mu_i^2} - 3\right)\right]_*^{[\mu_i^2/m_b]} \end{aligned} \tag{4.44}$$

that was matched at the intermediate scale μ_i. The star distributions are generalized plus distributions (compare Section 2.2.1) and were introduced in [92]. Note, that if the logarithm in (4.44) is evaluated at a soft scale $\mu_i \sim p_+$ it relates to the problematic large logarithms of Equation (2.33). It is an advantage of the factorization that the scale μ_i can be set to the more appropriate value of $\mathcal{O}(\sqrt{\Lambda_{\text{QCD}} m_b})$. Just like the hard functions, the jet functions are known at two-loop order [93]. After performing the two matching steps and separating all the scales of the problem it is now possible to determine the RG running of the quantities involved in the calculation. This will be the topic of the next Section.

4.4 Renormalization Group Running

Although somewhat outside the main line of this work, the procedure of resumming the large logarithms will be briefly reviewed in order to further motivate the usage of the effective theory. So far the decay rate has been factorized into three components, that

each encode the physics at a certain scale. In the first matching step from QCD to SCET the hard function H_γ appeared as the Wilson coefficient. If the matching is performed at the hard scale $\mu_h \sim m_b$ it contains no large logarithms and the one-loop result is given in (4.30). The second matching step from SCET onto non-local HQET operators needs to be performed at the intermediate scale $\mu_i \sim \sqrt{\Lambda_{\rm QCD} m_b}$, where the logarithms are again small. This leads to the one-loop result in (4.44). The typical scale of the remaining soft matrix element is of order $\Lambda_{\rm QCD}$. Thus, it can not be calculated perturbatively but must be modeled [2] and the model parameters related to experimental quantities. As was discussed in Section 3.3.4 the leading power shape function can be extracted from the form of the photon spectrum. The modeling must be performed at the soft scale $\mu_0 \sim \Lambda_{\rm QCD}$. By using the RG equations the three results can be evolved to a common scale (compare Section 2.1.3), which cancels the dependence of the decay rate on the hard and intermediate scales. Explicitly one proceeds as follows. First the hard function is determined at the hard scale and evolved down to the intermediate scale by solving

$$\frac{d}{d\ln\mu} H_\gamma(\bar n\cdot p,\mu) = \gamma_J(\bar n\cdot p,\mu) H_\gamma(\bar n\cdot p,\mu)\,, \tag{4.45}$$

where γ_J is the anomalous dimension of the heavy-to-light SCET current. Due to the simple Dirac structure of the leading power SCET Lagrangian (4.14) the anomalous dimension is the same for all type of Dirac structures in the current. Next one starts with a model of the shape function at the soft scale and evolves it up to the intermediate scale by solving the integro-differential evolution equation

$$\frac{d}{d\ln\mu} S(\omega,\mu) = -\int d\omega'\, \gamma_S(\omega,\omega',\mu) S(\omega',\mu). \tag{4.46}$$

Since the shape function is related to a non-local operator it is renormalized by a convolution, instead of multiplicatively.

The anomalous dimension γ_J can be determined from the singularities of the diagrams on the right of Figure 4.2 (in addition to the diagrams necessary to calculate the field-strength renormalization). At the leading order it can be written as [7, 94]

$$\gamma_J(\bar n\cdot p,\mu) = -\Gamma_{\rm cusp}(\alpha_s)\ln\frac{\mu}{\bar n\cdot p} + \gamma'(\alpha_s) = \frac{C_F\alpha_s}{\pi}\left(-\ln\frac{\mu}{\bar n\cdot p} - \frac{5}{4}\right) + \dots\,, \tag{4.47}$$

where $\Gamma_{\rm cusp}$ is the universal cusp anomalous dimension governing the UV singularities of Wilson lines with light-like segments [95]. Therefore the solution to the RG equation is given by

$$H_\gamma(\bar n\cdot p,\mu_i) = \exp\int_{\alpha_s(\mu_h)}^{\alpha_s(\mu_i)} \frac{d\alpha}{\beta(\alpha)}\left[\Gamma_{\rm cusp}(\alpha)\left(\ln\frac{\bar n\cdot p}{\mu_h} - \int_{\alpha_s(\mu_h)}^{\alpha}\frac{d\alpha'}{\beta(\alpha')}\right) + \gamma'(\alpha)\right] H_\gamma(\bar n\cdot p,\mu_h) \tag{4.48}$$

where $\beta(\alpha)$ is the QCD β-function. The cusp anomalous dimension has so far been derived up to three-loop order [96], while a conjecture for the two-loop expression of γ' has been suggested in [13].

In order to determine the anomalous dimension γ_S of the shape function one has to calculate the HQET amplitudes from the diagrams in Figure 4.5. Of course, a perturbative

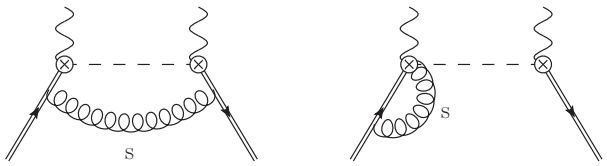

Figure 4.5: Diagrams relevant for the calculation of the shape function anomalous dimension. A mirror diagram of the second graph is not shown.

calculation of the hadronic operators will not yield a realistic result for the functional form of the shape function. However, the UV behavior, i.e., the μ dependence of the shape function may be determined that way. The one-loop calculation of γ_S as well as a review of earlier calculations has been presented in [1]. There, the result is given as

$$\gamma_S(\omega,\omega',\mu) = \frac{C_F\alpha_s}{\pi}\left[\left(2\ln\frac{\mu}{\bar{\Lambda}-\omega}-1\right)\delta(\omega-\omega') - 2\left(\frac{\theta(\omega'-\omega)}{\omega'-\omega}\right)_+\right], \tag{4.49}$$

which leads to the following solution of the RG equation

$$S(\omega,\mu_i) = e^{V_S(\mu_i,\mu_0)}\frac{1}{\Gamma(\eta)}\int_{\bar{\Lambda}-\omega}^{0} d\omega' \frac{S(\omega',\mu_0)}{\mu_0^{\eta}(\omega'-\omega)^{1-\eta}}, \tag{4.50}$$

where η is an integral over the cusp anomalous dimension and together with the evolution function V_S is defined in [1]. Improving on this calculation, a two-loop analysis was performed in [97].

Using Equations (4.48) and (4.50) all quantities in the factorized decay rate (4.40) can be calculated at their appropriate scale and then run to a common scale, thereby eliminating the scale dependencies on μ_i and μ_h. This running resums the large leading logs that appeared in the partonic calculation. Thus, the problem stated in the conclusions of Chapter 2 is solved.

4.5 Conclusions of this Chapter

This chapter analyzed the differential $\bar{B} \to X_s\gamma$ decay rate at leading power in the SCET expansion. It was shown that the effective theory approach using SCET could be used to write down a factorization theorem for the leading power decay rate. Schematically it can be represented as

$$d\Gamma(\bar{B} \to X_s\gamma) \sim H\, J \otimes S \tag{4.51}$$

where H is the hard function, J the jet function and S the shape function each encoding the physics at their respective scales. The symbol $\otimes$ denotes a convolution. This approach solved the two major issues worked out in the previous chapters. On the one

hand, the factorization of the leading power decay rate allowed for the resummation of the large logarithms appearing in the partonic calculation of Chapter 2. On the other hand the systematic power counting naturally introduced the shape function of Chapter 3 and extended the definition to any order in α_s. The framework presented in this chapter points out two possible directions for improvements. First, the perturbative calculations can always be pushed to some higher order. However, since these calculations have already been performed at the NNLO [93, 97], the next step is the extension of the analysis to the next order in the power counting. This will be the topic of the next chapter.

Chapter 5

Subleading Contributions in SCET

Historically, the first SCET analysis beyond the leading power dealt with the $1/m_b$ suppressed contributions due to two operator insertions of the electromagnetic dipole operator $Q_{7\gamma}$. This chapter will on the one hand review the well-known results of this analysis and on the other hand set the basis for an extension of the formalism to include any operator insertions beyond the leading power. For this it is necessary to discuss the general procedure of determining the relevant SCET operator basis in Section 5.1. As a first application of this procedure the suppressed SCET operators deriving from $Q_{7\gamma}$ will be derived in Section 5.2.1. Inserting these operators into the formula for the decay rate and matching the result onto HQET leads to a factorization theorem at subleading power. At this order the subleading jet and shape functions arise, which are discussed in Section 5.2.3 and 5.2.4. Concluding the discussion of the $Q_{7\gamma} - Q_{7\gamma}$ interference, the results will be related to the QCD calculation.

When other operator interferences are considered, anti-hard-collinear fields play an important role. It is due to their appearance that a distinction between "direct" and "resolved" photon contributions can be made. These concept, along with the derivation of a general factorization theorem will be discussed in Section 5.3. In the last section of this chapter the subleading SCET operators, relevant for the resolved photon contributions will be derived from the QCD effective operators. A complete list of the subleading operators, some of which are required for the direct photon contributions, will be given in Appendix B.

5.1 Matching onto SCET

The previous chapter introduced the leading power heavy-to-light SCET operator (4.27) that was shown to scale like $\lambda^{5/2}$. It was found that at tree level only the QCD operator $Q_{7\gamma}$ (see (2.17)) has a non-vanishing matching coefficient. At the loop level, there are also contributions from Q_{8g} and Q_1^q as well as from the penguin operators $Q_{3\ldots6}$ which were absorbed into the effective Wilson coefficient $C_{7\gamma}^{\text{eff}}$ (see (4.30)). This chapter will deal with SCET operators beyond the leading power. The ultimate goal is to calculate the $\bar{B} \to X_s\gamma$ differential decay rate at subleading power, i.e., including contributions suppressed by $1/m_b$

compared to the leading power. Since the decay rate contains at least two SCET operator insertions, it is necessary to find the operators that are suppressed by $\lambda^{1/2}$ (denoted with a superscript (1)) as well as those suppressed by λ (denoted with a superscript (2)) compared to the leading power.

Once again, the possible SCET operators can be determined by starting from the QCD operators and replacing each field by its SCET counterpart. Afterwards the operator is expanded in powers of λ. Further suppressed operators are introduced by considering time ordered products of effective QCD operators and QCD Lagrangian insertions and integrating out the internal lines not present in SCET. One example was already given in Figure 4.1. There, the heavy quark emitted an arbitrary number of hard-collinear gluons, that put the heavy quark far off-shell. These off-shell modes were integrated out of the effective SCET+HQET Lagrangian, leading to a single leading power operator that contained the large components of the hard-collinear gluons resummed into a Wilson line. Beyond leading power the SCET operator may also contain the smaller components of hard-collinear gluons. However, since they scale with a higher power of λ it would make no sense to resum them into eikonal form. Thus, only a limited number of them are emitted from the heavy-quark line, which is thereby put off-shell. It was already demonstrated in Section 3.2 that integrating out this off-shell mode corresponds to solving the classical equation of motion of the off-shell field. This time it is not the small component of a nearly on-shell heavy quark that is integrated out, but the far off-shell component. Following References [10, 85] one decomposes the QCD heavy-quark field into a nearly on-shell and a far off-shell part

$$b(x) = e^{-imv\cdot x}\big(b_v^{\text{on}}(x) + b_v^{\text{off}}(x)\big), \tag{5.1}$$

inserts this into the QCD Lagrangian and solves the equation of motion for b_v^{off} which formally leads to

$$b_v^{\text{off}} = -\frac{1}{i\not{D} - m(1-\not{v})} g\not{\mathcal{A}}_{\text{hc}} b_v^{\text{on}}. \tag{5.2}$$

The nearly on-shell part b_v^{on} can be further decomposed into a large component spinor h and a small component spinor H as was done in (3.10). By explicitly solving this equation order by order in λ and introducing the gauge invariant building blocks (4.23) it is possible to write down the necessary replacement, that derives the SCET operator from the corresponding QCD operator. Writing down only the terms relevant for $\bar{B} \to X_s\gamma$, one finds

$$b \to W_{\text{hc}}\Big[1 - \frac{\not{n}}{2m_b}\not{\mathcal{A}}_{\text{hc}\perp} + \frac{i\not{D}_s}{2m_b} - \frac{\not{n}\not{\bar{n}}}{4m_b} n\cdot\mathcal{A}_{\text{hc}} - \frac{1}{i\bar{n}\cdot\partial}\, n\cdot\mathcal{A}_{\text{hc}} - \frac{1}{m_b}\frac{1}{i\bar{n}\cdot\partial}\, i\partial\!\!\!/_\perp \not{\mathcal{A}}_{\text{hc}\perp} + \ldots,\Big] h \tag{5.3}$$

where operators containing more than one hard-collinear gluon have been dropped, since they are not required for the matching performed in this work. By the power counting rules of Section 4.1 the first term on the right hand side is of order $\lambda^{3/2}$, the second of order λ^2 while the rest is of order $\lambda^{5/2}$. In general, it is also possible that the anti-hard-collinear photon is emitted from the heavy-quark line. In that case the hard-collinear quark field is replaced by the photon field, with the corresponding interchanges of n and $\bar{n}$. As usual, the $+i\varepsilon$ prescription regulating the inverse derivatives is not explicitly shown.

The expansion for a hard-collinear quark field can also be obtained by writing down time ordered products of QCD operators with gluon emissions from the hard-collinear line and integrating out the appropriate internal lines. For the case of hard-collinear gluon emissions this leads to

$$\psi_{\rm hc} \to W_c\big[1 - \frac{1}{i\bar{n}\cdot\partial}\frac{\bar{n}\!\!\!/}{2}\, i\mathcal{D}\!\!\!/_\perp\big]\xi_{\rm hc}\,, \tag{5.4}$$

where the first term on the right hand side is of order $\lambda^{1/2}$ and the second of order λ. The analogous relation applies to the anti-hard-collinear quark field. If a photon is emitted from the light quark field, the perpendicular covariant derivative is replaced by a photon field.

After the above expansions have been inserted into the heavy-to-light operator, all soft fields must be multipole expanded as given in (4.21). Furthermore all vector fields can be decomposed in the usual way (3.22). With this procedure it is an easy task to determine the relevant operators up to $\lambda^{7/2}$. The matching onto the SCET operators will be performed at the leading order in the strong coupling constant g. Therefore the Wilson coefficients of the QCD to SCET matching step are just products of the Wilson coefficients C_i of the weak effective Lagrangian (see Section 2.1.5). In order to describe $\bar{B} \to X_s\gamma$, each operator must contain at least one hard-collinear particle which will be part of the jet, as well as one anti-hard-collinear particle, either the photon or light partons that can be converted into a photon and soft partons. Anti-hard-collinear particles can not be part of the final state jet, since this would imply an invariant mass of $\mathcal{O}(m_b)$ which is excluded by definition. In principle the operator can contain any number of hard-collinear and soft particles that is consistent with the desired order in the power counting. In the following, all the operators relevant for $\bar{B} \to X_s\gamma$ will be considered. It was explained in Section 2.1.5 and 2.2.1 that the operators Q_1^q, $Q_{7\gamma}$ and Q_{8g} are the most relevant. The next section will deal with the SCET operators descending from the QCD operator $Q_{7\gamma}$.

5.2 The Subleading $Q_{7\gamma} - Q_{7\gamma}$ Contribution

Before dealing with the subleading operators on more general grounds, the contribution due to the electromagnetic dipole operator $Q_{7\gamma}$ will be considered in detail. Although already introducing some new concepts (subleading jet and shape functions), it only represents a certain type of contribution (direct). The detailed discussion of all possible types will be postponed to the next section.

5.2.1 Tree Level Matching

By using the replacement rules of the last section it is possible to determine the SCET operators that the QCD operator $Q_{7\gamma}$ matches onto at tree level. At higher orders in α_s other QCD operators may also match onto these SCET operators. Furthermore, new operators can be introduced by radiative corrections. In order to determine the full set of operators at a certain order in the power counting, a more systematic approach is necessary.

In [98,99] reparameterization invariance (redefinition of the light-cone vectors) of SCET as well as the invariance under the SCET gauge transformations was used to perform this task. At tree level, $Q_{7\gamma}$ matches onto the leading power operator already given in (4.27). Beyond leading power it matches onto a set of operators already given in [85]. Suppressing a factor $-\frac{em_b}{4\pi^2}\, e^{-im_b\, v\cdot x}$ and assuming an external photon with a momentum in the n-direction one finds

$$\begin{aligned} Q_{7\gamma A}^{(1)} &= \bar\xi_{\rm hc}\, \frac{\bar n\!\!\!/}{2}\, [in\cdot\partial A\!\!\!/_\perp^{\rm em}]\,(1+\gamma_5)\, x_\perp^\mu D_\mu h\,, \\ Q_{7\gamma A}^{(2)} &= \bar\xi_{\rm hc}\, \frac{\bar n\!\!\!/}{2}\, [in\cdot\partial A\!\!\!/_\perp^{\rm em}]\,(1+\gamma_5)\left[\frac{n\cdot x}{2}\bar n\cdot Dh + \frac{x_\perp^\mu x_\perp^\nu}{2} D_\mu D_\nu h + \frac{i\not{D}}{2m_b}\, h\right], \end{aligned} \tag{5.5}$$

and

$$\begin{aligned} Q_{7\gamma B}^{(1)} &= \bar\xi_{\rm hc}\, \frac{[in\cdot\partial A\!\!\!/_\perp^{\rm em}]}{m_b}\, g\, \mathcal{A}\!\!\!/_{\rm hc\perp}(1+\gamma_5)h\,, \\ Q_{7\gamma B}^{(2)} &= -\bar\xi_{\rm hc}\, \frac{\bar n\!\!\!/}{2}\, [in\cdot\partial A\!\!\!/_\perp^{\rm em}]\,(1+\gamma_5)\, \frac{1}{i\bar n\cdot\partial}\, g\, n\cdot\mathcal{A}_{\rm hc} h + \bar\xi_{\rm hc}\, \frac{[in\cdot\partial A\!\!\!/_\perp^{\rm em}]}{m_b}\, g\, n\cdot\mathcal{A}_{\rm hc}(1-\gamma_5)h \\ &\quad + \bar\xi_{\rm hc} \frac{[in\cdot\partial A\!\!\!/_\perp^{\rm em}]}{m_b}\, g\, \mathcal{A}\!\!\!/_{\rm hc\perp}(1+\gamma_5) x_\perp^\mu D_\mu h \\ &\quad - \bar\xi_{\rm hc}\, \frac{\bar n\!\!\!/}{2}\, [in\cdot\partial A\!\!\!/_\perp^{\rm em}]\,(1+\gamma_5)\, \frac{1}{i\bar n\cdot\partial}\, \frac{(i\partial\!\!\!/_\perp\, g\, \mathcal{A}\!\!\!/_{\rm hc\perp})}{m_b} h\,, \end{aligned} \tag{5.6}$$

where the covariant derivative D^μ only contains soft fields. The operators are separated into an "A" and "B" group depending on whether they contain hard-collinear gluon fields or not. As usual, the soft fields depend on x_- while the hard-collinear fields depend on x. The $+i\varepsilon$ prescription of the inverse derivative is not explicitly given. Since every operator deriving from $Q_{7\gamma}$ already contains the photon, there is no room for further anti-hard-collinear particles. With these operators it is now possible to calculate the decay rate using the effective theory.

5.2.2 Factorization and the Decay Rate

The subleading contribution to the $\bar B \to X_s\gamma$ decay rate due to insertions of the operator $Q_{7\gamma}$ (henceforth called $Q_{7\gamma} - Q_{7\gamma}$ contribution) can now be determined by inserting (5.5) and (5.6) into the decay rate formula (3.4). In addition, insertions of the SCET or HQET Lagrangians are possible. It turns out that the product of a leading power operator and an operator suppressed by $\lambda^{1/2}$ vanishes due to chirality and the fact that the heavy-to-light operators contain only left handed particles [10]. Therefore the first correction to the leading power decay rate is suppressed by $\lambda \sim 1/m_b$. If expressed in absolute powers of λ the leading power operators are of order $\lambda^{5/2}$, which implies that operators with a scaling of λ^3 and $\lambda^{7/2}$ are needed to determine the subleading decay rate. Schematically

the following operator insertions contribute at subleading power

$$Q_i^{(0)}Q_j^{(2)}, \quad Q_i^{(1)}Q_j^{(1)}, \quad Q_i^{(0)}Q_j^{(0)}\int d^4x\mathcal{L}^{(2)}, \quad Q_i^{(0)}Q_j^{(1)}\int d^4x\mathcal{L}^{(1)},$$
$$Q_i^{(0)}Q_j^{(2)}\int d^4x\mathcal{L}^{(0)}, \quad Q_i^{(0)}Q_j^{(0)}\int d^4x\mathcal{L}^{(1)}\int d^4x\mathcal{L}^{(1)}\,, \tag{5.7}$$

as well as the mirror contributions and with $i = j = 7\gamma$. Since all operators deriving from $Q_{7\gamma}$ already contain a photon field, no further anti-hard-collinear fields are allowed. Thus the matrix element in the decay rate (3.4) has the generic form

$$\mathrm{Disc}\langle\bar{B}|\bar{h}(x)[\phi_{\mathrm{s}}(x_i)\ldots\phi_{\mathrm{hc}}(y_i)\ldots]h(0)|\bar{B}\rangle\,, \tag{5.8}$$

where ϕ_{s} and ϕ_{hc} are soft and hard-collinear fields respectively. If they originate from an operator their position argument will be either x (or x_-) or 0. If they originate from a Lagrangian insertion, they can be located at any point along the n light-cone between the two heavy-quark fields. When matching onto HQET, the hard-collinear fields are integrated out, while the soft fields remain in the matrix element. Thus there must be at least two hard-collinear fields in the square brackets, whereas the number of soft fields is only constrained by the power counting. So far the soft and hard-collinear fields can still interact via the exchange of soft gluons. However, just as in the leading power case in Section 4.3.3, the hard-collinear fields may be decoupled by the introduction of the soft Wilson lines. The matrix element therefore factorizes into a hard-collinear and a soft part

$$\langle\bar{B}|\bar{h}(x_-)[\phi_{\mathrm{s}}(x_{i-})\ldots]h(0)|\bar{B}\rangle\times\mathrm{Disc}\langle\Omega|\phi_{\mathrm{hc}}^{(0)}(y_i)\ldots|\Omega\rangle\,, \tag{5.9}$$

thereby proving a factorization formula for the subleading contribution due to two insertions of $Q_{7\gamma}$. The soft Wilson lines introduced by the decoupling transformation still reside in the soft matrix element. In analogy to the procedure at leading power, a jet function can be defined by the Fourier transform of the discontinuity of the vacuum matrix element of the hard-collinear fields. At the leading power, the non-locality of the soft matrix element leads to a convolution of the jet and soft function. Since the additional soft fields in the subleading matrix element introduce even more non-localities one might expect multi-dimensional convolution integrals. By using partial-fraction identities on the hard-collinear propagators connecting the soft fields it was shown in [100] that there is in fact only one convolution integral in the case of the tree-level $Q_{7\gamma} - Q_{7\gamma}$ interference. However, as will be demonstrated in Chapter 6 multi-dimensional convolution integrals do appear for other operator combinations at the subleading power.

In general, the subleading contributions to the decay rate can be divided into two types. One type contains operator insertions that are suppressed by the small components of additional hard-collinear fields or their derivatives. The other type is suppressed by additional soft fields. They will be considered in turn.

5.2.3 The Subleading Jet Functions

First the case of additional hard collinear fields will be analyzed. One example of such a contribution is given by two insertions of the operator $Q_{7\gamma B}^{(1)}$ of Equation (5.6) which leads

to an α_s/m_b suppressed contribution and is depicted on the left of Figure 5.1. Another

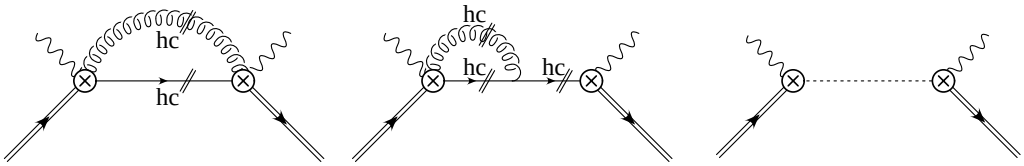

Figure 5.1: Subleading SCET diagrams containing hard-collinear loops. The short double lines indicate possible cuts (recall that the photon lines are already drawn cut). The diagram to the right represents the non-local HQET operator remaining after integrating out the hard-collinear fields.

contribution of this type (depicted in the second diagram of Figure 5.1) is generated by the interference of the leading power $Q_{7\gamma}^{(0)}$ with the suppressed $Q_{7\gamma B}^{(2)}$ plus an insertion of the leading power SCET Lagrangian (4.14). Since there are no additional soft fields in these examples, they both match onto an HQET matrix element that is of the same form as the one at leading power (its space-time structure is depicted in the third diagram of Figure 5.1). The jet function on the other hand will contain additional hard-collinear fields. The factorization formula can therefore symbolically be written as

$$d\Gamma(\bar{B} \to X_s\gamma) \sim \frac{1}{m_b} \sum_i H\, j_i \otimes S\,, \tag{5.10}$$

where H is the hard function (corresponding to $|C_{7\gamma}(\mu)|^2$ in the case of tree level matching), S is the leading power shape function introduced in Section 4.3.3, j_i are the so-called *subleading jet functions* and the symbol $\otimes$ denotes a convolution. There are several different subleading jet functions corresponding to the different terms in Equation (5.6), all of which have been calculated in [101]. In general they are divergent quantities and need to be renormalized at the intermediate scale μ_i. This scale dependence cancels with the scale dependence of the subleading soft functions which can be determined by considering the one-loop corrections. The sum of all renormalized subleading jet functions is given as

$$j(p^2, \mu_i) = \frac{C_F \alpha_s(\mu_i)}{4\pi} \left(16 \ln \frac{p^2}{\mu_i^2} + 25 - 16 c_{\mathrm{RS}}\right) \theta(p^2)\,, \tag{5.11}$$

where c_{RS} is a constant depending on the renormalization scheme whose importance will become apparent later on (Section 5.2.5). It vanishes in the $\overline{\mathrm{MS}}$ scheme and is 1 in the dimensional reduction scheme which corresponds to evaluating all Dirac structures in $d = 4$ dimensions, while loop integrals are evaluated with $d = 4 - 2\varepsilon$. The step function θ is introduced by taking the imaginary part of the hard-collinear correlation function. This result only applies if the SCET operators are matched at tree level. If the hard functions are determined at NLO, additional subleading jet functions suppressed by $\alpha_s(\mu_h)\alpha_s(\mu_i)/m_b$ are to be expected. In conclusion, the subleading $Q_{7\gamma} - Q_{7\gamma}$ jet function contribution to

the decay rate is given by

$$\frac{d\Gamma_{77}^{\rm SJF}}{dE_\gamma} = \frac{G_F^2 \overline{m}_b^2(\mu)\alpha}{2\pi^4} |C_{7\gamma}^{\rm eff}(\mu)\lambda_t|^2 E_\gamma^3 \frac{1}{m_b} \int_{-p_+}^{\bar\Lambda} d\omega\, m_b\, j(m_b(p_+ + \omega),\mu) S(\omega,\mu). \tag{5.12}$$

where j is given in (5.11). When integrating the differential decay rate over a range much larger than the endpoint region, the leading shape function may be approximated by the first term its moment expansion (3.38). It is then possible to perform the integration over the terms of the subleading jet function by using

$$\begin{aligned} \int_{E_0 \ll M_B}^{\frac{M_B}{2}} dE_\gamma\, 1 &\approx \frac{1}{2}(m_b - 2E_0)\,, \\ \int_{E_0 \ll M_B}^{\frac{M_B}{2}} dE_\gamma\, \ln\frac{m_b(m_b-2E_\gamma)}{\mu_i^2} &\approx \frac{1}{2}(m_b-2E_0)\left(\ln\frac{m_b(m_b-2E_0)}{\mu_i^2} - 1\right), \end{aligned} \tag{5.13}$$

where the approximate expressions on the right are valid up to $\mathcal{O}(1/(m_b-2E_0)^2)$ (see Section 3.3.4). It follows that the subleading jet function contributions are promoted to leading power in the limit $E_0 \to 0$ which is consistent with the observation that power corrections to the total rate due to $Q_{7\gamma} - Q_{7\gamma}$ interference appear only at $\mathcal{O}(1/m_b^2)$. The other subleading contributions due to insertions of $Q_{7\gamma}$ originate from additional soft fields in the matrix elements. These will be considered now.

5.2.4 The Subleading Shape Functions

In contrast to the subleading jet functions, subleading contributions due to additional soft fields (or derivatives) in the SCET operators already appear at tree level. The relevant diagrams for the $Q_{7\gamma} - Q_{7\gamma}$ interference are given in Figure 5.2. The first diagram in the top

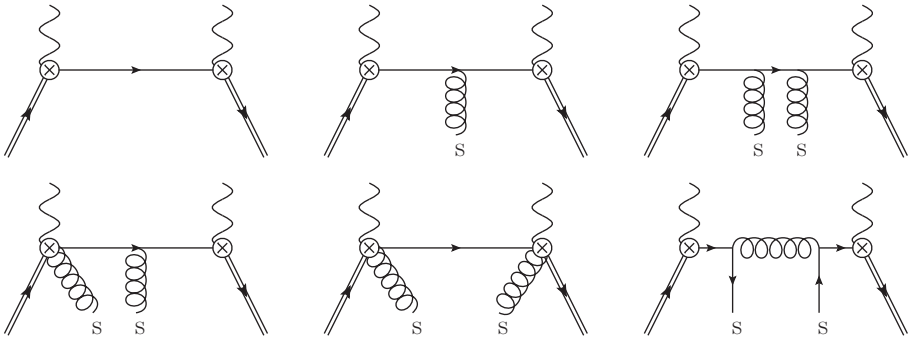

Figure 5.2: Examples for diagrams contributing at subleading power due to additional soft fields or derivatives of soft fields (first diagram).

row might represent the product of two times the first term of $Q_{7\gamma A}^{(1)}$ with the additional soft derivative responsible for the suppression, or the interference of the leading power operator

with $Q^{(2)}_{7\gamma A}$. The second diagram of the top row contains the insertion of a power suppressed SCET interaction term. Due to the additional gluons these contributions contain a factor $g^2 = 4\pi\alpha_s$.

In References [9,10,100] it was proven that contributions of this type obey a factorization formula that can be schematically represented as

$$d\Gamma(\bar{B} \to X_s\gamma) \sim \frac{1}{m_b} \sum_i H\, J \otimes s_i\,, \tag{5.14}$$

where J is the leading power jet function (4.43) and s_i are the *subleading shape functions*. These shape functions correspond to non-local HQET matrix elements that contain additional soft fields or derivatives compared to the leading power shape function. Using the notation of [100] the first five diagrams in Figure 5.2 introduce the following non-local HQET operators defining the subleading shape functions.

$$\begin{aligned}
s(\omega) &= m_b \int \frac{dt}{2\pi}\, e^{-i\omega t} \int d^4z\, \frac{\langle \bar{B}|\mathbf{T}\{(\bar{h}S_n)(tn)(S_n^\dagger h)(0)\mathcal{L}(z)\}|\bar{B}\rangle}{2M_B} \\
t(\omega) &= -\int \frac{dt}{2\pi}\, e^{-i\omega t} \int_0^t dr\, \frac{\langle \bar{B}|(\bar{h}S_n)(tn)\frac{\hbar}{2}\gamma_\mu^\perp n_\nu (S_n^\dagger g G_s^{\mu\nu} S_n)(rn)(S_n^\dagger h)(0)|\bar{B}\rangle}{2M_B} \\
u(\omega) &= -\int \frac{dt}{2\pi}\, e^{-i\omega t} \int_0^t dr\, \frac{\langle \bar{B}|(\bar{h}S_n)(tn)(S_n^\dagger i(iD_\perp)^2 S_n)(rn)(S_n^\dagger h)(0)|\bar{B}\rangle}{2M_B} \\
v(\omega) &= -\int \frac{dt}{2\pi}\, e^{-i\omega t} \int_0^t dr\, \frac{\langle \bar{B}|(\bar{h}S_n)(tn)\frac{\hbar}{2} i\sigma_{\mu\nu} (S_n^\dagger g G_{s\perp}^{\mu\nu} S_n)(rn)(S_n^\dagger h)(0)|\bar{B}\rangle}{2M_B}
\end{aligned} \tag{5.15}$$

The soft Wilson lines were introduced by the decoupling transformation (4.33). They reflect the space-time topology of the diagram after integrating out the hard-collinear fields and they guarantee gauge invariance of the HQET operators. Note, that even though the additional soft fields introduce new non-localities, the subleading shape functions depend only on one convolution variable ω. As was already mentioned above, this property only holds at the tree level of the $Q_{7\gamma} - Q_{7\gamma}$ contribution. One can interpret t and v as non-local generalizations of the B-meson matrix element of the subleading HQET chromomagnetic operator (see (3.14)), and u as a non-local generalization of the matrix element of the kinetic operator. The function s is related to the second diagram in Figure 5.2. In addition to the shape functions given above, there is a four quark operator appearing at $\mathcal{O}(\alpha_s)$ which is depicted in the last diagram of Figure 5.2. It is generated by the insertion of two hard-collinear-soft interaction terms of the SCET Lagrangian (4.24) together with two leading

power $Q_{7\gamma}^{(0)}$ operators. This contribution defines the following shape functions

$$\begin{aligned} f_u^{(q)}(\omega) =& -2\int \frac{dt}{2\pi}\, e^{-i\omega t}\int_0^t dr\int_r^t du \\ &\times \frac{\langle \bar B|[(\bar h S_n)(tn)T^a]_k[T^a(S_n^\dagger h)(0)]_l[(\bar q S_n)(rn)]_l \not{n}[(S_n^\dagger q)(un)]_k|\bar B\rangle}{2M_B}\,, \\ f_v^{(q)}(\omega) =& -2\int \frac{dt}{2\pi}\, e^{-i\omega t}\int_0^t dr\int_r^t du \\ &\times \frac{\langle \bar B|[(\bar h S_n)(tn)T^a]_k \not{n}\gamma_5[T^a(S_n^\dagger h)(0)]_l[(\bar q S_n)(rn)]_l \not{n}\gamma_5[(S_n^\dagger q)(un)]_k|\bar B\rangle}{2M_B}\,, \end{aligned} \tag{5.16}$$

where k and l are color indices and T^a are the $SU(3)_c$ generators. These non-local operators exhibit another interesting property. Since the hard-collinear fields in SCET carry large momentum components, the particles created by these fields always propagate forward in time. There is no interaction term in SCET that can turn a forward moving quark into a backward moving anti-quark, since this would require a hard fluctuation. As a result, after the convolution with the jet function, the quantum fields in the definition of the subleading shape functions are ordered in the same way as they appear in the Feynman graphs [100]. In the above formulas this corresponds to the requirement that $t > u > r$.

The subleading shape function presented in this section also contribute, in other combinations, to the semi-leptonic $\bar B \to X_u l\bar\nu$ decay in the endpoint region. If these shape functions were the only ones appearing in $\bar B \to X_s\gamma$ one might try to find weighted distributions of $\bar B \to X_s\gamma$ and $\bar B \to X_u l\bar\nu$ events, in which the subleading shape functions enter in the same combinations [102]. However, it will be shown in Chapter 6 that there are several additional unique shape functions that are relevant for $\bar B \to X_s\gamma$. The tree level subleading shape function contribution due to the $Q_{7\gamma} - Q_{7\gamma}$ interference can be written as

$$\begin{aligned} \frac{d\Gamma_{77}^{\rm SSF}}{dE_\gamma} =& \frac{G_F^2\overline{m}_b^2(\mu)\alpha}{2\pi^4}\,|C_{7\gamma}^{\rm eff}(\mu)\lambda_t|^2 E_\gamma^3\frac{1}{m_b}\int_{-p_+}^{\bar\Lambda} d\omega\, m_b\, J(m_b(p_+ + \omega),\mu) \\ &\times\Big(-\omega S(\omega,\mu) + s(\omega,\mu) - t(\omega,\mu) + u(\omega,\mu) - v(\omega,\mu) - \pi\alpha_s\left[f_u^{(s)}(\omega,\mu) + f_v^{(s)}(\omega,\mu)\right]\Big)\,, \end{aligned} \tag{5.17}$$

where J is the leading power jet function and the soft functions are given in (5.15) and (5.16). Since the shape functions only have support over the endpoint region, integrating the differential decay rate over a range much larger than $\Lambda_{\rm QCD}$ justifies the replacement

$$\int_{E_0\ll M_B}^{\frac{M_B}{2}} dE_\gamma \int_{2E_\gamma - m_b}^{\bar\Lambda} d\omega\,\delta(m_b - 2E_\gamma + \omega)e^{-i\omega t}F(E_\gamma,t) \to \delta(t)\frac{F(\frac{m_b}{2},t)}{2}\,, \tag{5.18}$$

where the exponential originates from the definition of the subleading shape functions and E_γ was set to $m_b/2$ which corresponds to the first order in the power counting. The function F contains all quantities of Equation (5.17) that are not explicitly given in (5.18),

specifically the non-local matrix element. It follows that the subleading shape functions of the $Q_{7\gamma} - Q_{7\gamma}$ contribution reduce to local matrix elements in the total rate. However, for $t = 0$ all subleading shape functions vanish as can be easily seen from their definitions. This zero normalization of the subleading shape functions corresponds to the vanishing $1/m_b$ corrections, discussed in Section 3.3.4. There, it was argued that the total rate was well approximated by the partonic calculation because of these vanishing corrections. As will be shown in Section 7.1, this does no longer hold when subleading shape functions of other operator interferences are taken into account. However, before discussing this, the relation of the QCD calculation to the effective theory calculation will be more carefully analyzed.

5.2.5 Kinematic vs Hadronic Power Corrections

From the discussion of the two preceding sections it becomes apparent that the subleading jet function and the subleading shape function contributions describe two fundamentally different types of corrections. The subleading shape functions introduce new matrix elements and are therefore related to hadronic parameters. The subleading jet functions on the other hand are perturbatively calculable and their importance increases when considering the total rate. They are therefore kinematically suppressed in the endpoint region, whereas the shape functions parameterize hadronic corrections through higher powers in the heavy-quark expansion. The two types of suppression imply, that the decay rate of the $Q_{7\gamma} - Q_{7\gamma}$ contribution integrated over a large enough range can be expressed in terms of local operators organized in a double expansion in powers of Δ/m_b and $\Lambda_{\rm QCD}/\Delta$ [13], where Δ is related to the photon energy cut $\Delta = m_b - 2E_0$. With a cut in the endpoint region, the factor $\Lambda_{\rm QCD}/\Delta$ is of $\mathcal{O}(1)$ which requires a resummation of the corresponding terms into a shape function (see Section 3.3.4).

Before the establishment of the systematic factorization (5.10) the kinematically suppressed contributions were deduced from the partonic calculation close to the endpoint. In that region the emission of hard-collinear and soft bremsstrahlung gluons is possible. Hard gluons, on the other hand are forbidden, since they would lead to an invariant mass of the final state of order m_b. Thus, the partonic calculation already contains all contributions due to the subleading jet functions, which originate from hard-collinear gluon bremsstrahlung, as was discussed in Section 5.2.3. However, since the different regions were not properly factorized, the partonic result will also contain contributions from the soft region. If this soft contribution appears at the same order in the power counting as the hard-collinear one, it must be absorbed into the subleading shape functions. Such an absorption is indeed necessary for the $Q_{7\gamma} - Q_{7\gamma}$ contribution, as will be shown in this section.

The general procedure of deriving the kinematic power corrections from the parton model was suggested in [13]. The starting point is the partonic results in (2.29), (2.33) and (2.35). The appropriate scale for the calculation is μ_i since one considers hard-collinear gluon emissions. The Wilson coefficients on the other hand are evaluated at the hard scale, as usual. Although the anomalous dimensions of the subleading SCET and HQET

operators are generally unknown, by using the solution to the RG equation derived at the leading power to run between the two scales, it is possible to resum the Sudakov double logarithms of the partonic result [13]. Finally, it is necessary to include the effects of the residual b-quark momentum in the $\bar{n}$ direction as it is of the same order as the hard-collinear momentum in that direction. This corresponds to the replacement

$$n \cdot p = m_b - 2E_\gamma \to n \cdot p + n \cdot k = m_b - 2E_\gamma + \omega. \tag{5.19}$$

The result must then be convoluted with the leading power shape function and expanded around $E_\gamma = m_b/2$. The first term in this expansion contains the subleading jet function contributions. For the case of he $Q_{7\gamma} - Q_{7\gamma}$ interference this leads to[1]

$$\frac{d\Gamma_{77}^{\text{part}}}{dE_\gamma} = \frac{G_F^2 \overline{m}_b^2(\mu)\alpha}{2\pi^4} |C_{7\gamma}^{\text{eff}}(\mu)\lambda_t|^2 E_\gamma^3 \frac{1}{m_b} \frac{C_F\alpha_s(\mu)}{4\pi} \int_{-p_+}^{\bar{\Lambda}} d\omega \left(16 \ln \frac{m_b}{p_+ + \omega} - 15\right) S(\omega, \mu). \tag{5.20}$$

Comparing this to the subleading jet function expression in (5.11) one finds that the $\ln(m_b)$ term agrees in both expressions, while the p_+-dependent terms and the constant accompanying the logarithms differ. This difference is due to the effects of the soft region in the partonic result. In order to prove that the effective theory approach properly factorizes the partonic result, it is necessary to calculate the partonic one-loop contributions to the subleading shape functions (5.15) as well as the tree-level matrix elements of the soft operators in (5.16). Since the perpendicular component of the heavy-quark velocity can be freely chosen it has been set to zero in this work. As a result the matrix elements of the soft operators corresponding to the subleading shape functions t and v vanish at one-loop order, since they only contain gluons with transverse polarization. The tree-level matrix elements of the soft operators corresponding to f_u and f_v also vanish, since they contain scaleless integrals over the $\bar{n}$-components of the light quark momenta. Finally, the matrix element of the soft operator corresponding to s is non-zero only when the heavy quarks are off-shell with a non-zero n-component of the residual momentum. As a result, it does not contribute if the residual momentum is set to zero in the partonic calculation. Therefore, the only remaining quantities left to be calculated from (5.17) are ωS and u. The relevant diagrams are depicted in Figure 4.5. The shape function ωS can be extracted from the calculation performed in [1]. Setting $v \cdot k = 0$ and using dimensional regularization one finds for the unrenormalized shape function

$$\omega\, S_{\text{bare}}(\omega) = \theta(-\omega) \frac{C_F\alpha_s(\mu)}{4\pi} \left(-\frac{4}{\bar{\epsilon}} - 4 \ln \frac{\mu^2}{(-\omega)^2} + 4\right), \tag{5.21}$$

where $1/\bar{\epsilon} = 1/\epsilon - \gamma_E + \ln 4\pi$ regularizes the UV pole. The one-loop correction to the subleading shape function u is calculated to [101]

$$u_{\text{bare}}(\omega) = \theta(-\omega) \frac{C_F\alpha_s(\mu)}{4\pi} \left(\frac{12}{\bar{\epsilon}} + 12 \ln \frac{\mu^2}{(-\omega)^2} - 20\right). \tag{5.22}$$

[1]Note, that a part of the subleading contributions of the $Q_{7\gamma} - Q_{7\gamma}$ interference is already included in the kinematic factor $E_\gamma^3 = (m_b + \omega)^3/8$ of the leading power in (4.40) (see [13] for details).

Subtracting the pole in the $\overline{\text{MS}}$ scheme, one obtains from (5.17) for the subleading shape function part of the differential decay rate

$$\frac{d\Gamma_{77}^{\text{SSF}}}{dE_\gamma}\Big|_{\text{part}} = \frac{G_F^2 \overline{m}_b^2(\mu)\alpha}{2\pi^4} |C_{7\gamma}^{\text{eff}}(\mu)\lambda_t|^2 E_\gamma^3 \frac{1}{m_b} \frac{C_F\alpha_s(\mu)}{4\pi} \left(16 \ln \frac{\mu^2}{p_+^2} - 24\right) , \tag{5.23}$$

where the subscript "part" indicates that the naive partonic expressions were used instead of the non-perturbative subleading shape functions. In order to compare the effective with the full theory result, the shape functions in (5.11) and (5.20) are replaced by δ-functions, which corresponds to the on-shell heavy quark of the partonic calculation. The sum of the partonic expression for the subleading jet function and the subleading shape functions (5.23) is then given by

$$\frac{d\Gamma_{77}^{\text{SJF}}}{dE_\gamma}\Big|_{\text{part}} + \frac{d\Gamma_{77}^{\text{SSF}}}{dE_\gamma}\Big|_{\text{part}} = \frac{G_F^2 \overline{m}_b^2(\mu)\alpha}{2\pi^4} |C_{7\gamma}^{\text{eff}}(\mu)\lambda_t|^2 E_\gamma^3 \frac{1}{m_b} \frac{C_F\alpha_s(\mu)}{4\pi} \left(16 \ln \frac{m_b}{p_+} + 1 - 16 c_{\text{RS}}\right) , \tag{5.24}$$

which coincides with the partonic expression in (5.20) if the renormalization scheme dependent constant is set to one. This choice is in fact the correct one, since (5.17) was derived in [100] by evaluating all traces of Dirac structures in $d = 4$ dimensions. Thus, the subleading jet function should be renormalized using the same scheme which just corresponds to setting $c_{\text{RS}} = 1$. Equation (5.24) then proves that the subleading contribution derived from the partonic expression contains contributions from the hard-collinear as well as the soft region. The logarithm in (5.20) originates from a combination of hard-collinear and soft scales

$$\ln \frac{m_b}{p_+} = \ln \frac{m_b p_+}{\mu^2} + \ln \frac{\mu^2}{p_+^2} \tag{5.25}$$

that are properly factorized in the effective theory approach.

The calculation presented above is equivalent to a method of regions analysis of the one-loop QCD forward scattering amplitudes contributing to $\bar{B} \to X_s\gamma$ [101]. The hard-collinear and soft regions exactly reproduce the partonic expressions for the subleading jet and shape functions, respectively. No further regions are necessary to reproduce the full QCD result. Hard gluon loops only play a role in the matching of the effective QCD operators onto SCET, but do not give rise to subleading contributions, as they only depend on scales of order m_b [101]. Before proceeding with operator interferences other than $Q_{7\gamma} - Q_{7\gamma}$ a final comment is in order concerning strange-quark mass effects.

5.2.6 Strange Quark Mass Effects

Throughout this thesis the strange-quark mass was set to zero, which turns out to be an excellent approximation numerically. However, taking m_s to be non-zero gives rise to a subleading jet function proportional to m_s^2/p_{hc}^2, where p_{hc} is the momentum of the hard-collinear jet containing the strange-quark [103]. If one adopts the scaling $m_s \sim \mathcal{O}(\Lambda_{\text{QCD}})$, this function scales as Λ_{QCD}/m_b in the endpoint region and contributes to F_{77}. From [103]

follows that the extra contribution is

$$F_{77}^{m_s}(E_\gamma,\mu) = -\tilde{H}_{77}\int_{-p_+}^{\bar{\Lambda}} d\omega\, m_b\, j_m(\omega+p_+,\mu)\, S(\omega,\mu)\,, \tag{5.26}$$

where it was defined $j_m = \frac{1}{\pi}\,\mathrm{Im}\, J_{m_b}^m$. Both $\tilde{H}_{77} = 1+\mathcal{O}(\alpha_s)$ and $J_{m_b}^m$ can be found in [103]. At the lowest order in α_s,

$$j_m(\omega+p_+,\mu) = \frac{m_s^2}{m_b}\,\delta'(\omega+p_+) + \mathcal{O}(\alpha_s)\,, \tag{5.27}$$

and indeed j_m is suppressed by $m_s^2/(m_b\Lambda_{\mathrm{QCD}})$ compared to the leading-order jet function $J(p^2,\mu)$. One could argue that for $m_s \approx 100\,\mathrm{MeV}$ and $\Lambda_{\mathrm{QCD}} \sim 500\,\mathrm{MeV}$ the parameter m_s should scale as a higher power of the SCET expansion parameter λ, e.g. $m_s \sim \lambda^2$. This would imply that j_m can be neglected at order $\Lambda_{\mathrm{QCD}}/m_b$. Contributions of j_m to coefficient functions F_{ij} other than F_{77} are further suppressed by hard functions $\tilde{H}_{ij} = \mathcal{O}(\alpha_s)$. They will not be considered in the following, since they are bound to be tiny.

This concludes the discussion of the subleading contribution due to two insertions of the operator $Q_{7\gamma}$. The next section will deal with the new effects that are introduced by the insertions of the other effective operators Q_1^q and Q_{8g}.

5.3 Factorization at Subleading Power

In the middle of the 2000s, the effective theory treatment of $\bar{B}\to X_s\gamma$ included the proof of the leading power factorization [12], the two loop calculation of the leading power soft and jet function [93, 97], the proof of tree-level factorization at subleading power for the $Q_{7\gamma}-Q_{7\gamma}$ contribution [9,10,100,106,107] as well as the the contribution of other operator insertions at one-loop order in the hard function and through kinematical power corrections [13]. Furthermore, hints at the importance of the non-perturbative corrections existed in the form of a soft scale dependence of the partonic result for the $Q_{8g}-Q_{8g}$ interference [64, 104] and a non-perturbative correction to the total rate from the interference of Q_1^c with $Q_{7\gamma}$ [108–111]. However, a detailed analysis of the subleading hadronic corrections was missing.

The distinguishing feature of the $Q_{7\gamma}-Q_{7\gamma}$ contributions is the fact that the photon is always emitted directly from the weak-interaction vertex. In principle, the operators Q_1^q and Q_{8g} can also match onto SCET operators with the photon directly emitted from the vertex. One possibility was discussed in Section 4.3.2 where QCD was matched to the leading power SCET operator at the one-loop level. In the case of Q_1^q and Q_{8g} it is also possible, that the photon couples to the light partons. Processes of this kind will be called *resolved photon* contributions to be contrasted with the *direct photon* contributions where the photon couples to the weak vertex. It is clear that all subleading contributions considered so far were direct ones. The resolved contributions can be interpreted as a probe of the hadronic substructure of the photon. There is no analogue to these contributions in

the semi-leptonic decays, because the lepton-neutrino pair can only couple to light partons via W-boson exchange.

In order for a light parton to emit the anti-hard-collinear photon it must be anti-hard-collinear itself. The conversion of an hard-collinear particle into an anti-hard-collinear one would require a hard fluctuation which is integrated out of SCET. Therefore an extension of the subleading factorization formulas (5.10) and (5.14) which only contained hard-collinear particles, is required. The proof of factorization proceeds in analogy to the direct case. First the QCD operators are matched at the hard scale onto SCET(hc,$\overline{\text{hc}}$,s). In the case of $Q_{7\gamma}$ the resulting SCET operator was not allowed to include anti-hard-collinear particles, since there was no way to convert them into hard-collinear or soft ones, and they were not allowed to appear in the final state jet. Now, however, anti-hard-collinear particles may be converted into a photon by an insertion of the SCET Lagrangian. The QCD operators therefore also match onto SCET operators including anti-hard-collinear modes. A general matrix element, appearing in the calculation of the differential decay rate then looks like

$$\text{Disc}_{\text{restr.}}\langle\bar{B}|\bar{h}(x)[\phi_{\text{s}}(x_i)\dots\phi_{\text{hc}}(y_i)\dots\phi_{\overline{\text{hc}}}(z_i)\dots\phi'_{\overline{\text{hc}}}(z'_i)\dots]h(0)|\bar{B}\rangle. \tag{5.28}$$

Note that it is now necessary to consider only the restricted cut, as explained in Section 3.1. For the same reason, two different types of anti-hard-collinear fields $\phi_{\overline{\text{hc}}}$ and $\phi'_{\overline{\text{hc}}}$ have been introduced. Each type only appears on one side of the cut, either connected to the initial or final state B-meson via the weak vertex. In other words, an anti-hard-collinear line must never be cut, since this would change the scaling of the invariant mass of the final state jet. In the case of $\bar{B}\to X_s\gamma$ the matrix element must contain at least two hard-collinear fields to generate the final state jet, either a pair of strange-quarks or of other light particles. In the latter case, the strange-quarks must appear as soft fields. Since each field scales with a certain power of λ, the maximum number of fields of each type is determined by the desired order in the power counting. If there are no anti-hard-collinear fields in the matrix element, the result will correspond to a direct contribution, otherwise to a resolved one.

Due to the presence of the anti-hard-collinear fields the multipole expansion of the soft fields becomes more subtle. The correct form of the expansion must then be determined on a case-by-case basis for each operator, rather than derived from a simple set of rules. It will be shown that the heavy-quark fields must always be expanded about x_-, while the other soft fields can depend on either x_- or x_+, or both. After the decoupling transformation (4.33) the matrix element decomposes into

$$\langle\bar{B}|\bar{h}(x)[\phi_{\text{s}}(x_i)\dots]h(0)|\bar{B}\rangle\times\text{Disc}\langle\Omega|\phi^{(0)}_{\text{hc}}(y_i)\dots|\Omega\rangle\times\langle\Omega|\phi^{(0)}_{\overline{\text{hc}}}(z_i)\dots|\Omega\rangle\langle\Omega|\phi'^{(0)}_{\overline{\text{hc}}}(z'_i)\dots|\Omega\rangle, \tag{5.29}$$

where the soft matrix element once again contains the soft Wilson lines, introduced by the decoupling transformation. Now they do not only connect the fields along the n-light-cone but also the fields that are displaced in the $\bar{n}$ direction by the anti-hard-collinear propagators. The soft matrix element is therefore gauge invariant.

The second matching step, from SCET to HQET is performed by integrating out the (anti-)hard-collinear fields. This can be done perturbatively since the corresponding scales belong to the short-distance regime. The Wilson coefficients of this matching are just the

vacuum expectation values of the time ordered product of the (anti-)hard-collinear fields. It is now possible to define general jet and shape functions through the Fourier transform of the matrix elements

$$J_i^{(n)} \sim \Big[\text{Disc}\,\langle\Omega|\phi_{\rm hc}^{(0)}(y_j)\dots|\Omega\rangle\Big]_{\rm F.T.}\,, \quad S_i^{(n)} \sim \Big[\langle\bar B|\bar h(x_-)[\phi_{\rm s}(x_{i\mp})\dots]h(0)|\bar B\rangle\Big]_{\rm F.T.}, \tag{5.30}$$

where the superscript (n) indicates the suppression in powers of $1/m_b$ and "F.T." designates a Fourier transform. The subleading shape functions of (5.15) fit into this scheme and correspond to $S_i^{(1)}$. In addition to these objects resolved photon contributions give rise to a new type of jet function

$$\bar J_i^{(n)} \sim \Big[\langle\Omega|[\phi_{\rm hc}^{(0)}(z_k)\dots]|\Omega\rangle\Big]_{\rm F.T.}\,, \tag{5.31}$$

which corresponds to an uncut anti-hard-collinear propagator dressed by Wilson lines. As was discussed in Section 4.3.3, the vacuum correlation function of the photon field factorizes trivially and is not considered in this discussion.

The above discussion suggests the validity of a general factorization formula for the differential $\bar B \to X_s\gamma$ decay rate in the endpoint region to all orders in $1/m_b$

$$\begin{aligned} d\Gamma(\bar B\to X_s\gamma) =& \sum_{n=0}^\infty \frac{1}{m_b^n}\sum_i H_i^{(n)} J_i^{(n)}\otimes S_i^{(n)} \\ &+\sum_{n=1}^\infty \frac{1}{m_b^n}\Big[\sum_i H_i^{(n)} J_i^{(n)}\otimes S_i^{(n)}\otimes \bar J_i^{(n)} + \sum_i H_i^{(n)} J_i^{(n)}\otimes S_i^{(n)}\otimes \bar J_i^{(n)}\otimes \bar J_i^{(n)}\Big] \end{aligned} \tag{5.32}$$

which generalizes and includes the previous formulas (4.51), (5.10) and (5.14). The first line contains the direct, the second line the resolved photon contributions. One can distinguish between single and double resolved contributions depending on whether there are anti-hard-collinear propagators on one or on both sides of the cut. Note that the notation is symbolic. Objects denoted by the same symbol in the various terms refer, in general, to different quantities. The symbol $\otimes$ denotes a convolution over all soft momentum variables shared by the jet functions and shape function. A graphical representation of the factorization formula is shown in Figure 5.3. The resolved contributions exhibit another interesting property, that will explicitly be demonstrated in Section 7.1: It was discussed in Sections 5.2.3 and 5.2.4 that the subleading $Q_{7\gamma}-Q_{7\gamma}$ (direct) contributions are only relevant in the endpoint region and vanish when the total rate is considered. This is no longer true for the resolved contributions.

When talking about factorization this always refers to the the kind of proof presented in this section. It implies that it is always possible to decompose the differential $\bar B \to X_s\gamma$ decay rate in the endpoint region into the parts considered above. But it does not imply, that this decomposition allows for a consistent resummation of large logarithms and that the renormalization procedure discussed in Section 4.4 will work at all orders in

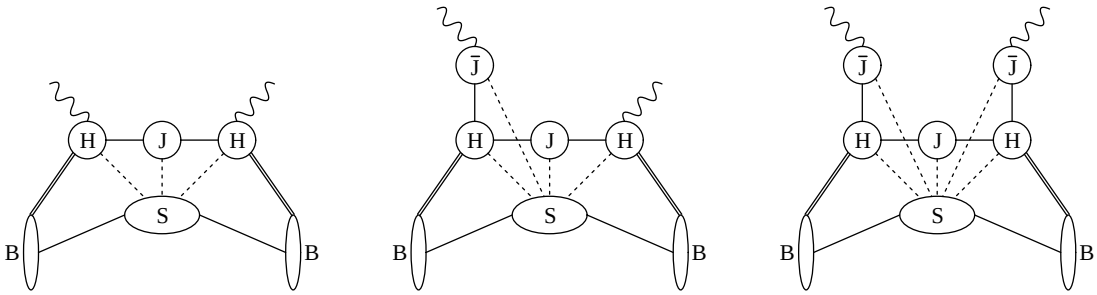

Figure 5.3: Graphical illustration of the three terms in the factorization formula (5.32). The dashed lines represent soft interactions that are factored off the remaining building blocks by the decoupling transformation and the heavy-quark expansion.

perturbation theory. These issues will be analyzed in more detail in Section 6.3.1, when an explicit example is available. The next step in the systematic analysis of the subleading corrections is to match the QCD operators Q_1^q and Q_{8g} onto the corresponding SCET operators.

5.4 Operator Matching onto SCET

It was motivated in Section 2.1.5 that the only QCD operators not severely suppressed by their Wilson coefficients are Q_1^q and Q_{8g}. The matching of these operators proceeds in analogy to the $Q_{7\gamma}$ matching by making the replacements discussed in Section 5.1. As was explained in Section 5.2.2, only operators with a scaling of $\lambda^{5/2}$, λ^3 and $\lambda^{7/2}$ are of relevance. For simplicity, the matching will only be performed at tree-level for hard quantum corrections. This procedure will generate a large number of possible SCET operators, all of which are collected in Appendix B. However, only a limited number of them are relevant for the calculation of the subleading resolved contributions. Their matching will be explicitly presented in this section.

The second matching step, from SCET onto HQET, will be performed at the one-loop level for (anti-)hard-collinear quantum fluctuations associated with the leading power shape function in (4.38). These correspond to direct contributions. Finally, the Wilson coefficients of the new subleading shape functions will be computed at tree-level, but including the $4\pi\alpha_s$ contributions resulting from tree-level (anti-)hard-collinear gluon exchange.

In order to determine which of the several possible subleading SCET operators are of relevance, the basic requirements will once again be collected from the previous sections. First, it is required that the final state only contains one anti-hard-collinear particle, namely the photon. All other particles in the final state must either be hard-collinear or soft. There must be at least one hard-collinear particle in the final state in order to have a jet with an invariant mass at the required scale $\sqrt{\Lambda_{\rm QCD} m_b}$. Furthermore, there can be an arbitrary number of anti-hard-collinear fields in the operators as long as they are converted to the final state photon plus soft particles by SCET Lagrangian insertions. The number of

these soft and hard-collinear particles is only restricted by the desired overall scaling of the operator. Before matching the operators themselves, the necessary conversions will be collected.

5.4.1 Photon Conversions

As can be seen from the discussion in Section 4.2.2 (with hc replaced by $\overline{\text{hc}}$) the conversion of an anti-hard-collinear field into a photon and a soft field is suppressed by at least $\lambda^{1/2}$. The interaction of the photon with an anti-hard-collinear field on the other hand is unsuppressed in (4.14). This leads to the possible conversions illustrated in Figure 5.4. The last diagrams of each line, which involve three gluon fields, are not needed for the

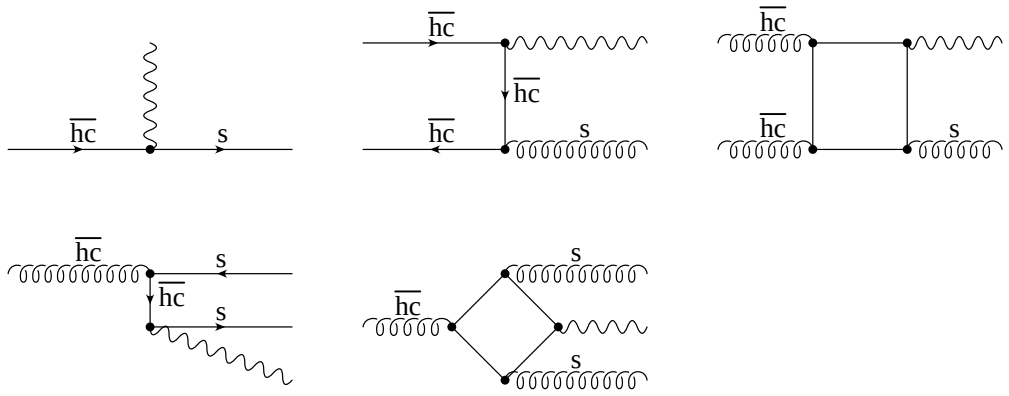

Figure 5.4: $\mathcal{O}(\lambda^{1/2})$ (top row) and $\mathcal{O}(\lambda)$ (bottom row) conversions of anti-hard-collinear particles into a photon accompanied by soft particles. Only some representative diagrams are shown.

tree-level analysis of this work. The scaling of the conversions does not change by adding any number of anti-hard-collinear gluons to the ingoing side. The conversions at order $\lambda^{1/2}$ can thus be written as

$$\xi_{\overline{\text{hc}}} \to A_\perp^{\text{em}} + q\,, \qquad \xi_{\overline{\text{hc}}} + \bar{\xi}_{\overline{\text{hc}}} \to A_\perp^{\text{em}} + A_s\,, \qquad \mathcal{A}_{\overline{\text{hc}}} + \mathcal{A}_{\overline{\text{hc}}} \to A_\perp^{\text{em}} + A_s\,, \tag{5.33}$$

while the ones at order λ are

$$\mathcal{A}_{\overline{\text{hc}}} \to A_\perp^{\text{em}} + q + \bar{q}\,, \qquad \mathcal{A}_{\overline{\text{hc}}} \to A_\perp^{\text{em}} + A_s + A_s\,. \tag{5.34}$$

With these conversion rules at hand it is possible to decide which SCET operators contribute to the subleading resolved photon contributions.

5.4.2 Operator Matching of Q_{8g}

When matching the chromomagnetic dipole operator Q_{8g} of (2.17), one can discard the non-abelian part of the field strength tensor $G^{\mu\nu}$, since only the first order in g needs to

be considered. A priori, it is possible to match the s-quark onto either a hard-collinear or anti-hard-collinear quark and the gluon onto a hard-collinear or anti-hard-collinear gluon. Matching the s-quark onto a soft particle would only give rise to a contribution beyond the subleading power. Also, the gluon and the s-quark can not both be anti-hard-collinear, since the necessary conversions would again lead to a suppression beyond the subleading power. However, for the resolved contribution one of them needs to be anti-hard collinear, which implies two possible SCET operators that descend from Q_{8g}. They are illustrated in Figure 5.5. The first one (first row) is suppressed by λ compared to the leading power

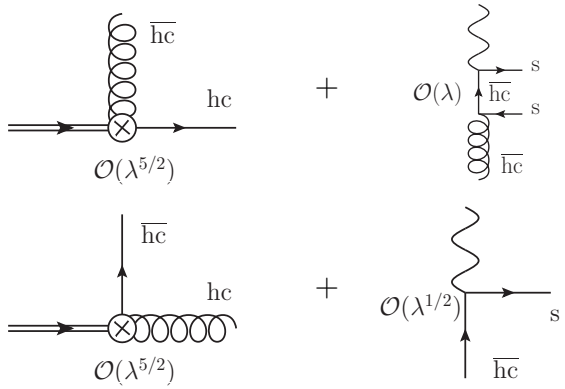

Figure 5.5: SCET Operators descending from Q_{8g} that give rise to resolved photon contributions plus the necessary conversions by Lagrangian insertions.

and can be written as follows. Here and in the rest of this section the factor $-\frac{g\,m_b}{4\pi^2}e^{-im_b\,v\cdot x}$ will be suppressed, leading to

$$Q^{(2)}_{8g,\,\overline{\text{hc}}\text{ gluon}}(x) = \bar{\xi}_{\overline{\text{hc}}}(x)\,\frac{\bar{n}\!\!\!/}{2}\,[in\cdot\partial \mathcal{A}_{\overline{\text{hc}}\perp}(x)]\,(1+\gamma_5)h(x_-)\,, \quad \text{followed by } \mathcal{O}(\lambda) \text{ conversion} \tag{5.35}$$

which contributes to the differential decay rate at subleading power in combination with the leading power operator (4.27). The superscript (i) now denotes the total suppression in powers of $\lambda^{1/2}$ of the complete set of fields on one side of the cut. In the present case it consists of the operator scaling of $\mathcal{O}(\lambda^{5/2})$ plus the $\mathcal{O}(\lambda)$ scaling of the Lagrangian insertion. In the above expression the gluon field strength tensor has been expanded after the introduction of the gauge invariant building block (4.23)

$$\begin{aligned}\sigma_{\mu\nu}igG^{\mu\nu} &= \sigma_{\mu\nu}[iD^\mu_{\overline{\text{hc}}}, iD^\nu_{\overline{\text{hc}}}] = \sigma_{\mu\nu}W_{\overline{\text{hc}}}[i\mathcal{D}^\mu_{\overline{\text{hc}}}, i\mathcal{D}^\nu_{\overline{\text{hc}}}]W^\dagger_{\overline{\text{hc}}} \\ &= W_{\overline{\text{hc}}}\Big[2\,\frac{\bar{n}\!\!\!/}{2}\,[in\cdot\partial \mathcal{A}_{\overline{\text{hc}}\perp}] \\ &\quad + 2\,[i\partial\!\!\!/_\perp \mathcal{A}_{\overline{\text{hc}}\perp} - i\partial_\perp\cdot\mathcal{A}_{\overline{\text{hc}}\perp}] \,+\, \left(\frac{\bar{n}\!\!\!/}{2}\frac{n\!\!\!/}{2} - \frac{n\!\!\!/}{2}\frac{\bar{n}\!\!\!/}{2}\right)[in\cdot\partial\,\bar{n}\cdot\mathcal{A}_{\overline{\text{hc}}}]\Big]W^\dagger_{\overline{\text{hc}}}\,,\end{aligned} \tag{5.36}$$

where the terms in the second and third line are of order $\lambda^{1/2}$ and λ, respectively.

If the s-quark is matched onto an anti-hard-collinear field it needs to be converted into the photon and a soft quark. This conversion costs $\lambda^{1/2}$, so the lowest power insertion possible is of order λ^3. This leads to (see second row of Figure 5.5)

$$Q^{(1)}_{8g,\,\overline{\text{hc}}\,\text{quark}}(x) = \bar{\xi}_{\overline{\text{hc}}}(x)\frac{\not{n}}{2}\left[i\bar{n}\cdot\partial\!\!\!/\mathcal{A}_{\text{hc}\perp}(x)\right](1+\gamma_5)h(x_-)\,, \quad \text{followed by } \mathcal{O}(\lambda^{1/2}) \text{ conversion.} \tag{5.37}$$

Two insertions of this operator give rise to a double resolved contribution. The subleading contributions due to insertions of a SCET operator descending from Q_{8g} will be discussed in Sections 6.3 and 6.4.

5.4.3 Operator Matching of Q_1^q

In order to determine the resolved photon contributions that include the current-current operator Q_1^q, it has to be matched onto a SCET operator containing at least one anti-hard-collinear field. The remaining quark fields in Q_1^q are then matched onto the heavy-quark field and two hard-collinear fields, since a soft quark would lead to a scaling larger than $\lambda^{7/2}$. However, such an operator can not interfere with the leading power SCET operator which only contains one hard-collinear field. It is therefore necessary to match Q_1^q onto a SCET operator containing two anti-hard-collinear fields and convert them into a soft gluon and the photon via a penguin loop, by using the appropriate conversion rule in (5.33). The situation is depicted in Figure 5.6. Note that the conversion into a single gauge boson

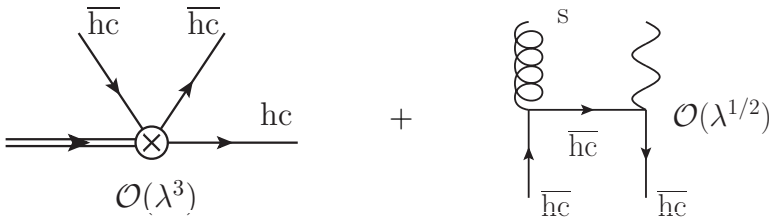

Figure 5.6: SCET Operator descending from Q_1^q that gives rise to resolved photon contributions plus the necessary conversion by Lagrangian insertions.

vanishes in the 't Hooft-Veltmann scheme, as was discussed in Section 2.1.5. The anti-hard-collinear fields can be either a charm- or up-quark, while the hard-collinear field must be the strange-quark. This leads to an $\mathcal{O}(\lambda^{7/2})$ SCET operator insertion, namely

$$Q_1^{q\,(2)} = e^{-im_b v\cdot x}\bar{\xi}_{\text{hc}}\gamma^\mu(1-\gamma_5)h(x_-)\,\bar{\xi}_{\overline{\text{hc}}}(x)\gamma_\mu(1-\gamma_5)\xi_{\overline{\text{hc}}}(x)\,, \quad \text{followed by } \mathcal{O}(\lambda^{1/2}) \text{ conversion.} \tag{5.38}$$

In the interference with the leading power SCET operator this gives rise to a single-resolved photon contribution. This contribution will be discussed in detail in Section 6.1.

5.5 Conclusions of this Chapter

In this chapter a factorization theorem for the subleading contribution to the differential $\bar{B} \to X_s\gamma$ decay rate in the endpoint region has been presented in (5.32). The concepts of subleading jet and shape functions were generally introduced in (5.30). In addition a new type of jet function (5.31) appeared in the calculation of resolved photon contributions. It was related to an uncut anti-hard-collinear propagator dressed by Wilson lines. After this general considerations about the subleading contributions to $\bar{B} \to X_s\gamma$, the remainder of this work will deal with each contribution in detail, using the SCET operators of Section 5.4 as a starting point. For this, it is convenient to write the CP-averaged $\bar{B} \to X_s\gamma$ differential decay rate in the endpoint region as

$$\begin{aligned}\frac{d\Gamma}{dE_\gamma} = \frac{G_F^2\alpha|V_{tb}V_{ts}^*|^2}{2\pi^4}\,\overline{m}_b^2(\mu)\,E_\gamma^3\Bigg[&|H_\gamma(\mu)|^2\int_{-p_+}^{\bar{\Lambda}} d\omega\, m_b\, J\big(m_b(\omega+p_+),\mu\big)\,S(\omega,\mu)\\ &+\frac{1}{m_b}\sum_{i\le j}\mathrm{Re}\big[C_i^*(\mu)\,C_j(\mu)\big]\,F_{ij}(E_\gamma,\mu)+\dots\Bigg],\end{aligned} \tag{5.39}$$

where the first and second line represent the leading and subleading power contribution, respectively, while the ellipses denote terms of even higher order in the power counting and the real part prescription originates from the CP-averaging. The leading power has been discussed in detail in Chapter 4 (compare Equation (4.40)). At the subleading power, the $Q_{7\gamma} - Q_{7\gamma}$ contribution has been discussed in this chapter. It was found that the function F_{77} decomposes into a subleading jet function part $F_{77}^{(a)}$ and a subleading shape function part $F_{77}^{(b)}$. The former is given in (5.12), the latter in (5.17). The other F_{ij} will be determined in the next chapter. In principle, all possible combinations of the operators Q_1^q, $Q_{7\gamma}$ and Q_{8g} contribute to $\bar{B} \to X_s\gamma$. However, only three of them, corresponding to F_{17}, F_{78} and F_{88} actually contribute at $\mathcal{O}(1/m_b)$, as will also be shown in the next chapter.

Chapter 6

Analysis of Subleading Contributions to the Photon Spectrum

In this chapter all the relevant subleading contributions to the differential $\bar{B} \to X_s\gamma$ decay rate in the endpoint region will be analyzed in detail. As was discussed in the previous chapter, this includes the interference of operators descending from Q_1^q with those descending from $Q_{7\gamma}$ in Section 6.1, the interference of operators descending from Q_{8g} with themselves in Section 6.3, as well as the interference of operators descending from Q_{8g} with those descending from $Q_{7\gamma}$ in Section 6.4. The results of the calculation will exemplify the factorization formula (5.32), introduced in the last chapter. However, there are some subtleties concerning the factorization of the $Q_{8g} - Q_{8g}$ contribution. These will be discussed in Section 6.3.1. Finally, some properties of the soft functions will be discussed in their respective sections and in Section 6.5.

6.1 Analysis of the $Q_1^q - Q_{7\gamma}$ Contributions

In order to determine the direct photon contribution for the interference of the operators Q_1^q and $Q_{7\gamma}$ one has to evaluate the diagrams in Figure 5.1. The first diagram in that Figure contains two insertions of $\mathcal{O}(\lambda^3)$ SCET operators, which can be read off from (5.6) and (B.13). There is more than one possibility for insertions that generate the second diagram in Figure 5.1. The vertex on the right can either be the leading power SCET operator (4.27) or an $\mathcal{O}(\lambda^3)$ operator from $Q_{7\gamma A}$. In the former case the vertex on the left corresponds to an $\mathcal{O}(\lambda^{7/2})$ operator from (B.13), else to an $\mathcal{O}(\lambda^3)$ operator. In either case an additional leading power SCET Lagrangian (4.14) insertion is necessary, to connect the hard-collinear gluon to the hard-collinear strange-quark. The calculation yields

$$F_{17}^{(a)}(E_\gamma,\mu) = \frac{C_F\alpha_s(\mu)}{4\pi}\left(-\frac{2}{3}\right)\int_{-p_+}^{\bar{\Lambda}} d\omega\, S(\omega,\mu)\,, \tag{6.1}$$

which involves a convolution of the leading shape function (4.38) with a jet function consisting of the cut of a hard-collinear loop. This result coincides with the kinematical power

corrections (see Section 5.2.5) derived from the partonic result in (2.29) by expanding around $E_\gamma = m_b/2$. To obtain this result the scaling $m_c^2 = \mathcal{O}(\Lambda_{\rm QCD} m_b)$ for the charm-quark mass was adopted, meaning that the ratio m_c^2/m_b remains a constant of order $\Lambda_{\rm QCD}$ in the heavy-quark limit.

Much more interesting is the single resolved photon contribution arising from this operator pair. As shown in the left graph of Figure 6.1, it is obtained by combining the $\mathcal{O}(\lambda^3)$ SCET four-quark operator in (5.38), which contains two anti-hard-collinear quark fields in addition to a hard-collinear strange-quark and a heavy quark, with the leading-power contribution (4.27) descending from $Q_{7\gamma}$. According to the rules (5.33), the conversion

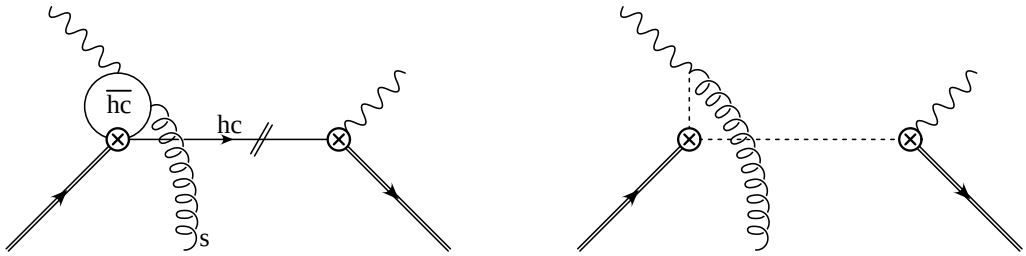

Figure 6.1: Diagrams arising from the matching of the $Q_1^q - Q_{7\gamma}$ contribution onto SCET (left) and HQET (right). As a resolved photon contribution, the diagram contains non-localities in the light-cone direction n, denoted by the vertical dashed line in the second diagram.

of the two anti-hard-collinear fields into a photon and a soft gluon costs a factor of $\lambda^{1/2}$, giving a total suppression with respect to the leading term of $\lambda \sim \Lambda_{\rm QCD}/m_b$. When the (anti-)hard-collinear fields are integrated out in the second matching step, one obtains the HQET diagram shown in the right graph of Figure 6.1. Here and below, horizontal (vertical) dotted lines represent Wilson lines along the n ($\bar{n}$) direction. The HQET matrix element corresponding to the graph on the right in Figure 6.1 contains a soft gluon field in addition to the two heavy quarks. In the language of the factorization formula (5.32) this corresponds to a single resolved contribution with a subleading shape function. For the contribution from the operator Q_1^c one obtains

$$\begin{aligned} F_{17,c}^{(b)}(E_\gamma,\mu) = \frac{2}{3}\,(1-\delta_u) \int_{-\infty}^{\bar\Lambda} d\omega\, \delta(\omega+p_+) \\ \times \,{\rm Re}\int_{-\infty}^{\infty} \frac{d\omega_1}{\omega_1+i\varepsilon} \left[1 - F\!\left(\frac{m_c^2-i\varepsilon}{2E_\gamma\,\omega_1}\right)\right] g_{17}(\omega,\omega_1,\mu)\,, \end{aligned} \tag{6.2}$$

where the CKM-suppressed parameter δ_u is defined by

$$\delta_q = \frac{{\rm Re}\,[\lambda_q^* C_1^*(\mu)(-\lambda_t) C_{7\gamma}(\mu)]}{|\lambda_t|^2 {\rm Re}\,[C_1^*(\mu) C_{7\gamma}(\mu)]}\,, \tag{6.3}$$

while the subleading shape function g_{17} is defined by

$$g_{17}(\omega,\omega_1,\mu) = \int \frac{dr}{2\pi}\, e^{-i\omega_1 r} \int \frac{dt}{2\pi}\, e^{-i\omega t} \times \frac{\langle \bar{B}|\big(\bar{h}S_n\big)(tn)\,\bar{n}\!\!\!/(1+\gamma_5)\big(S_n^\dagger S_{\bar{n}}\big)(0)\,i\gamma_\alpha^\perp \bar{n}_\beta\,\big(S_{\bar{n}}^\dagger\, gG_s^{\alpha\beta} S_{\bar{n}}\big)(r\bar{n})\,\big(S_{\bar{n}}^\dagger h\big)(0)|\bar{B}\rangle}{2M_B}\,. \tag{6.4}$$

The penguin function $F(x)$ is defined in Appendix A.1. For $0 < x < 1/4$ this function develops an imaginary part. Note that a power counting for the charm-quark mass is adopted such that $m_c^2 = \mathcal{O}(m_b\Lambda_{\rm QCD})$. The argument of the penguin function in the convolution (6.2) then counts as $\mathcal{O}(1)$. Another comment concerning the charm-quark mass is in order. In the analysis of the $\bar{B} \to X_s\gamma$ decay rate and photon spectrum, it is customary to adopt for the charm-quark mass a running mass defined at a hard-collinear scale $\mu_{hc} \sim \sqrt{m_b\Lambda_{\rm QCD}} \sim m_c$ [52]. For instance, the default value adopted in [5] is $m_c = \overline{m}_c(1.5\,\text{GeV})$. This scale choice is indeed appropriate for charm-quark mass effects residing in the jet functions entering the factorization formula (5.32). On the other hand, charm-quark mass effects also enter some of the hard functions in the factorization formula, for instance via the coefficient $H_\gamma(\mu)$ in (4.30) [13], or via phase-space functions such as those shown in (2.29). In this case the charm-penguin loops are probed at virtualities of order m_b, and it is therefore appropriate to use a running mass $m_c = \overline{m}_c(\mu_h)$ evaluated at a hard scale $\mu_h \sim m_b$. This can have important numerical effects, enhancing the theoretical prediction for the total decay rate by up to 3%.

The structure of the soft Wilson lines in (6.4), which are directed either along n or $\bar{n}$, follows when the decoupling transformation is applied to the (anti-)hard-collinear fields in SCET to remove their soft interactions from the effective Lagrangian and absorb them into eikonal factors. The Wilson lines reflect the space-time topology of the HQET diagrams shown on the right-hand side in Figure 6.1. The two weak vertices shall be labeled by coordinates 0 (left) and $x = tn + x_+ + x_\perp$ (right), and the vertex of the soft gluon by $y = r\bar{n} + y_- + y_\perp$. The multipole expansion of the effective-theory fields implies that $x_{+,\perp}$ and $y_{-,\perp}$ can be set to zero at this order. Gauge invariance then requires that the fields $\bar{h}(tn)$ and $G_s(r\bar{n})$ are joined by a Wilson line, and the rules of SCET determine that this line consists of two segments: a straight line $[tn, 0]$ along the light-like direction n followed by a straight line $[0, r\bar{n}]$ along the light-like direction $\bar{n}$. The fields $G_s(r\bar{n})$ and $h(0)$ are joined by a straight Wilson line $[r\bar{n}, 0]$ along the light-like direction $\bar{n}$. Using that $[tn, 0] = S_n(tn)S_n^\dagger(0)$ etc., one recovers the structure of the Wilson lines in the non-local operator in (6.4). It is noted for completeness that soft functions closely related to the functions g_{17} in (6.4) and g_{11} in (6.23) were introduced, in a context not related to $\bar{B} \to X_s\gamma$ decay, in [112].

There is more to the space-time structure of the soft operator that is worth pointing out. Since hard-collinear fields in SCET carry large momentum components, the particles created by these fields always move forward in time. As a result, after convolution with the jet functions, the quantum fields in the definition of the subleading shape functions are

ordered in the same way as they appear in Feynman graphs [100]. The operators considered in this work contain fields that propagate along the two light-like directions n and $\bar{n}$, as indicated by the dotted lines in the right graph in Figure 6.1. If one assigns coordinate 0 to the first of the weak vertices in the figure, the gluon is emitted at space-time point $r\bar{n}$ with $r > 0$. This is ensured by the $i\varepsilon$ prescription in the jet function in (6.2), since

$$\int d\omega_1 \, e^{-i\omega_1 r} \, \frac{i}{\omega_1 + i\varepsilon} = 2\pi \, \theta(r) \,. \tag{6.5}$$

The gluon thus lives at a later time than the field $h(0)$ (recall that $n^0 = \bar{n}^0 = +1$), and indeed it appears to the left of that field.

Another comment is in order concerning the structure of the result (6.2). From the diagrams shown in Figure 6.1 one derives one half times the expression (6.2) without the real-part prescription in front of the integral and in expression (6.3). The mirror diagrams not shown in the figure, in which the two weak vertices are interchanged, give an analogous contribution with the complex conjugate Wilson coefficients and CKM matrix elements, the complex conjugate penguin function $F^*(r)$,[1] the propagator factor $1/(\omega_1 - i\varepsilon)$, and the soft function

$$\begin{aligned} g_{17}'(\omega, \omega_1, \mu) \;&=\; \int \frac{dr}{2\pi} \, e^{i\omega_1 r} \int \frac{dt}{2\pi} \, e^{-i\omega t} \\ &\times \frac{\langle \bar{B} | \big(\bar{h} S_{\bar{n}}\big)(tn) \, (-i\gamma_\alpha^\perp \bar{n}_\beta) \, \big(S_{\bar{n}}^\dagger \, g G_s^{\alpha\beta} S_{\bar{n}}\big)(tn + r\bar{n}) \, \big(S_{\bar{n}}^\dagger S_n\big)(tn) \, \bar{\not{n}} (1 + \gamma_5) \big(S_n^\dagger h\big)(0) | \bar{B} \rangle}{2 M_B} \,, \end{aligned} \tag{6.6}$$

which is related to the original one by complex conjugation: $g_{17}'(\omega, \omega_1, \mu) = [g_{17}(\omega, \omega_1, \mu)]^*$. To show this, one uses translational invariance to shift all position arguments by $-tn$ and then changes the sign of the integration variable t. The sum of the diagrams in Figure 6.1 plus their mirror graphs thus gives a real result, and after averaging over CP-conjugate decay modes one obtains (6.2).

The real-part symbols in (6.3) and (6.2) refer to different kinds of complex parameters. The various products of Wilson coefficients and CKM factors carry, in general, CP-violating weak phases. The convolution of the jet and soft functions, on the other hand, can carry CP-even, strong-rescattering phases, which in principle can result either from anti-hard-collinear loops (i.e., the jet functions $\bar{J}_i$) or from the soft matrix elements themselves. (However, in Section 6.5 it will be argued that the soft functions are real.) When both types of phases are present, a non-zero direct CP asymmetry arises. The subleading power corrections provide new mechanisms for generating such an asymmetry. This will be discussed in Chapter 8.

The range of support of the soft functions in HQET can be derived in analogy to Section 4.3.3 by noting that the light-cone projections $n \cdot p_i$ and $\bar{n} \cdot p_i$ of all parton momenta in the B meson must be non-negative, and that the total momentum of all partons in the B meson is $M_B v$. Since in HQET the momentum of a heavy quark is decomposed as

[1] This is because the fields in the charm-quark loop of the mirror graphs are anti-time-ordered.

$p_b = m_b v + k$, where k is the residual momentum, it follows that

$$\sum_{i\neq b} n\cdot p_i + n\cdot k = \bar\Lambda\,, \qquad \sum_{i\neq b} \bar n\cdot p_i + \bar n\cdot k = \bar\Lambda\,, \tag{6.7}$$

where $n\cdot k > -m_b$ and $\bar n\cdot k > -m_b$. In the heavy-quark limit $m_b\to\infty$ it follows that $-\infty < n\cdot k \le \bar\Lambda$ and $0 \le n\cdot p_i < \infty$ (for $i\neq b$), and similarly for $\bar n\cdot k$ and $\bar n\cdot p_i$. In the special case of the soft function g_{17} in (6.4), the variable ω corresponds to the residual-momentum component $n\cdot k$ of the initial-state heavy quark, while ω_1 can either correspond to the component $\bar n\cdot p_g$ of a gluon in the final-state B meson or to the component $-\bar n\cdot p_g$ of a gluon in the initial-state B meson. It thus follows that $-\infty<\omega\le\bar\Lambda$ and $-\infty<\omega_1<\infty$. This implies that the penguin-loop function $F(x)$ is sampled over both positive and negative values of its argument.

In principle, each of the six QCD penguin four-quark operators in the effective weak Hamiltonian can give rise to a similar contribution, either via loops of massless quarks ($q=u,d,s$) or via a charm-quark loop. (b-quark loops lead to further power suppression.) Of these options only Q_1^c has both a large Wilson coefficient $C_1\sim 1$ and a large CKM factor $V_{cb}V_{cs}^* = \mathcal{O}(\lambda^2)$, so it will give rise to the dominant effects. However, for later use the case of the CKM-suppressed operator Q_1^u will also be considered. Using that $F(0)=0$, it follows that the resolved photon contribution resulting from this operator is given by

$$F_{17,u}^{(b)}(E_\gamma,\mu) = \frac{2}{3}\,\delta_u\,\mathrm{Re}\int_{-\infty}^{\bar\Lambda} d\omega\,\delta(\omega+p_+)\int_{-\infty}^{\infty}\frac{d\omega_1}{\omega_1+i\varepsilon}\,g_{17}(\omega,\omega_1,\mu)\,. \tag{6.8}$$

Note that the soft function is the same as in (6.2).

Next the convergence properties of the convolution integrals in (6.2) and (6.8) will be investigated. In the UV region, for $\omega_1\gg\Lambda_{\rm QCD}$, the first integral approaches the form of the second one, since mass effects become negligible. It follows that the convolution over ω_1 converges as long as the soft function g_{17} vanishes for $\omega_1\to\pm\infty$. In general, the asymptotic behavior of the soft functions for large values of the ω_i variables can be analyzed using short-distance methods [1]. This shows, for instance, that the leading shape function behaves as $S(\omega,\mu)\sim 1/\omega$ modulo logarithms for $\omega\to-\infty$. For the present case, naive dimensional analysis suggests the behavior $g_{17}(\omega,\omega_1,\mu)\propto\omega_1$ for large ω_1 but fixed ω, in which case the convolution integral would diverge linearly. To obtain such a contribution, however, would require a non-zero matrix element of the soft operator between two on-shell b-quarks. But this matrix element vanishes by Lorentz invariance. A non-zero contribution is only obtained if, in addition to the heavy quarks, one adds a soft external gluon. This costs two orders in power counting, so that the asymptotic fall-off is at least as strong as $g_{17}(\omega,\omega_1,\mu)\propto 1/\omega_1$ for $\omega_1\to\pm\infty$. It follows that the convolution integrals (6.2) and (6.8) are UV convergent.

The behavior of the soft functions in the IR region can not be derived from a perturbative analysis. In the present case, however, it suffices to make the reasonable assumption that $g_{17}(\omega,\omega_1,\mu)$ is non-singular at $\omega_1=0$. Using the expansion

$$1-F(x) = -\frac{1}{12x} - \frac{1}{90x^2} - \frac{1}{560x^3} - \ldots \tag{6.9}$$

valid for large x, one finds that for small ω_1 the convolution integral (6.2) arising from the charm-quark loop behaves as

$$\int\limits_{\omega_1\approx 0} \frac{d\omega_1}{\omega_1+i\varepsilon}\left[1-F\left(\frac{m_c^2-i\varepsilon}{2E_\gamma\,\omega_1}\right)\right] g_{17}(\omega,\omega_1,\mu) \approx -\frac{E_\gamma}{6m_c^2}\int\limits_{\omega_1\approx 0} d\omega_1\, g_{17}(\omega,\omega_1,\mu)\,. \tag{6.10}$$

For the convolution integral (6.8) arising from the up-quark loop, one finds instead

$$\int \frac{d\omega_1}{\omega_1+i\varepsilon}\, g_{17}(\omega,\omega_1,\mu) = \mathrm{P}\!\int \frac{d\omega_1}{\omega_1}\, g_{17}(\omega,\omega_1,\mu) - i\pi\, g_{17}(\omega,0,\mu)\,, \tag{6.11}$$

where the symbol P denotes the Cauchy principal value of the integral. It follows that the convolution integrals indeed exist as long as the subleading shape function is non-singular at $\omega_1 = 0$. Note that for the case of the up-quark loop it is important that the integral over ω_1 runs over both positive and negative values. Previous authors have already pointed out that the up-quark loop contribution to the $\bar{B}\to X_s\gamma$ decay rate, while strongly CKM suppressed, is described by an uncalculable long-distance contribution [108, 110, 111]. The relation (6.11) provides a rigorous field-theoretic definition of this contribution in terms of a well-defined, non-local soft matrix element.

For phenomenological purposes it is useful to define a new function

$$f_{17,q}(\omega,\mu) = \frac{2}{3}\int_{-\infty}^{\infty}\frac{d\omega_1}{\omega_1+i\varepsilon}\left[1-F\left(\frac{m_q^2-i\varepsilon}{(m_b+\omega)\,\omega_1}\right)\right] g_{17}(\omega,\omega_1,\mu)\,. \tag{6.12}$$

The final expression for the $Q_1^q - Q_{7\gamma}$ contribution can then be written as

$$F_{17}(E_\gamma,\mu) = \frac{C_F\alpha_s(\mu)}{4\pi}\left(-\frac{2}{3}\right)\int_{-p_+}^{\bar\Lambda} d\omega\, S(\omega,\mu) + \sum_{q=c,u}\delta_q\,\mathrm{Re}\, f_{17,q}(-p_+,\mu)\,. \tag{6.13}$$

Note that the argument of the penguin function entering $f_{17,q}(-p_+,\mu)$ is $m_q^2/[(m_b - p_+)\,\omega_1] = m_q^2/(2E_\gamma\,\omega_1)$, as it should be. It was already mentioned at the beginning of this section, that the direct part in (6.13) corresponds just to the result derived by expanding the parton model expression in (2.29) around the endpoint (for $m_c^2 \sim \Lambda_{\rm QCD} m_b$). The resolved part on the other hand is a new hadronic effect. Even though there is no way to explicitly calculate these non-perturbative contributions, some information about them is obtainable.

6.1.1 $Q_1^q - Q_{7\gamma}$: Facts about the Soft Function

One fact that is known about this non-perturbative contribution is that the definition of the soft function g_{17} in (6.4) implies the normalization condition

$$\int_{-\infty}^{\bar\Lambda} d\omega \int_{-\infty}^{\infty} d\omega_1\, g_{17}(\omega,\omega_1,\mu) = \frac{\langle\bar B|\,\bar h\,\bar{\not n}\, i\gamma_\alpha^\perp \bar n_\beta\, gG_s^{\alpha\beta}\, h\,|\bar B\rangle}{2M_B} = 2\lambda_2\,, \tag{6.14}$$

where (3.39) was used to evaluate the matrix element of the local quark-gluon operator in terms of the hadronic parameter λ_2. Moreover, the HQET trace formalism of Section 3.3.3 implies that the soft function can be written as

$$\begin{aligned} g_{17}(\omega,\omega_1,\mu) &= \text{tr}\,\Big[\overline{\mathcal{M}}\,\bar{n}\!\!\!/(1+\gamma_5)\,i\gamma_\alpha^\perp\,\mathcal{M}\,\Xi^\alpha(v,\bar{n},\omega,\omega_1,\mu)\Big] \\ &= M_B\text{tr}\,\left[\frac{1+v\!\!\!/}{2}\,\bar{n}\!\!\!/(1+\gamma_5)\,i\gamma_\alpha^\perp\,\frac{1+v\!\!\!/}{2}\,\Big(i\gamma^{\alpha_\perp}\Xi_1(\omega,\omega_1,\mu)+i\gamma^{\alpha_\perp}\bar{n}\!\!\!/\,\Xi_2(\omega,\omega_1,\mu)\Big)\right] \\ &= 4M_B\Xi_2(\omega,\omega_1,\mu) \end{aligned} \tag{6.15}$$

where the most general decomposition of Ξ^α was used. It follows from this argument that the factor $(1+\gamma_5)$ in (6.4) can be replaced by 1, since the part of the trace involving γ_5 vanishes. It is then easy to see that

$$\int_{-\infty}^{\bar\Lambda} d\omega\, g_{17}(\omega,\omega_1,\mu) = \int_{-\infty}^{\bar\Lambda} d\omega\,\Big[g_{17}(\omega,-\omega_1,\mu)\Big]^*. \tag{6.16}$$

One can constrain the function $g_{17}(\omega,\omega_1,\mu)$ further by looking at its first moments with respect to ω and ω_1. These can be related to linear combinations of HQET matrix elements with three covariant derivatives. Such matrix elements can be expressed in terms of two hadronic parameters, ρ_1 and ρ_2, via [113]

$$\frac{\langle\bar B|\,\bar h\,\Gamma_{\alpha\delta\beta}\,iD^\alpha iD^\delta iD^\beta h\,|\bar B\rangle}{2M_B} = \frac{1}{2}\,\text{tr}\,\left(\Gamma_{\alpha\delta\beta}\,\frac{1+v\!\!\!/}{2}\,\Big[(g^{\alpha\beta}-v^\alpha v^\beta)\,v^\delta\,\frac{\rho_1}{3}+i\sigma^{\alpha\beta}v^\delta\,\frac{\rho_2}{2}\Big]\,\frac{1+v\!\!\!/}{2}\right). \tag{6.17}$$

Thus, one finds

$$\begin{aligned} \int_{-\infty}^{\bar\Lambda} d\omega\,\omega\int_{-\infty}^{\infty} d\omega_1\, g_{17}(\omega,\omega_1,\mu) &= \frac{\langle\bar B|\,\bar h\,\bar{n}\!\!\!/\gamma_{\perp\alpha}\,in\cdot D\,[iD_\perp^\alpha, i\bar n\cdot D]\,h\,|\bar B\rangle}{2M_B} = -\rho_2\,, \\ \int_{-\infty}^{\bar\Lambda} d\omega\int_{-\infty}^{\infty} d\omega_1\,\omega_1\, g_{17}(\omega,\omega_1,\mu) &= \frac{\langle\bar B|\,\bar h\,\bar{n}\!\!\!/\gamma_{\perp\alpha}\,[[iD_\perp^\alpha, i\bar n\cdot D], i\bar n\cdot D]\,h\,|\bar B\rangle}{2M_B} = 0\,, \end{aligned} \tag{6.18}$$

where the HQET parameter ρ_2 is related to the parameter ρ_{LS}^3 introduced in [114] via $\rho_{LS}^3 = 3\rho_2$. The vanishing of the first moment with respect to ω_1 of g_{17} is not a coincidence. As will be shown in Section 6.5, g_{17} is in fact a real function. Relation (6.16) then implies that all the odd moments in ω_1 vanish.

As a final comment it is added that even in the limit where the charm-quark is treated as a heavy quark, $m_c = \mathcal{O}(m_b)$, the penguin contribution to the photon spectrum must still be described by a subleading shape function. In this limit the argument of the penguin function in (6.2) is of order $m_b/\Lambda_{\rm QCD}$. Expanding then the function $[1-F(x)]$ to first order in $1/x$ leads to[2]

$$f_{17,c}(\omega,\mu) \to -\frac{m_b+\omega}{18m_c^2}\int\frac{dt}{2\pi}\,e^{-i\omega t}\,\frac{\langle\bar B|\big(\bar h S_n\big)(tn)\,\bar{n}\!\!\!/(1+\gamma_5)\,i\gamma_\alpha^\perp\bar n_\beta\,\big(S_n^\dagger\,gG_s^{\alpha\beta}\,h\big)(0)|\bar B\rangle}{2M_B}\,. \tag{6.19}$$

[2]Only the first term in this expansion gives rise to a UV-convergent convolution integral.

Integrating this expression over ω, and dropping higher power corrections, one obtains a contribution to the total decay rate proportional to

$$\int_{-\bar{\Lambda}}^{m_b} dp_+ \, f_{17,c}(-p_+,\mu) \to -\frac{m_b \lambda_2}{9 m_c^2} \,. \tag{6.20}$$

This non-perturbative correction to the total rate was already considered in [108–111] (the correct sign was obtained in the last reference). This gave an early hint at the weaknesses of the local OPE approach on $\bar{B} \to X_s\gamma$. With the above derivation its origin can be related to the effect of a resolved photon contribution.

6.2 Analysis of the $Q_1^q - Q_1^q$ and $Q_1^q - Q_{8g}$ Contributions

The power-counting rules described in Appendix B show that for these two cases there do not exist operators arising at order $1/m_b$ in the heavy-quark expansion that contain soft fields other than the two heavy quarks. In particular, the diagrams shown in Figure 6.2 contribute to the $\bar{B} \to X_s\gamma$ photon spectrum only at order $1/m_b^2$. This is an important

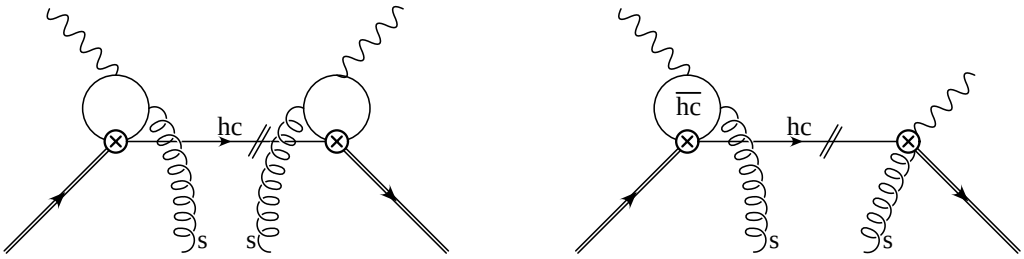

Figure 6.2: Examples of SCET diagrams giving rise to resolved photon contributions suppressed by at least two powers of of $1/m_b$. The left graph arises from the pairing $Q_1^q - Q_1^q$, while the right one contributes to the $Q_1^q - Q_{8g}$ term.

finding. Since for the case of two charm-quark loops the first diagram in the figure is proportional to the large Wilson coefficient $|C_1|^2 \sim 1$, it has sometimes been mentioned as a potentially dangerous source of power corrections. It follows from the present analysis that this contribution scales as $(\Lambda_{\rm QCD}/m_b)^2$ relative to the leading term. It is therefore expected to be a small correction (see below).

It thus remains to calculate the leading power corrections to the direct photon term in the factorization formula, by analyzing graphs of the type shown in Figure 5.1. Note that here only the first diagram on the left in this figure can contribute. After a straightforward calculation (summing over $q = c, u$), one finds once again contributions involving a convolution of the leading shape function with a jet function consisting of the cut of a hard-collinear loop. The results are the same in the two cases and given by

$$F_{11}^{(a)}(E_\gamma,\mu) = \frac{2E_\gamma}{m_b} F_{18}^{(a)}(E_\gamma,\mu) = \frac{C_F\alpha_s(\mu)}{4\pi} \frac{2}{9} \int_{-p_+}^{\bar{\Lambda}} d\omega \, S(\omega,\mu) \,. \tag{6.21}$$

This is the obvious generalization of the parton-model results in (2.29). Note that the prefactor $m_b/2E_\gamma$ in the result for F_{18} follows from the SCET calculation, and therefore it is presented here. In the endpoint region this factor equals 1 up to power corrections, and it could therefore be omitted.

In order to substantiate the statement about the smallness of the $\mathcal{O}(1/m_b^2)$ double resolved photon contribution represented by the first diagram in Figure 6.2, this graph is evaluated explicitly. The result is

$$F_{11}^{(b)}(E_\gamma,\mu) = -\frac{1}{m_b}\left|\frac{\lambda_c}{\lambda_t}\right|^2 \frac{2}{9}\int_{-\infty}^{\bar\Lambda} d\omega\,\delta(\omega+p_+)\int_{-\infty}^{\infty}d\omega_1\int_{-\infty}^{\infty}d\omega_2 \\ \times\frac{1}{\omega_1+i\varepsilon}\left[1-F\left(\frac{m_c^2-i\varepsilon}{2E_\gamma\,\omega_1}\right)\right]\frac{1}{\omega_2-i\varepsilon}\left[1-F^*\left(\frac{m_c^2-i\varepsilon}{2E_\gamma\,\omega_2}\right)\right] g_{11}(\omega,\omega_1,\omega_2,\mu)\,, \tag{6.22}$$

where the $1/m_b$ prefactor indicates the additional power suppression. The soft function is defined as

$$g_{11}(\omega,\omega_1,\omega_2,\mu) = \int\frac{dt}{2\pi}\,e^{-i\omega t}\int\frac{dr}{2\pi}\,e^{-i\omega_1 r}\int\frac{du}{2\pi}\,e^{i\omega_2 u}\,g_{\mu\nu}\,\bar n^\alpha\bar n^\beta \\ \times\frac{\langle\bar B|\big(\bar h S_{\bar n}\big)(tn)\big(S_{\bar n}^\dagger\,gG_s^{\nu\beta}S_{\bar n}\big)(tn+u\bar n)\Gamma\big(S_{\bar n}^\dagger S_n\big)(tn)\big(S_n^\dagger S_{\bar n}\big)(0)\big(S_{\bar n}^\dagger\,gG_s^{\mu\alpha}S_{\bar n}\big)(r\bar n)\big(S_{\bar n}^\dagger h\big)(0)|\bar B\rangle}{2M_B}, \tag{6.23}$$

where $\Gamma=\bar n\!\!\!/(1-\gamma_5)$. This function satisfies $g_{11}(\omega,\omega_1,\omega_2,\mu)=[g_{11}(\omega,\omega_2,\omega_1,\mu)]^*$, which implies that $F_{11}^{(b)}$ is real. In order to obtain an estimate of the magnitude of this contribution, the penguin functions are expanded to first order using (6.9). This yields

$$F_{11}^{(b)}(E_\gamma,\mu) \approx -\frac{1}{648}\left(\frac{2E_\gamma}{m_b}\right)^2\left|\frac{\lambda_c}{\lambda_t}\right|^2\frac{m_b}{m_c^4}\int_{-\infty}^{\infty}d\omega_1\int_{-\infty}^{\infty}d\omega_2\;g_{11}(-p_+,\omega_1,\omega_2,\mu)\,, \tag{6.24}$$

where the remaining double integral over the soft function scales like $\Lambda_{\rm QCD}^3$. For any reasonable value of this quantity, the prefactor 1/648 and the additional $1/m_b$ suppression render this contribution negligible. For instance, if one models the double integral by $\Lambda_{11}^4\,S(-p_+,\mu)$ with some hadronic scale $\Lambda_{11}\sim\Lambda_{\rm QCD}$, the contribution of this term relative to the leading direct photon contribution in (4.40) is approximately given by

$$-\frac{1}{648}\left|\frac{C_1(\mu)}{C_{7\gamma}(\mu)}\right|^2\left(\frac{\Lambda_{11}}{m_c}\right)^4 \approx -2\cdot10^{-4}\left(\frac{\Lambda_{11}}{0.5\,\text{GeV}}\right)^4. \tag{6.25}$$

6.3 Analysis of the $Q_{8g}-Q_{8g}$ Contribution

As it will turn out, this contribution is more subtle than the remaining ones, so its calculation will be presented in more detail. The direct contribution is generated by two insertions

of the operator $Q^{(1)}_{8g,\,\text{hc quark}}$ given in (B.2). Since there is no leading power operator containing a photon and descending from Q_{8g} (at tree level in the matching) only the first diagram of Figure 5.1 is relevant for the direct photon contribution. The same diagram is given more suggestively in the first line of Figure 6.3. The second line of Figure 6.3 shows

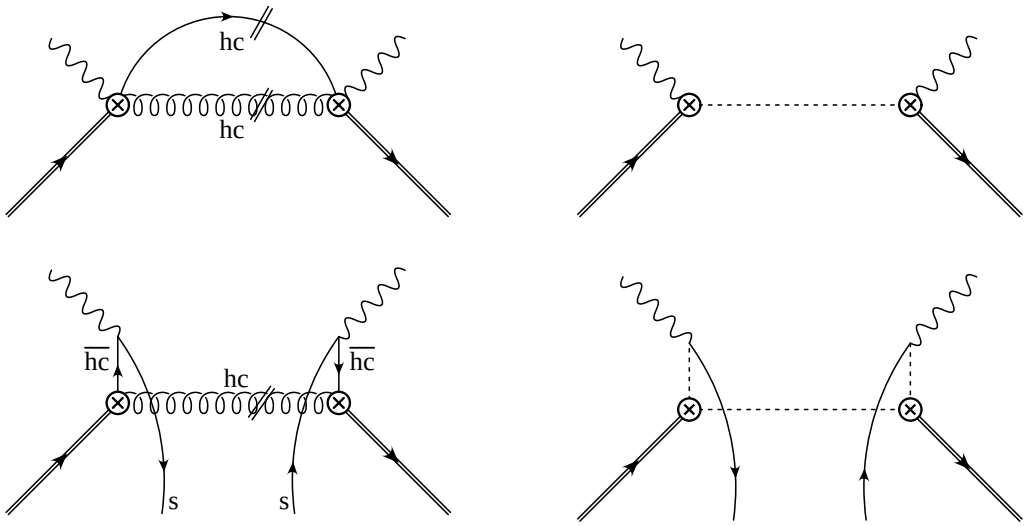

Figure 6.3: Diagrams arising from the matching of the $Q_{8g} - Q_{8g}$ contribution onto SCET (left) and HQET (right). Dashed lines denote non-localities obtained after (anti-)hard-collinear fields have been integrated out.

the resolved contribution which is generated by two insertions of the operator (5.37) and its associated conversion. The operator in (5.35) does not contribute to the $Q_{8g} - Q_{8g}$ interference, since it is already suppressed by λ compared to the leading power and there is no leading power operator descending from Q_{8g} to combine it with. Also, there is no contribution due to a matching of Q_{8g} onto an operator containing any soft fields at order $1/m_b$ in the heavy-quark expansion. The right panel of Figure 6.3 shows the HQET diagrams obtained after the (anti-)hard-collinear fields have been integrated out in the second matching step.

The direct photon contribution involves a convolution of the leading shape function in (4.38) with a subleading jet function consisting of the cut of a hard-collinear loop. In the present case the jet function is divergent and needs to be regularized. Using dimensional regularization and subtracting its $1/\bar{\epsilon}$ pole in the $\overline{\text{MS}}$ scheme yields

$$F_{88}^{(a)}(E_\gamma,\mu) = \frac{C_F\alpha_s(\mu)}{4\pi}\left(\frac{m_b}{2E_\gamma}\right)^2 \int_{-p_+}^{\bar{\Lambda}} d\omega \left(\frac{2}{9}\ln\frac{m_b(\omega+p_+)}{\mu^2} + \frac{1}{9} - \frac{4}{9}\,c_{\text{RS}}\right) S(\omega,\mu)\,. \quad (6.26)$$

The scheme-dependent constant c_{RS} vanishes in the $\overline{\text{MS}}$ scheme, $c_{\overline{\text{MS}}} = 0$. If, on the other hand, the dimensional reduction scheme is adopted, in which the Dirac algebra is performed

in 4 rather than $d = 4 - 2\epsilon$ dimensions, then $c_{\overline{\rm DR}} = 1$. It will be shown later that the final answer for F_{88} is scheme independent.

The double resolved photon contribution gives rise to a more complicated structure, as the resulting soft matrix element contains four quark fields located at different space-time points. One finds

$$F_{88}^{(b)}(E_\gamma,\mu) = \frac{8}{9}\,\pi\alpha_s(\mu)\left(\frac{m_b}{2E_\gamma}\right)^2\int_{-\infty}^{\bar\Lambda} d\omega\,\delta(\omega+p_+)\int_{-\infty}^{\infty}\frac{d\omega_1}{\omega_1+i\varepsilon}\int_{-\infty}^{\infty}\frac{d\omega_2}{\omega_2-i\varepsilon}\,g_{88}^{\rm cut}(\omega,\omega_1,\omega_2,\mu), \tag{6.27}$$

where the subleading shape function has been defined by

$$\begin{aligned} g_{88}^{\rm cut}(\omega,\omega_1,\omega_2,\mu) &= \int\frac{dr}{2\pi}\,e^{-i\omega_1 r}\int\frac{du}{2\pi}\,e^{i\omega_2 u}\int\frac{dt}{2\pi}\,e^{-i\omega t}\sum\!\!\!\!\!\!\int_{\mathcal{X}_s} \\ &\times\frac{\langle\bar B|\big(\bar h S_n\big)(tn)\,T^A\big(S_n^\dagger S_{\bar n}\big)(tn)\,\overline{\Gamma}_{\bar n}\big(S_{\bar n}^\dagger s\big)(tn+u\bar n)|\mathcal{X}_s\rangle\,\langle\mathcal{X}_s|\big(\bar s S_{\bar n}\big)(r\bar n)\Gamma_{\bar n}\big(S_{\bar n}^\dagger S_n\big)(0)\,T^A\big(S_n^\dagger h\big)(0)|\bar B\rangle}{2M_B} \\ &= \int\frac{dr}{2\pi}\,e^{-i\omega_1 r}\int\frac{du}{2\pi}\,e^{i\omega_2 u}\int\frac{dt}{2\pi}\,e^{-i\omega t} \\ &\times\frac{\langle\bar B|\big(\bar h S_n\big)(tn)\,T^A\big(S_n^\dagger S_{\bar n}\big)(tn)\,\overline{\Gamma}_{\bar n}\big(S_{\bar n}^\dagger s\big)(tn+u\bar n)\big(\bar s S_{\bar n}\big)(r\bar n)\Gamma_{\bar n}\big(S_{\bar n}^\dagger S_n\big)(0)\,T^A\big(S_n^\dagger h\big)(0)|\bar B\rangle}{2M_B}\,. \end{aligned} \tag{6.28}$$

As before, the Wilson lines render the soft matrix element gauge invariant. The sum over soft intermediate states $\mathcal{X}_s$ with strangeness $S = -1$ in the first equation arises since in this particular case the hard-collinear jet does not contain the strange-quark. Note that only color-octet partonic states contribute to the sum, not physical hadronic ones. As was already argued in Section 3.1 a complete sum can be performed, since the operators ensure the correct quantum number for the intermediate states. This gives rise to the second equation, in which the two strange-quark fields are *not* time ordered but appear in the order shown in the formula. In the definition above

$$\Gamma_{\bar n} = \frac{\bar{n}\!\!\!/ n\!\!\!/}{4}\,(1+\gamma_5)\,, \qquad \overline{\Gamma}_{\bar n} = \frac{n\!\!\!/\bar{n}\!\!\!/}{4}\,(1-\gamma_5) \tag{6.29}$$

are projectors onto two-component light-quark spinors. In deriving the result (6.27) the Dirac structure has been simplified using the identity [115]

$$\gamma_\perp^\alpha\,\frac{n\!\!\!/\bar{n}\!\!\!/}{4}\,\gamma_\perp^\mu\otimes\gamma_{\perp\mu}\,\frac{\bar{n}\!\!\!/ n\!\!\!/}{4}\,\gamma_{\perp\alpha} = (d-2)^2\,\frac{n\!\!\!/\bar{n}\!\!\!/}{4}\otimes\frac{\bar{n}\!\!\!/ n\!\!\!/}{4}\,, \tag{6.30}$$

where d is the number of space-time dimensions.

According to the discussion of Section 6.1, it follows that $g_{88}^{\rm cut}$ has support for $-\infty < \omega \le \bar\Lambda$ and $-\infty < \omega_{1,2} < \infty$. Note the difference in the sign of the $i\varepsilon$ terms in the two anti-hard-collinear propagators in (6.27), which is due to the fact that the anti-hard-collinear fields connected to the right weak vertex in the diagrams are anti-timed-ordered. Consequently, after convolution with the jet functions the position variables r and u in

(6.28) are restricted to positive values, such that the fields in the soft $\langle \mathcal{X}_s| \dots |\bar{B}\rangle$ matrix elements are time ordered, while those in the $\langle \bar{B}| \dots |\mathcal{X}_s\rangle$ matrix elements are anti-time-ordered, as it should be. Finally, the second equality in (6.28) implies the relation

$$\Big[g_{88}^{\rm cut}(\omega,\omega_1,\omega_2,\mu)\Big]^* = g_{88}^{\rm cut}(\omega,\omega_2,\omega_1,\mu)\,, \tag{6.31}$$

and since the convolution in (6.27) is symmetric in ω_1 and ω_2 up to complex conjugation, it follows that the final result is real. Contrary to (6.14) there is no useful normalization condition for the soft function $g_{88}^{\rm cut}$.

For phenomenological purposes, it will be convenient to define a new, real function

$$f_{88}(\omega,\mu) = \frac{2}{9}\int_{-\infty}^{\infty}\frac{d\omega_1}{\omega_1+i\varepsilon}\int_{-\infty}^{\infty}\frac{d\omega_2}{\omega_2-i\varepsilon}\,g_{88}^{\rm cut}(\omega,\omega_1,\omega_2,\mu)\,, \tag{6.32}$$

in terms of which the second contribution to the photon spectrum is simply

$$F_{88}^{(b)}(E_\gamma,\mu) = 4\pi\alpha_s(\mu)\left(\frac{m_b}{2E_\gamma}\right)^2 f_{88}(-p_+,\mu)\,. \tag{6.33}$$

Note that the poles at $\omega_1 = 0$ and $\omega_2 = 0$ are regularized by the $i\varepsilon$ prescriptions, in analogy with (6.11).

One comment is in order concerning the structure of this result in light of the general factorization formula (5.32). The present case is the only example of a double resolved photon contribution at order $1/m_b$. The jet function for the hard-collinear gluon is given by the cut of the gluon propagator, which up to trivial prefactors yields $J(p^2) = \delta(p^2)$ with $p^2 = m_b(\omega + p_+)$, in analogy with the tree-level expression for the quark jet function of (4.43). The jet functions for the two anti-hard-collinear quark propagators are, up to a trivial numerator factor, given by $\bar{J}(p^2) = 1/(p^2+i\varepsilon)$, where $p^2 = 2E_\gamma\,\omega_{1,2}$ in the present case. Hence, the triple convolution can be recast in the form (omitting scale dependences for brevity)

$$\begin{aligned}&\int d\omega\,\delta(p_+ + \omega)\int\frac{d\omega_1}{\omega_1+i\varepsilon}\int\frac{d\omega_2}{\omega_2-i\varepsilon}\,g_{88}^{\rm cut}(\omega,\omega_1,\omega_2)\\ &= H\int m_b\,d\omega\,J\big(m_b(p_+ + \omega)\big)\int 2E_\gamma\,d\omega_1\,\bar{J}(2E_\gamma\,\omega_1)\int 2E_\gamma\,d\omega_2\,\big[\bar{J}(2E_\gamma\,\omega_2)\big]^*\,g_{88}^{\rm cut}(\omega,\omega_1,\omega_2),\end{aligned} \tag{6.34}$$

with the hard matching coefficient corresponding at tree level to the product of Wilson coefficients $|C_{8g}|^2$ in (5.39). This result is in agreement with the factorization formula (5.32). Even though all seems well with the above formula, the presentation has hidden an important subtlety. The next section will deal with the renormalization properties of the individual quantities in the factorization formula.

6.3.1 $Q_{8g} - Q_{8g}$: Details about the Factorization

A priori, each of the quantities in Equation (6.34) is scale dependent. However, the scale dependence should cancel (up to terms of order α_s^2) in the sum of the two contributions (6.26) and (6.27). This is in correspondence to the cancellation of divergences between the hard-collinear and soft region in a method of regions analysis of $Q_{8g} - Q_{8g}$ in full QCD. In order for this cancellation to happen the convolution (6.32) must contain a μ-dependent term at zeroth order in the strong coupling. This fact is incompatible with a multiplicative renormalization of SCET operators as given in Equation (4.46). The situation can be contrasted to the $Q_{7\gamma} - Q_{7\gamma}$ case in Section 5.2.5, whose matrix element turned out to be less singular. The resolution of this puzzle is that the additional convolution integrals over the soft function themselves are not convergent. In order to demonstrate this, one calculates the asymptotic behavior of the soft function for large values $\omega_{1,2} \gg \Lambda_{\rm QCD}$, corresponding to highly energetic light quarks. This behavior can be extracted using short-distance methods [1]. At leading order in perturbation theory, one just has to replace the light-quark fields in the definition (6.28) by a cut propagator and perform some phase-space integrations. Working in $d = 4 - 2\epsilon$ dimensions leads to

$$g_{88}^{\rm cut}(\omega,\omega_1,\omega_2,\mu)\Big|_{\omega_{1,2}\gg\Lambda_{\rm QCD}} = \frac{C_F}{(4\pi)^{2-\epsilon}}\,\frac{\theta(\omega_1)\,\omega_1^{1-\epsilon}}{\Gamma(1-\epsilon)}\,\delta(\omega_1-\omega_2)\int_\omega^{\bar\Lambda} d\omega'\,S(\omega',\mu)\,(\omega'-\omega)^{-\epsilon}+\dots\,. \tag{6.35}$$

Corrections to this result are suppressed by powers of α_s or $\Lambda_{\rm QCD}/\omega_{1,2}$. The limit $\epsilon \to 0$ is smooth and gives rise to a dependence $g_{88}^{\rm cut} \propto \omega_1\,\delta(\omega_1 - \omega_2)$. It is then obvious that the double convolution integral in (6.32) is logarithmically divergent in the UV region.[3] When the convolution is understood in the usual sense as an integral over renormalized functions, then this divergence is not regularized.

On the other hand, the explicit expression (6.35) shows that the convolution integral would be regularized by the dimensional regulator if the limit $\epsilon \to 0$ was taken after the convolutions have been evaluated. In that case one obtains a $1/\epsilon$ pole from the UV-divergent convolution integral, which needs to be subtracted in the $\overline{\rm MS}$ scheme. Thus the following procedure will be applied: a hard cutoff $\Lambda_{\rm UV}$ is introduced and the convolution integral is split up in a low-momentum region defined by $\omega_1, \omega_2 < \Lambda_{\rm UV}$ and a high-momentum region defined by the complement. In the high-momentum region it is possible to replace the soft function by the perturbative expression (6.35) up to higher-order terms in α_s and power-suppressed contributions. Then the high-momentum contribution to the double convolution integral is evaluated before taking the limit $\epsilon \to 0$. In doing so, it is important to reinstate a factor $(1-\epsilon)^2$ from the Dirac algebra, see (6.30), and a factor $\mu^{2\epsilon}$ from the conversion of the bare coupling constant g^2 into the renormalized coupling $4\pi\alpha_s(\mu)$. This

[3] Note that according to (6.35) there are no UV divergences from the region of large negative values of $\omega_{1,2}$. In this region the convolution integrals are cut off by non-perturbative dynamics.

leads to

$$\begin{aligned} f_{88}(\omega,\mu) &= \frac{2}{9}\left[(1-\epsilon)^2\,\mu^{2\epsilon}\int_{-\infty}^{\infty}\frac{d\omega_1}{\omega_1+i\varepsilon}\int_{-\infty}^{\infty}\frac{d\omega_2}{\omega_2-i\varepsilon}\,g_{88}^{\text{cut,bare}}(\omega,\omega_1,\omega_2)\right]_{\overline{\text{MS}}\text{ subtracted}} \\ &= \frac{2}{9}\int_{-\infty}^{\Lambda_{\text{UV}}}\frac{d\omega_1}{\omega_1+i\varepsilon}\int_{-\infty}^{\Lambda_{\text{UV}}}\frac{d\omega_2}{\omega_2-i\varepsilon}\,g_{88}^{\text{cut}}(\omega,\omega_1,\omega_2,\mu) \\ &\quad - \frac{C_F}{72\pi^2}\int_{\omega}^{\bar\Lambda}d\omega'\,S(\omega',\mu)\left(\ln\frac{\Lambda_{\text{UV}}(\omega'-\omega)}{\mu^2}+2-2c_{\text{RS}}\right), \end{aligned} \tag{6.36}$$

where c_{RS} is the same scheme-dependent constant as in (6.26). This expression is independent of the auxiliary scale Λ_{UV}, which for consistency should be taken to be several times Λ_{QCD}, so that perturbation theory can be trusted. In the above result the dependence on the factorization scale of dimensional regularization is explicit, and it is now evident that the sum of the two contributions (6.26) and (6.27) is both scale and scheme independent. Indeed, one finds

$$\begin{aligned} F_{88}(E_\gamma,\mu) &= \frac{C_F\alpha_s(\mu)}{4\pi}\left(\frac{m_b}{2E_\gamma}\right)^2\left(\frac{2}{9}\ln\frac{m_b}{\Lambda_{\text{UV}}}-\frac{1}{3}\right)\int_{-p_+}^{\bar\Lambda}d\omega\,S(\omega,\mu) \\ &\quad + \frac{8}{9}\,\pi\alpha_s(\mu)\left(\frac{m_b}{2E_\gamma}\right)^2\int_{-\infty}^{\Lambda_{\text{UV}}}\frac{d\omega_1}{\omega_1+i\varepsilon}\int_{-\infty}^{\Lambda_{\text{UV}}}\frac{d\omega_2}{\omega_2-i\varepsilon}\,g_{88}^{\text{cut}}(-p_+,\omega_1,\omega_2,\mu)\,. \end{aligned} \tag{6.37}$$

The large logarithm $\ln(m_b/\Lambda_{\text{UV}})$ in the first term results from the ratio of the hard-collinear scale $m_b(\omega+p_+)$ in (6.26) and the soft (yet perturbative) scale $\Lambda_{\text{UV}}(\omega+p_+)$ contained in the function $f_{88}(-p_+,\mu)$ in (6.33). Resumming these large logarithms would require solving evolution equations in the effective theory. In the case of UV-divergent convolution integrals, the derivation of such equations is an open problem.

The problem of divergent convolution integrals in SCET has been encountered previously in the context of heavy-to-light form factors [88, 115–117] and power-suppressed contributions to hadronic B-meson decays [35, 118]. It is to some extent still an open question whether these integrals indicate a failure of factorization, or whether they can be cured by a generalization of the theoretical framework of SCET (an attempt in this direction was initiated in [119]). An important difference is that in all previous cases these divergences were of IR origin. In the current case, however, the convolution integrals diverge in the UV. Such divergences appear to be rather generic in the description of higher-order power corrections, because the resulting convolution integrals contain higher powers of soft momentum variables. Still, the presence of this effect casts doubt on the factorization proof in Section 5.3. It is not obvious that the treatment discussed in this section will work at higher orders in perturbation theory and allow for a consistent resummation of large logarithms. In that sense the derivation of factorization is incomplete.

Note that the result (6.37) is insensitive to the mass of the strange-quark, as it should be. This is in contrast with the parton-model expression derived in [64] and shown in (2.29). The IR regulator m_s introduced in the parton-model calculation is replaced in real QCD by a subleading shape function, i.e., by a hadronic matrix element of a non-local operator.

One recovers the parton-model expression for F_{88} if one calculates the soft matrix element in perturbation theory, i.e., if one assumes the validity of (6.35) also at small values of $\omega_{1,2}$ and introduces m_s as an IR regulator, which replaces $\omega_1^{-\epsilon}(\omega'-\omega)^{-\epsilon} \to [\omega_1(\omega'-\omega)-m_s^2]^{-\epsilon}$ in this formula. Of course, such a treatment can not be justified due to the non-perturbative nature of QCD at low energies.

It was argued in [104] that the IR-sensitive terms in the $Q_{8g} - Q_{8g}$ contribution to the $\bar{B} \to X_s\gamma$ photon spectrum can be absorbed into photon fragmentation functions of a strange-quark or gluon. While no formal proof of this assertion was given in that paper, it is likely to be true in the kinematic region away from the endpoint, where the splitting processes $s \to \gamma + s$ and $g \to \gamma + g$ can be treated using the collinear approximation. In the language of SCET this means that the partons after the splitting are still anti-hard-collinear fields, and hence the photon energy can not be near the endpoint. In the endpoint region, on the other hand, these partons are soft, and they do not factorize from the remaining soft matrix element. Hence, in this region the non-perturbative physics is encoded in a complicated subleading four-quark shape function rather than a simpler fragmentation function.

6.4 Analysis of the $Q_{7\gamma} - Q_{8g}$ Contribution

Evaluating the diagrams in Figure 5.1 for this operator pair, yields for the direct photon contribution

$$F_{78}^{(a)}(E_\gamma,\mu) = \frac{C_F\alpha_s(\mu)}{4\pi}\,\frac{m_b}{2E_\gamma}\,\frac{10}{3}\int_{-p_+}^{\bar\Lambda} d\omega\, S(\omega,\mu)\,, \tag{6.38}$$

which generalizes the parton-model result (2.29) in the endpoint region. The case of the $Q_{7\gamma}-Q_{8g}$ interference term is special in that, even though the parton-model expression does not indicate any problematic feature that would call for non-trivial soft contributions, there actually do exist some $\mathcal{O}(1/m_b)$ effects that are described by subleading shape functions. Moreover, these effects remain non-local even for the total decay rate [14] (see also [105]).

In order to study the resolved photon contributions, either one of the two SCET operators in (5.35) and (5.37) arising from the matching relation for Q_{8g} is combined with the leading-order operator in (4.27) descending from $Q_{7\gamma}$. In both cases, the conversion of the anti-hard-collinear fields gives rise to one or more soft quark fields. The relevant SCET diagrams are depicted in the left panels in Figure 6.4, while the corresponding soft graphs resulting after the second matching step are shown in the right panels. In the first case, the second soft quark is generated by an insertion of a subleading term of the SCET Lagrangian. Evaluating the first contribution in detail yields

$$\begin{aligned} F_{78}^{(b)}(E_\gamma,\mu) = \frac{16}{3}\,\pi\alpha_s(\mu)\,\frac{m_b}{2E_\gamma}\,\mathrm{Re}\int_{-\infty}^{\bar\Lambda} d\omega\,\delta(\omega+p_+)\int_{-\infty}^{\infty}\frac{d\omega_1}{\omega_1+i\varepsilon}\int_{-\infty}^{\infty}\frac{d\omega_2}{\omega_2-i\varepsilon} \\ \times\left[\bar g_{78}(\omega,\omega_1,\omega_2,\mu) - \bar g_{78}^{\rm cut}(\omega,\omega_1,\omega_2,\mu)\right]. \end{aligned} \tag{6.39}$$

The soft function $\bar g_{78}$ arises when the hard-collinear strange-quark line in the left diagram in the first row of Figure 6.4 is cut, while the function $\bar g_{78}^{\rm cut}$ originates from the cut through

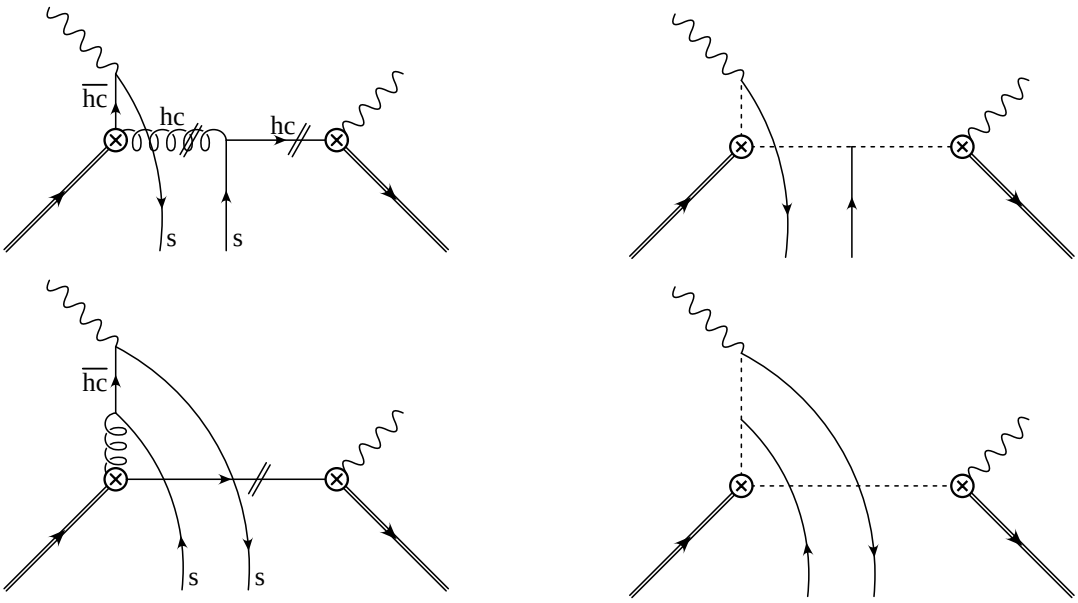

Figure 6.4: Diagrams arising from the matching of the $Q_{7\gamma} - Q_{8g}$ contribution onto SCET (left) and HQET (right). Dashed lines denote non-localities obtained after (anti-)hard-collinear fields have been integrated out.

the hard-collinear gluon line. In this latter case the soft strange-quark line must also be cut. Specifically, the corresponding subleading shape functions are defined as

$$\begin{aligned}\bar{g}_{78}(\omega,\omega_1,\omega_2,\mu) &= \int\frac{dr}{2\pi}\,e^{-i\omega_1 r}\int\frac{du}{2\pi}\,e^{i\omega_2 u}\int\frac{dt}{2\pi}\,e^{-i\omega t}\\ &\times\frac{\langle\bar{B}|\big(\bar{h}S_n\big)(tn)\,T^A\,\overline{\Gamma}_n\,\big(S_n^\dagger s\big)(un)\big(\bar{s}S_{\bar{n}}\big)(r\bar{n})\,\Gamma_{\bar{n}}\,\big(S_{\bar{n}}^\dagger S_n\big)(0)\,T^A\big(S_n^\dagger h\big)(0)|\bar{B}\rangle}{2M_B}\,,\end{aligned}\tag{6.40}$$

and

$$\begin{aligned}\bar{g}_{78}^{\rm cut}(\omega,\omega_1,\omega_2,\mu) &= \int\frac{dr}{2\pi}\,e^{-i\omega_1 r}\int\frac{du}{2\pi}\,e^{i\omega_2 u}\int\frac{dt}{2\pi}\,e^{-i\omega t}\sum\!\!\!\!\!\!\int_{\mathcal{X}_s}\\ &\times\frac{\langle\bar{B}|\big(\bar{h}S_n\big)(tn)\,T^A\,\overline{\Gamma}_n\,\big(S_n^\dagger s\big)((t+u)n)|\mathcal{X}_s\rangle\,\langle\mathcal{X}_s|\big(\bar{s}S_{\bar{n}}\big)(r\bar{n})\,\Gamma_{\bar{n}}\,\big(S_{\bar{n}}^\dagger S_n\big)(0)\,T^A\big(S_n^\dagger h\big)(0)|\bar{B}\rangle}{2M_B}\\ &= \int\frac{dr}{2\pi}\,e^{-i\omega_1 r}\int\frac{du}{2\pi}\,e^{i\omega_2 u}\int\frac{dt}{2\pi}\,e^{-i\omega t}\\ &\times\frac{\langle\bar{B}|\big(\bar{h}S_n\big)(tn)\,T^A\,\overline{\Gamma}_n\,\big(S_n^\dagger s\big)((t+u)n)\big(\bar{s}S_{\bar{n}}\big)(r\bar{n})\,\Gamma_{\bar{n}}\,\big(S_{\bar{n}}^\dagger S_n\big)(0)\,T^A\big(S_n^\dagger h\big)(0)|\bar{B}\rangle}{2M_B}\,,\end{aligned}\tag{6.41}$$

where $\Gamma_{\bar{n}}$ was introduced in (6.29), and Γ_n is defined in the same way as $\Gamma_{\bar{n}}$ but with n and $\bar{n}$ interchanged. One half of the contribution shown in (6.39), but without the real part

prescription, arises from the original diagrams, while the mirror diagrams not shown in the figure give the complex conjugate of the above expressions. The two results combined give a real result, as indicated in (6.39). Note that there is no need to insert a time-ordering symbol in front of the light-quark fields in the definition of $\bar{g}_{78}$ in (6.40), since after convolution with the jet functions the integration variables r and u are restricted to take positive values, and hence the light-quark fields have a space-like separation. In the second equation in (6.42), on the other hand, the fields are not time ordered because the non-local four-fermion operator arises upon performing a sum over intermediate states, as shown in the first equation.

Consider next the contribution shown in the second row of Figure 6.4. In this case the soft light-quark pair can carry any flavor. This yields

$$\begin{aligned} F_{78}^{(c)}(E_\gamma,\mu) &= 4\pi\alpha_s(\mu)\,\frac{m_b}{2E_\gamma}\,\mathrm{Re}\int_{-\infty}^{\bar\Lambda} d\omega\,\delta(\omega+p_+)\int_{-\infty}^{\infty}d\omega_1\int_{-\infty}^{\infty}d\omega_2\,\frac{1}{\omega_1-\omega_2+i\varepsilon} \qquad (6.42)\\ &\times\left[\left(\frac{1}{\omega_1+i\varepsilon}+\frac{1}{\omega_2-i\varepsilon}\right)g_{78}^{(1)}(\omega,\omega_1,\omega_2,\mu)-\left(\frac{1}{\omega_1+i\varepsilon}-\frac{1}{\omega_2-i\varepsilon}\right)g_{78}^{(5)}(\omega,\omega_1,\omega_2,\mu)\right], \end{aligned}$$

where the subleading shape functions have been defined by

$$\begin{aligned} g_{78}^{(1)}(\omega,\omega_1,\omega_2,\mu) &= \int\frac{dr}{2\pi}\,e^{-i\omega_1 r}\int\frac{du}{2\pi}\,e^{i\omega_2 u}\int\frac{dt}{2\pi}\,e^{-i\omega t}\\ &\times\frac{\langle\bar B|\big(\bar h S_n\big)(tn)\big(S_n^\dagger S_{\bar n}\big)(0)\,T^A\,\bar{\not n}(1+\gamma_5)\,\big(S_{\bar n}^\dagger h\big)(0)\,\mathbf{T}\sum_q e_q\,\big(\bar q S_{\bar n}\big)(r\bar n)\,\bar{\not n}\,T^A\big(S_{\bar n}^\dagger q\big)(u\bar n)|\bar B\rangle}{2M_B},\\ g_{78}^{(5)}(\omega,\omega_1,\omega_2,\mu) &= \int\frac{dr}{2\pi}\,e^{-i\omega_1 r}\int\frac{du}{2\pi}\,e^{i\omega_2 u}\int\frac{dt}{2\pi}\,e^{-i\omega t}\\ &\times\frac{\langle\bar B|\big(\bar h S_n\big)(tn)\big(S_n^\dagger S_{\bar n}\big)(0)\,T^A\,\bar{\not n}(1+\gamma_5)\,\big(S_{\bar n}^\dagger h\big)(0)\,\mathbf{T}\sum_q e_q\,\big(\bar q S_{\bar n}\big)(r\bar n)\,\bar{\not n}\gamma_5\,T^A\big(S_{\bar n}^\dagger q\big)(u\bar n)|\bar B\rangle}{2M_B}, \end{aligned} \qquad (6.43)$$

where the sum extends over light quark flavors ($q=u,d,s$), and e_q denote the quark electric charges in units of e. Again, one half of the contribution shown in (6.42), but without the real part prescription, arises from the original diagrams, while the mirror diagrams not shown in the figure give the complex conjugate of the above expressions.

In these definitions the light-quark fields are time-ordered, as indicated by the **T** symbols. That this is the appropriate ordering can be seen as follows. After convolution with the jet functions, for the terms containing the propagator $1/(\omega_1+i\varepsilon)$ in the second line of (6.42) the integration variables r and u are restricted to the range $r>u>0$. These terms correspond to the Feynman graph shown on the left in the second row of Figure 6.4, in which $\bar q(r\bar n)$ should appear to the left of $q(u\bar n)$. For the terms containing the propagator $1/(\omega_2-i\varepsilon)$ the integration variables are restricted to the range $u>r>0$. These terms correspond to the analogous Feynman graph with the opposite direction of the fermion arrow on the light-quark line, for which $\bar q(r\bar n)$ should appear to the right of $q(u\bar n)$. Hence, the proper ordering is indeed the ordering according to (light-cone) time. On the other

hand, arguments along the lines discussed in [120] suggest that the time-ordering prescription is, in fact, not required for forward matrix elements and fields at light-like separation. In what follows it will be assumed that the **T** symbol can be dropped in (6.43).

Very little is known about the complicated four-quark shape-functions defined in (6.40), (6.42), and (6.43). By the general arguments presented in Section 6.1 it follows that the soft functions $\bar{g}_{78}$ and $g_{78}^{(1,5)}$ have support for $-\infty < \omega \leq \bar{\Lambda}$ and $-\infty < \omega_{1,2} < \infty$. However, in the case of $\bar{g}_{78}^{\rm cut}$ it is necessary that $\omega_{1,2} > 0$. Note also the symmetry property

$$\int_{-\infty}^{\bar{\Lambda}} d\omega \left[g_{78}^{(1,5)}(\omega, \omega_1, \omega_2, \mu) \right]^* = \int_{-\infty}^{\bar{\Lambda}} d\omega \, g_{78}^{(1,5)}(\omega, \omega_2, \omega_1, \mu) \,, \tag{6.44}$$

which follows from the definitions of the soft functions in (6.43). While nothing specific could be said about the subleading shape function in the $Q_{8g} - Q_{8g}$ interference, the situation is slightly improved in the $Q_{7\gamma} - Q_{8g}$ case.

6.4.1 $Q_{7\gamma} - Q_{8g}$ in the Vacuum Insertion Approximation

The fact that in the case of $g_{78}^{(1,5)}$ the operators involve light quarks of all flavors offers a strategy for modeling their matrix elements between B-meson states. Unlike the case of the four-quark operators encountered for $g_{88}^{\rm cut}$, $\bar{g}_{78}$, and $\bar{g}_{78}^{\rm cut}$, here it is possible to (very roughly) estimate the matrix element by inserting the vacuum intermediate state between the two light-quark fields. The "vacuum-insertion approximation" (VIA) is used extensively in the study of local four-quark operator matrix elements, and a priori there is no reason why it should work less accurately for non-local operators. Following [14] leads to

$$\int_{-\infty}^{\bar{\Lambda}} d\omega \, g_{78}^{(1,5)}(\omega, \omega_1, \omega_2, \mu)\Big|_{\rm VIA} = -e_{\rm spec} \, \frac{F^2(\mu)}{8} \left(1 - \frac{1}{N_c^2} \right) \phi_+^B(-\omega_1, \mu) \, \phi_+^B(-\omega_2, \mu) \,, \tag{6.45}$$

where $e_{\rm spec}$ denotes the charge of the spectator quark inside the B meson, i.e., $e_{\rm spec} = 2/3$ for $B^\pm$, and $e_{\rm spec} = -1/3$ for B^0 and $\bar{B}^0$. The quantity $F(\mu)$ is the HQET matrix element corresponding to the asymptotic value of the product $f_B\sqrt{M_B}$ in the heavy-quark limit [121]. Finally, $\phi_+^B(\omega, \mu)$ is the leading light-cone distribution amplitude of the B meson [122]. It is a real function with support for $\omega > 0$, which vanishes at $\omega = 0$ and asymptotically falls off like $1/\omega$ modulo logarithms [123]. Useful forms for this function have been derived based on QCD sum rules [122,124,125], the relativistic quark model [126], and model-independent moment relations obtained using the operator-product expansion [123, 127]. The support of $\phi_+^B(\omega, \mu)$ implies that only negative values of ω_1 and ω_2 give rise to non-zero contributions in (6.45), which is in accordance with the fact that $\bar{q}$ (q) describes an anti-quark in the initial (final) state.

To conclude this analysis, the following phenomenological functions are defined

$$\begin{aligned} f_{78}^{(\mathrm{I})}(\omega,\mu) &= \frac{4}{3}\int_{-\infty}^{\infty}\frac{d\omega_1}{\omega_1+i\varepsilon}\int_{-\infty}^{\infty}\frac{d\omega_2}{\omega_2-i\varepsilon}\left[\bar{g}_{78}(\omega,\omega_1,\omega_2,\mu)-\bar{g}_{78}^{\mathrm{cut}}(\omega,\omega_1,\omega_2,\mu)\right], \\ f_{78}^{(\mathrm{II})}(\omega,\mu) &= \int_{-\infty}^{\infty}d\omega_1\int_{-\infty}^{\infty}d\omega_2\,\frac{1}{\omega_1-\omega_2+i\varepsilon} \\ &\quad\times\left[\left(\frac{1}{\omega_1+i\varepsilon}+\frac{1}{\omega_2-i\varepsilon}\right)g_{78}^{(1)}(\omega,\omega_1,\omega_2,\mu)-\left(\frac{1}{\omega_1+i\varepsilon}-\frac{1}{\omega_2-i\varepsilon}\right)g_{78}^{(5)}(\omega,\omega_1,\omega_2,\mu)\right]. \end{aligned} \tag{6.46}$$

In the VIA, one finds

$$\begin{aligned} \int_{-\infty}^{\bar{\Lambda}}d\omega\, f_{78}^{(\mathrm{II})}(\omega,\mu)\Big|_{\mathrm{VIA}} &= -e_{\mathrm{spec}}\,\frac{F^2(\mu)}{8}\left(1-\frac{1}{N_c^2}\right)\left\{\frac{1}{\lambda_B^2(\mu)}+2\pi i\int_0^{\infty}d\omega\,\frac{\left[\phi_+^B(\omega,\mu)\right]^2}{\omega}\right\}, \\ \int_{-\infty}^{\bar{\Lambda}}d\omega\,\mathrm{Re}\, f_{78}^{(\mathrm{II})}(\omega,\mu)\Big|_{\mathrm{VIA}} &= -e_{\mathrm{spec}}\,\frac{F^2(\mu)}{8}\left(1-\frac{1}{N_c^2}\right)\frac{1}{\lambda_B^2(\mu)}, \end{aligned} \tag{6.47}$$

where $\lambda_B=\int_0^{\infty}d\omega\,\phi_+^B(\omega,\mu)/\omega$ denotes the first inverse moment of the B-meson light-cone distribution amplitude [35]. In terms of the functions $f_{78}^{(\mathrm{I,II})}$, the direct and resolved photon contributions to the $\bar{B}\to X_s\gamma$ photon spectrum can be summarized as

$$\begin{aligned} F_{78}(E_\gamma,\mu) = \frac{C_F\alpha_s(\mu)}{4\pi}\,\frac{m_b}{2E_\gamma}\,\frac{10}{3}\int_{-p_+}^{\bar{\Lambda}}d\omega\,S(\omega,\mu) \\ +4\pi\alpha_s(\mu)\,\frac{m_b}{2E_\gamma}\,\mathrm{Re}\left[f_{78}^{(\mathrm{I})}(-p_+,\mu)+f_{78}^{(\mathrm{II})}(-p_+,\mu)\right]. \end{aligned} \tag{6.48}$$

This concludes the analysis of each of the subleading contributions to the $\bar{B}\to X_s\gamma$ differential decay rate in the endpoint region. Some information about the new subleading shape functions appearing in this analysis was already extracted in Section 6.1.1 and this section. The next section will consider the properties of the subleading shape functions under PT transformations.

6.5 Constraints from PT Invariance

In the expressions presented in the previous sections there are four potential sources of complex phases: weak (CP-violating) phases from the CKM matrix elements and the Wilson coefficients, and strong (CP-conserving) phases from the new jet functions $\bar{J}_i$ and the various subleading shape functions. The CKM phases are non-zero only for the $Q_1^q-Q_{7\gamma}$ contributions (with $q=c,u$), where they are suppressed by two powers of the Cabbibo angle. The Wilson coefficients are real in the Standard Model, although they can be complex in many of its extensions (see e.g. [128]).

A unique property of the resolved photon contribution is that the new jet functions $\bar{J}_i$ are given in terms of full propagators (dressed by Wilson lines) and not by cut propagators.

As a result, these functions are in general complex and give rise to strong phases. Since the relevant scale of the jet functions is $\sqrt{2E_\gamma\,\Lambda_{\rm QCD}}$, which is perturbative in the endpoint region, these strong phases are calculable in perturbation theory. The other potential source of strong phases are the soft functions, whose phases are of a non-perturbative nature. When studying the effects of the resolved photon contributions on the rate and CP asymmetry in $B\to X_s\gamma$ decay, it is important to obtain some handle on these non-perturbative phases. In order to do so, the invariance of strong-interaction matrix elements under parity (P) and time reversal (T) is employed.

Under the combined transformation PT, a spinor field $\psi(x)$ transforms as $PT\psi(x)PT=\Lambda_{PT}\,\psi(-x)$, where in the Weyl representation of the Dirac matrices $\Lambda_{PT}=-\gamma^0\gamma^1\gamma^3$ up to an irrelevant phase factor. The soft Wilson line $S_n(x)$ in (4.38) transforms into $S_n(-x)$.[4] Finite-length Wilson lines, as they appear in the definitions of the soft functions, transform as $PT\,[tn,0]\,PT=PT\,S_n(tn)\,S_n^\dagger(0)\,PT=S_n(-tn)\,S_n^\dagger(0)=[-tn,0]$. Finally, the external B-meson states transform as $PT\,|\bar B(v)\rangle=-|\bar B(v)\rangle$. Also, because the time-reversal transformation is anti-linear, matrix elements get complex conjugated under application of PT.

Consider now the definition of the soft function g_{17} in (6.4). Using the fact that the position-space strong-interaction matrix element is PT invariant leads to

$$\begin{aligned} g_{17}(\omega,\omega_1,\mu) &= \int\frac{dr}{2\pi}\,e^{-i\omega_1 r}\int\frac{dt}{2\pi}\,e^{-i\omega t} \\ &\times\frac{\langle\bar B|\big(\bar h S_n\big)(-tn)\,\bar n\!\!\!/(1-\gamma_5)\big(S_n^\dagger S_{\bar n}\big)(0)\,i\gamma_\alpha^\perp\bar n_\beta\,\big(S_{\bar n}^\dagger\,gG_s^{\alpha\beta}S_{\bar n}\big)(-r\bar n)\,\big(S_{\bar n}^\dagger h\big)(0)|\bar B\rangle^*}{2M_B}\,, \end{aligned} \tag{6.49}$$

where it was used that $\Lambda_{PT}^\dagger\,\bar n\!\!\!/\,i\gamma_\alpha^\perp\,\Lambda_{PT}=\bar n\!\!\!/\,i\gamma_\alpha^\perp$ and $\Lambda_{PT}^\dagger\,\bar n\!\!\!/\gamma_5\,i\gamma_\alpha^\perp\,\Lambda_{PT}=-\bar n\!\!\!/\gamma_5\,i\gamma_\alpha^\perp$. However, it was already argued after (6.15) that the term containing γ_5 vanishes. Hence, PT transforms the position-space matrix element into the complex conjugate of the same matrix element with all position arguments x_i replaced by $-x_i$. By taking the complex conjugate of relation (6.50) and reversing the sign of the integration variables r and t, it then follows that $g_{17}(\omega,\omega_1,\mu)$ is a real function.

An analogous argument can be presented for the soft functions $\bar g_{78}$ in (6.40) and $g_{78}^{(1,5)}$ in (6.43), where it is important however that it is possible to avoid the time-ordering prescription for the soft light-quark fields. The HQET trace formalism can be used to show that in the definitions of these matrix elements only even numbers of γ_5 matrices can give rise to non-vanishing contributions, and then the Dirac structures are in all cases even under PT. In contrast to (6.15) the shape function $\bar g_{78}$ corresponds to a four-quark matrix element. Therefore there are two possibilities for additional Dirac structures at higher order. They can appear either between the two light quarks or between a light quark and

[4] Strictly speaking the lower limit of integration is also changed from $-\infty$ to $+\infty$, but this provides an equally valid definition of the same object.

an external state. This leads to

$$\begin{aligned}\bar{g}_{78}(\omega,\omega_1,\omega_2,\mu) = M_B\mathrm{tr}\left[\frac{1+\not v}{2}\,\Gamma_A\,\Xi_1(v,\bar n)\,\Gamma_B\,\frac{1+\not v}{2}\,\Xi_2(v,\bar n)\right]\\ + M_B\mathrm{tr}\left[\gamma_5\,\frac{1+\not v}{2}\,\Gamma_A\,\Xi_3(v,\bar n)\right]\,\mathrm{tr}\left[\Xi_4(v,\bar n)\,\Gamma_B\,\frac{1+\not v}{2}\,\gamma_5\right],\end{aligned} \tag{6.50}$$

where $\Gamma_A = \overline{\Gamma}_n$ and $\Gamma_B = \Gamma_{\bar n}$, and for brevity the dependence of the coefficient functions Ξ_i on ω, ω_1, ω_2, and μ has been suppressed. A similar expression, but with different matrices Γ_A and Γ_B, holds for $g_{78}^{(1,5)}$ after a Fierz transformation. The most general Lorentz-invariant decompositions of the functions Ξ_i involve products of up to four $\not v$, $\not{\bar n}$, and $\gamma_\perp^\alpha$ matrices, where all transverse indices must be contracted. No γ_5 matrices appear in this decomposition. Note also that by using the relation $n + \bar n = 2v$ $\not n$ can be eliminated in favor of $\not v$ and $\not{\bar n}$. With only two independent external vectors v and $\bar n$, however, it is impossible to saturate the four indices of an $\epsilon_{\alpha\beta\gamma\delta}$ symbol, and hence only even numbers of γ_5 matrices in the product structure $\Gamma_A \otimes \Gamma_B$ can give rise to non-zero traces. For the case of $\bar g_{78}$ considered above, it follows that one can replace $16\,\overline{\Gamma}_n \otimes \Gamma_{\bar n} \to \not{\bar n}\not n \otimes \not{\bar n}\not n - \not{\bar n}\not n\gamma_5 \otimes \not{\bar n}\not n\gamma_5$. Both of these product structures are even under PT. In the case of $g_{78}^{(1)}$ and $g_{78}^{(5)}$, it follows similarly that $\not{\bar n}(1+\gamma_5) \otimes \not{\bar n} \to \not{\bar n} \otimes \not{\bar n}$ and $\not{\bar n}(1+\gamma_5) \otimes \not{\bar n}\gamma_5 \to \not{\bar n}\gamma_5 \otimes \not{\bar n}\gamma_5$. Once again, these product structures are even under PT. Therefore the functions $\bar g_{78}$, $g_{78}^{(1)}$, and $g_{78}^{(5)}$ are all real.

Finally the functions $\bar g_{88}^{\rm cut}$ in (6.28) and $\bar g_{78}^{\rm cut}$ in (6.42) will be considered. They are defined in terms of sums over intermediate states $|\mathcal{X}_s\rangle$, which without loss of generality can be chosen to be eigenstates of PT with eigenvalues ± 1. After summing over the polarizations of the intermediate states and integrating over their momenta, one finds that each term in the sum over states can be written as a product of two traces, in analogy to the second term in (6.50). The same arguments as above then show that $\bar g_{88}^{\rm cut}$ and $\bar g_{78}^{\rm cut}$ are real.

In conclusion, all of the subleading shape functions are real. The strong phases mentioned in the introduction to this section thus arise only from the new jet functions $\bar J_i$. Given that the soft functions are real, it now follows from (6.16), (6.31), and (6.44) that $\int d\omega\, g_{17}(\omega,\omega_1)$ is an even function of ω_1, and that $g_{88}^{\rm cut}(\omega,\omega_1,\omega_2)$ and $\int d\omega\, g_{78}^{(1,5)}(\omega,\omega_1,\omega_2)$ are symmetric under the exchange of ω_1 and ω_2.

6.6 Conclusions of this Chapter

This chapter presented a systematic and throughout analysis of the $1/m_b$ corrections to the $\bar B \to X_s\gamma$ photon spectrum in the endpoint region. The results can be summarized by

giving the complete list of the quantities F_{ij} appearing in (5.39). They are

$$\begin{aligned}
F_{77}(E_\gamma,\mu) &= \frac{C_F\alpha_s(\mu)}{4\pi}\int_{-p_+}^{\bar\Lambda} d\omega\left(16\ln\frac{m_b(\omega+p_+)}{\mu^2}+9\right)S(\omega,\mu)+F_{77}^{\rm SSF}(E_\gamma,\mu)\,,\\
F_{88}(E_\gamma,\mu) &= \frac{C_F\alpha_s(\mu)}{4\pi}\int_{-p_+}^{\bar\Lambda} d\omega\left(\frac{2}{9}\ln\frac{m_b(\omega+p_+)}{\mu^2}-\frac{1}{3}\right)S(\omega,\mu)+4\pi\alpha_s(\mu)\,f_{88}(-p_+,\mu)\,,\\
F_{78}(E_\gamma,\mu) &= \frac{C_F\alpha_s(\mu)}{4\pi}\,\frac{10}{3}\int_{-p_+}^{\bar\Lambda} d\omega\,S(\omega,\mu)+4\pi\alpha_s(\mu)\,{\rm Re}\left[f_{78}^{(\rm I)}(-p_+,\mu)+f_{78}^{(\rm II)}(-p_+,\mu)\right],\\
F_{17}(E_\gamma,\mu) &= \frac{C_F\alpha_s(\mu)}{4\pi}\left(-\frac{2}{3}\right)\int_{-p_+}^{\bar\Lambda} d\omega\,S(\omega,\mu)+\sum_{q=c,u}\delta_q\,{\rm Re}\,f_{17,q}(-p_+,\mu)\,,\\
F_{11}(E_\gamma,\mu) &= F_{18}(E_\gamma,\mu)=\frac{C_F\alpha_s(\mu)}{4\pi}\,\frac{2}{9}\int_{-p_+}^{\bar\Lambda} d\omega\,S(\omega,\mu)\,,
\end{aligned}\tag{6.51}$$

with the leading shape function defined in (4.38), δ_q in (6.3), and $F_{77}^{\rm SSF}$ in (5.17) while the the phenomenological functions f_{ij} are convolutions of subleading shape functions and defined in the previous sections of this chapter. These results provide important informations for phenomenological applications. The following chapters will analyze them in detail. In Chapter 7 the effect of the new subleading shape functions on the partially integrated decay rate will be considered. Since these non-perturbative quantities can not be calculated explicitly, they constitute a hadronic uncertainty in the determination of the integrated decay rate. This is also true for an integration range much larger than the endpoint region. In contrast to the subleading shape functions of the $Q_{7\gamma}-Q_{7\gamma}$ contribution, the new subleading shape functions do not reduce to local matrix elements if integrated over a large range. The reason for this lies in the non-local structure of the HQET matrix elements in the n direction. This non-locality is due to the anti-hard-collinear propagators and is not "integrated out" by considering the total rate.

The other phenomenological application is the determination of the hadronic uncertainty in the direct CP asymmetry, observed in the decays of B- and $\bar B$-mesons. This will be considered in Chapter 8.

Chapter 7

Phenomenology I: Hadronic Uncertainties in the Integrated Decay Rate

It has been argued in Chapter 1 that the branching fraction of $\bar{B} \to X_s\gamma$ contains useful information concerning the determination of SM parameters, as well as for restricting the parameter space of new physics models. For practical reasons explained in Section 1.3, this branching fraction only includes photons with an energy above a certain cut. The corresponding theoretical prediction, based on the parton model, was given in (2.38). In this calculation the uncertainty due to non-perturbative effects was estimated to be about 5% [5].

The last chapter systematically identified the non-perturbative corrections to the $\bar{B} \to X_s\gamma$ photon spectrum in the endpoint region at $\mathcal{O}(1/m_b)$. By integrating these results over the photon energy, it is now possible to estimate the size of the non-perturbative corrections to the branching fraction. As it turns out, some of these corrections fall outside the realm of the local OPE and need to be parameterized by integrals over subleading shape functions. In Section 7.1 the partially integrated decay rate with a lower cutoff will be defined and related to the results of the previous chapter. Section 7.2 will then define a set of hadronic quantities that parameterize the uncertainties due to the new subleading contributions. Subsequently, each of the relevant contributions will be considered in Sections 7.3 to 7.5. Finally, the results will be summed up in Section 7.6 and an improved estimate of the hadronic uncertainties in the partonic calculation of the branching fraction will be given.

7.1 Partially Integrated Decay Rate

For phenomenological purposes, it is most interesting to study the partial $\bar{B} \to X_s\gamma$ decay rate

$$\Gamma(E_0) := \int_{E_0}^{M_B/2} dE_\gamma \, \frac{d\Gamma}{dE_\gamma} \,, \tag{7.1}$$

obtained by integrating the photon spectrum over a region $E_0 < E_\gamma < M_B/2$. Provided that $\Delta := m_b - 2E_0$ is much larger than $\Lambda_{\rm QCD}$, the direct photon contributions to this integrated rate can be calculated in terms of local operator matrix elements [13] using a combined expansion in powers of Δ/m_b and $\Lambda_{\rm QCD}/\Delta$. The latter expansion corresponds to the moment expansion of the leading shape function, given in (3.38). In the limit $E_0 \to 0$ one obtains the total decay rate, and $\Delta = m_b$; however, as was discussed in Section 1.3, the rates measured experimentally are obtained with values of E_0 larger than 1.7 GeV, so that $\Delta < 1.25\,\text{GeV}$.

An important feature of the resolved photon contributions studied in this work is that they do not reduce to local operator matrix element in the limit $\Delta \gg \Lambda_{\rm QCD}$. Rather, the corresponding contributions to the integrated decay rate must still be described in terms of matrix elements of non-local operators. This implies that the corresponding theoretical uncertainties do not reduce significantly as the cutoff E_0 is taken out of the endpoint region. This will now be illustrated by deriving expressions for the first-order power corrections to the integrated decay rate

$$\begin{aligned}\Gamma(E_0) = \frac{G_F^2\alpha|V_{tb}V_{ts}^*|^2}{32\pi^4}\,\overline{m}_b^2(\mu)\,m_b^3\Bigg[&|H_\gamma(\mu)|^2\,[1+\mathcal{O}(\alpha_s)]\\ &+\frac{1}{m_b}\sum_{i\le j}\text{Re}\big[C_i^*(\mu)\,C_j(\mu)\big]\,\bar F_{ij}(\Delta,\mu)+\dots\Bigg],\end{aligned} \tag{7.2}$$

valid for $\Delta \gg \Lambda_{\rm QCD}$. Here m_b denotes the pole mass of the b-quark. The dots represent terms of order $1/m_b^2$ and higher, which are ignored. The integrated coefficient functions are obtained as

$$\bar F_{ij}(\Delta,\mu) = \int_{-\bar\Lambda}^{\Delta} dp_+\,F_{ij}(E_\gamma,\mu)\,, \tag{7.3}$$

where $p_+ = m_b - 2E_\gamma$. As will be explained below, with the exception of $g_{88}^{\rm cut}$ the non-perturbative soft functions have support for values $\omega = \mathcal{O}(\Lambda_{\rm QCD})$.[1] In the limit $\Delta \gg \Lambda_{\rm QCD}$, the ω integrals in the definitions of the subleading shape function can then be performed over the entire range from $-\infty$ to $\bar\Lambda$, and this leads to simplifications. However, the integrals over the remaining ω_i variables can not be simplified.

For the direct photon contributions, the integrals (5.13) will again be needed

$$\begin{aligned}\int_{-\bar\Lambda}^{\Delta} dp_+ \int_{-p_+}^{\bar\Lambda} d\omega\,S(\omega,\mu) &\approx \Delta\,,\\ \int_{-\bar\Lambda}^{\Delta} dp_+ \int_{-p_+}^{\bar\Lambda} d\omega\,\ln\frac{m_b(\omega+p_+)}{\mu^2}\,S(\omega,\mu) &\approx \Delta\left(\ln\frac{m_b\Delta}{\mu^2}-1\right).\end{aligned} \tag{7.4}$$

It follows that the direct photon terms contribute to (7.2) at order Δ/m_b in power counting and can be computed using a local operator-product expansion. In the formal limit $E_0 \to 0$ these terms are promoted to $\mathcal{O}(1)$ contributions.

[1] Radiative tails of these functions, which can exhibit power behavior and extend to larger ω values will be ignored. These effects only contribute at higher orders in α_s.

Next the subleading shape-function contributions to the integrated decay rate will be discussed. For the operator pair $Q_{7\gamma} - Q_{7\gamma}$, the subleading shape-function contributions also reduce to matrix elements of local operators, as discussed in detail in [9, 10, 100, 107]. From (5.24) it then follows that

$$\bar{F}_{77}(\Delta,\mu) = \frac{C_F\alpha_s(\mu)}{4\pi}\,\Delta\left(16\ln\frac{m_b}{\Delta}+1\right). \tag{7.5}$$

Note that, at order $1/m_b$, the non-zero strange-quark mass effect discussed in Section 5.2.6 integrates to zero in the partially integrated decay rate (at tree level in α_s), as long as $\Delta \gg \Lambda_{\rm QCD}$. Similarly, for the operator pairs $Q_1^q - Q_1^q$ and $Q_1^q - Q_{8g}$, only direct photon contributions contribute at order $1/m_b$, and one obtains

$$\bar{F}_{11}(\Delta,\mu) = \bar{F}_{18}(\Delta,\mu) = \frac{C_F\alpha_s(\mu)}{4\pi}\,\frac{2}{9}\,\Delta\,. \tag{7.6}$$

The remaining contributions, all of which contain resolved photon terms, are more interesting. For the operator pairs $Q_1^q - Q_{7\gamma}$, one obtains

$$\bar{F}_{17}(\Delta,\mu) = \frac{C_F\alpha_s(\mu)}{4\pi}\,\left(-\frac{2}{3}\right)\Delta + \frac{2}{3}\,(1-\delta_u)\,{\rm Re}\int_{-\infty}^{\infty}\frac{d\omega_1}{\omega_1+i\varepsilon}\left[1-F\left(\frac{m_c^2-i\varepsilon}{m_b\,\omega_1}\right)\right]h_{17}(\omega_1,\mu)\,, \tag{7.7}$$

where

$$\begin{aligned} h_{17}(\omega_1,\mu) &= \int_{-\Delta}^{\bar\Lambda} d\omega\, g_{17}(\omega,\omega_1,\mu) \approx \int_{-\infty}^{\bar\Lambda} d\omega\, g_{17}(\omega,\omega_1,\mu) \\ &= \int\frac{dr}{2\pi}\,e^{-i\omega_1 r}\,\frac{\langle\bar B|\big(\bar h S_{\bar n}\big)(0)\,\bar n\!\!\!/\, i\gamma_\alpha^\perp\bar n_\beta\,\big(S_{\bar n}^\dagger\, gG_s^{\alpha\beta}S_{\bar n}\big)(r\bar n)\,\big(S_{\bar n}^\dagger h\big)(0)|\bar B\rangle}{2M_B}\,. \end{aligned} \tag{7.8}$$

The integral over p_+ in (7.3) eliminates the $\delta(\omega+p_+)$ distribution in (6.2), and integrating the soft function $g_{17}(\omega,\omega_1,\mu)$ in (6.4) over ω then eliminates the t-integral and sets $t=0$, so that part of the non-localities of the operator are eliminated. However, the gluon field is still smeared out on the $\bar n$ light-cone. Note that there is no contribution from the up-quark penguin loop to the integrated rate. As noted in Section 6.5, the integral over ω of $g_{17}(\omega,\omega_1,\mu)$ is symmetric in ω_1, so that the integral over $F_{17,u}^{(b)}$ in (6.8) vanishes.[2]

The case of the $Q_{7\gamma} - Q_{8g}$ interference leads to

$$\bar{F}_{78}(\Delta,\mu) = \frac{C_F\alpha_s(\mu)}{4\pi}\,\frac{10}{3}\,\Delta + 4\pi\alpha_s(\mu)\,{\rm Re}\int_{-\infty}^{\infty}\frac{d\omega_1}{\omega_1+i\varepsilon}\int_{-\infty}^{\infty}\frac{d\omega_2}{\omega_2-i\varepsilon}\,h_{78}^{(5)}(\omega_1,\omega_2,\mu)\,, \tag{7.9}$$

[2]It has been pointed out in the past that up-quark penguin loops might give rise to an $\mathcal{O}(\Lambda_{\rm QCD}/m_b)$ uncertainty in the integrated rate for $\bar B\to X_d\gamma$ decay [111], where unlike in $\bar B\to X_s\gamma$ they are not CKM suppressed. Applying the present analysis to $\bar B\to X_d\gamma$ shows that this contribution actually vanishes, removing that source of uncertainty in the integrated decay rate. Note that the same is not true for the CP asymmetry in $\bar B\to X_d\gamma$ decay, where the corresponding contribution is proportional to $h_{17}(0)$, which is non-zero in general.

where in analogy with (7.8) it has been defined

$$h_{78}^{(5)}(\omega_1,\omega_2,\mu) = \int\frac{dr}{2\pi}\,e^{-i\omega_1 r}\int\frac{du}{2\pi}\,e^{i\omega_2 u} \times\frac{\langle\bar B|\big(\bar h S_{\bar n}\big)(0)\,T^A\,\bar n\!\!\!/\gamma_5\,\big(S_{\bar n}^\dagger h\big)(0)\,\sum_q e_q\,\big(\bar q S_{\bar n}\big)(r\bar n)\,\bar n\!\!\!/\gamma_5\,T^A\big(S_{\bar n}^\dagger q\big)(u\bar n)|\bar B\rangle}{2M_B}\,. \tag{7.10}$$

Note that the contribution from $g_{78}^{(1)}$ vanishes, since the integral over ω of this function is symmetric under the exchange of ω_1 and ω_2. Likewise, the contributions from the functions $\bar g_{78}$ and $\bar g_{78}^{\rm cut}$ to the integrated decay rate cancel each other. This follows from the fact that the two non-local operators in (6.40) and (6.42) coincide for $t=0$. In the VIA one finds

$$\bar F_{78}(\Delta,\mu)\Big|_{\rm VIA} = \frac{C_F\alpha_s(\mu)}{4\pi}\,\frac{10}{3}\,\Delta - \frac{\pi\alpha_s(\mu)}{2}\,e_{\rm spec}\left(1-\frac{1}{N_c^2}\right)\frac{F^2(\mu)}{\lambda_B^2(\mu)}\,. \tag{7.11}$$

The second term coincides with the result derived first in [14].

Finally, for the case of the operator pair $Q_{8g}-Q_{8g}$, it follows from (6.37)

$$\begin{aligned}\bar F_{88}(\Delta,\mu) &= \frac{C_F\alpha_s(\mu)}{4\pi}\left(\frac{2}{9}\,\ln\frac{m_b}{\Lambda_{\rm UV}}-\frac{1}{3}\right)\Delta \\ &\quad+\frac{8}{9}\,\pi\alpha_s(\mu)\int_{-\infty}^{\Lambda_{\rm UV}}\frac{d\omega_1}{\omega_1+i\varepsilon}\int_{-\infty}^{\Lambda_{\rm UV}}\frac{d\omega_2}{\omega_2-i\varepsilon}\,h_{88}^{\rm cut}(\Delta,\omega_1,\omega_2,\mu)\,,\end{aligned} \tag{7.12}$$

where

$$h_{88}^{\rm cut}(\Delta,\omega_1,\omega_2,\mu) = \int_{-\Delta}^{\bar\Lambda} d\omega\, g_{88}^{\rm cut}(\omega,\omega_1,\omega_2,\mu)\,. \tag{7.13}$$

Naively, one would expect that for $\Delta\gg\Lambda_{\rm QCD}$ this function becomes independent of Δ and reduces to the expression

$$h_{88}^{\rm cut}(\omega_1,\omega_2,\mu) \stackrel{?}{=} \int\frac{dr}{2\pi}\,e^{-i\omega_1 r}\int\frac{du}{2\pi}\,e^{i\omega_2 u} \times\frac{\langle\bar B|\big(\bar h S_n\big)(0)\,T^A\big(S_n^\dagger S_{\bar n}\big)(0)\,\overline{\Gamma}_{\bar n}\big(S_{\bar n}^\dagger s\big)(u\bar n)\big(\bar s S_{\bar n}\big)(r\bar n)\Gamma_{\bar n}\big(S_{\bar n}^\dagger S_n\big)(0)\,T^A\big(S_n^\dagger h\big)(0)|\bar B\rangle}{2M_B}\,, \tag{7.14}$$

in which case the second term in (7.12) would be strictly positive. However, in the present case the limit $t\to 0$ in (6.28) is singular, since then the separation between the two light-quark fields s and $\bar s$ becomes light-like. As a result, the integral over ω in (7.13) diverges linearly as Δ is raised to infinity, and hence it must be evaluated at large but finite Δ. In other words, unlike for the other soft functions, the support of the function $g_{88}^{\rm cut}$ is not restricted to values $\omega=\mathcal{O}(\Lambda_{\rm QCD})$ but extends to large negative values of ω. This is in accordance with the asymptotic behavior derived in (6.35).

The convolutions of the soft functions with anti-hard-collinear jet functions in the results given above can not be expressed in terms of local operator matrix elements, but rather define unknown hadronic parameters of order $\Lambda_{\rm QCD}$. These are the sources of genuine, first-order power corrections to the integrated decay rate, which are not reduced by lowering the cutoff E_0 on the photon energy. In the following sections the size of these hadronic effects will be estimated.

7.2 Hadronic Uncertainties

The results of the previous sections can be used to quantify the effect of the resolved photon terms on the $\bar{B} \to X_s\gamma$ photon spectrum. In this section the decay rate integrated over a sufficiently wide energy range will be considered.

In order to estimate the irreducible theoretical uncertainty from these new non-local effects on the integrated decay rate, it is useful to define the function

$$\mathcal{F}_E(\Delta) = \frac{\Gamma(E_0) - \Gamma(E_0)|_{\rm OPE}}{\Gamma(E_0)|_{\rm OPE}} \tag{7.15}$$

where E_0 is the lower cutoff on the photon energy, and $\Delta = m_b - 2E_0$. This definition is such that the true decay rate $\Gamma(E_0)$ is obtained from the theoretical expression $\Gamma(E_0)|_{\rm OPE}$ obtained using a *local* operator product expansion by multiplying it with $[1 + \mathcal{F}_E(\Delta)]$. Note that $\Gamma(E_0)|_{\rm OPE}$ refers to the formula used in previous calculations of the $\bar{B} \to X_s\gamma$ rate, see e.g. [5]. The function $\mathcal{F}_E(\Delta)$ corresponds to the relative theoretical error made in these calculations due to the neglect of non-local power corrections from resolved photon contributions. Note that the non-perturbative effect from (6.20) is already included in the OPE result.

At order $1/m_b$ this yields

$$\begin{aligned}
\mathcal{F}_E(\Delta) = \frac{1}{m_b}\Bigg\{ & \left[\bar{F}_{77}(\Delta,\mu) - \frac{C_F\alpha_s(\mu)}{4\pi}\,\Delta\left(16\ln\frac{m_b}{\Delta} + 1\right)\right] \\
& + \frac{C_1(\mu)}{C_{7\gamma}(\mu)}\left[\bar{F}_{17}(\Delta,\mu) + \frac{C_F\alpha_s(\mu)}{4\pi}\,\frac{2}{3}\,\Delta + \frac{m_b\lambda_2}{9m_c^2}\right] \\
& + \frac{C_{8g}(\mu)}{C_{7\gamma}(\mu)}\left[\bar{F}_{78}(\Delta,\mu) - \frac{C_F\alpha_s(\mu)}{4\pi}\,\frac{10}{3}\,\Delta\right] \\
& + \left(\frac{C_{8g}(\mu)}{C_{7\gamma}(\mu)}\right)^2\left[\bar{F}_{88}(\Delta,\mu) - \frac{C_F\alpha_s(\mu)}{4\pi}\,\Delta\left(\frac{2}{9}\ln\frac{m_b\Delta}{m_s^2} - \frac{5}{9}\right)\right]\Bigg\} + \dots\,,
\end{aligned} \tag{7.16}$$

where it was assumed that the Wilson coefficients are real (like in the Standard Model) and effects proportional to V_{ub} have been neglected. Note that the terms in the first line on the right-hand side vanish due to the relation (7.5). The various other contributions can be expressed in terms of suitably defined hadronic parameters of order $\Lambda_{\rm QCD}$, using the expressions for the quantities $\bar{F}_{ij}(\Delta,\mu)$ derived in the previous section under the assumption that $\Delta \gg \Lambda_{\rm QCD}$. Making explicit the dependence on the Wilson coefficients and factors of the strong coupling $g^2 = 4\pi\alpha_s$ leads to

$$\begin{aligned}
\mathcal{F}_E(\Delta) = & \frac{C_1(\mu)}{C_{7\gamma}(\mu)}\,\frac{\Lambda_{17}(m_c^2/m_b,\mu)}{m_b} + \frac{C_{8g}(\mu)}{C_{7\gamma}(\mu)}\,4\pi\alpha_s(\mu)\,\frac{\Lambda_{78}^{\rm spec}(\mu)}{m_b} \\
& + \left(\frac{C_{8g}(\mu)}{C_{7\gamma}(\mu)}\right)^2\left[4\pi\alpha_s(\mu)\,\frac{\Lambda_{88}(\Delta,\mu)}{m_b} - \frac{C_F\alpha_s(\mu)}{9\pi}\,\frac{\Delta}{m_b}\,\ln\frac{\Delta}{m_s}\right] + \dots\,,
\end{aligned} \tag{7.17}$$

where

$$\Lambda_{17}\Big(\frac{m_c^2}{m_b},\mu\Big) = e_c\,\mathrm{Re}\int_{-\infty}^{\infty}\frac{d\omega_1}{\omega_1}\left[1-F\left(\frac{m_c^2-i\varepsilon}{m_b\,\omega_1}\right)+\frac{m_b\,\omega_1}{12m_c^2}\right]h_{17}(\omega_1,\mu)\,,$$
$$\Lambda_{78}^{\rm spec}(\mu) = \mathrm{Re}\int_{-\infty}^{\infty}\frac{d\omega_1}{\omega_1+i\varepsilon}\int_{-\infty}^{\infty}\frac{d\omega_2}{\omega_2-i\varepsilon}\,h_{78}^{(5)}(\omega_1,\omega_2,\mu)\,,$$
$$\Lambda_{88}(\Delta,\mu) = e_s^2\left[\int_{-\infty}^{\Lambda_{\rm UV}}\frac{d\omega_1}{\omega_1+i\varepsilon}\int_{-\infty}^{\Lambda_{\rm UV}}\frac{d\omega_2}{\omega_2-i\varepsilon}\,2h_{88}^{\rm cut}(\Delta,\omega_1,\omega_2,\mu)-\frac{C_F}{8\pi^2}\,\Delta\left(\ln\frac{\Lambda_{\rm UV}}{\Delta}-1\right)\right]. \tag{7.18}$$

In the case of Λ_{17} and Λ_{88} the appropriate powers of the quark electric charges have been factored out. Because of the sum over light-quark flavors in (7.11), the parameter $\Lambda_{78}^{\rm spec}$ receives contributions proportional to any one of the light-quark charges. The resulting hard breaking of isospin symmetry implies that its value will be different for charged and neutral B mesons, even in the limit of exact isospin symmetry of the strong interaction. It will be show in Section 7.4 that, in certain approximation schemes, $\Lambda_{78}^{\rm spec}$ is proportional to the electric charge of the spectator quark in the B meson.

Note that the parameters m_c^2/m_b and Δ entering the arguments of Λ_{17} and Λ_{88} count as $\mathcal{O}(\Lambda_{\rm QCD})$. The dependence on the strange-quark mass in (7.17) arises only because the function $\mathcal{F}_E(\Delta)$ is defined as the deviation from the partonic rate $\Gamma_{\rm part}(E_0)$. The true decay rate $\Gamma(E_0)$ in (7.15) is independent of m_s. Note also that the result for Λ_{88} is formally independent of the UV cutoff $\Lambda_{\rm UV}$, and that it is the only hadronic parameter in (7.17) that depends on the quantity Δ. In the formal limit where the cut on the photon energy is removed, $\Delta\to m_b$, the linear growth (modulo logarithms) of the parameter Λ_{88} with Δ implies that the corresponding contribution to $\mathcal{F}_E(\Delta)$ is promoted from a power-suppressed to a leading-order effect. Indeed, it is well known that in this limit there exists a leading-power, non-perturbative $Q_{8g}-Q_{8g}$ contribution related to the photon fragmentation off a strange-quark or gluon [104]. For practical applications this observation is irrelevant. It will be argued in Section 7.5 that, for realistic values of E_0 outside the endpoint region, the dependence of Λ_{88} on Δ is very weak, and therefore the function $\mathcal{F}_E(\Delta)$ is almost equal to a constant.

Without further information about the soft functions, the Λ_{ij} parameters are expected to be of order $\Lambda_{\rm QCD}$ apart from the electric charges factored out in (7.18). This would lead to very large effects of up to 30% on the decay rate. Fortunately, it is possible to constrain the values of Λ_{17} and $\Lambda_{78}^{\rm spec}$ by means of simple considerations, as will now be discussed. The input parameters used for the estimates in the following discussion are collected in Appendix A.2. The accuracy of the calculations is such that the scale dependence of the subleading soft functions and the corresponding hadronic parameters is irrelevant. Even though their μ dependence is indicated in the formulae given above, to properly control this dependence would require to extend the calculations to the next order in the expansion in powers of $\alpha_s(\mu)$.

7.3 Analysis of the $Q_1^c - Q_{7\gamma}$ Contribution

In order to obtain a reasonable estimate for the parameter Λ_{17}, first everything known about the function $h_{17}(\omega_1, \mu)$ defined below (7.8) will be collected. As proven in Section 6.5, this function must be real, and the symmetry relation (6.16) then implies that it is an even function of ω_1. It follows that all odd moments of h_{17} vanish. Moreover, from (6.14) the normalization of h_{17} is fixed to $2\lambda_2$. About the higher even moments nothing definite is known, but one can expect them to be proportional to an appropriate power of $\Lambda_{\rm QCD}$ times a not too large numerical factor. Finally, as a soft function, h_{17} should not have any significant structures, such as peaks or zeros, outside the hadronic energy range.

The first functions that come to mind are an exponential and a Gaussian,

$$h_{17}(\omega_1,\mu) = \frac{\lambda_2}{\sigma}\, e^{-\frac{|\omega_1|}{\sigma}}\,, \quad \text{or} \quad h_{17}(\omega_1,\mu) = \frac{2\lambda_2}{\sqrt{2\pi}\sigma}\, e^{-\frac{\omega_1^2}{2\sigma^2}}\,, \tag{7.19}$$

for which all even moments are finite. As long as $\sigma \ll 4m_c^2/m_b \approx 1.1\,\text{GeV}$, which with the power counting adopted in this thesis is formally of order $\Lambda_{\rm QCD}$, then for all relevant ω_1 values the argument of the penguin function $F(x)$ entering the definition of Λ_{17} in (7.18) is much larger than $1/4$, which is the radius of convergence for the Taylor expansion given in (6.9). It is then a good approximation to expand the penguin function $[1 - F(x)]$ to $\mathcal{O}(1/x^3)$. The first term in this expansion corresponds to the non-perturbative correction identified in [108], which was already included in the partonic result and subtracted in (7.18). It therefore does not contribute to $\mathcal{F}_E(\Delta)$. The next term gives rise to an odd moment of h_{17} and thus vanishes. The third term in the expansion contributes the amount

$$\Lambda_{17}^{\rm expanded} = -\frac{e_c}{280}\,\frac{m_b^3}{m_c^6}\,\lambda_2\,\langle\omega_1^2\rangle \tag{7.20}$$

to Λ_{17}. Here $\langle\omega_1^2\rangle$ denotes the (normalized) variance of the function $h_{17}(\omega_1,\mu)$, which equals $2\sigma^2$ for the exponential form and σ^2 for the Gaussian. For a typical hadronic scale $\sigma = 0.5\,\text{GeV}$ this gives $\Lambda_{17}^{\rm expanded} = -6.9\,\text{MeV}$ and $-3.4\,\text{MeV}$, respectively. Here and below the input parameters collected in Appendix A.2 have been used. The corresponding contributions to the decay rate are very small, below 0.5% in magnitude.

It is an interesting observation that, due to a weaker numerical suppression, certain $1/m_b$ corrections to Λ_{17} can give a contribution of comparable size. They arise from the fact that the first moment of the function $g_{17}(\omega,\omega_1,\mu)$ with respect to ω does not vanish, see (6.18). In order to calculate the resulting power-suppressed term, one replaces the first relation in (7.18) by

$$\begin{aligned}\Lambda_{17}\Big(\frac{m_c^2}{m_b},\mu\Big) = e_c\,\text{Re}\int_{-\infty}^{\bar\Lambda} d\omega \int_{-\infty}^{\infty}\frac{d\omega_1}{\omega_1}\\ \times\left\{\left(\frac{m_b+\omega}{m_b}\right)^3\left[1-F\left(\frac{m_c^2-i\varepsilon}{(m_b+\omega)\,\omega_1}\right)\right]+\frac{m_b\,\omega_1}{12m_c^2}\right\} g_{17}(\omega,\omega_1,\mu)\,,\end{aligned} \tag{7.21}$$

where the factor $(\frac{m_b+\omega}{m_b})^3$ appears because of the prefactor E_γ^3 in (5.39). Expanding now the penguin function to first order yields

$$\Lambda_{17}\Big(\frac{m_c^2}{m_b},\mu\Big) = e_c\,\mathrm{Re}\int_{-\infty}^{\bar\Lambda} d\omega \int_{-\infty}^{\infty}\frac{d\omega_1}{\omega_1}\left\{-\left(1+\frac{\omega}{m_b}\right)^4\frac{m_b\,\omega_1}{12m_c^2}+\frac{m_b\,\omega_1}{12m_c^2}+\ldots\right\} g_{17}(\omega,\omega_1,\mu)\,, \tag{7.22}$$

where the dots represent higher-order terms in the expansion of the penguin function, which in particular give rise to the contribution (7.20). The expression shown above yields a $1/m_b$-suppressed contribution to the parameter Λ_{17}, which is denoted by $\delta\Lambda_{17}$. It is proportional to the normalized first moment of the function g_{17} with respect to ω, which according to (6.14) and (6.18) is given by $\langle\omega\rangle = -\rho_{LS}^3/(6\lambda_2) \approx 0.24\,\mathrm{GeV}$. This leads to

$$\delta\Lambda_{17} = \frac{2\rho_{LS}^3}{27m_c^2} \approx -(9.8\pm 5.2)\,\mathrm{MeV}\,, \tag{7.23}$$

which is formally a power correction proportional to $\Lambda_{\rm QCD}^2/m_b$ to the result in (7.20). Here $\rho_{LS}^3 = 3\rho_2$ corresponds to the spin-orbit term of the HQET Lagrangian introduced in (3.14).

In practice, it turns out that (7.20) provides a reasonable approximation only as long as $\sigma < 0.3\,\mathrm{GeV}$. Performing the convolution integral in (7.18) exactly, one finds that for both model functions in (7.19) the resulting value of $|\Lambda_{17}|$ is maximized for certain values of σ, which depend on the functional form of h_{17}. Using the input parameters collected in Appendix A.2, one obtains $(\Lambda_{17}^{\rm exp})_{\rm max} = -4.6\,\mathrm{MeV}$ for $\sigma = 0.51\,\mathrm{GeV}$ with the exponential model, and $(\Lambda_{17}^{\rm Gauss})_{\rm max} = -8.1\,\mathrm{MeV}$ for $\sigma = 0.77\,\mathrm{GeV}$ with the Gaussian model. Note that the maximum values are smaller in magnitude than those one would derive from (7.20) with these values of σ.

The above estimates do not provide a conservative bound on the size of the hadronic parameter Λ_{17}. A significantly larger effect can be obtained if the soft function $g_{17}(\omega,\omega_1,\mu)$ exhibits a tail outside the region $|\omega_1| \ll 4m_c^2/m_b$. In analogy with the leading-order shape function, it is to be expected that the function g_{17} exhibits a radiative tail proportional to $1/\omega_1$ for large ω_1. But even at the non-perturbative level, it is conceivable that a significant contribution to the integral results from the region of larger ω_1 values. Consider, as an example, the model

$$h_{17}(\omega_1,\mu) = \frac{2\lambda_2}{\sqrt{2\pi}\sigma}\,\frac{\omega_1^2-\Lambda^2}{\sigma^2-\Lambda^2}\,e^{-\frac{\omega_1^2}{2\sigma^2}}\,, \tag{7.24}$$

which for Λ and σ of order $\Lambda_{\rm QCD}$ satisfies all requirements one would reasonably impose on the soft function. The solid curve in Figure 7.1 shows this function evaluated with $\sigma = 0.5\,\mathrm{GeV}$ and $\Lambda = 0.425\,\mathrm{GeV}$. It features regions of positive and negative values and hence is less constrained at larger ω_1 by the fact that the normalization is fixed to $2\lambda_2$. Having values of either sign is not problematic, because there is no probabilistic interpretation of the subleading soft functions. The long-dashed line in the figure shows the weight function under the convolution integral in the definition of Λ_{17} in (7.18), including the charge factor e_c. With the above parameter choices for the soft function, it follows that

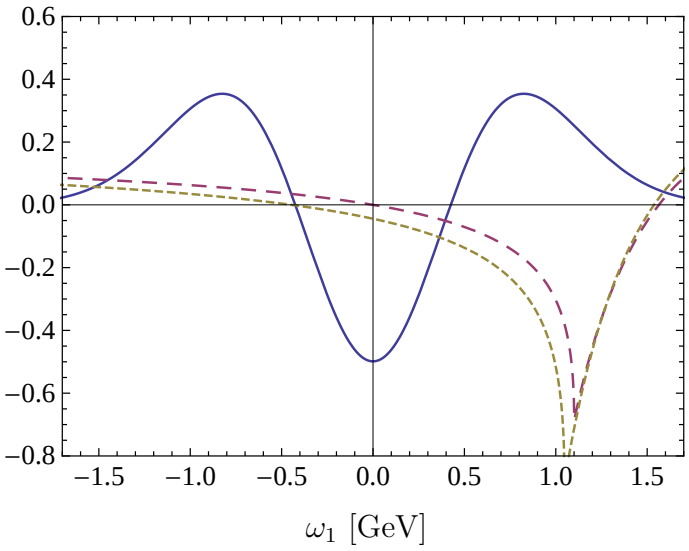

Figure 7.1: Model function $h_{17}(\omega_1, \mu)$ from (7.24) in units of GeV, with $\sigma = 0.5\,\text{GeV}$ and $\Lambda = 0.425\,\text{GeV}$ (solid line); weight function under the convolution integral in the definition of Λ_{17} in (7.18) in units of GeV^{-1} (long-dashed line); weight function including $1/m_b$ corrections, obtained by the substitution $\omega \to \langle\omega\rangle$ in (7.21) (short-dashed line). See text for explanations.

$\Lambda_{17} = -42\,\text{MeV}$. By using another set of values, a correction with the opposite sign and of the same magnitude can be obtained. For example, taking $\sigma = 0.5\,\text{GeV}$ and $\Lambda = 0.575\,\text{GeV}$ yields $\Lambda_{17} = 27\,\text{MeV}$. If the $1/m_b$ corrections as shown in (7.21) are included, using $(m_b + \omega) \to (m_b + \langle\omega\rangle) = (m_b - \rho_{LS}^3/6\lambda_2)$, one finds $-62\,\text{MeV}$ and $21\,\text{MeV}$, respectively. Of course, these are just illustrative values, and one could obtain even larger negative or positive values by reducing the separation between σ and Λ, which however will also increase the value of the soft function at $\omega_1 = 0$. Nevertheless, based on these considerations, it seems that

$$-60\,\text{MeV} < \Lambda_{17} < 25\,\text{MeV} \tag{7.25}$$

is a reasonably conservative range, which will be adopted for the analysis below. While this allows for a value significantly larger in magnitude than the naive estimate (7.20), it nevertheless strongly suggests that Λ_{17} is considerably smaller in magnitude than Λ_{QCD}. Note that the effect of a value of Λ_{17} near the extreme values indicated above would be of the same magnitude as the effect of the leading-order, non-perturbative correction from [108], which corresponds to $-m_b\lambda_2/(9m_c^2) \approx -48\,\text{MeV}$.

7.4 Analysis of the $Q_{7\gamma} - Q_{8g}$ Contribution

It is instructive to analyze this contribution using the language of flavor symmetry of the strong interaction. Due to the weighting by the quark electric charges, the relevant four-quark operator in (6.43) is a pure $SU(3)$ octet, which can be decomposed into two parts

corresponding to isospin $I = 0, 1$. The Wigner-Eckart theorem implies that

$$\Lambda_{78}^{\rm spec} = \frac{1}{6}\,\Lambda_{I=0}^{(8)} \pm \frac{1}{2}\,\Lambda_{I=1}^{(8)} = \frac{1}{6}\left(\Lambda_{I=0}^{(8)} - \Lambda_{I=1}^{(8)}\right) + e_{\rm spec}\,\Lambda_{I=1}^{(8)}\,, \tag{7.26}$$

where the upper (lower) sign in the first equation refers to charged (neutral) B mesons, and as before $e_{\rm spec}$ denotes the electric charge of the spectator quark in units of e. In the limit of unbroken $SU(3)$ flavor symmetry, it follows that $\Lambda_{I=0}^{(8)} = \Lambda_{I=1}^{(8)}$, since both parameters arise from the matrix element of the same $SU(3)$ octet operator. Hence, in this limit one obtains

$$\Lambda_{78}^{\rm spec}\big|_{SU(3)} = e_{\rm spec}\,\Lambda_{I=1}^{(8)}\,. \tag{7.27}$$

Interestingly, the VIA discussed in Section 6.4.1 also predicts that $\Lambda_{78}^{\rm spec}$ is proportional to $e_{\rm spec}$ [14], and this fact can be used to obtain a model estimate of the relevant $SU(3)$ reduced matrix element. From (6.47) it follows

$$\Lambda_{I=1}^{(8)}\big|_{\rm VIA} = \Lambda_{I=0}^{(8)}\big|_{\rm VIA} = -\left(1 - \frac{1}{N_c^2}\right)\frac{F^2(\mu)}{8\lambda_B^2(\mu)} \in [-386\,{\rm MeV}, -35\,{\rm MeV}]\,, \tag{7.28}$$

where in the last step the parameter ranges discussed in Appendix A.2 have been used.

According to (7.26), the isospin-averaged decay rate $[\Gamma(\bar B^0 \to X_s\gamma) + \Gamma(B^- \to X_s\gamma)]/2$ depends only on $\Lambda_{I=0}^{(8)}$, while the isospin difference $[\Gamma(\bar B^0 \to X_s\gamma) - \Gamma(B^- \to X_s\gamma)]$ is proportional to $\Lambda_{I=1}^{(8)}$. While *a priori* these two non-perturbative parameters are unrelated, they coincide both in the $SU(3)$ flavor-symmetry limit and in the VIA as has just been shown. It was first pointed out in [129] that, in the limit of exact $SU(3)$ flavor symmetry, the isospin-averaged decay rate can be related to the isospin asymmetry,

$$\Delta_{0-} = \frac{\Gamma(\bar B^0 \to X_s\gamma) - \Gamma(B^- \to X_s\gamma)}{\Gamma(\bar B^0 \to X_s\gamma) + \Gamma(B^- \to X_s\gamma)}\,, \tag{7.29}$$

without employing the VIA. This asymmetry has been measured by the BaBar Collaboration using two different experimental methods. For the "sum-over-exclusive-modes method" with $E_\gamma > 1.9\,{\rm GeV}$, they find $\Delta_{0-} = (-0.6 \pm 5.8 \pm 0.9 \pm 2.4)\%$ [130], where the errors are statistical, systematic, and due to the production ratio $\bar B^0/B^-$, respectively. For the "recoil method" with $E_\gamma > 2.2\,{\rm GeV}$, they obtain instead $\Delta_{0-} = (-6 \pm 15 \pm 7)\%$ [131], where the errors are statistical and systematic, respectively. The naive average of these two results is $\Delta_{0-} = (-1.3 \pm 5.9)\%$. At the order of the present calculation, the parameter $\Lambda_{I=1}^{(8)}$ is related to Δ_{0-} via

$$\Lambda_{I=1}^{(8)}\big|_{\rm exp} = -\frac{C_{7\gamma}(\mu)}{C_{8g}(\mu)}\,\frac{m_b}{2\pi\alpha_s(\mu)}\,\Delta_{0-} \approx (59 \pm 268)\,{\rm MeV}\,, \tag{7.30}$$

where in the last step the average experimental result with its large uncertainty given above has been used. This value is consistent with the prediction (7.28) obtained in the VIA within errors, even though the central value has the opposite sign.

Allowing for $SU(3)$ flavor-symmetry breaking at the level of 30%, i.e. $\Lambda^{(8)}_{I=0} = (1 \pm 0.3)\,\Lambda^{(8)}_{I=1}$, one finally obtains

$$\Lambda^{\rm spec}_{78} = (e_{\rm spec} \pm 0.05)\,\Lambda^{(8)}_{I=1} \approx -4.5\,{\rm GeV}\,(e_{\rm spec} \pm 0.05)\,\Delta_{0-}\,, \tag{7.31}$$

which is meant as a range, not an error bar. This formula implies that, within the quoted uncertainty, the isospin asymmetry also determines the *flavor-averaged value* of $\Lambda^{\rm spec}_{78}$. For the corresponding contribution to the flavor-averaged value of the function $\mathcal{F}_E(\Delta)$, it follows that

$$\mathcal{F}_E^{\rm avg}(\Delta)\big|_{78} = -(1 \pm 0.3)\,\frac{\Delta_{0-}}{3}\,, \tag{7.32}$$

which adds $SU(3)$-breaking effects to the estimate derived in [129]. Note that this relation is independent of the values of the Wilson coefficients and other theoretical parameters.

Due to the current large experimental uncertainties in the measurement of the isospin asymmetry, it is difficult to give a reliable estimate for $\Lambda^{\rm spec}_{78}$. Based on (7.28) and (7.30), the parameter $\Lambda^{(8)}_{I=1}$ is expected to be negative (assuming that the VIA is sufficiently reliable to predict the sign correctly), but since the experimental value allows for the entire range in (7.28) at the level of two standard deviations, it is not possible to restrict that range further at present. A future, more accurate measurement of Δ_{0-} could improve the situation.

7.5 Analysis of the $Q_{8g} - Q_{8g}$ Contribution

Unfortunately, very little is known about the soft function $h^{\rm cut}_{88}$ entering the definition of the hadronic parameter Λ_{88} in (7.18). Its asymptotic behavior for large values of ω_1 and ω_2 can be derived from (6.35), and it ensures that Λ_{88} is independent of the UV cutoff $\Lambda_{\rm UV}$. Note that the second term in the definition of Λ_{88}, which contains the logarithm of $\Lambda_{\rm UV}/\Delta$, is bound to give a very small contribution to Λ_{88}, because $(C_F e_s^2 \Delta)/(8\pi^2) < 3\,{\rm MeV}$ is very small for realistic values $E_0 \geq 1.6\,{\rm GeV}$. Thus, it is expected that the hadronic parameter Λ_{88} receives its dominant contributions from values $\omega_{1,2} = \mathcal{O}(\Lambda_{\rm QCD})$, for which no useful constraints on the soft function $h^{\rm cut}_{88}$ exist. For the same reason, it is expected that the linear growth of Λ_{88} for large Δ is a numerically irrelevant effect. It then follows that the function $h^{\rm cut}_{88}(\Delta, \omega_1, \omega_2, \mu)$ is *approximately* equal to the function $h^{\rm cut}_{88}(\omega_1, \omega_2, \mu)$ shown in (7.15), even though this relation is not strictly valid. As mentioned earlier in the paragraph following that equation, this form would imply that the contribution to Λ_{88} resulting from the double integral in (7.18) were strictly positive.

In summary, the hadronic parameter $\Lambda_{88}(\Delta, \mu)$ is expected to be, to a good approximation, independent of Δ and given by a positive, non-perturbative constant of order $e_s^2\,\Lambda_{\rm QCD}$:

$$\Lambda_{88}(\Delta, \mu) \approx e_s^2\,\Lambda(\mu)\,, \qquad \Lambda(\mu) > 0\,. \tag{7.33}$$

This expectation is supported by using different models for the soft function $h^{\rm cut}_{88}$, for example by writing it as a product of two functions $f_1(\omega_1)\,f_2(\omega_2)$ and using various models such as exponentials or Gaussians. A particularly simple example is provided by functions

$h_{88}^{\rm cut}(\omega_1,\omega_2,\mu)$ that are symmetric in both ω_i variables and have support for $\omega_i = \mathcal{O}(\Lambda_{\rm QCD})$. In this case the third relation in (7.18) implies $\Lambda(\mu) \approx 2\pi^2 h_{88}^{\rm cut}(0,0,\mu)$, and the value at the origin scales like $h_{88}^{\rm cut}(0,0,\mu) \sim \Lambda_{\rm QCD}$. For the numerical analysis, the rather generous range $0 < \Lambda(\mu) < 1\,\text{GeV}$ will be considered. Even for the largest value, the suppression by the charge factor $e_s^2 = 1/9$ in (7.33) implies that the effect of this term on the decay rate is very small.

7.6 Conclusions of this Chapter

With the estimates of the hadronic parameters Λ_{ij} at hand it is now possible to study the implications of the analysis for the function $\mathcal{F}_E(\Delta)$ in (7.17). Using the parameter values collected in Appendix A.2, one obtains from (7.25) and (7.33) the contributions

$$\begin{aligned} \mathcal{F}_E\big|_{17} &\in [-1.7, +4.0]\,\%\,, \\ \mathcal{F}_E\big|_{88} &\in [-0.3, +1.9]\,\%\,. \end{aligned} \tag{7.34}$$

The value of $\mathcal{F}_E|_{88}$ depends slightly on Δ and is obtained using $\Delta = 1.45\,\text{GeV}$, corresponding to a cut at $E_0 = 1.6\,\text{GeV}$. For the case of $\mathcal{F}_E|_{78}$, the charge-averaged contribution will be considered and the estimates will be given using both methods, the VIA and the isospin asymmetry. In the latter case, the extremal values are obtained by assuming 30% $SU(3)$ violation and taking the 95% confidence level experimental range. This yields

$$\begin{aligned} \mathcal{F}_E\big|_{78}^{\rm VIA} &\in [-2.8, -0.3]\,\%\,, \\ \mathcal{F}_E\big|_{78}^{\rm exp} &\in [-4.4, +5.6]\,\% \quad (95\%\ \text{CL})\,. \end{aligned} \tag{7.35}$$

In order to obtain a conservative estimate of the combined theoretical analysis, a Bayesean approach will be adopted and various contributions added up using the scanning method. In this way, the final result turns out to be

$$-4.8\% < \mathcal{F}_E(\Delta) < +5.6\% \quad (\text{VIA for } \Lambda_{78}^{\rm spec})\,, \tag{7.36}$$

where the theoretical estimate for $\mathcal{F}_E|_{78}$ has been used. When the experimental estimate is used instead, the range is expanded to

$$-6.4\% < \mathcal{F}_E(\Delta) < +11.5\% \quad (\Lambda_{78}^{\rm spec} \text{ from } \Delta_{0-})\,. \tag{7.37}$$

It is emphasized that the estimates in this sections should be considered as *ranges*, within which the actual values of $\mathcal{F}_E$ are expected to lie, without making a statement about the most likely values within these ranges.

If in the future a more precise value of the isospin asymmetry can be measured, this could be used to reduce the uncertainty range somewhat. If, for example, it is assumed that the true isospin asymmetry lies in the center of the interval predicted by the VIA, $\Delta_{0-} = +4.6\%$, then in the absence of experimental uncertainties one would derive $\mathcal{F}_E|_{78}^{\rm exp} \in$

$[-2.0, -1.1]\,\%$, where the remaining uncertainty stems from the unknown effects of $SU(3)$ breaking. In this "ideal" case, the combined result would be

$$-4.0\% < \mathcal{F}_E(\Delta) < +4.8\% \quad \text{(ideal case)}\,. \tag{7.38}$$

There seems to be no possibility to reduce this uncertainty in the foreseeable future, given that no theoretical tools exist to constrain the non-local matrix elements defining the soft functions entering the various resolved photon contributions studied in this work. Thus, the range in (7.38) can be considered as the *irreducible* theoretical uncertainty affecting any theoretical prediction of the $\bar{B} \to X_s\gamma$ branching fraction.

Chapter 8

Phenomenology II: Direct CP Violation

This chapter will discuss the effects of the resolved photon contributions of Chapter 6 on the direct CP asymmetry. Since these effects are not covered within the local OPE approach, they constitute a new non-perturbative uncertainty on the partonic calculations of the past. After a short introduction on CP violation in Section 8.1, the relevant formulae are worked out in Section 8.2 and the non-perturbative effects of the resolved contributions are parameterized. Sections 8.3 and 8.4 will then present a numerical analysis of the new effects in the SM and beyond. Finally the CP asymmetry in $\bar{B} \to X_s\gamma$ is contrasted to the one in $\bar{B} \to X_d\gamma$ in Section 8.5.

8.1 Preliminaries

A certain process is said to violate the CP symmetry *directly*, if the rate of this process differs from the rate of the CP-conjugate process. In the case of $\bar{B} \to X_s\gamma$ this can be written as

$$\Delta\Gamma = \Gamma(\bar{B} \to X_s\gamma) - \Gamma(B \to X_{\bar{s}}\gamma) \neq 0\,. \tag{8.1}$$

Such a difference is possible when at least two partial amplitudes contributing to the process carry different weak and strong phases. The weak phase is associated with the coupling constants in the Lagrangian, while a non-zero strong phase is generated by Feynman diagrams with internal lines, that are able to go on-shell. In the SM a weak phase is introduced through the complex parameters of the CKM matrix.

The partonic calculation of the $\bar{B} \to X_s\gamma$ amplitude introduces different strong phases at $\mathcal{O}(\alpha_s)$, which give rise to CP violation. The calculation was performed in [128] under the assumption that the rate can be expressed in terms of a local OPE if integrated over a large enough range. However, it was discussed in the previous chapters that there exist contributions that do not fit into the local OPE approach, even in the total rate. These contributions could be expressed in terms of convolutions of subleading shape functions with jet functions J and $\bar{J}$ (see Section 5.3). It was noted, that even though the subleading

shape functions are real, the corresponding jet functions can introduce a strong phase. This gives rise to a non-perturbative CP violating contribution.

An appropriate quantity to parameterize CP violating effects is the CP asymmetry A_{CP} defined by

$$A_{CP} = \frac{\Gamma(\bar{B} \to X_s\gamma) - \Gamma(B \to X_{\bar{s}}\gamma)}{\Gamma(\bar{B} \to X_s\gamma) + \Gamma(B \to X_{\bar{s}}\gamma)}\,. \tag{8.2}$$

Just like the CP averaged decay rate discussed in the previous chapters, the CP asymmetry can be used as a probe for new physics. In particular, new physics models can generate complex Wilson coefficients, thereby introducing new phases for CP violation. On the other hand, while the experimental error of the CP averaged rate has been reduced below the 10 % level (see Section 1.3), the CP asymmetry is much less certain. The current world average is [24]

$$A_{CP} = -(1.2 \pm 2.8)\,\%\,. \tag{8.3}$$

The theoretical analysis, based on the parton model predicts for the CP asymmetry in the SM [132]

$$A_{CP}^{\rm SM} = (0.44^{+0.15}_{-0.10} \pm 0.03^{+0.19}_{-0.09})\,\%\,, \tag{8.4}$$

where the errors refer to uncertainties associated with the quark-mass ratio m_c/m_b, CKM parameters, and higher-order perturbative corrections. It follows from this prediction, that any measured value for the CP asymmetry outside the range $0 < A_{CP} < 1\,\%$ would be a clear signal of new physics. Such models have been considered in [13, 17, 133–141].

The CP asymmetry defined above contains the partially integrated decay rate. As usual, the integration is defined with a lower cut E_0 on the photon energy (see Section 7.1). The experimental result given in (8.2) is an averaged value from measurements using values for E_0 between 1.9 and 2.2 GeV. The theoretical prediction used $E_0 = 1.6\,\text{GeV}$. In this case, however, it was demonstrated in [128] that the dependence of A_{CP} on the cut is relatively small (a few percent).

The effective theory analysis of $\bar{B} \to X_s\gamma$ presented in the previous chapters established the following contributions to the differential decay rate (compare Equation (5.39)). The leading power contribution is at leading order in α_s irrelevant for an analysis of CP violation, since it contains neither weak nor strong phase differences (recall that the leading shape function is CP invariant). At NLO the leading power contains both, weak and strong phase differences, encoded in the hard function $|H_\gamma|^2$, see (4.30). The strong phases are due to hard virtual corrections as depicted in Figure 2.6. When integrated over a range much larger than the endpoint region, the leading shape function can be expanded in powers of $\Lambda_{\rm QCD}/\Delta$ with $\Delta = m_b - 2E_0$, as explained in Section 3.3.4. The first term in that expansion corresponds to the partonic calculation of the hard virtual loops. At subleading power there are direct and resolved contributions. It has been shown explicitly in Chapter 6, that the direct contributions correspond to QCD bremsstrahlung diagrams, expanded around the endpoint. If integrated over a large enough range the direct contributions are promoted to leading power. These can also give rise to CP violating phases. Finally, the resolved contributions can potentially contribute to CP violation. However, some of them vanish in the integrated rate (see Section 5.2.4). Thus, if the cut on the

photon energy is assumed to be sufficiently low, i.e., such that $\Delta = \text{few} \times \Lambda_{\rm QCD}$, the direct contributions (at any power) can be calculated in terms of a local operator matrix elements using a combined expansion in Δ/m_b and $\Lambda_{\rm QCD}/\Delta$. The partonic result corresponds to the leading power in $\Lambda_{\rm QCD}/\Delta$ and includes all powers in Δ/m_b. However, the resolved contributions can never be expressed in terms of local matrix elements. Their effects have to be added to the partonic result. In the following sections, the CP asymmetry including direct as well as resolved contributions will be given, assuming a sufficiently low cut. While the direct contributions will depend explicitly on the cut, the cut effect for the resolved contributions can be ignored as explained in Section 7.1.

8.2 The CP Asymmetry

The direct photon contribution to the CP asymmetry is given by the expressions for the CP asymmetry from [128] and the $Q_1^c - Q_1^u$ interference term from [142]

$$\begin{aligned}
A_{CP}^{\rm dir}(\delta) &= \left.\frac{\Gamma(\bar B \to X_s\gamma) - \Gamma(B \to X_{\bar s}\gamma)}{\Gamma(\bar B \to X_s\gamma) + \Gamma(B \to X_{\bar s}\gamma)}\right|_{E_\gamma > (1-\delta)m_b/2} \\
&= \frac{\alpha_s}{|C_{7\gamma}|^2}\left\{\frac{40}{81}\,{\rm Im}[C_1 C_{7\gamma}^*] - \frac{8z}{9}\Big[v(z) + b(z,\delta)\Big]\,{\rm Im}[(1+\epsilon_s) C_1 C_{7\gamma}^*]\right. \\
&\qquad - \frac{4}{9}\,{\rm Im}[C_{8g} C_{7\gamma}^*] + \frac{8z}{27}\,b(z,\delta)\,{\rm Im}[(1+\epsilon_s) C_1 C_{8g}^*] \\
&\qquad \left. + \frac{16z}{27}\,\tilde b(z,\delta)\,|C_1|^2\,{\rm Im}[\epsilon_s]\right\} + \mathcal{O}(\alpha_s^2)\,,
\end{aligned} \tag{8.5}$$

where $z = m_c^2/m_b^2$, $\delta = 1 - 2E_0/m_b$, $b(z,\delta) = g(z,1) - g(z,1-\delta)$, and $\tilde b(z,\delta) = \tilde g(z,1) - \tilde g(z,1-\delta)$, with

$$\begin{aligned}
v(z) &= \left(5 + \ln z + \ln^2 z - \frac{\pi^2}{3}\right) + \left(\ln^2 z - \frac{\pi^2}{3}\right) z + \left(\frac{28}{9} - \frac{4}{3}\ln z\right) z^2 + \mathcal{O}(z^3), \\
g(z,y) &= \theta(y-4z)\left\{(y^2 - 4yz + 6z^2)\ln\left(\sqrt{\frac{y}{4z}} + \sqrt{\frac{y}{4z}-1}\right) - \frac{3y(y-2z)}{4}\sqrt{1-\frac{4z}{y}}\right\} \\
\tilde g(z,y) &= \theta(y-4z)\,y\left\{2L_2\left[-\left(\sqrt{\frac{y}{4z}} + \sqrt{\frac{y}{4z}-1}\right)^2\right] + 2\ln\left(\sqrt{\frac{y}{4z}} + \sqrt{\frac{y}{4z}-1}\right)^2 + \frac{\pi^2}{6}\right. \\
&\qquad - \left[2 + y - \frac{4z}{y} - 4z + \frac{6z^2}{y} - 2\ln\left(\frac{y}{z}\right)\right]\ln\left(\sqrt{\frac{y}{4z}} + \sqrt{\frac{y}{4z}-1}\right) \\
&\qquad \left. + \left(\frac{4+3y-6z}{4}\right)\sqrt{1-\frac{4z}{y}}\right\}.
\end{aligned} \tag{8.6}$$

The parameter ϵ_s is the only source of CP violation in the SM and is defined as in [128] to be

$$\epsilon_s = \frac{\lambda_u}{\lambda_t} = \frac{V_{ub}V_{us}^*}{V_{tb}V_{ts}^*} = \frac{\lambda^2(i\bar{\eta}-\bar{\rho})}{1-\lambda^2(1-\bar{\rho}+i\bar{\eta})} + \mathcal{O}(\lambda^6), \tag{8.7}$$

with the Wolfenstein parameters $\lambda = \sin\theta_C \approx 0.225$, $\bar{\rho} = 0.144$ and $\bar{\eta} = 0.342$. For brevity the scale dependencies of the Wilson coefficients C_i and the strong coupling α_s have been dropped. The numerically most important contributions arise from the interference of charm- and up-quark penguin graphs with virtual or real gluon emission with the leading electromagnetic dipole amplitude.

The CP asymmetry due to resolved contributions can be easily derived from the results in Chapter 6. Keeping in mind that the earlier results were CP averaged, it is obvious that the dual real part prescriptions in (5.39) and in the definition of the $\bar{F}_{ij}$ need to be replaced by imaginary part prescriptions times -2. By decomposing the uncut propagators in $\bar{J}$ into a Cauchy principle value and a δ-function, some of the integrals in the definition of the $\bar{F}_{ij}$ can be explicitly performed. This leads to

$$\begin{aligned} A_{CP}^{\text{res}} &= \left.\frac{\Gamma(\bar{B}\to X_s\gamma)-\Gamma(B\to X_{\bar{s}}\gamma)}{\Gamma(\bar{B}\to X_s\gamma)+\Gamma(B\to X_{\bar{s}}\gamma)}\right|_{\delta\approx 1} \\ &= \frac{\pi}{m_b|C_{7\gamma}|^2}\left\{\text{Im}\left[(1+\epsilon_s)C_1C_{7\gamma}^*\right]\tilde{\Lambda}_{17}^c - \text{Im}\left[\epsilon_s C_1 C_{7\gamma}^*\right]\tilde{\Lambda}_{17}^u + \text{Im}\left[C_{8g}C_{7\gamma}^*\right]4\pi\alpha_s\tilde{\Lambda}_{78}^{\bar{B}}\right\}, \end{aligned} \tag{8.8}$$

where (once again omitting the scale dependence of the Wilson coefficients and the $\tilde{\Lambda}_{ij}$ parameters)

$$\begin{aligned} \tilde{\Lambda}_{17}^u &= \frac{2}{3}h_{17}(0)\,, \\ \tilde{\Lambda}_{17}^c &= \frac{2}{3}\int_{\frac{4m_c^2}{m_b}}^{\infty}\frac{d\omega}{\omega}\,f\left(\frac{m_c^2}{m_b\omega}\right)h_{17}(\omega)\,, \\ \tilde{\Lambda}_{78}^{\bar{B}} &= 2\int_{-\infty}^{\infty}\frac{d\omega}{\omega}\,\left[h_{78}^{(1)}(\omega,\omega)-h_{78}^{(1)}(\omega,0)\right]\,, \end{aligned} \tag{8.9}$$

and where the h_{ij} are defined in Section 7.1 and f is the imaginary part of the penguin function (see Appendix A.1)

$$f(x) = 4x\ln\left(\sqrt{\frac{1}{4x}}+\sqrt{\frac{1}{4x}-1}\right)\,. \tag{8.10}$$

Note that the contribution from $g_{78}^{(5)}$ vanishes, since the integral over ω of this function is symmetric under the exchange of ω_1 and ω_2. Likewise, the contributions from the functions $\bar{g}_{78}$ and $\bar{g}_{78}^{\text{cut}}$ to the CP asymmetry cancel each other. Note also that the soft function $h_{78}^{(1)}(\omega_1,\omega_2,\mu)$ is symmetric under the exchange of ω_1 and ω_2. Compared to the

direct photon contributions which are α_s suppressed, the resolved photon contributions are $1/m_b$ suppressed.

The total CP asymmetry is given by the sum of (8.5) and (8.8)

$$\begin{aligned} A_{CP}^{\rm tot}(\delta) = \frac{\pi}{|C_{7\gamma}|^2}\Bigg\{ & \left(\frac{40}{81}\,\frac{\alpha_s}{\pi} - \frac{8z}{9}\,\frac{\alpha_s}{\pi}\Big[v(z)+b(z,\delta)\Big] + \frac{\tilde\Lambda_{17}^c}{m_b}\right) \mathrm{Im}\,[C_1 C_{7\gamma}^*] \\ & - \left(\frac{\tilde\Lambda_{17}^u - \tilde\Lambda_{17}^c}{m_b} + \frac{8z}{9}\,\frac{\alpha_s}{\pi}\Big[v(z)+b(z,\delta)\Big]\right) \mathrm{Im}\,[\epsilon_s C_1 C_{7\gamma}^*] \\ & - \left(\frac{4}{9}\,\frac{\alpha_s}{\pi} - 4\pi\alpha_s(\mu)\,\frac{\tilde\Lambda_{78}^{\bar B}}{m_b}\right) \mathrm{Im}\,[C_{8g} C_{7\gamma}^*] \\ & + \frac{8z}{27}\,\frac{\alpha_s}{\pi}\,b(z,\delta)\,\mathrm{Im}\,[(1+\epsilon_s) C_1 C_{8g}^*] + \frac{16z}{27}\,\frac{\alpha_s}{\pi}\,\tilde b(z,\delta)\,|C_1|^2\,\mathrm{Im}\,[\epsilon_s]\Bigg\} + \dots\,, \end{aligned} \tag{8.11}$$

where the ellipses represent terms of order $\alpha_s^2, \alpha_s/m_b, 1/m_b^2$ and higher. This formula is model independent and is valid also for extensions of the SM, in which the dipole coefficients $C_{7\gamma}$ and C_{8g} receive new CP violating contributions. The phenomenological implication of this formula will be explored in the following sections.

8.3 Phenomenology in the SM

In order to properly estimate the importance of each term in (8.11), a few approximations will be made. However, the numerical calculations will always be performed with the full formula. If the charm-quark mass is assumed to scale like $m_c^2 = \mathcal{O}(\Lambda_{\rm QCD} m_b)$, the above expression may be expanded in powers of $z, \delta = \mathcal{O}(\Lambda_{\rm QCD}/m_b)$. Then contributions proportional to $b(z,\delta)$ and $\tilde b(z,\delta)$ scale as $(\Lambda_{\rm QCD}/m_b)^2$ and can be neglected to a good approximation, while the term proportional to $v(z)$ contributes at first order in $\Lambda_{\rm QCD}/m_b$ and can be simplified by expanding $v(z)$ to zeroth order in z. This yields the approximation

$$\begin{aligned} A_{CP}^{\rm tot}(\delta) \approx \frac{\pi}{|C_{7\gamma}|^2}\Bigg\{ & \left(\left[\frac{40}{81} - \frac{40}{9}\,\frac{\Lambda_c}{m_b}\right]\frac{\alpha_s}{\pi} + \frac{\tilde\Lambda_{17}^c}{m_b}\right) \mathrm{Im}\,[C_1 C_{7\gamma}^*] \\ & - \left(\frac{\tilde\Lambda_{17}^u - \tilde\Lambda_{17}^c}{m_b} + \frac{40}{9}\,\frac{\Lambda_c}{m_b}\,\frac{\alpha_s}{\pi}\right) \mathrm{Im}\,[\epsilon_s C_1 C_{7\gamma}^*] - \left(\frac{4\alpha_s}{9\pi} - 4\pi\alpha_s(\mu)\,\frac{\tilde\Lambda_{78}^{\bar B}}{m_b}\right) \mathrm{Im}\,[C_{8g} C_{7\gamma}^*]\Bigg\}, \end{aligned} \tag{8.12}$$

which is independent of the cutoff in δ. The scale parameter Λ_c is just like the parameters $\tilde\Lambda_{ij}$ of $\mathcal{O}(\Lambda_{\rm QCD})$ and defined by

$$\Lambda_c := \frac{m_c^2}{m_b}\left(1 - \frac{2}{5}\ln\frac{m_b}{m_c} + \frac{4}{5}\ln^2\frac{m_b}{m_c} - \frac{\pi^2}{15}\,,\right) \approx 0.38\,\mathrm{GeV}, \tag{8.13}$$

where the parameters given in Appendix A.2 have been used. As can be seen from (8.12) the resolved photon contributions yield numerically significant corrections to the direct terms since $\alpha_s/\pi \sim \Lambda_{\rm QCD}/m_b$. In the second term, which is the only one present in the SM, the resolved contribution is likely more important due to the double suppression of the direct term.

In order to obtain ranges for the non-perturbative parameters $\tilde{\Lambda}_{ij}$ the same methods are employed as for the integrated rate in Chapter 7. Note, that the parameter $\tilde{\Lambda}_{78}^{\bar{B}}$ in (8.8) depends on the flavor of the spectator quark inside the $\bar{B}$-meson. It has been shown in Section 7.4 that $\tilde{\Lambda}_{78}^{\bar{B}} = e_{\rm spec}\tilde{\Lambda}_{78}$, where $e_{\rm spec}$ denotes the electric charge of the spectator quark in units of e. Evaluating the hadronic matrix element of the corresponding non-local four-quark operator in the VIA yields

$$\tilde{\Lambda}_{78}^{\bar{B}} \approx e_{\rm spec}\frac{2f_B^2 M_B}{9}\int_0^\infty d\omega\,\frac{\phi_+^B(\omega)}{\omega}\,. \tag{8.14}$$

Therefore the size of the hadronic parameter

$$\frac{1}{\nu_B(\mu)^2} := \int_0^\infty d\omega_1\,\frac{\left[\phi_+^B(\omega_1,\mu)\right]^2}{\omega_1}. \tag{8.15}$$

with the light-cone distribution amplitude ϕ_+^B needs to be estimated. Although it was not discussed in the literature in the past, one can use the analysis of [123] to estimate its size. The results are summarized in Table 8.1. The other parameters in (8.15) are given

μ [GeV]	1.0	1.5	2.0	2.5
ν_B^{-2} [GeV^{-2}]	1.21 ± 0.26	0.91 ± 0.16	0.77 ± 0.12	0.68 ± 0.10

Table 8.1: Values of ν_B^{-2} using the analysis of [123]. See text for a discussion of the appropriate scale.

in Appendix A.2. In order to be conservative, ν_B will be taken to be between 0.5 GeV and 1.5 GeV, which covers the range in Table 8.1 as well as the value that can be obtained from a QCD sum rules analysis similar to that of [125]. This leads to a range

$$17\,{\rm MeV} < \tilde{\Lambda}_{78} < 190\,{\rm MeV}\,. \tag{8.16}$$

The parameters $\tilde{\Lambda}_{17}^q$ can be estimated by employing the same models as studied in Section 7.3. Note that $\tilde{\Lambda}_{17}^u$ only depends on the value of the soft function h_{17} at the origin. This leads to the following ranges

$$\begin{aligned} -330\,{\rm MeV} < \tilde{\Lambda}_{17}^u < 525\,{\rm MeV}\,,\\ -9\,{\rm MeV} < \tilde{\Lambda}_{17}^c < 11\,{\rm MeV}\,. \end{aligned} \tag{8.17}$$

One observes that $\tilde{\Lambda}_{17}^u$ and $\tilde{\Lambda}_{78}$ are of order $\Lambda_{\rm QCD}$, while the charm-loop contribution $\tilde{\Lambda}_{17}^c$ is much smaller. The slight preference for positive values of $\tilde{\Lambda}_{17}^q$ is due to the normalization

constraint (6.14). Note that in the formal limit $m_c \to m_u = 0$ the values of $\tilde{\Lambda}^c_{17}$ and $\tilde{\Lambda}^u_{17}$ coincide. However, a strong GIM violation is to be expected, owing to the fact that the integral in the second relation in (8.9) starts at $4m_c^2/m_b \approx 1.1\,\text{GeV}$, at which the soft function es expected to take already rather small values, since it is governed by non-perturbative dynamics and must vanish for $\omega \to 0$.

With the above results at hand, the SM CP asymmetry can be predicted and the effect of the non-perturbative corrections estimated. The factorization scale is chosen to be $\mu = 2\,\text{GeV}$ (for which $\alpha_s(\mu) = 0.307$, and $C_1(\mu) = 1.204$, $C_{7\gamma}(\mu) = -0.381$, $C_{8g}(\mu) = -0.175$ at leading order), since the strong phases required for a non-zero CP asymmetry arise either from GIM violations related to charm-quark loops (for which $\mu \sim 2m_c$), or from cut hard-collinear propagators (for which $\mu \sim \sqrt{\Lambda_{\text{QCD}} m_b}$). This leads to

$$A_{CP}^{\text{SM}} \approx \left(1.15 \times \frac{\tilde{\Lambda}^u_{17} - \tilde{\Lambda}^c_{17}}{300\,\text{MeV}} + 0.71\right)\%. \tag{8.18}$$

Although the $\tilde{\Lambda}^c_{17}$ is much smaller than $\tilde{\Lambda}^u_{17}$, it is still given in (8.18) to make explicit the fact, that the CP asymmetry vanishes in the formal limit $m_c = m_u$ due to the GIM mechanism. The numerically most important contribution arises from the up-quark penguin graph with emission of a soft gluon at a light-like distance from the heavy quarks. Uncertainties associated with the input parameters are not shown, since they are much smaller than the non-perturbative uncertainty. The central value $0.71\,\%$ for the direct photon term is larger than the one obtained in [132] since smaller values for μ and m_c have been used here.

It is observed that the resolved photon term is parametrically larger than the direct photon term, which contains an additional α_s suppression. Using the model estimates for $\tilde{\Lambda}_{ij}$ given above leads to the range

$$-0.6\,\% < A_{CP}^{\text{SM}} < 2.8\,\%\,, \tag{8.19}$$

which covers most of the experimentally allowed range. Only a value of the asymmetry below $-2\,\%$ could be interpreted as a sign of new physics, as in this case $\tilde{\Lambda}^u_{17} < -700\,\text{MeV}$ would be much larger than the model expectations. The case of new physics will be explored in more detail in the next section.

8.4 Phenomenology beyond the SM

In order to illustrate the impact of the resolved photon terms, a class of new physics models is considered in which the dominant non-standard effects are encoded in the values of the dipole operators which will be parameterized in the form

$$\frac{C_{7\gamma}}{C_1} = \frac{C_{7\gamma}^{\text{SM}}}{C_1^{\text{SM}}}\, r_7 e^{i\theta_7}\,, \qquad \frac{C_{8g}}{C_1} = \frac{C_{8g}^{\text{SM}}}{C_1^{\text{SM}}}\, r_8 e^{i\theta_8}\,. \tag{8.20}$$

Using that $\arg(-\epsilon_s) \approx -\gamma$ in the SM, one obtains for the default parameters

$$\begin{aligned} A_{CP}^{e_{\rm spec}}\,[\%] \,=\, & \left(6.27 + 11.98\, e_{\rm spec} \times \frac{\tilde\Lambda_{78}}{100\,\text{MeV}}\right) \frac{r_8}{r_7}\sin(\theta_7-\theta_8) \\ & + \left(10.12 + 2.14 \times \frac{\tilde\Lambda_{17}^c}{10\,\text{MeV}}\right)\frac{1}{r_7}\sin\theta_7 + \left(0.74 + 1.26 \times \frac{\tilde\Lambda_{17}^u - \tilde\Lambda_{17}^c}{300\,\text{MeV}}\right)\frac{1}{r_7}\sin(\gamma+\theta_7) \\ & + 0.18\,\frac{r_8}{r_7^2}\sin(\theta_8) + \frac{0.037}{r_7^2}\sin\gamma - 0.004\,\frac{r_8}{r_7^2}\sin(\gamma+\theta_8)\,. \end{aligned} \tag{8.21}$$

The flavor-averaged CP asymmetry $(A_{CP}^{e_u} + A_{CP}^{e_d})/2$ can be obtained by replacing $e_{\rm spec} \to 1/6$. Then the resolved photon contributions are subdominant except for the third term, which is already present in the SM. In principle, very large asymmetries are possible from the first and second terms [128], which however are already ruled out by the data.

A non-trivial feature of this analysis is that the resolved photon contributions induce a flavor dependent term in the CP asymmetry already at order $\Lambda_{\rm QCD}/m_b$. In the SM such effects are suppressed, compared with (8.18), by at least one additional factor of $\Lambda_{\rm QCD}/m_b$ and are thus bound to be negligible. This suggests the measurement of the CP asymmetry difference

$$\Delta A_{CP} := A_{CP}^{e_u} - A_{CP}^{e_d} \approx 4\pi^2\alpha_s\,\frac{\tilde\Lambda_{78}}{m_b}\,\text{Im}\,\frac{C_{8g}}{C_{7\gamma}} \approx 12\,\% \times \frac{\tilde\Lambda_{78}}{100\,\text{MeV}}\,\frac{r_8}{r_7}\sin(\theta_8-\theta_7) \tag{8.22}$$

as a sensitive probe for flavor physics beyond the SM. Even though it will be difficult to determine the value of the hadronic parameter $\tilde\Lambda_{78}$ with any reasonable accuracy, the difference ΔA_{CP} can easily reach the level of 10 % in magnitude if either the electromagnetic or the chromomagnetic dipole coefficients (or both) receive a sizable CP violating new-physics phase. It is important in this context that the Wilson coefficient of the chromomagnetic operator can be much enhanced with regard to the SM value, so that $r_8/r_7 \sim$ a few is possible [128]. Before concluding, it is interesting to consider the the case of $\bar B \to X_d\gamma$ and compare it to $\bar B \to X_s\gamma$.

8.5 Comments on $\bar B \to X_d\gamma$ and $\bar B \to X_{s+d}\gamma$

All of the expressions in the previous sections also apply to the CP asymmetry in $\bar B \to X_d\gamma$, where one only needs to change ϵ_s to ϵ_d, defined as

$$\epsilon_d = \frac{V_{ub}V_{ud}^*}{V_{tb}V_{td}^*} = \frac{\bar\rho - i\bar\eta}{1-\bar\rho+i\bar\eta} = \mathcal{O}(1)\,. \tag{8.23}$$

As a result, the CP asymmetry for the $\bar B \to X_d\gamma$ decay in the SM differs by a factor $\text{Im}\,\epsilon_d/\text{Im}\,\epsilon_s \approx -22$ from the $\bar B \to X_s\gamma$ case.

In the endpoint region, there are two other potential sources of difference between $b \to s\gamma$ and $b \to d\gamma$ that however *do not* contribute to the integrated CP asymmetry at order $1/m_b$. The first is the four-quark shape functions which are sensitive to the flavor of q in $b \to q\gamma$ [9, 10, 100]. However, as shown in Section 7.1 these effects integrate to zero in the partially inclusive CP asymmetry at order $\Lambda_{\rm QCD}/m_b$. The second potential source arises if one adopts the scaling $m_s \sim \mathcal{O}(\Lambda_{\rm QCD})$. This gives rise to a new subleading jet function which is suppressed by $\Lambda_{\rm QCD}/m_b$ in the endpoint region (see Section 5.2.6). At order $\Lambda_{\rm QCD}/m_b$, it only contributes to the interference $Q_{7\gamma}$ with itself and not to the CP asymmetry. The interference of $Q_{7\gamma}$ with other operators is suppressed by two powers of $\Lambda_{\rm QCD}/m_b$ in the endpoint region. Outside of the endpoint region these strange-quark mass effects are even further suppressed.

Another observable of interest is the CP asymmetry for $\bar{B} \to X_{s+d}\gamma$. Considering only the direct photon contributions, the sum of the SM CP asymmetries of $\bar{B} \to X_d\gamma$ and $\bar{B} \to X_s\gamma$ vanishes in the U-spin limit ($m_s = m_d$), as was first pointed out in [143]. This can be seen explicitly by applying unitarity of the CKM matrix

$$\Delta\Gamma_{\rm SM}(\bar{B} \to X_s\gamma) + \Delta\Gamma_{\rm SM}(\bar{B} \to X_d\gamma) \propto \mathrm{Im}\left[V_{ub}V_{tb}^*(V_{us}^*V_{ts} + V_{ud}^*V_{td})\right] = 0. \tag{8.24}$$

From the discussion in the previous section it follows that the resolved photon contributions do not violate this relation at order $\Lambda_{\rm QCD}/m_b$. It is not inconceivable, though, that beyond this order there could be resolved photon contributions that might affect this relation, but these are beyond the scope of this work.

8.6 Conclusions of this Chapter

It was demonstrated in Chapter 6 that resolved photon contributions give rise to new, calculable CP violating strong phases related to (anti-)hard-collinear jet functions, which are convoluted with real, non-perturbative shape functions. These phases are responsible for a sizable hadronic uncertainty in the partonic calculation of the CP asymmetry. In this chapter it was shown, that the dominant part of these uncertainties is related to the interference of the electromagnetic dipole amplitude with the amplitude for an up-quark penguin transition accompanied by soft gluon emission. It was parameterized in the form of $\tilde{\Lambda}_{17}^u$ in (8.9) and a possible range of values for this quantity was estimated. It turned out, that the long-distance contribution encoded in $\tilde{\Lambda}_{17}^u$ is parametrically leading in the SM and will be difficult to disentangle from possible new physics effects. A measurement of the CP asymmetry difference (8.22) seems more promising as a new physics probe. Finally it was found that the untagged CP asymmetry for the $\bar{B} \to X_{s+d}\gamma$ decay vanishes in the SM (up to U-spin breaking corrections [128, 143, 144]) even after the resolved terms are taken into account.

Chapter 9

Conclusions

9.1 Summary and Outlook

This work explored the origin and implications of non-perturbative contributions to the decay rate of $\bar{B} \to X_s\gamma$. The charmless, radiative and inclusive decay $\bar{B} \to X_s\gamma$ is relevant as a test of the SM as well as a probe for physics beyond the SM. For example, it is used in combination with the semi-leptonic decay $\bar{B} \to X_u l\bar{\nu}$ to determine the CKM matrix element V_{ub}. On the other hand it is able to provide stringent bounds on several new physics models [3].

The partonic calculation of the $\bar{B} \to X_s\gamma$ decay rate considers the decay of a free, on-shell b-quark and has been performed practically completely up to NNLO [5] (see Chapter 2). This calculation predicts a branching fraction of $\mathcal{B}(\bar{B} \to X_s\gamma) = (3.15 \pm 0.23) \cdot 10^{-4}$ for all $\bar{B} \to X_s\gamma$ decays containing a photon with an energy above a cut $E_0 > 1.6\,\text{GeV}$. This cut on the photon energy is necessary in order to eliminate the $B\bar{B}$ background from the experimental measurements (see Chapter 1).

Of course, there are several effects that are not considered in the partonic prediction. The most relevant one stems from non-perturbative corrections, due to the large QCD coupling constant at low (hadronic) energies. In the framework of HQET it can be shown that the partonic calculation corresponds to the leading term in an expansion in powers of $1/m_b$ and that the non-perturbative corrections only appear at higher orders in the expansion (see Chapter 3). However, this only applies to situations where the cut on the photon energy is chosen sufficiently low (so that $m_b - 2E_0 \to m_b$). The cut of $E_0 > 1.6\,\text{GeV}$ was chosen to satisfy this requirement. It was already known for some time that the expansion can no longer be expressed in terms of local operators when considering the endpoint region ($E_\gamma \to m_b/2$). In that case the partonic result has to be convoluted with a shape function, that is defined by the Fourier transform of a non-local HQET matrix element, and that can be interpreted as the momentum distribution of the heavy quark within the meson [81] (see Chapter 4).

Later on it was discovered, that there are contributions to the integrated $\bar{B} \to X_s\gamma$ decay rate at $\mathcal{O}(1/m_b)$ which do not fit into the framework of a local OPE even if the cut

is taken outside the endpoint region [14]. It was one of the major objectives of this work to systematically analyze all $1/m_b$ suppressed contributions of this type at tree level in perturbation theory. The appropriate approach for such an analysis makes use of SCET [6,7] (see Chapter 4). By employing SCET it was possible to proof a factorization formula for the differential $\bar{B} \to X_s\gamma$ decay rate in the endpoint region which is valid at any order in the $1/m_b$ expansion (see Chapter 5). This formula can be written as

$$\begin{aligned} d\Gamma(\bar{B} \to X_s\gamma) = &\sum_{n=0}^{\infty} \frac{1}{m_b^n} \sum_i H_i^{(n)} J_i^{(n)} \otimes S_i^{(n)} \\ &+ \sum_{n=1}^{\infty} \frac{1}{m_b^n} \left[\sum_i H_i^{(n)} J_i^{(n)} \otimes S_i^{(n)} \otimes \bar{J}_i^{(n)} + \sum_i H_i^{(n)} J_i^{(n)} \otimes S_i^{(n)} \otimes \bar{J}_i^{(n)} \otimes \bar{J}_i^{(n)} \right], \end{aligned} \tag{9.1}$$

where $H_i^{(n)}$ are hard functions appearing in the matching of QCD onto SCET at the hard scale $\mu_h \sim m_b$, $J_i^{(n)}$ and $\bar{J}_i^{(n)}$ are the jet functions corresponding to the matching coefficient from SCET onto HQET at $\mu_i \sim \sqrt{\Lambda_{\rm QCD} m_b}$, and $S_i^{(n)}$ represents the shape functions, which encode the non-perturbative dynamics. The explicit formula is given in (5.39). On the one hand this factorization resolves some of the issues of the partonic calculation, like large logarithms or the dependence on low-energy parameters in (2.35). On the other hand it provides new insights concerning the possible space-time structure of the relevant contributions. While the usual jet functions $J_i^{(n)}$ are defined as cut propagators of hard-collinear particles, the new type of jet function $\bar{J}_i^{(n)}$ corresponds to full propagators dressed by Wilson lines. They appear in the so-called resolved photon contributions, in which the photon is not emitted directly from the vertex but from one of the light partons. The contributions that do not contain a $\bar{J}_i^{(n)}$ are called direct photon contributions and they can be expressed as a double expansion in powers of $\Lambda_{\rm QCD}/\Delta$ and Δ/m_b when considering the integrated rate with a cut far outside the endpoint region.

In contrast, the resolved contributions are new and not covered in the local OPE approach, yet they have important implications for phenomenology. They significantly contribute to the uncertainty in the prediction of the branching fraction as well as in the determination of the direct CP asymmetry. The second major topic of this work was to estimate the possible size of these effects. Due to their non-perturbative nature, they can not be calculated analytically. Unfortunately it is also not possible to determine their values on the lattice, since they contain non-local matrix elements separated by light-like distances.

A careful analysis revealed that the phenomenologically relevant resolved contributions at $\mathcal{O}(1/m_b)$ are due to interferences of weak effective operators $Q_1^q - Q_{7\gamma}$, $Q_{7\gamma} - Q_{8g}$ and $Q_{8g} - Q_{8g}$ (see Chapter 6). Models for the shape functions and a relation to the measured isospin asymmetry have been used to estimate the influence of these contributions on the integrated rate with a cut outside the endpoint region (see Chapter 7). It turned out that a simple dimensional estimate of $\Lambda_{\rm QCD}/m_b$ (possibly enhanced by Wilson coefficients) tends to overestimate the effect. In the $Q_1^q - Q_{7\gamma}$ case the normalization (6.14) restricted the size,

while the contributions due to $Q_{7\gamma} - Q_{8g}$ in (6.45) and $Q_{8g} - Q_{8g}$ in (6.32) were suppressed by charge factors. Nevertheless, it was found that the resolved photon contributions are responsible for an irreducible uncertainty of at least

$$-4.0\% < \mathcal{F}_E(\Delta) < +4.8\%\,, \tag{9.2}$$

where the $Q_{7\gamma} - Q_{8g}$ contribution was extracted from the measured isospin asymmetry in the hypothetical limit of no experimental uncertainties. This result therefore represents the "ideal" case and it is hard to conceive a way to further reduce this uncertainty.

The effect of the resolved contributions on the direct CP asymmetry can be determined by considering the imaginary parts of the convolutions of the jet and shape functions. All shape functions are real (see Chapter 6), yet the new jet functions $\bar{J}_i^{(n)}$ carry a strong phase. This phase generates new long-distance contributions to the CP asymmetry (see Chapter 8), which turn out to be the dominant effects in the SM, since they are enhanced by a factor $1/\alpha_s$ compared to the SM in (8.18). The largest of these effects is due to the interference of the electromagnetic dipole amplitude with an up-quark penguin amplitude accompanied by a soft gluon emission. It was found that the SM prediction for the direct CP asymmetry should be given as a range

$$-0.6\,\% < A_{CP}^{\rm SM} < 2.8\,\%\,, \tag{9.3}$$

compared to the $\sim 0.5\,\%$ prediction of the parton model [132]. Since such a large range can possibly hide new physics effects, a measurement of the asymmetry rate difference in (8.22) was suggested.

In summary, the analysis presented in this thesis established the factorization formula (9.1) for the photon spectrum in the endpoint region, and provided estimates for the effects of the resolved photon contributions on the branching fraction (9.2) and the direct CP asymmetry (9.3). In the light of pending advances on the intensity frontier [25,26], the results will have important implications for the determination of SM parameters, as well as for the search for new physics, which might be hidden by the non-perturbative effects analyzed in this thesis. Even though these effects can only be estimated at present, the systematic approach based on the effective theories SCET and HQET has been shown to provide a suitable framework for their identification and their exact field theoretic definition.

Appendix A

Definitions and Numbers

A.1 The Penguin Function

This appendix will introduce the penguin function, appearing in calculations where two lines of a four-quark operator are contracted to a penguin loop. Feynman diagrams, such as the last one in Figure 2.6 generally are proportional to a function [63]

$$\frac{2G(t)+t}{(q\cdot q')\,t} \tag{A.1}$$

where q and q' are the momenta of the gauge bosons emitted from the loop, $t = 2q\cdot q'/m_c^2$ (for a charm-quark loop) and $G(t)$ is defined by

$$G(t) = \int_0^1 \frac{dy}{y}\,\ln\big(1-t(1-y)-i\varepsilon\big). \tag{A.2}$$

It is now convenient to introduce the *penguin function* $F(x)$ through

$$F(x) = -2xG\left(\frac{1}{x}\right) \tag{A.3}$$

which implies

$$F(x) = 4x\arctan^2\left(\frac{1}{\sqrt{4x-1}}\right) \tag{A.4}$$

which is real for $x<0$ and $x>1/4$ and whose real and imaginary parts for $0<x<1/4$ are also given by

$$\mathrm{Re}\,F(x) = \pi^2 x - 4x\ln^2\left(\sqrt{\frac{1}{4x}}+\sqrt{\frac{1}{4x}-1}\right) \tag{A.5}$$

$$\mathrm{Im}\,F(x) = 4\pi x\ln\left(\sqrt{\frac{1}{4x}}+\sqrt{\frac{1}{4x}-1}\right). \tag{A.6}$$

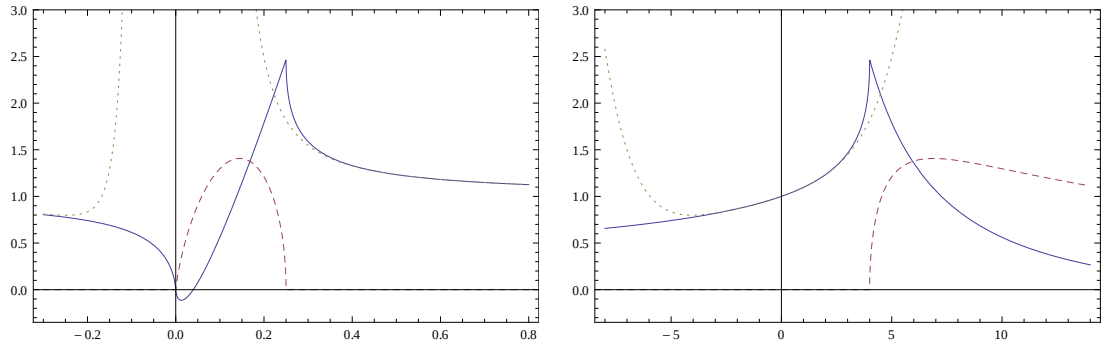

Figure A.1: The penguin function $F(x)$ (on the left) and $F(1/x)$ (on the right). The full and dashed lines represent the real and imaginary part, respectively. Also illustrated are the expansions for large x (on the left) and small x (on the right).

Due to the definition (A.3) the penguin function of the inverse argument as well as the penguin function itself are plotted in Figure A.1. The expansion in (6.9) converges for $|x| > 1/4$ and is also illustrated in the Figure. Furthermore, it can be seen that $F(x)$ vanishes for $x \to 0$ which justifies the approximation $F(z/x) \to 0$ in (2.29) for $m_c^2 \sim \Lambda_{\rm QCD} m_b$.

A.2 Input Parameters

In this Appendix all input parameter values used in the various numerical calculations are collected. As the default choice for the factorization scale μ entering the Wilson coefficients, the strong coupling constant, and the various hadronic quantities, the hard-collinear scale $\mu = 1.5\,\text{GeV}$ is taken, which is indeed a scale of order $\sqrt{m_b \Lambda_{\text{QCD}}}$. This is an appropriate scale choice, given that RG evolution effects are neglected.

The b-quark mass enters the expressions either via the photon energy ($E_\gamma \approx m_b/2$ near the peak of the spectrum) or as the heavy-quark expansion parameter. It is therefore appropriate to adopt a low-scale subtracted heavy-quark mass, such as the mass defined in the shape-function scheme [1]. Specifically, $m_b = 4.65\,\text{GeV}$ will be used. The charm-quark mass enters as a running mass in charm-penguin diagrams with a soft gluon emission, which are characterized by a hard-collinear virtuality. Therefore $m_c = \overline{m}_c(\mu)$ defined in the $\overline{\text{MS}}$ scheme will be used, with $\mu = 1.5\,\text{GeV}$ fixed as described above. This corresponds to the choice adopted in [5], and following these authors $\overline{m}_c(\mu) = 1.131\,\text{GeV}$ is assumed. Finally, for the strange-quark mass $m_s = m_b/50$ is taken, which is the value commonly adopted in the literature on $\bar{B} \to X_s\gamma$ decay.

Furthermore input values for some HQET matrix elements are needed. The parameters λ_2 and ρ^3_{LS} are extracted from a global fit to $\bar{B} \to X_c l\,\bar{\nu}$ experimental data by the Heavy Flavor Averaging Group (HFAG) [24]. Unfortunately, in many cases these and other parameters are extracted from a combined fit to $\bar{B} \to X_c l\,\bar{\nu}$ and $\bar{B} \to X_s\gamma$, an approach that was criticized in [145]. Only recently HFAG has started quoting also values obtained using only semi-leptonic data. The most recent results are $\lambda_2 = (0.12 \pm 0.02)\,\text{GeV}^2$ and $\rho^3_{LS} = (-0.17 \pm 0.09)\,\text{GeV}^3$ [146]. For simplicity, the central values for these quantities will always be used. For the first inverse moment of the B-meson light-cone distribution amplitude, the range $250\,\text{MeV} < \lambda_B < 750\,\text{MeV}$ is taken, which covers predictions obtained using QCD sum rules and other methods [122–127]. Finally, to the level of accuracy of the calculations in this work, the parameter F can be extracted from the relation $F = f_B\sqrt{M_B}$, and using $f_B = (193 \pm 10)\,\text{MeV}$ [147] one obtains $0.177\,\text{GeV}^3 < F^2 < 0.217\,\text{GeV}^3$.

Appendix B

Operator Matching onto SCET

This appendix will complete the list of SCET operators relevant for $\bar{B} \to X_s\gamma$ and descending from Q_{8g} and Q_1^q up to a suppression of $1/m_b$ compared to the leading power operator (4.27). The operators descending from $Q_{7\gamma}$ were already given in (5.5) and (5.6). In order to determine the SCET operators the methods introduced in Section 5.1 will be applied.

B.1 Tree-Level Matching of Q_{8g}

As was already discussed in Section 5.4, there are three relevant possibilities to match the gluon and the light quark onto SCET fields. Either they are both hard-collinear or one is hard-collinear and the other anti-hard-collinear. Soft fields are excluded by the power counting. The leading operators for the combination of hard-collinear and anti-hard-collinear fields were already given in Section 5.4 but will be repeated here for completeness.

For the case of Q_{8g} containing an anti-hard-collinear gluon and a hard-collinear s-quark, the conversion of the anti-hard-collinear gluon into a photon is $\mathcal{O}(\lambda)$ in power counting. In this case, Q_{8g} is matched onto a single operator (suppressing the a factor $-\frac{g\,m_b}{4\pi^2}e^{-im_b\,v\cdot x}$):

$$Q^{(2)}_{8g,\,\overline{\text{hc}}\text{ gluon}} = \bar{\xi}_{\text{hc}}\,\frac{\bar{n}\!\!\!/}{2}\,[in\cdot\partial \mathcal{A}_{\overline{\text{hc}}\perp}]\,(1+\gamma_5)h\,, \quad \text{followed by } \mathcal{O}(\lambda) \text{ conversion.} \tag{B.1}$$

If the s-quark is matched onto a hard-collinear field, the anti-hard-collinear photon needs to be emitted from either the b or s-quark lines. This is illustrated in Figure B.1. The operator Q_{8g} would then match onto SCET operators that contain both a hard-collinear gluon and an anti-hard-collinear photon suppressed by m_b if the photon is emitted from the b-quark line, and by $\bar{n}\cdot\partial$ if the photon is emitted from the s-quark line. Furthermore the expansion of $G^{\mu\nu}$ given in (5.36) and the multipole expansion of the heavy-quark field

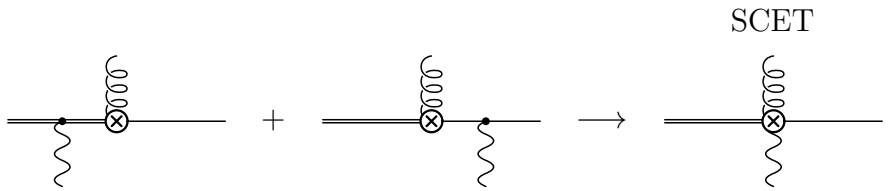

Figure B.1: Graphical illustration of the tree-level matching procedure for the operator Q_{8g} for the case when the s-quark is matched onto a hard-collinear field.

need to be considered. This leads to

$$\begin{aligned}
Q^{(1)}_{8g,\,\text{hc quark}} &= \bar\xi_{\text{hc}}\frac{1}{i\bar n\cdot\overleftarrow{\partial}}e_d e\!\not\!A^{\text{em}}_\perp[i\bar n\cdot\partial\!\not\!\mathcal{A}_{\text{hc}\perp}]\,(1+\gamma_5)h\,,\\
Q^{(2)}_{8g,\,\text{hc quark}} &= \bar\xi_{\text{hc}}\frac{1}{i\bar n\cdot\overleftarrow{\partial}}e_d e\!\not\!A^{\text{em}}_\perp[i\bar n\cdot\partial\!\not\!\mathcal{A}_{\text{hc}\perp}]\,(1+\gamma_5)x^\mu_\perp D_\mu h\\
&\quad-\bar\xi_{\text{hc}}\frac{i\overleftarrow{\partial\!\!\!/}_\perp}{i\bar n\cdot\overleftarrow{\partial}}\frac{\bar n\!\!\!/}{2m_b}\,[i\bar n\cdot\partial\!\not\!\mathcal{A}_{\text{hc}\perp}]e_d e\!\not\!A^{\text{em}}_\perp(1+\gamma_5)h\\
&\quad+\bar\xi_{\text{hc}}\frac{1}{i\bar n\cdot\overleftarrow{\partial}}e_d e\!\not\!A^{\text{em}}_\perp\frac{\bar n\!\!\!/}{2}\,[i\partial\!\!\!/_\perp\!\not\!\mathcal{A}_{\text{hc}\perp}-i\partial_\perp\cdot\mathcal{A}_{\text{hc}\perp}]\,(1+\gamma_5)h\\
&\quad-\bar\xi_{\text{hc}}\,[i\partial\!\!\!/_\perp\!\not\!\mathcal{A}_{\text{hc}\perp}-i\partial_\perp\cdot\mathcal{A}_{\text{hc}\perp}]\,\frac{\bar n\!\!\!/}{2m_b}e_d e\!\not\!A^{\text{em}}_\perp(1+\gamma_5)h\\
&\quad+\bar\xi_{\text{hc}}\frac{1}{i\bar n\cdot\overleftarrow{\partial}}e_d e\!\not\!A^{\text{em}}_\perp\frac{\bar n\!\!\!/}{2}\left[\frac{i}{2}\bar n\cdot\partial\,n\cdot\mathcal{A}_{\text{hc}}\right](1+\gamma_5)h\\
&\quad+\bar\xi_{\text{hc}}\frac{\bar n\!\!\!/}{2m_b}\left[\frac{i}{2}\bar n\cdot\partial\,n\cdot\mathcal{A}_{\text{hc}}\right]e_d e\!\not\!A^{\text{em}}_\perp(1+\gamma_5)h\,.
\end{aligned}\tag{B.2}$$

If the s-quark is matched onto an anti-hard-collinear field, it can only be converted to an anti-hard-collinear photon and a soft s-quark. The conversion costs $\lambda^{1/2}$, so the lowest-order operator possible is $\mathcal{O}(\lambda^3)$. Considering all the possible structures for $G^{\mu\nu}$ and the multipole expansion, one finds

$$\begin{aligned}
Q^{(1)}_{8g,\,\overline{\text{hc}}\,\text{quark}} &= \bar\xi_{\overline{\text{hc}}}\frac{n\!\!\!/}{2}\,[i\bar n\cdot\partial\!\not\!\mathcal{A}_{\text{hc}\perp}]\,(1+\gamma_5)h\,,\quad\text{followed by }\mathcal{O}(\lambda^{1/2})\text{ conversion,}\\
Q^{(2)}_{8g,\,\overline{\text{hc}}\,\text{quark}} &= \bar\xi_{\overline{\text{hc}}}\frac{n\!\!\!/}{2}\,[i\bar n\cdot\partial\!\not\!\mathcal{A}_{\text{hc}\perp}]\,(1+\gamma_5)x^\mu_\perp D_\mu h\,,\quad\text{followed by }\mathcal{O}(\lambda^{1/2})\text{ conversion,}\\
&\quad+\bar\xi_{\overline{\text{hc}}}\,[i\partial\!\!\!/_\perp\!\not\!\mathcal{A}_{\text{hc}\perp}-i\partial_\perp\cdot\mathcal{A}_{\text{hc}\perp}]\,(1+\gamma_5)h\,,\quad\text{followed by }\mathcal{O}(\lambda^{1/2})\text{ conversion,}\\
&\quad+\bar\xi_{\overline{\text{hc}}}\,\frac{n\!\!\!/}{2}\left[\frac{i}{2}\bar n\cdot\partial\,n\cdot\mathcal{A}_{\text{hc}}\right](1+\gamma_5)h\,,\quad\text{followed by }\mathcal{O}(\lambda^{1/2})\text{ conversion.}
\end{aligned}\tag{B.3}$$

B.2 Tree-Level Matching of Q_1^q

The tree-level matching of Q_1^q onto a SCET operator containing two anti-hard-collinear and one hard-collinear field was already given in Section 5.4. There, it was argued, that all other possibilities for the matching of the light quark fields do not contribute to subleading $\bar{B} \to X_s\gamma$ since there is no operator they can interfere with to generate a $1/m_b$ suppressed contribution to the differential decay rate. However, at order $1/m_b^2$ there are more possibilities to match Q_1^q. To simplify the notation the operator will be written as as $Q_1^q = \bar{s}\,\Gamma_1 q\,\bar{q}\,\Gamma_2 b$, where $\Gamma_1 \otimes \Gamma_2 = \gamma^\mu(1-\gamma_5) \otimes \gamma_\mu(1-\gamma_5)$. At tree level, the light quarks can only be matched onto hard-collinear or anti-hard-collinear fields. A matching of any of the light quarks onto even one soft field would lead to a suppression of $\mathcal{O}(\lambda^4)$. As a result, Q_1^q is matched at $\mathcal{O}(\lambda^3)$, before taking into account any conversions. When there is more than one anti-hard-collinear quark field, no conversion is allowed at tree-level. Hence, the following cases remain (suppressing the $e^{-im_b\, v\cdot x}$ factor).

$\bar{s} = \bar{\xi}_{\rm hc}$, $q = \xi_{\rm hc}$, $\bar{q} = \bar{\xi}_{\rm hc}$: The anti-hard-collinear photon can either be emitted from the heavy or one of the hard-collinear quark lines. This leads to four possible $\mathcal{O}(\lambda^{7/2})$ operators:

$$\begin{aligned} Q_1^{q\,(2)} = &- \bar{\xi}_{\rm hc}\Gamma_1 \frac{\bar{n}\!\!\!/}{2m_b} e_d e A\!\!\!/_\perp^{\rm em} h\, \bar{\xi}_{\rm hc}\Gamma_2\xi_{\rm hc} + \bar{\xi}_{\rm hc}\, e_d e A\!\!\!/_\perp^{\rm em} \frac{\bar{n}\!\!\!/}{2} \frac{1}{i\bar{n}\cdot \overleftarrow{\partial}} \Gamma_1 h\, \bar{\xi}_{\rm hc}\Gamma_2\xi_{\rm hc} \\ &+ \bar{\xi}_{\rm hc}\Gamma_1 h\, \bar{\xi}_{\rm hc}\, e_d e A\!\!\!/_\perp^{\rm em} \frac{\bar{n}\!\!\!/}{2} \frac{1}{i\bar{n}\cdot \overleftarrow{\partial}} \Gamma_{2\mu}\xi_{\rm hc} - \bar{\xi}_{\rm hc}\Gamma_1 h\, \bar{\xi}_{\rm hc}\Gamma_2 \frac{\bar{n}\!\!\!/}{2}\, e_d e A\!\!\!/_\perp^{\rm em} \frac{1}{i\bar{n}\cdot \overrightarrow{\partial}} \xi_{\rm hc}\,. \end{aligned} \tag{B.4}$$

$\bar{s} = \bar{\xi}_{\rm hc}$, $q = \xi_{\overline{\rm hc}}$, $\bar{q} = \bar{\xi}_{\rm hc}$ and **$\bar{s} = \bar{\xi}_{\rm hc}$, $q = \xi_{\rm hc}$, $\bar{q} = \bar{\xi}_{\overline{\rm hc}}$:** In this case the anti-hard-collinear quark needs to be converted to a photon via $\xi_{\overline{\rm hc}} \to A_\perp^{\rm em} + q$ and $\bar{\xi}_{\overline{\rm hc}} \to A_\perp^{\rm em} + \bar{q}$, which is of $\mathcal{O}(\lambda^{1/2})$. This yields

$$\begin{aligned} Q_1^{q\,(2)} = &\,\bar{\xi}_{\rm hc}\Gamma_1 h\, \bar{\xi}_{\overline{\rm hc}}\Gamma_2\xi_{\rm hc}\,, \quad \text{followed by } \mathcal{O}(\lambda^{1/2}) \text{ conversion,} \\ &+ \bar{\xi}_{\rm hc}\Gamma_1 h\, \bar{\xi}_{\rm hc}\Gamma_2\xi_{\overline{\rm hc}}\,, \quad \text{followed by } \mathcal{O}(\lambda^{1/2}) \text{ conversion.} \end{aligned} \tag{B.5}$$

$\bar{s} = \bar{\xi}_{\overline{\rm hc}}$, $q = \xi_{\rm hc}$, $\bar{q} = \bar{\xi}_{\rm hc}$: Supplemented with SCET Lagrangian for $\bar{\xi}_{\overline{\rm hc}} \to A_\perp^{\rm em} + \bar{q}$, only one $\mathcal{O}(\lambda^{7/2})$ operator is possible:

$$Q_1^{q\,(2)} = \bar{\xi}_{\overline{\rm hc}}\Gamma_1 h\, \bar{\xi}_{\rm hc}\Gamma_2\xi_{\rm hc}\,, \quad \text{followed by } \mathcal{O}(\lambda^{1/2}) \text{ conversion.} \tag{B.6}$$

B.3 Loop-Level Matching of Q_1^q

Loop-level matching is only relevant for Q_1^q, when the two up-type quarks are contracted and a number of gauge bosons are emitted from the internal lines. The contribution of three gauge bosons would lead to further power or loop suppression, so only one or two

bosons need to be considered. The one gauge boson loops are already included in the effective Wilson coefficients C_i^{eff} defined in Section 2.1.5.

A more involved contribution arises for the loops with two external bosons, which is the main focus of this section. These can only be one photon and one gluon. Two external gluons would lead to further power or loop suppression. As usual, the b-quark is matched onto the heavy-quark field h. Since there is already a photon in the operator, the s-quark can not be anti-hard-collinear. On the other hand, a soft s-quark would lead to power suppression, so it must be hard-collinear. There are two possibilities to match the gluon emitted from the loop: it can either be hard-collinear or it can be soft. If the gluon is hard-collinear, the loop momentum is hard for momentum conservation reasons. If the gluon is soft, the loop momentum is anti-hard-collinear which just corresponds to the case considered in Section 6.1. For the first case, a photon and a hard-collinear gluon, it is necessary to calculate the loop diagram in QCD in order to perform the matching. For the second case, a photon and and a soft gluon, one would need the tree-level matching of Q_1^q onto the operator of (5.38). The conversion of the two anti-hard collinear quarks to a photon and a soft gluon would be calculated in SCET. Alternatively, one can calculate the process in QCD and use the fact that the two calculations are equivalent, since only one momentum region, anti-hard-collinear, contributes in this case. The result can be read off from the two gluon calculation in [148], where one of the gluons is replaced by a photon. Using the notation of [148] the amplitude is given by

$$\mathcal{A} = \frac{e\, e_q}{4\pi}\frac{g}{4\pi}(T^a)_{mn}\bar{s}_m\Gamma_2 A_{\mu\nu}\Gamma_1 b_n \epsilon_1^{*\mu}(q_1)\epsilon_2^{*a\,\nu}(q_2)\delta_{ij}\delta_{kl}\,, \tag{B.7}$$

where

$$\begin{aligned} A_{\mu\nu} = {} & [(4r-1)F(r)-4r]\left[\frac{m_q}{2r}\,g_{\mu\nu} - \frac{q_\mu q_\nu}{m_q}\right] + [F(r)-1]\, i\epsilon_{\rho\alpha\mu\nu}\,(q_1^\rho - q_2^\rho)\,\gamma^\alpha\gamma^5 \\ & + \frac{2r}{m_q^2}\,[F(r)-1]\,[q_\mu i\epsilon_{\rho\sigma\alpha\nu}q_1^\rho q_2^\sigma - q_\nu i\epsilon_{\rho\sigma\alpha\mu}q_1^\rho q_2^\sigma]\,\gamma^\alpha\gamma^5 - \frac{F(r)}{m_q} i\epsilon_{\rho\sigma\mu\nu}q_1^\rho q_2^\sigma\gamma^5\,. \end{aligned} \tag{B.8}$$

Here m_q and e_q are the mass and charge of the quark in the loop, q_1, ϵ_1 (q_2, ϵ_2) are the momentum and polarization of the photon (gluon), $r = m_q^2/q^2 - i\epsilon$, $q^2 = (q_1+q_2)^2$, and $F(r)$ is the penguin function defined in Appendix A.1. Alternatively, one could write in a gauge-invariant notation

$$\begin{aligned} A_{\mu\nu}\epsilon_1^{*\mu}(q_1)\epsilon_2^{*a\,\nu}(q_2) = {} & [(1-4r)F(r)+4r]\,\frac{1}{2m_q}F^{\mu\nu}G^a_{\mu\nu} + \frac{F(r)}{2m_q}\,\tilde{G}^a_{\rho\mu}F^{\rho\mu}i\gamma_5 \\ & + [1-F(r)]\,\frac{2}{q^2}\left(G^a_{\mu\alpha}\tilde{F}^{\mu\beta} + F_{\mu\alpha}\tilde{G}^{a\,\mu\beta}\right) iq^\alpha\gamma_\beta\gamma_5\,. \end{aligned} \tag{B.9}$$

Here the convention

$$\tilde{F}^{\mu\nu} = -\frac{1}{2}\epsilon^{\mu\nu\alpha\beta}F_{\alpha\beta} \quad (\epsilon^{0123} = -1) \tag{B.10}$$

was used in addition to the fact that for an external gluon $q_2\cdot\epsilon_2^{*a} = 0$. In the following sections the cases of an anti-hard-collinear and a hard loop momentum will be considered

in turn. As already mentioned above, the former case is equivalent to the calculation of the SCET diagram in Section 6.1. The latter case on the other hand is necessary to determine the direct photon contributions involving insertions of the operator Q_1^q.

B.3.1 Matching with $A^{\rm em}_{\perp\overline{\rm hc}}$ and $A^{\rm gluon}_s$

The diagram with an anti-hard-collinear photon and a soft gluon emitted from the internal line already contributes at $\mathcal{O}(\lambda^{7/2})$. Since $A^{\rm gluon}_{\rm s}$ scales homogeneously $\sim(\lambda,\lambda,\lambda)$, it is natural to use the gauge invariant form for the resulting operators, rather than decomposing the gauge fields into their light-cone components. Furthermore, only the axial part of $A_{\mu\nu}$ in (B.9) yields a non-zero result, as the Γ_i in (B.7) are the usual $V-A$ Dirac structures, when matching Q_1^q. Therefore one only needs

$$\begin{aligned} A_{\mu\nu}\epsilon_1^{*\mu}(q_1)\epsilon_2^{*a\,\nu}(q_2) &= \frac{2}{q^2}\left(G^a_{\mu\alpha}\tilde F^{\mu\beta}+F_{\mu\alpha}\tilde G^{a\,\mu\beta}\right) iq^\alpha\gamma_\beta\gamma_5[1-F(r)] \\ &\approx \frac{2}{q^2}\left(G^a_{\mu\alpha}\tilde F^{\mu\beta}\right) iq^\alpha\gamma_\beta\gamma_5[1-F(r)]\,, \end{aligned} \tag{B.11}$$

which follows from the fact, that $q^\alpha F_{\mu\alpha}$ vanishes at the lowest order in λ.

The loop can consist of any up-type quark that is not integrated out in the weak effective Lagrangian. When matching onto SCET the u quark should be taken to be massless, so $F(m_u^2/q^2)$ can be replaced by 0 (see Appendix A.1). The charm-quark mass scales like $m_c^2\sim m_b\Lambda_{\rm QCD}$, which is of the same order as q^2. As a result, $F(m_c^2/q^2)$ should not be expanded for c-quarks.

Thus, in position space the Q_1^q operators are matched onto

$$\begin{aligned} Q_1^{u\,(2)}(x) &= \left(\frac{ee_u}{4\pi^2}\right)\bar\xi_{\rm hc}(x)\,T^a\gamma^\beta(1-\gamma_5)h(x)e^{-im_bv\cdot x} \\ &\quad\times\int\frac{d^4q_1}{(2\pi)^4}\frac{d^4q_2}{(2\pi)^4}e^{i(q_1+q_2)x}\frac{1}{(q_1+q_2)^2+i\epsilon}i(q_1^\alpha+q_2^\alpha)gG^a_{\mu\alpha}(q_2)\,\epsilon^{\mu\beta\rho\sigma}F_{\rho\sigma}(q_1)\,, \\ Q_1^{c\,(2)}(x) &= \left(\frac{ee_c}{4\pi^2}\right)\bar\xi_{\rm hc}(x)\,T^a\gamma^\beta(1-\gamma_5)h(y)e^{-im_bv\cdot x}\int\frac{d^4q_1}{(2\pi)^4}\frac{d^4q_2}{(2\pi)^4}e^{i(q_1+q_2)x} \\ &\quad\times\frac{1}{(q_1+q_2)^2+i\epsilon}\left[1-F\left(\frac{m_c^2}{(q_1+q_2)^2}-i\epsilon\right)\right]i(q_1^\alpha+q_2^\alpha)gG^a_{\mu\alpha}(q_2)\,\epsilon^{\mu\beta\rho\sigma}F_{\rho\sigma}(q_1)\,, \end{aligned} \tag{B.12}$$

where the dependence of the momentum-space $F_{\rho\sigma}$ and $G^a_{\mu\alpha}$ on q_1 and q_2 is shown explicitly.

B.3.2 Matching with $A^{\rm em}_{\perp\overline{\rm hc}}$ and $A^{\rm gluon}_{\perp\rm hc}$

In this case q^2 is hard, i.e. $q^2\sim m_b^2$. Therefore $F(m_q^2/q^2)$ can be expanded around zero for charm-quarks as well as for up-quarks. The first order correction resulting from this expansion gives a power suppressed contribution, so $F(m_q^2/q^2)$ can be set to zero. Depending

on the polarization of the gluon field Q_1^q either matches onto a $\mathcal{O}(\lambda^3)$ or an $\mathcal{O}(\lambda^{7/2})$ operator. Furthermore corrections from the multipole expansion of the heavy-quark need to be included. In total one finds that Q_1^q is matched onto (suppressing a factor $\frac{ee_q g}{4\pi^2}\, e^{-im_b\, v\cdot x}$)

$$\begin{aligned}
Q_1^{q\,(1)} &= \bar{\xi}_{\rm hc}\frac{\bar{n}\!\!\!/}{2}\,\epsilon_{\perp\mu\nu}[\mathcal{A}^\nu_{{\rm hc}\perp}\, n\cdot\partial A_\perp^{{\rm em}\,\mu}]\,(1-\gamma_5)h\,,\\
Q_1^{q\,(2)} &= \bar{\xi}_{\rm hc}\,\epsilon_{\perp\mu\nu}[A_\perp^{\rm em}\cdot\partial_\perp\mathcal{A}^\nu_{{\rm hc}\perp}]\,\gamma_\perp^\mu(1-\gamma_5)h\\
&\quad+\frac{1}{2}\,\bar{\xi}_{\rm hc}\,\epsilon_{\perp\mu\nu}[A_\perp^{{\rm em}\,\nu}\bar{n}\cdot\partial\, n\cdot\mathcal{A}_{\rm hc}]\,\gamma_\perp^\mu(1-\gamma_5)h\\
&\quad-\bar{\xi}_{\rm hc}\frac{i\overleftarrow{\partial\!\!\!/}_\perp}{i\bar{n}\cdot\overleftarrow{\partial}}\,\epsilon_{\perp\mu\nu}[A_\perp^{{\rm em}\,\mu}\bar{n}\cdot\partial\mathcal{A}^\nu_{{\rm hc}\perp}]\,(1-\gamma_5)h\\
&\quad+\bar{\xi}_{\rm hc}\frac{\bar{n}\!\!\!/}{2}\,\epsilon_{\perp\mu\nu}[\mathcal{A}^\nu_{{\rm hc}\perp}n\cdot\partial A_\perp^{{\rm em}\,\mu}]\,(1-\gamma_5)x_\perp^\mu D_\mu h\,,
\end{aligned}\tag{B.13}$$

where $\epsilon_{\perp\mu\nu}=\frac{1}{2}\epsilon_{\alpha\beta\mu\nu}\bar{n}^\alpha n^\beta$.

Bibliography

[1] S. W. Bosch, B. O. Lange, M. Neubert and G. Paz, Nucl. Phys. B **699** (2004) 335 [arXiv:hep-ph/0402094].

[2] B. O. Lange, M. Neubert and G. Paz, Phys. Rev. D **72** (2005) 073006 [arXiv:hep-ph/0504071].

[3] U. Haisch, arXiv:0805.2141 [hep-ph].

[4] M. Neubert, Phys. Rept. **245** (1994) 259 [arXiv:hep-ph/9306320].

[5] M. Misiak *et al.*, Phys. Rev. Lett. **98** (2007) 022002 [arXiv:hep-ph/0609232].

[6] C. W. Bauer, S. Fleming and M. E. Luke, Phys. Rev. D **63** (2000) 014006 [arXiv:hep-ph/0005275].

[7] C. W. Bauer, S. Fleming, D. Pirjol and I. W. Stewart, Phys. Rev. D **63** (2001) 114020 [arXiv:hep-ph/0011336].

[8] T. Becher and M. Neubert, Phys. Rev. Lett. **98** (2007) 022003 [arXiv:hep-ph/0610067].

[9] M. Beneke, F. Campanario, T. Mannel and B. D. Pecjak, JHEP **0506** (2005) 071 [arXiv:hep-ph/0411395].

[10] K. S. M. Lee and I. W. Stewart, Nucl. Phys. B **721** (2005) 325 [arXiv:hep-ph/0409045].

[11] G. P. Korchemsky and G. F. Sterman, Phys. Lett. B **340** (1994) 96 [arXiv:hep-ph/9407344].

[12] C. W. Bauer, D. Pirjol and I. W. Stewart, Phys. Rev. D **65** (2002) 054022 [arXiv:hep-ph/0109045].

[13] M. Neubert, Eur. Phys. J. C **40** (2005) 165 [arXiv:hep-ph/0408179].

[14] S. J. Lee, M. Neubert and G. Paz, Phys. Rev. D **75**, 114005 (2007) [arXiv:hep-ph/0609224].

[15] M. Benzke, S. J. Lee, M. Neubert and G. Paz, JHEP **1008** (2010) 099 [arXiv:1003.5012 [hep-ph]].

[16] M. Benzke, S. J. Lee, M. Neubert and G. Paz, arXiv:1012.3167 [hep-ph].

[17] T. Hurth, Rev. Mod. Phys. **75** (2003) 1159 [arXiv:hep-ph/0212304].

[18] T. Hurth and M. Nakao, Ann. Rev. Nucl. Part. Sci. **60** (2010) 645 [arXiv:1005.1224 [hep-ph]].

[19] `http://www.slac.stanford.edu/BF/`

[20] `http://belle.kek.jp/`

[21] E. H. Thorndike [Cleo collaboration], arXiv:hep-ex/0206067.

[22] A. Limosani *et al.* [Belle Collaboration], Phys. Rev. Lett. **103** (2009) 241801 [arXiv:0907.1384 [hep-ex]].

[23] O. Buchmuller and H. Flacher,Phys. Rev. D **73** (2006) 073008 [arXiv:hep-ph/0507253].

[24] The Heavy Flavor Averaging Group *et al.*, arXiv:1010.1589 [hep-ex].

[25] B. O'Leary *et al.* [SuperB Collaboration], arXiv:1008.1541 [hep-ex].

[26] T. Kuhr and f. t. B. Collaboration, arXiv:1101.1916 [hep-ex].

[27] A. J. Buras, arXiv:hep-ph/9806471.

[28] M. Neubert, arXiv:hep-ph/0512222.

[29] M. E. Peskin and D. V. Schroeder, *Reading, USA: Addison-Wesley (1995) 842 p*

[30] N. Cabibbo, Phys. Rev. Lett. **10** (1963) 531.
M. Kobayashi and T. Maskawa, Prog. Theor. Phys. **49** (1973) 652.

[31] K. G. Wilson, Phys. Rev. **179** (1969) 1499.

[32] V. A. Smirnov, Commun. Math. Phys. **134** (1990) 109.
F. V. Tkachov, Int. J. Mod. Phys. A **8** (1993) 2047 [arXiv:hep-ph/9612284].

[33] K. G. Wilson and W. Zimmermann, Commun. Math. Phys. **24** (1972) 87.
W. Zimmermann, Annals Phys. **77** (1973) 570 [Lect. Notes Phys. **558** (2000) 278].

[34] E. C. G. Stueckelberg and A. Petermann, Helv. Phys. Acta **26** (1953) 499.
M. Gell-Mann and F. E. Low, Phys. Rev. **95** (1954) 1300.
K. Symanzik, Commun. Math. Phys. **18** (1970) 227.

[35] M. Beneke, G. Buchalla, M. Neubert and C. T. Sachrajda, Nucl. Phys. B **606** (2001) 245 [arXiv:hep-ph/0104110].

[36] B. Grinstein, R. P. Springer and M. B. Wise, Nucl. Phys. B **339** (1990) 269.

[37] M. Ciuchini, E. Franco, G. Martinelli, L. Reina and L. Silvestrini, Phys. Lett. B **316** (1993) 127 [arXiv:hep-ph/9307364].

[38] A. J. Buras, M. Misiak, M. Munz and S. Pokorski, Nucl. Phys. B **424** (1994) 374 [arXiv:hep-ph/9311345].

[39] G. Cella, G. Curci, G. Ricciardi and A. Vicere, Phys. Lett. B **325** (1994) 227 [arXiv:hep-ph/9401254].

[40] G. Buchalla, A. J. Buras and M. E. Lautenbacher, Rev. Mod. Phys. **68** (1996) 1125 [arXiv:hep-ph/9512380].

[41] S. Bertolini, F. Borzumati and A. Masiero, Phys. Rev. Lett. **59** (1987) 180.

[42] A. Ali and C. Greub, Z. Phys. C **60** (1993) 433.

[43] K. G. Chetyrkin, M. Misiak and M. Munz, Phys. Lett. B **400** (1997) 206 [Erratum-ibid. B **425** (1998) 414] [arXiv:hep-ph/9612313].

[44] A. J. Buras, A. Kwiatkowski and N. Pott, Phys. Lett. B **414** (1997) 157 [Erratum-ibid. B **434** (1998) 459] [arXiv:hep-ph/9707482].

[45] G. Altarelli, G. Curci, G. Martinelli and S. Petrarca, Nucl. Phys. B **187** (1981) 461.

[46] M. Ciuchini, E. Franco, G. Martinelli and L. Reina, Nucl. Phys. B **415** (1994) 403 [arXiv:hep-ph/9304257].

[47] A. J. Buras, M. Jamin, M. E. Lautenbacher and P. H. Weisz, Nucl. Phys. B **370** (1992) 69 [Addendum-ibid. B **375** (1992) 501].

[48] K. Adel and Y. P. Yao, Phys. Rev. D **49** (1994) 4945 [arXiv:hep-ph/9308349].

[49] C. Greub and T. Hurth, Phys. Rev. D **56** (1997) 2934 [arXiv:hep-ph/9703349].

[50] M. Misiak and M. Munz, Phys. Lett. B **344** (1995) 308 [arXiv:hep-ph/9409454].

[51] C. Greub, T. Hurth and D. Wyler, Phys. Rev. D **54** (1996) 3350 [arXiv:hep-ph/9603404].

[52] P. Gambino and M. Misiak, Nucl. Phys. B **611** (2001) 338 [arXiv:hep-ph/0104034].

[53] C. Bobeth, M. Misiak and J. Urban, Nucl. Phys. B **574** (2000) 291 [arXiv:hep-ph/9910220].

[54] M. Misiak and M. Steinhauser, Nucl. Phys. B **683** (2004) 277 [arXiv:hep-ph/0401041].

[55] M. Gorbahn and U. Haisch, Nucl. Phys. B **713** (2005) 291 [arXiv:hep-ph/0411071].

[56] M. Gorbahn, U. Haisch and M. Misiak, Phys. Rev. Lett. **95** (2005) 102004 [arXiv:hep-ph/0504194].

[57] M. Czakon, U. Haisch and M. Misiak, JHEP **0703** (2007) 008 [arXiv:hep-ph/0612329].

[58] K. Bieri, C. Greub and M. Steinhauser, Phys. Rev. D **67** (2003) 114019 [arXiv:hep-ph/0302051].

[59] M. Misiak and M. Steinhauser, Nucl. Phys. B **764** (2007) 62 [arXiv:hep-ph/0609241].

[60] I. R. Blokland, A. Czarnecki, M. Misiak, M. Slusarczyk and F. Tkachov, Phys. Rev. D **72** (2005) 033014 [arXiv:hep-ph/0506055].

[61] H. M. Asatrian, A. Hovhannisyan, V. Poghosyan, T. Ewerth, C. Greub and T. Hurth, Nucl. Phys. B **749** (2006) 325 [arXiv:hep-ph/0605009].

[62] H. M. Asatrian, T. Ewerth, A. Ferroglia, P. Gambino and C. Greub, Nucl. Phys. B **762** (2007) 212 [arXiv:hep-ph/0607316].

[63] A. Ali and C. Greub, Z. Phys. C **49** (1991) 431.

[64] A. Ali and C. Greub, Phys. Lett. B **361** (1995) 146 [arXiv:hep-ph/9506374].

[65] N. Pott, Phys. Rev. D **54** (1996) 938 [arXiv:hep-ph/9512252].

[66] A. L. Kagan and M. Neubert, Eur. Phys. J. C **7** (1999) 5 [arXiv:hep-ph/9805303].

[67] A. Ali and E. Pietarinen, Nucl. Phys. B **154** (1979) 519.

G. Altarelli, N. Cabibbo, G. Corbo, L. Maiani and G. Martinelli, Nucl. Phys. B **208** (1982) 365.

[68] M. Neubert, Phys. Rev. D **49** (1994) 3392 [arXiv:hep-ph/9311325].

[69] D. Benson, I. I. Bigi and N. Uraltsev, Nucl. Phys. B **710** (2005) 371 [arXiv:hep-ph/0410080].

[70] J. S. Schwinger, J. Math. Phys. **2** (1961) 407.

L. V. Keldysh, Zh. Eksp. Teor. Fiz. **47** (1964) 1515 [Sov. Phys. JETP **20** (1965) 1018].

[71] T. Becher, M. Neubert and G. Xu, JHEP **0807** (2008) 030 [arXiv:0710.0680 [hep-ph]].

[72] T. Mannel, W. Roberts and Z. Ryzak, Nucl. Phys. B **368** (1992) 204.

[73] E. Eichten and B. R. Hill, Phys. Lett. B **234** (1990) 511.

[74] H. Georgi, Phys. Lett. B **240** (1990) 447.

[75] A. F. Falk and M. Neubert, Phys. Rev. D **47** (1993) 2965 [arXiv:hep-ph/9209268].

[76] N. Isgur and M. B. Wise, Phys. Lett. B **232** (1989) 113.

[77] A. F. Falk, H. Georgi, B. Grinstein and M. B. Wise, Nucl. Phys. B **343** (1990) 1.

[78] A. F. Falk, Nucl. Phys. B **378** (1992) 79.

[79] E. Eichten, Nucl. Phys. Proc. Suppl. **4** (1988) 170.

[80] B. A. Thacker and G. P. Lepage, Phys. Rev. D **43** (1991) 196.

[81] M. Neubert, Phys. Rev. D **49** (1994) 4623 [arXiv:hep-ph/9312311].

[82] I. I. Y. Bigi, M. A. Shifman, N. G. Uraltsev and A. I. Vainshtein, Int. J. Mod. Phys. A **9** (1994) 2467 [arXiv:hep-ph/9312359].

[83] H. D. Politzer, Nucl. Phys. B **172** (1980) 349.

[84] A. F. Falk, M. E. Luke and M. J. Savage, Phys. Rev. D **49** (1994) 3367 [arXiv:hep-ph/9308288].

[85] M. Beneke, A. P. Chapovsky, M. Diehl and T. Feldmann, Nucl. Phys. B **643** (2002) 431 [arXiv:hep-ph/0206152].

[86] M. Beneke and V. A. Smirnov, Nucl. Phys. B **522** (1998) 321 [arXiv:hep-ph/9711391].

[87] R. J. Hill and M. Neubert, Nucl. Phys. B **657** (2003) 229 [arXiv:hep-ph/0211018].

[88] M. Beneke and T. Feldmann, Nucl. Phys. B **685** (2004) 249 [arXiv:hep-ph/0311335].

[89] T. Becher, R. J. Hill and M. Neubert, Phys. Rev. D **69** (2004) 054017 [arXiv:hep-ph/0308122].

[90] M. Beneke and T. Feldmann, Phys. Lett. B **553** (2003) 267 [arXiv:hep-ph/0211358].

[91] C. W. Bauer and A. V. Manohar, Phys. Rev. D **70** (2004) 034024 [arXiv:hep-ph/0312109].

[92] F. De Fazio and M. Neubert, JHEP **9906** (1999) 017 [arXiv:hep-ph/9905351].

[93] T. Becher and M. Neubert, Phys. Lett. B **637** (2006) 251 [arXiv:hep-ph/0603140].

[94] S. W. Bosch, R. J. Hill, B. O. Lange and M. Neubert, Phys. Rev. D **67** (2003) 094014 [arXiv:hep-ph/0301123].

[95] G. P. Korchemsky and A. V. Radyushkin, Nucl. Phys. B **283** (1987) 342.
I. A. Korchemskaya and G. P. Korchemsky, Phys. Lett. B **287** (1992) 169.

[96] S. Moch, J. A. M. Vermaseren and A. Vogt, Nucl. Phys. B **688** (2004) 101 [arXiv:hep-ph/0403192].

[97] T. Becher and M. Neubert, Phys. Lett. B **633** (2006) 739 [arXiv:hep-ph/0512208].

[98] R. J. Hill, T. Becher, S. J. Lee and M. Neubert, JHEP **0407** (2004) 081 [arXiv:hep-ph/0404217].

[99] D. Pirjol and I. W. Stewart, Phys. Rev. D **67** (2003) 094005 [Erratum-ibid. D **69** (2004) 019903] [arXiv:hep-ph/0211251].

[100] S. W. Bosch, M. Neubert and G. Paz, JHEP **0411** (2004) 073 [arXiv:hep-ph/0409115].

[101] G. Paz, JHEP **0906** (2009) 083 [arXiv:0903.3377 [hep-ph]].

[102] K. S. M. Lee, Phys. Rev. D **78** (2008) 013002 [arXiv:0802.0873 [hep-ph]].

[103] J. Chay, C. Kim and A. K. Leibovich, Phys. Rev. D **72** (2005) 014010 [arXiv:hep-ph/0505030].

[104] A. Kapustin, Z. Ligeti and H. D. Politzer, Phys. Lett. B **357** (1995) 653 [arXiv:hep-ph/9507248].

[105] J. F. Donoghue and A. A. Petrov, Phys. Rev. D **53** (1996) 3664 [arXiv:hep-ph/9510227].

[106] G. Paz, arXiv:hep-ph/0607217.

[107] C. W. Bauer, M. E. Luke and T. Mannel, Phys. Rev. D **68** (2003) 094001 [arXiv:hep-ph/0102089].

[108] M. B. Voloshin, Phys. Lett. B **397** (1997) 275 [arXiv:hep-ph/9612483].

[109] Z. Ligeti, L. Randall and M. B. Wise, Phys. Lett. B **402** (1997) 178 [arXiv:hep-ph/9702322].

[110] A. K. Grant, A. G. Morgan, S. Nussinov and R. D. Peccei, Phys. Rev. D **56** (1997) 3151 [arXiv:hep-ph/9702380].

[111] G. Buchalla, G. Isidori and S. J. Rey, Nucl. Phys. B **511** (1998) 594 [arXiv:hep-ph/9705253].

[112] J. Chay, C. Kim, A. K. Leibovich and J. Zupan, Phys. Rev. D **76** (2007) 094031 [arXiv:0708.2466 [hep-ph]].

[113] T. Mannel, Phys. Rev. D **50** (1994) 428 [arXiv:hep-ph/9403249].

[114] I. I. Y. Bigi, M. A. Shifman, N. G. Uraltsev and A. I. Vainshtein, Phys. Rev. D **52** (1995) 196 [arXiv:hep-ph/9405410].

[115] B. O. Lange and M. Neubert, Nucl. Phys. B **690** (2004) 249 [Erratum-ibid. B **723** (2005) 201] [arXiv:hep-ph/0311345].

[116] M. Beneke, G. Buchalla, M. Neubert and C. T. Sachrajda, Nucl. Phys. B **591** (2000) 313 [arXiv:hep-ph/0006124].

[117] C. W. Bauer, D. Pirjol and I. W. Stewart, Phys. Rev. D **67** (2003) 071502 [arXiv:hep-ph/0211069].

[118] C. M. Arnesen, Z. Ligeti, I. Z. Rothstein and I. W. Stewart, Phys. Rev. D **77** (2008) 054006 [arXiv:hep-ph/0607001].

[119] A. V. Manohar and I. W. Stewart, Phys. Rev. D **76** (2007) 074002 [arXiv:hep-ph/0605001].

[120] R. L. Jaffe, Nucl. Phys. B **229** (1983) 205.

[121] M. Neubert, Phys. Rev. D **45** (1992) 2451.

[122] A. G. Grozin and M. Neubert, Phys. Rev. D **55** (1997) 272 [arXiv:hep-ph/9607366].

[123] S. J. Lee and M. Neubert, Phys. Rev. D **72** (2005) 094028 [arXiv:hep-ph/0509350].

[124] P. Ball and E. Kou, JHEP **0304** (2003) 029 [arXiv:hep-ph/0301135].

[125] V. M. Braun, D. Y. Ivanov and G. P. Korchemsky, Phys. Rev. D **69** (2004) 034014 [arXiv:hep-ph/0309330].

[126] A. Le Yaouanc, L. Oliver and J. C. Raynal, Phys. Rev. D **77** (2008) 034005 [arXiv:0707.3027 [hep-ph]].

[127] H. Kawamura and K. Tanaka, Phys. Rev. D **81** (2010) 114009 [arXiv:1002.1177 [hep-ph]].

[128] A. L. Kagan and M. Neubert, Phys. Rev. D **58** (1998) 094012 [arXiv:hep-ph/9803368].

[129] M. Misiak, Acta Phys. Polon. B **40** (2009) 2987 [arXiv:0911.1651 [hep-ph]].

[130] B. Aubert *et al.* [BABAR Collaboration], Phys. Rev. D **72** (2005) 052004 [arXiv:hep-ex/0508004].

[131] B. Aubert *et al.* [BABAR Collaboration], Phys. Rev. D **77** (2008) 051103 [arXiv: 0711.4889 [hep-ex]].

[132] T. Hurth, E. Lunghi and W. Porod, Nucl. Phys. B **704** (2005) 56 [arXiv:hep-ph/0312260].

[133] L. Wolfenstein and Y. L. Wu, Phys. Rev. Lett. **73** (1994) 2809 [arXiv:hep-ph/9410253].

[134] G. M. Asatrian and A. Ioannisian, Phys. Rev. D **54** (1996) 5642 [arXiv:hep-ph/9603318].

H. M. Asatrian, G. K. Egiian and A. N. Ioannisian, Phys. Lett. B **399** (1997) 303.

[135] F. Borzumati and C. Greub, Phys. Rev. D **58** (1998) 074004 [arXiv:hep-ph/9802391].

[136] M. Blanke, A. J. Buras, A. Poschenrieder, C. Tarantino, S. Uhlig and A. Weiler, JHEP **0612** (2006) 003 [arXiv:hep-ph/0605214].

[137] J. R. Ellis, J. S. Lee and A. Pilaftsis, Phys. Rev. D **76** (2007) 115011 [arXiv:0708.2079 [hep-ph]].

[138] W. Altmannshofer, A. J. Buras, S. Gori, P. Paradisi and D. M. Straub, Nucl. Phys. B **830** (2010) 17 [arXiv:0909.1333 [hep-ph]].

[139] A. Soni, A. K. Alok, A. Giri, R. Mohanta and S. Nandi, Phys. Rev. D **82** (2010) 033009 [arXiv:1002.0595 [hep-ph]].

[140] A. J. Buras, B. Duling, T. Feldmann, T. Heidsieck, C. Promberger and S. Recksiegel, JHEP **1009** (2010) 106 [arXiv:1002.2126 [hep-ph]].

[141] M. Jung, A. Pich and P. Tuzon, arXiv:1011.5154 [hep-ph].

[142] H. H. Asatryan, H. M. Asatrian, G. K. Yeghiyan and G. K. Savvidy, Int. J. Mod. Phys. A **16** (2001) 3805 [arXiv:hep-ph/0012085].

[143] J. M. Soares, Nucl. Phys. B **367** (1991) 575.

[144] T. Hurth and T. Mannel, Phys. Lett. B **511** (2001) 196 [arXiv:hep-ph/0103331].

[145] M. Neubert, arXiv:0801.0675 [hep-ph].

[146] `http://www.slac.stanford.edu/xorg/hfag/semi/fpcp2009/gbl\_fits/kinetic/nobsg.txt`

[147] J. Laiho, E. Lunghi and R. S. Van de Water, Phys. Rev. D **81** (2010) 034503 [arXiv:0910.2928 [hep-ph]].

[148] M. Beneke and M. Neubert, Nucl. Phys. B **651** (2003) 225 [arXiv:hep-ph/0210085].